Cell assemblies : recruitment of heterogeneous networks and readout mechanisms

Céline Boucly

Cell assemblies: recruitment of heterogeneous networks and readout mechanisms

Assemblées de neurones: recrutement de réseaux hétérogènes et mécanismes de lecture

Thèse de doctorat de l'université Sorbonne Université

présentée par

Céline BOUCLY

pour obtenir le grade de

Docteure en Neurosciences

Soutenue publiquement le 25 septembre 2020 devant le jury composé de :

Dr. David DUPRET Université d'Oxford, Oxford	*Rapporteur*
Dr. Adrien PEYRACHE Université McGill, Montréal	*Rapporteur*
Dr. Mehdi KHAMASSI Sorbonne Université, Paris	*Examinateur*
Dr. Clément LÉNA École Normale Supérieure, Paris	*Examinateur invité*
Dr. Michaël ZUGARO Collège de France, Paris	*Directeur de thèse*

Ecole doctorale N°158 : **Cerveau, Cognition, Comportement**

Remerciements

Je voudrais tout d'abord remercier les membres du jury, qui ont accepté d'évaluer ce travail. Merci aux deux rapporteurs, *David Dupret* et *Adrien Peyrache*, qui ont du lire ma thèse durant l'été. En particulier, merci à vous, *Clément Lénat* et *Mehdi Khamassi*, qui avez suivi l'évolution de mes travaux depuis le début à l'occasion des comités.

Merci à toi *Michaël*, d'avoir acueillie dans l'équipe la physicienne égarée que j'étais (mais qu'est donc une ripple, au juste?). Toutes nos discussions scientifiques m'ont permise d'avancer et de mieux comprendre le vaste (très vaste) sujet des 'assemblées cellulaires' mais ce que je retiendrai le plus, ce sont nos déjeuners animés à la cantine et tes discours passionnés. Sid, merci pour ton encadrement, tes conseils et bien sûr tes relectures. Si le texte qui suit est écrit dans un anglais à peu près intelligible, c'est en grande partie grâce à toi!

Merci mille fois à super *Raly*, la grande experte de Matlab qui pense et parle plus vite que son ombre, toujours disponible pour débugger un code, relire des chapitres de thèse ou bien boire du pastis. Dans la même veine, deux superbes rencontres, Marco, le monsieur à tout faire du labo, respo tiramisu et opinioniste, Virginie, capable de faire de la photosynthèse, record woman du plus long temps passée au labo d'affilé sans dormir (72h), amatrice de saké. Merci à tous les deux pour vos données que vous avez si dûrement acquises, sans vous ce manuscript aurait été bien vide! Maintenant, on croise les doigts et on attend avec impatience nos deux publis. Une pensée pour *Raphaël*, la relève du labo, on compte sur toi pour nous sortir des résultats du feu de dieu avec tes enregistrements dans 46 structures en parallèle. *Nadia, Ariane*, on voit le bout du tunnel, d'ici quelques jours nous serons toutes les trois docteures ! Merci à vous deux et bonne chance pour la suite. Merci à *Théo* et *Ombeline*, nos exilés de l'ENS, courage, courage pour votre beau projet d'imagerie. Une dédicace aux anciens membres de l'équipe : *Gabriel, Eulalie, Elena, Sara, Diane, Maïna, Alexandra, Ahmed, Arthem, Fanny*, et à *Céline D*, je m'en vais du labo et ta maison n'est toujours pas dans "old", un scandale. Une pensée à *Angelo* et *Elisa* de *l'Institut de la vision*, qui m'ont donnée l'envie de me lancer dans cette aventure qu'est la thèse.

Je voudrais également remercier tous les autres membres du CIRB que j'ai pu croisé et qui m'ont aidé au cours de ces trois années. En particulier merci à *Nicole* et le service de gestion, merci pour votre compréhension et votre patience (des ordres de mission pas toujours remplis en temps et en heure, pardon). Merci à la team Venance aka les copains du couloir, notamment

Gaëtan, mon acolyte de pauses thé, *Nicolas* l'expert Top chef, et *Willy* les bons plans. J'envoie toutes mes ondes positive à *Amaury* et au GreenCom, notre asso écolo, vous allez faire de grandes choses (j'y crois!)

Je remercie tous les copains de l'ENS Lyon (aux surnoms très enfantins) : mes anciens colocs de choc, *Lulu* et *Percy*, *Dédé* la surdouée de LLG, *Sousou* et *Clem* exilés à Amiensse, *Guigui* le cycliste fou, *Lilou* et *Thibaut*, thésards en magie noire, *Trotro* respo marcel et vente privée, *Marie* la future avocate, *Sami* notre plongeur olympique, ma petite *Adeline*, *Christochèvre*, bon courage pour la fin de thèse. Un grand merci aux copains de Paris, les ptits potes, comme on dit : *Alexis* le déconneur régaleur, *Casto* le grand fan du Secret H. (droit dans ses bottes), *Aude* aka madame Poup, *Chloé*, la seule et l'unique, la douce *Valentine*, JB le parasite , *Vianney*, l'élégance même, *Artiom*, toujours positif, *Camcam* et *Valou* les expert de l'escape game, le grand *Gus*, *Marius*, *Léa* et *Bruneel*, bientôt docteurs, *Hadrien* (promis je viendrai bientôt te voir dans le Sud). Merci à tous pour votre soutien durant ces trois années, merci à ceux qui me demandaient régulièrement comment se passait LA thèse mais merci aussi à ceux qui ne me demandaient pas comment avançaient mes grandes recherches.

Merci à *Eliette*, *Philippe*, *Loulou*, *Thoumsi*, la famille Rosell qui m'a epaulée tout au long de ce parcours, à base d'apéros, diners et le fameux voyage en Thaïlande (encore heureux, on est partis l'année dernière!). Un grand merci à ma famille, mon petit Michel, les frérots Seb et Lolo, mes parents chéris, merci papa, merci maman. Merci pour tout ce que vous avez fait pour moi toutes ces années, merci mille fois.

Enfin, Baptiste, tu pensais que je t'avais oublié? Merci de t'être occupé de moi pendant que j'écrivais ce manuscript (comment aurais-je donc fait pour me nourrir sinon?), merci d'être là, merci d'être toi tout simplement.

Contents

Prologue

How do billions of neurons cooperate to process information and mediate cognitive function? An influential hypothesis is that groups of neurons can synchronize within brief time windows to represent a cognitive entity or a concept (Hebb 1949). These groups, called 'cell assemblies' are thought to be the functional units of the brain. Recent advances in large-scale neuronal recordings have permitted to investigate such synchronous activity within single areas of the brain. Yet, the functional relevance of these ensembles remains largely unexplored, especially within and among higher order brain areas.

The *Introduction* of this thesis is structured in three parts and discusses the background knowledge for my thesis research on cell assemblies.
Chapter 1 presents the historical evolution of the cell assembly concept. Cell assemblies were first proposed in a representational framework by Hebb (1949). In this view, the role of a cell assembly is to 'code' for an item, for example, an apple. This motivated many studies in the sensory system. Their goal was to find neurons that preferentially activated in response to specific stimuli. Decades later, Buzsáki proposed that the functional relevance of synchronous activation should be considered from the perspective of the internal mechanisms of the brain itself, not that of the experimenter. For example, downstream neurons could rely on temporally organized inputs to discharge. This chapter also discusses the issues of cell assembly time scales, and how brain rhythms could help to shape them. A brief section presents sequences of cell assemblies, hypothetical 'neural words' that could underpin elaborated cognitive processes. Finally, this chapter proposes a working definition of cell assemblies applicable for the rest of this manuscript, that is: ensembles of cells that are co-active in a brief temporal window.
Chapter 2 is dedicated to the numerous existing methods to identify cell assemblies. This chapter covers elementary cross-correlation tools, model-based techniques and unsupervised frameworks. A particular focus is set on principal and independent component analyses. These methods form the basis of my two research projects described in the *Result* section.
Chapter 3 exposes the neurophysiological mechanisms involved in memory consolidation during sleep. In particular, this chapter describes 'reactivations', i.e., repeated activations of cell assemblies and 'replay', i.e., temporally ordered sequences of neural activity, both of which occur in many brain regions.

The *Results* section of this manuscript presents the computational projects of my PhD work, in collaboration with team members and under the supervision of Michaël Zugaro and Sidney Wiener at the Collège de France.

Chapter 4 consists of a manuscript currently under consideration at *Nature Communications*. In this project, we aimed at investigating whether cell assemblies existed within and among two high order brain areas. My contribution was to demonstrate and characterize synchronous activity spanning different parts of the prefrontal cortex and the striatum in freely behaving rats, members of the cortico-basal ganglia loop. These distributed cell assemblies exhibited behaviorally correlated activation in rats performing a set-shifting task, and synchrony emerged when members shifted their phase relative to ongoing brain rhythms.
Chapter 5 presents a manuscript in preparation for submission. The goal of this project is to study the functional relevance of cell assemblies from the perspective of a downstream neuron. To this end, we analyzed the neural activity from hundreds of single units in the prefrontal-amygdalar networks in rats during sleep. Our results suggest that the synchronous activity of cell assemblies facilitate and amplify the discharge of downstream neurons, termed 'readers' of the assembly. Finally, the paper shows that the assembly-reader communication changes with learning.

The *General Discussion* presents some general considerations and possible perspectives for future work.
Chapter 6 is dedicated to discussing the main findings of Chapter 4. It also addresses future data analyses aimed at further characterizing assembly-reader relationship described in Chapter 5.
In **Chapter 7**, I discuss some of the main limitations of the computing method employed here to detect cell assemblies. Finally, I also suggest a possible strategy for overcoming them.

Part I

Introduction

1 How does information flow within the brain?

How do billions of neurons work together to process information and enable cognitive functions? One strategy to try to answer this question, is to present various stimuli such as a the sound of Chopin sonata, the scent of an orange, a Degas painting of dancers, and record the responses of neurons in a brain. However, in the early years of neuroscience, only one or few single neurons could be examined at a time. Therefore, experimenters focused on finding the relevant stimulus that induce reliable firing of single cells. Afterwards, with technological advances increasing the number of neurons simultaneously recorded, electrophysiologists suggested that: a single cell might not code only for a single stimulus and conversely a stimulus may not be represented by only a single cell. These considerations led to the popularization of the cell assembly concept, first developed by Hebb (1949): groups of anatomically interconnected neurons are the functional units of the brain that can represent distinct objects, concepts or cognitive entities. The 'representational concept' of cell assemblies proposed by Hebb was recently challenged and refined by Buzsáki (2010). To be functionally relevant, cell assemblies should provide

meaningful signals for downstream neurons or network mechanisms reading the assembly activity, rather than simply being detectable by the experimenter seeking the external stimulus best correlating with assembly activity. In this chapter, I will first retrace the paradigm shift from the neuron doctrine to cell assemblies. Subsequent sections are dedicated to time scales that define cell assemblies but also sequences of assemblies: neural words.

1.1 From the neuron doctrine to cell assemblies

Popular in the 1970s, an extension to the neuron doctrine stated that a neuron is not only the anatomical and functional unit of the nervous system but also its perceptual unit (Barlow 1972). In this view, each neuron is a feature detector of a specific stimulus, object, event. This assumption was based on visual system studies, especially on frog retina ganglion cells ("fly detector neurons", particularly active when a bug is moving; Barlow 1953), and later in the cat visual cortex (Hubel & Wiesel 1962). Neurons that respond to the orientation of a bar stimulus in a particular part of the visual field[1] would converge onto other cells in hierarchically superior structures to be combined into more complex percepts (see Figure 1.1, a). This builds up a hierarchy of coding that ultimately leads to cells at the top of the pyramid (ironically) named "gnostic neuron" (Konorski 1967) or "grand-mother cells" (Lettvin 1967, Gross 2002). Grand-mother cells are hypothetical neurons that would uniquely code for a highly complex stimulus, such as the concept of a person, e.g. the face, the voice or the name of my grand mother. Interestingly, face selective cells have been recorded in the highest level of the hierarchy of the visual areas (i.e. in the inferior temporal cortex) of monkeys (Gross *et al.* 1969, Perrett *et al.* 1982, Desimone *et al.* 1984). For example, in the human medial temporal lobe, neurons exhibit selective response to particular faces or objects (Kreiman *et al.* 2000), such as the well known 'Jennifer Aniston cell' (Quiroga, Reddy, *et al.* 2005), particularly active when a patient was looking at a picture of the actress[2].

However, these neurons (celebrity cells or face selective cells in monkeys) typically respond to more than one or several stimulus. Even the popular Jennifer Aniston neuron responded in a subsequent session also to Lisa Kudrow, one of her co-stars in the show *Friends*. Theoretical work estimated that each cell most probably responds to between 50 and 150 distinct percepts (Waydo *et al.* 2006). Similarly, in higher order areas such as the prefrontal cortex (PFC), neurons exhibit complex and multi-modal tuning (see Eichenbaum 2018 for a review). The fact that neurons are specifically activated by particular inputs may not necessarily mean that this is their role in the circuit (Yuste 2015).
The mean by which a neuron encode a given information could be related to

[1] These neurons are located in the primary visual cortex V1 and are arranged in columns, perpendicular to the surface of the cortex

[2] Interestingly, such cells are multi-modal, that is, a Jennifer Anniston cell may respond to a picture of the actress but also to hearing her name (auditory stimuli; Quian Quiroga *et al.* 2009)

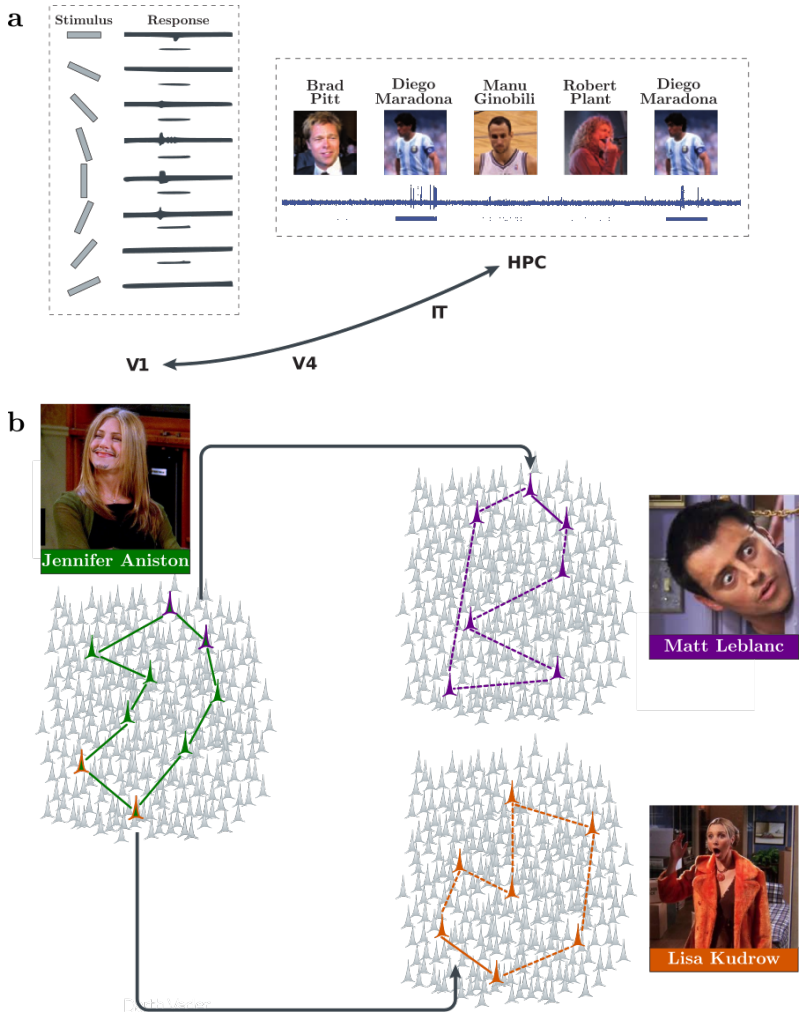

Figure 1.1: a) Tuning of a neuron recorded in cat V1 (the first visual cortical area) to the local orientations of moving visual stimulus(Hubel & Wiesel 1962). Note that this neuron is more active when the bar is vertical. This information is further processed along the ventral visual pathway. The neuronal representation in V1 is combined into more complex patterns in higher areas (V1 to V4), and in the inferotemporal cortex (the hierarchically highest purely visual area) neurons fire selectively to the sight of faces (Gross *et al.* 1969, Perrett *et al.* 1982, Desimone *et al.* 1984). The inferotemporal cortex (IT) has numerous connections to the medial temporal lobe (which includes the hippocampus, HPC), in which neurons were found to respond selectively to persons or objects, such as, in the example shown, the football player Diego Maradona (Quiroga, Reddy, *et al.* 2005). **b)** Distributed representation of concepts (e.g., TV show *Friends* actors) in the medial temporal lobe.

Figure 1.1: On the left is a hypothetical cell assembly encoding the concept 'Jennifer Aniston' (group of neurons colored in green). Of these neurons, some also fired in response to Lisa Kudrow (identified with an orange line contour), and some others fired in response to Matt Leblanc (identified with a purple line contour). The activation of the 'Jennifer Aniston cell assembly', for example, after seeing her picture, can then trigger other associated concepts, such as Lisa Kudrow or Matt Leblanc, through the firing of the neurons with an overlapping representation. Such partially overlapping representation could be the basis of the encoding and learning of associations and episodic memories. Note that this schematic example is an extrapolation proposed by Quiroga 2012 following numerous studies from the Itzak Fried lab (Quiroga, Reddy, *et al.* 2005, Quiroga, Kreiman, *et al.* 2008, Gelbard-Sagiv *et al.* 2008), in particular the Jennifer Aniston cell (Quiroga, Reddy, *et al.* 2005; which also fired for Lisa Kudrow in subsequent session). Panel a) and b) are adapted from Quiroga 2012.

its firing or its lack of firing (rate code), to the exact time at which it fires (temporal code), but also to whether or not it fires in synchrony with other neurons (ensemble coding).

Perhaps one of the strongest arguments in favor of cell assembly coding is the following: considering the millions of neurons existing in the medial temporal lobe, how can the investigators be lucky enough to record a neuron that codes for the face of a particular person (which happens to be represented in of the 30 pictures selected for the experiment)? It is more likely that coding for any particular face is distributed across a large population of neurons. Distributed encoding in the visual system is explained by the binding-theory: the different features of a stimulus (edges, colour, motion, texture) are treated separately by feature detector neurons in different visual areas, and then this information is integrated when these neurons fire together so the representation of the stimulus can emerge. In this view, there are no unique 'grandmother cells' or 'Jennifer Aniston cells' that could detect the unique collection of features that characterize a person but rather a 'Jennifer Aniston assembly' combining several features, (e.g. her voice, blond hair, blue eyes; Gross 2002, Quiroga, Kreiman, *et al.* 2008; see also section 1.3 for an hypothetical mechanism of binding). Notably, Quiroga 2012 suggested that related cognitive representations (e.g. actors casted in the same TV show, see Figure 1.1, b) could be encoded by overlapping groups of cells. These groups are also referred to as 'cell assemblies'. Cell assemblies are the central topic of this thesis, therefore, before moving further, I will provide a working definition of what assemblies are.

1.2 Conceptual definition of cell assemblies

The literature, employs many terms, such as *'ensemble', 'population', 'group of neurons', 'cell assemblies'* or even *'states'*, to describe the activity of a certain number of neurons (ranging 'from more than one', to 'all the neurons we could record'), without explicitly defining what these terms actually refer to. In this section, I will present the original conceptual definition of a cell

assembly, proposed by Hebb (1949), but also a more recent one proposed by Buzsáki (2010), providing a framework for the scientific questions addressed in the Result section 5.

1.2.1 Cell assemblies in a representational framework

The term 'cell assembly' was first coined by Donald O. Hebb in 1949 in his book *the Organization of behavior* where he proposed a paradigm shift: cell assemblies rather than single cells are the functional units of the brain (as opposed to the neuron doctrine, see 1.1). But what was the originally proposed definition a cell assembly? A cell assembly is a group of physically interconnected neurons. This theory is based on Hebb's rule : *"The general idea is an old one, any two cells or systems of cells that are repeatedly active at the same time will tend to become "associated", so that activity in one facilitates activity in the other* (Hebb 1949). Thus, mutual excitation of a sufficient number of cells can activate them as a cell assembly. Their interconnections would then be reinforced, so that subsequent excitation of a subset of the assembly would reactivate the rest. Because of this plasticity and high-interconnectivity, Hebb hypothesized that an assembly could maintain its activity and manifest a reverberatory activity that would persist[3], without requiring any further input. The simplest examples of such processes are closed loop systems, i.e. A triggers B, B triggers C and C leads back to A. However, the best analogy to the network structure defined by Hebb, instead of a ring or a loop is a *closed solid cage-work or a 3D lattice* with no regular structure and with connections possible from any one cell (intersection) to any other. In turn, the reverberatory activity of an assembly can serve as an input to another assembly, thus resulting in 'chains', denominated as 'phase sequences' by Hebb. He proposed that phase sequences are the neural substrate of perception and internal complex cognitive processes such as thinking, planning, or decision making (see Figure 1.2a).

However, Hebb defined assemblies in the context of study of the visual system in particular within the 'representational framework' (i.e. finding the relevant stimulus that elicit the activation of a single cell or an assembly, see examples in the section 1.1 above). However, when studying complex cognitive function such as thinking, emotion, or memory at higher hierarchical levels, it may become difficult to find a relevant stimulus. Representation of external features is only part of the story: Gelbard-Sagiv *et al.* (2008) found a stimulus, an episode of *The Simpsons*, triggering activity of a subset of neurons in the hippocampus and the entorhinal cortex. Interestingly, firing rate of these neurons increased during free conscious recall, when the sensory stimuli was absent and no external cues were provided. Thus, the firing pattern of neurons reflects not only the physical nature of a stimulus, but also internal factors (even in primary sensory cortices; Kreiman *et al.* 2000). These considerations led Buzsáki (2010) to refine the definition of cell assemblies, as activity patterns mean-

[3] at least transciently, Hebb theorized a time limit up to 500 ms

ingful for internal processing by the brain rather than for the experimenters seeking the best stimulus associated with the cell assembly's activation.

1.2.2 Cell assemblies in the framework of internal processing: 'reader' mechanisms

Buzsáki (2010) proposed a functional definition of cell assemblies, without invoking representations, while keeping some features of Hebb's definition. He suggested that cell assemblies are meaningful events for neuronal computation, only from the point of view of a 'reader' mechanism and within a given temporal frame. The reader observes, integrates and sends an action in response to a particular input pattern (presumed cell assembly). In other words, cell assemblies are defined by their predictable consequences on downstream readers. Unlike Hebb's proposition, members of an assembly are not necessarily connected together, since only the generation of a coherent output is meaningful in this framework. Which candidates can qualify as reader mechanism? In Buzsáki's view, readers may be a neuron, a group of neurons[4], a motor response such as a muscle contraction or even a machine interpreting neural activity and producing an output. Hence, the time scales of assemblies could range from milliseconds to several seconds. However, here we will consider cell assemblies to exist on a brief timescale, from the perspective of readers that are one or several downstream neurons. In the next section, I will present the time scale of such cell assemblies and explain why these are relevant.

Box 1.1 Concepts related to cell assemblies

- **Hopfield networks** : inspired by Hebb's rule and his definition of the cell assembly, these networks can store externally presented patterns through the modification of recurrent excitatory synapses (Hopfield 1982). In time, the reverberant excitatory activity of the Hopfield network converges onto a stable state, an 'attractor', which matches one of the original input. However, once an attractor is reached, the network is locked there and can no longer evolve. This stationarity is in opposition with the dynamical view of cell assemblies : they can drop or recruit members over time, a fundamental property common to Hebb's and Buzsáki's definitions.

- **Synfire chains**. These refer to models of feed-forward neurons with many layers (Abeles 1982). Neurons in the same layer are not necessarily connected together but at least one of them projects onto a neuron in the target layer. This models sequences of cell assemblies, propagating in cascade from one layer to an other.

[4] Resulting in a sequence of assembly activations, similar to Hebb's phase sequences (see Figure 1.2b).

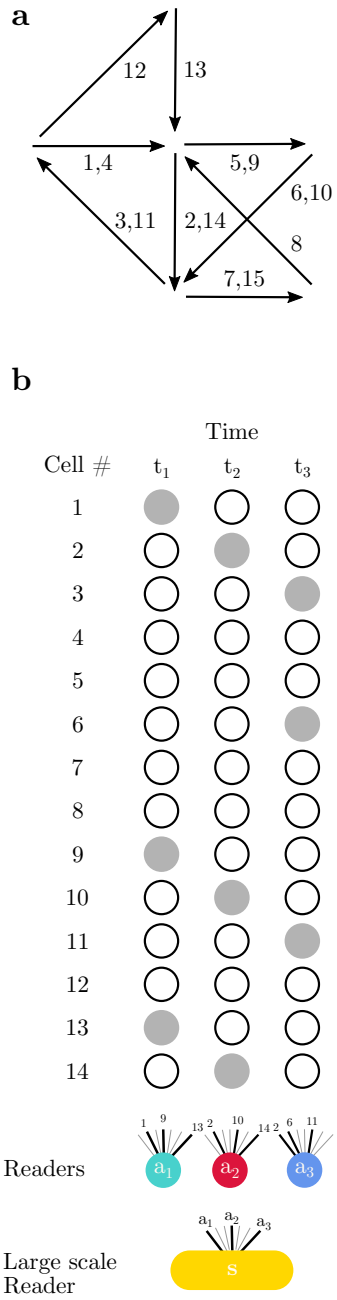

Figure 1.2: Conceptual definitions of cell assemblies. **a)** Hebb's reverberating cell assembly sequences (after Figure 10 of *The Organization of Behavior*). Arrows represent transitions between individual assemblies and numbers indicate the order of activation in the sequence. The direction of activity flow across assemblies (edges) is determined by the stronger synaptic strengths among assembly members relative to other connections (not shown). The same assembly can participate in a sequence more than once (e.g., pathway 1, 4 indicates recurring transitions). No mechanism is postulated to explain why activity does not spread to all parts of the network and reverberate forever. **b)** Cell assemblies in the framework of reader mechanisms (Buzsáki 2010). Cells firing within the time integrating window of a reader mechanism define an assembly (irrespective of whether assembly members are connected synaptically or not). Readers a_1, a_2 and a_3 may receive inputs from many neurons but respond only to a combination of spiking neurons (gray circles) to which they are most strongly connected. Thus reader a_1 responds preferentially to cofiring of neurons 1, 9, and 13 at t_1 (bold lines), even though it may be synaptically innervated by other neurons neurons (gray lines). The large scale reader mechanism s (yellow) integrates over a longer time period and, therefore, can link together assemblies into "neural words" reading out a new quality not present in the individual representations of a_1, a_2 and a_3.

1.3 A question of time windows

The working definition of cell assemblies here is a set of upstream neurons jointly firing in a given time window to be received by downstream neurons. In this section, I will explain the role of cell assembly synchronous activations in triggering an action potential of a downstream neuron and discuss the relevant time scale[5]. I will particularly focus on a window of electrophysiological interest: the 10-30 ms window corresponding to the membrane time constant of several cells in the brain (Spruston & Johnston 1992; Koch *et al.* 1996), as well as the time scale of plasticity mechanisms.

1.3.1 Coincidence detectors

What exactly causes a neuron to fire an action potential and which time scale is relevant? A neuron fires when its input current exceeds a certain threshold. Precisely, the threshold for action potential generation is the lowest at the initial segment of the axon, 'the trigger zone', since the density of Na+ channel is high in this region[6] (Figure 1.3a). However, the amplitude of a single excitatory postsynaptic potential (EPSP) does not usually drive the cell to reach this spiking threshold. Indeed, it is rather the summation of multiple synaptic potentials, propagating from dendrites to the soma and the trigger zone (and thus, undergoing severe attenuation, Segev & London 2000), that generates an action potential[7]. Theoretical studies have shown that excitatory inputs from multiple synapses arriving synchronously (e.g. from converging inputs from a cell assembly activation) within a short window, the width of an EPSP, are most effective in generating output spikes (Abeles 1982, König *et al.* 1996; see Figure 1.3c). Such mechanisms are referred to as coincidence detection or spatial summation, as opposed to temporal integration. In a temporal integration mode, the efficacy of EPSP summation results from sequential activation of the same input (Figure 1.3 b) whereas in a 'coincidence detection' mode, a neuron fires action potentials whenever a sufficient number of presynaptic neurons are precisely synchronously active. These two modes are not completely antagonistic: integrators are simply characterized by longer EPSPs. Thus, multiple inputs from the same synapse can be integrated (but also asynchronous activation of different inputs) while coincidence detectors by short ones, hence spatially separated inputs are favored[8] (Magee 2000). However, EPSP time

[5] Note that cell assemblies could have other downstream effects such as routing, gating as well as shunting.

[6] Na+ channels are voltage-gated protein embedded in the membrane of a neuron. They remain closed when the neuron membrane potential is close to the resting potential but they can open when the potential increases (for instance, because of the current induced by synaptic transmission). This causes more sodium ions to enter the cell which further increases the membrane potential, and so on, eventually reaching the action potential threshold. Following the action potential, Na+ channels becomes inactivated, Na+ ions are transported back outside of the cell. The resting potential is then restored with K+ channels opening.

[7] Neural integration also occurs at dendrites which can affect the propagation of synaptic potential to the cell body.

[8] Because of refractory periods, one neuron, can spike only one or two times in a short windows, say 20 ms.

widths are difficult to measure in vivo and depend on multiple factors: the morphology of the cell, the location of the synapses, and the time course of the synaptic currents from the dendrites to the trigger zone.

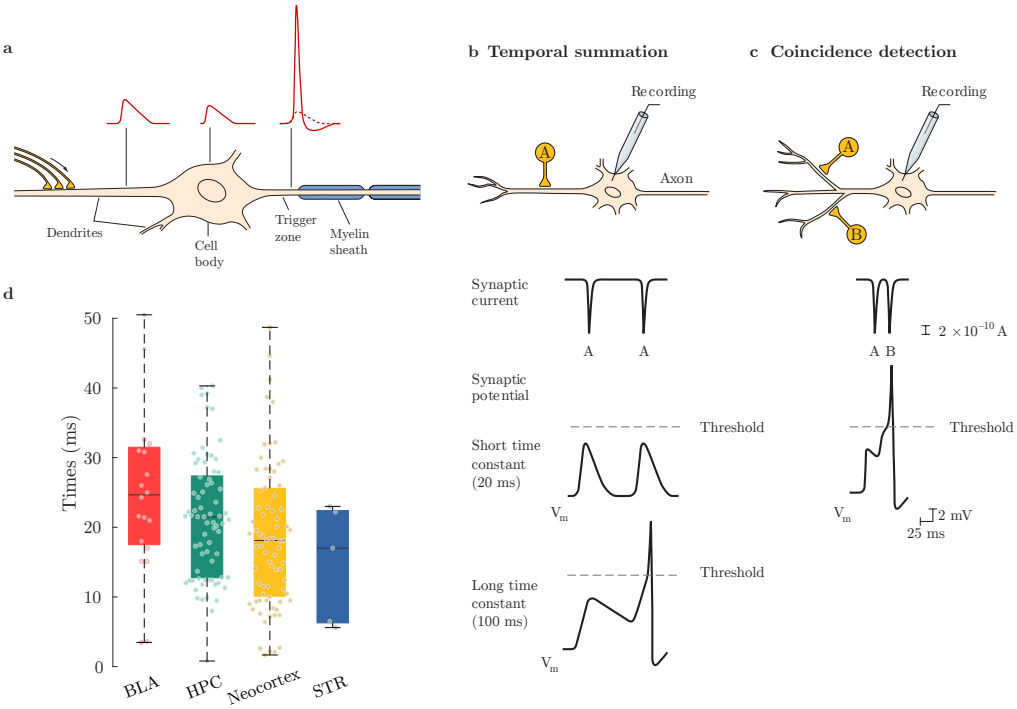

Figure 1.3: Neural integration. **a)** An excitatory synaptic potential originating in the dendrites decreases with distance as it propagates passively to the soma. Nevertheless, an action potential can be initiated at the trigger zone (the axon initial segment) because the density of the Na+ channels in this region is high, and thus the threshold is low. **b)** Temporal summation. In a cell with a short time constant (20 ms) the first EPSP decays to the resting potential before the second EPSP is triggered. EPSPs alone can not cause enough depolarization to trigger an action potential. However, in a cell with a long time constant the first EPSP does not fully decay by the time the second EPSP is triggered. Therefore, the depolarizing effects of both potentials are additive, bringing the membrane potential above the threshold and triggering an action potential. **c)** The summation of two potentials produced by two proximal synaptic neurons results in enough depolarization to exceed threshold, triggering an action potential, in a cell with short time constant (20 ms). **d)** Distribution of membrane time constants for different type of neurons : amygdala basolateral nucleus pyramidal neuron (BLA), Hippocampal CA1 pyramidal cell (HPC), Neocortex pyramidal cell layer 2-3, Nucleus accumbens medium spiny neuron (STR). Distributions first and third quartiles are indicated by boxplots, median by horizontal black bars (BLA = 25 ms; HPC = 21,5 ms; Neocortex = 18 ms; STR = 17 ms). Panels a,b and c are adapted from Kandel *et al.* 2000. Pannel d was produced with data from Tripathy *et al.* 2015.

Experimental studies in anesthetized animals provided evidence for the existence of coincidence detectors, reporting a 6 to 8 ms integration window of thalamic inputs in the somatosensory cortex (Roy & Alloway 2001) and in the visual system (Alonso *et al.* 1996; Usrey *et al.* 2000). Also, the integration time or EPSP width can be approximated by the measure of related parameters such as the neuron membrane time constant. The membrane time constant (τ) is the product of the resistance r_m and capacitance c_m of the membrane ($\tau = r_m c_m$) and represents the duration within which the membrane potential decays to approximately 37% ($= e^{-1}$) of the resting potential following an voltage step. Membrane time constants range from 5 to 100 ms depending on the type of cell and/or the brain area (for an impressive database including time constant measurements from 968 studies, see Tripathy *et al.* 2015). Typically, the membrane time constants of neurons in the neocortex, the striatum as well as in the amygdala, are ∼20 ms[9] (between 10 and 30 ms, see Figure 1.3d, see Box 1.2 for a brief description of these structures). Hence, cell assemblies time scale in these brain structures should lie within these values (as we reported in Result chapters 4 and 5, but see also Figure 1.5).

Box 1.2 Three brain structures of interest: the amydgala, the medial prefrontal cortex and the striatum

In this manuscript, experimental and computational studies aimed at investigating neural communication within and among three brain structures:

- **The amygdala** is a heterogeneous group of ∼13 nuclei. The basal and lateral nulcei called 'cortical-like', because, like the cortex, are mainly composed of excitatory projection neurons (∼85%) with a small percentage of local inhibitory interneurons (∼15%), and contain cortical-like neurons with pyramidal and stellate morphologies. Conversely, the centromedial nuclei, on the other hand, are considered striatal-like, because, like the striatum, they are composed almost exclusively of inhibitory neurons, and the projecting cells resemble the medium spiny neurons of the striatum. The amygdala is an emotional and motivational processor, implicated notably in aversion and reward processing (Pignatelli & Beyeler 2019). The amygdala also modulates fear learning in other brain regions, like the hippocampus and cortical areas (McGaugh 2004).

- **The striatum** (STR) is the main entry point of the basal ganglia. The basal ganglia system has been attributed various functions such as action selection, certain types of learning and memory as well as motivated behavior. The STR integrates multiple inputs, in particular, from diverse cortical areas and these connections are functionally organized. The striatum can be divided into multiple anatomo-functional subregions: dorsolateral, dorsomedial and the ventral stria-

[9] Note that these constants may vary depending on the synaptic background activity (Koch *et al.* 1996, Destexhe *et al.* 2003)

tum (vSTR), also called nucleus accumbens, which is subdivided into core and shell subregions. Striatal projection neurons are the GABAergic medium spiny neurons (MSNs) and comprise in rodents 90-95% of the striatal neuronal population (Rymar et al., 2004). The STR also contains GABAergic and cholinergic interneurons.

- **The medial prefrontal cortex** (mPFC) is implicated in a broad range of cognitive functions related to attention, executive control and working memory. As the other neocortical areas, the mPFC mostly contains two types of neurons: glutamatergic pyramidal projection neurons (PN) and GABAergic interneurons (IN) which represent respectively 80% and 20% of the cortical neural population (DeFelipe & Fariñas 1992). the mPFC is reciprocally connected with other subcortical structures including the amygdala, the hippocampus, and the striatum (Groenewegen *et al.* 1997).

1.3.2 Synaptic plasticity

Coincidental inputs from multiple pre-synaptic neurons (i.e. a cell assembly), within 20 ms, facilitate the discharge of a neuron. In this section, we will see that plasticity mechanisms occurs at similar time scales resulting in synaptic weight changes between one pre-synaptic neuron, e.g. a member of an assembly, and a post-synaptic neuron; e.g. a downstream target[10].
In *The Organisation of Behavior*, Hebb stated : "*when an axon of cell A is near enough to excite a cell B and repeatedly or persistently takes part in firing it, some growth process or metabolic change takes place in one or both cells such that its efficiency, as one of the cells firing B, is increased*". This was summarized by the well-known expression "*neurons that fire together, wire together*" (Shatz 1992).

However, the first experimental proof of Hebb's postulate came 30 years later, with the discovery of long term potentiation by Bliss & Lømo (1973). Their experiments were carried out in the rabbit hippocampus with tetanic stimulation of efferent fibers from the perforant pathway that projects monosynaptically to the dentate gyrus. These high frequency train of stimuli caused strong excitatory postsynaptic potentials in pyramidal cells of the dentate gyrus(see Figure 1.4a). Hence the following postsynaptic responses to further single stimulus pulses were enhanced. Since then, LTP has been observed in a variety of neural structures such as visual (Artola & Singer 1987), somatosensory (Bindman *et al.* 1988), motor (Iriki *et al.* 1989) and prefrontal cortical areas (Hirsch & Crepel 1992), the amygdala (Clugnet & LeDoux 1990), the nucleus accumbens (Pennartz, Ameerun, *et al.* 1993) and the midbrain reward system (Liu *et al.* 2005). A decade later, the opposite effect was discovered in cerebellum: a persistent decrease of synaptic efficacy resulting from another

[10] Plasticity mechanisms may as well occur between two members of an assembly if those happen to be anatomically connected, but this not necessarily the case in the 'reader' view of assemblies

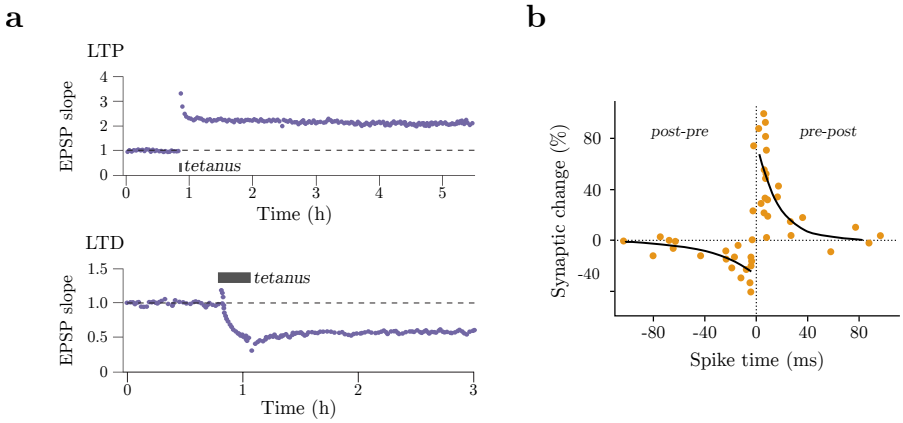

Figure 1.4: Plasticity mechanisms. **a)** Alterations in field EPSP (rising slope normalized to baseline) over time, during LTP (100 Hz tetanic stimulation, 1 s, baseline intensity) or after the induction of LTD (1 Hz stimulation, 15 min, baseline intensity). The gray bar represents the duration of the stimulus (from Collingridge *et al.* 2004). **b)** In STDP protocols, the synapse is either potentiated or depotentiated according to the delay between the pre-and post-synaptic spikes (from Bi & Poo 2001).

type of stimulus timing, called long term depression (LTD, see Figure 1.4a; Ito & Kano 1982). LTP can last more than a year and thus is capable of serving as a mechanism for long-lasting storage of information (Abraham *et al.* 2002).

Yet, the powerful tetanic stimulations used in early experiments to trigger LTP are much stronger than physiological conditions in vivo. Moreover, in these protocols, the Hebbian pairing rule is not respected since the spiking of the postsynaptic neurons is not controlled. Spiking-Timing-Dependant-Plasticity (STDP) provides a framework to understand plasticity one postsynaptic spike at a time. In 1997, Markram *et al.* and Magee & Johnston demonstrated that LTD occurs if a postsynaptic action potential precedes presynaptic activity by 20 to 100 ms while LTP occurs if the postsynaptic action potential follows presynaptic activity by ∼20 ms (Figure 1.4b). Thus repeated co-activations of multiple neurons within 20 ms can strengthen their reciprocal connections and/or their connection with a common downstream target (with ∼20 ms conduction delay). This provides a possible mechanism of structural changes that are thought to support memory formation and consolidation.

1.4 Cell assemblies within the brain

While experimental evidence for cell pair synchronization is abundant, work concerning cell assemblies (n≥3) is more rare. This is probably due to the technical difficulties of recording hundreds of single units simultaneously. Still, in the literature, cell assemblies have been reported in different brain region

including the hippocampus (Harris *et al.* 2003; O'Neill, Senior, *et al.* 2008), the prefrontal cortex (Fujisawa, Amarasingham, *et al.* 2008; Peyrache, Khamassi, *et al.* 2009; Benchenane *et al.* 2010), the visual cortex (Dong *et al.* 2008; Martin & von der Heydt 2015), the motor cortex (Riehle *et al.* 1997; Gulati, Won, *et al.* 2015; Ramanathan *et al.* 2015), the somatosensory cortex (Deolindo *et al.* 2018), as well as the olfactory cortex (Perez-Orive *et al.* 2002). However, the time scale of synchrony may vary greatly from one study to another (see Figure 1.5 and Table *2*). Also, these time scales may exceeded the membrane time constant of neurons from one to several orders of magnitude, especially in the prefrontal cortex. It is difficult to imagine the functional synchrony at such long time scales since they would not trigger spiking in downstream neurons (discussed in Chapter 5). Note that in the ventral striatum and the amygdala, none or very few studies have described cell assemblies.

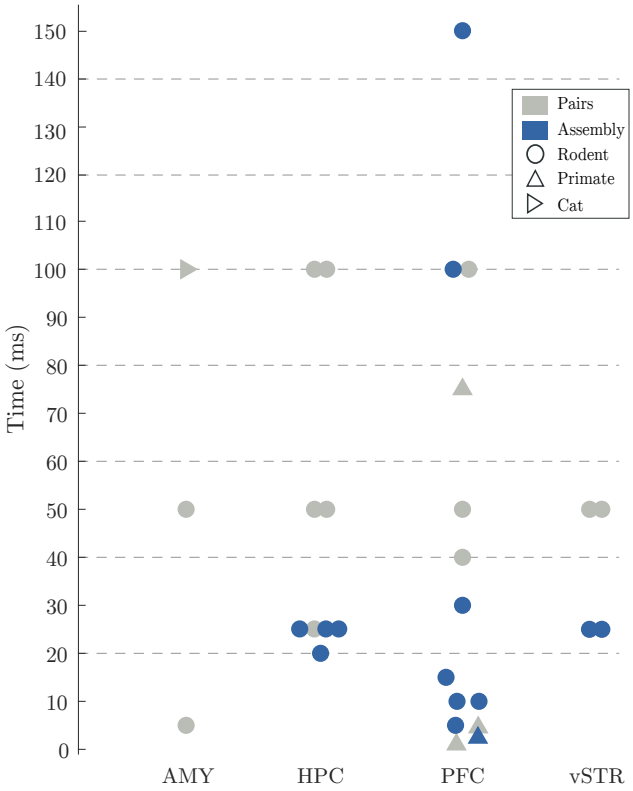

Figure 1.5: Time scales of assembly synchrony in the literature. Reported time scale of co-activations (pairs, n=2; assembly, n>2) within 4 brain regions: the amygdala (AMY), the hippocampus (HPC), the prefrontal cortex (PFC) and the ventral striatum (vSTR) in different species (rodent, primate and cat). Data are from Table *2*.

Also, the vast majority of synchronous activity reports concerns cell assemblies within a single structure. Yet, some cross-structural correlated pairs have been found within the cortex but rarely between cortical and sub-cortical structures (and nor at the level of the assembly). These considerations will be further developed in Chapters 4 and 5.

Inhibition in cell assemblies. Since Hebb's definition predicted synapses strengthening between assembly members upon synchronous activation, most studies focused on excitatory connections. However, cell assemblies, defined as a group of co-active cells (in a relevant time window), could benefit from inhibitory members:

- Interneurons may prevent interference by silencing local cells (Geisler *et al.* 2007).
- Inhibitory projection neurons, such as medium spiny neurons in the striatum, can disinhibit downstream targets through feed-forward mechanisms.
- The activity of interneurons may be informative of their inputs and this could shed light on many pre-synaptic principal cells that are not sampled in the recording. Hence, interneurons may be integrated into cell assemblies, although not directly leading to synaptic strengthening, not as 'real' members but as proxies for undetected principal cells (in addition to possibly being 'real' members too).

1.5 Synchronization of neural activity through brain rhythms

We have seen the relevant time scales of assembly formation and discussed their electrophysiological significance for brain processes. In this section I will describe candidate mechanisms that organize and synchronize neural activity: brain rhythms. More specifically, I will focus on gamma rhythms (∼30-90 Hz), that are oscillations with a half-cycle duration of ∼5-15 ms close to the presumed assembly time scale, in the assumption of downstream coincidence detectors.

1.5.1 Brain rhythms

Like many other complex, dynamical systems, neural networks oscillate (Izhikevich 2007). Single neurons are natural oscillators, and the constant flux of ions through their membranes contributes to intrinsic resonance and oscillation of their membrane potential and therefore of their spiking activity (Buzsáki & Wang 2012). Synchronization leads networks of densely interconnected neurons to oscillate, generating those that are commonly called brain rhythms. The first to report brain-produced oscillatory activity was Berger (1929) while he was searching for potential telepathic phenomena. He succeeded in recording the human electroencephalogram (EEG) and observed for

the first time large oscillatory electrical signals in the brain. The electric field that can be measured with EEG electrodes on the scalp, but also with intracranial electrodes closer to nerve cells in the extracellular medium ('LFP', Figure 1.6 and Method Box 1.3). LFP is mostly the resultant of the averaged sums of excitatory and inhibitory post-synaptic potentials at the synaptic level[11]. LFP oscillations are naturally segregated in different frequency bands that have been associated to specific brain and behavioral states.

Box 1.3. Recording electrical signals in the brain

The current fluxes in the dendritic tree of each cell generate an electrical potential and the electrical field recorded with an electrode in the vicinity of a group of neurons is called LFP; also known as intra-cranial EEG). LFP Therefore, the LFP is the average of the potentials generated by each cell acting as a dipole (an antenna). However, despite its name, the LFP also reflects the electrical field reaching the recording electrode after travelling from further away neural sources through the brain tissue. This phenomenon is called volume conduction and, as brain oscillations can travel relatively large distances in the nervous tissue (especially slow waves), it contribute significantly to the recorded LFP. Extracellular recordings, as used in the experimental work described in this manuscript, record a signal composed by the LFP and the action potentials of the neurons in the vicinity of the microelectrode [a]. See also Figure 1.6.

[a] Depending upon the impedance of the microelectrode, within a spheric volume with a radius of ∼60-100μm (Buzsáki & Draguhn 2004)

Brain oscillations can span five orders of magnitude in frequency from approximately 0.05 Hz to 500 Hz and play critical roles in network synchronization, as we will see in the following paragraphs. These will focus on gamma oscillations. Gamma frequencies may vary widely across species but typically the gamma band is 30-90 Hz for mammalian[12] and (10-30 Hz) for insects (Kay 2015). Gamma oscillations have been described in several areas such as: the neocortex (Gray & Singer 1989; Singer & Gray 1995, Sirota, Montgomery, *et al.* 2008; Popa, Spolidoro, *et al.* 2013), the enthorinal cortex (Chrobak & Buzsáki 1998), the amygdala (Halgren *et al.* 1977), the hippocampus(Buzsáki, Lai-Wo S., *et al.* 1983), the striatum (Berke *et al.* 2004; Tort, Kramer, *et al.* 2008), the olfactory bulb (Adrian 1942; Laurent & Davidowitz 1994) as well as others. Many reviews are available on this topic: Engel, Fries, *et al.* 2001, Laurent 2002; Fries 2005; Fries 2009; Wang 2010, Buzsáki & Wang 2012; Bosman, Lansink, *et al.* 2014).

[11] However, other sources like Na^+ and Ca^{2+} spikes, ionic fluxes through voltage- and ligand-gated channels, and intrinsic membrane oscillation also participate

[12] Note that an important issue and possible caveat when detecting gamma oscillations is to distinguish true gamma oscillation from an increase in gamma power caused by greater spike activity (Ray & Maunsell 2011) and spike waveform spectral leakage (Schomburg *et al.* 2014).

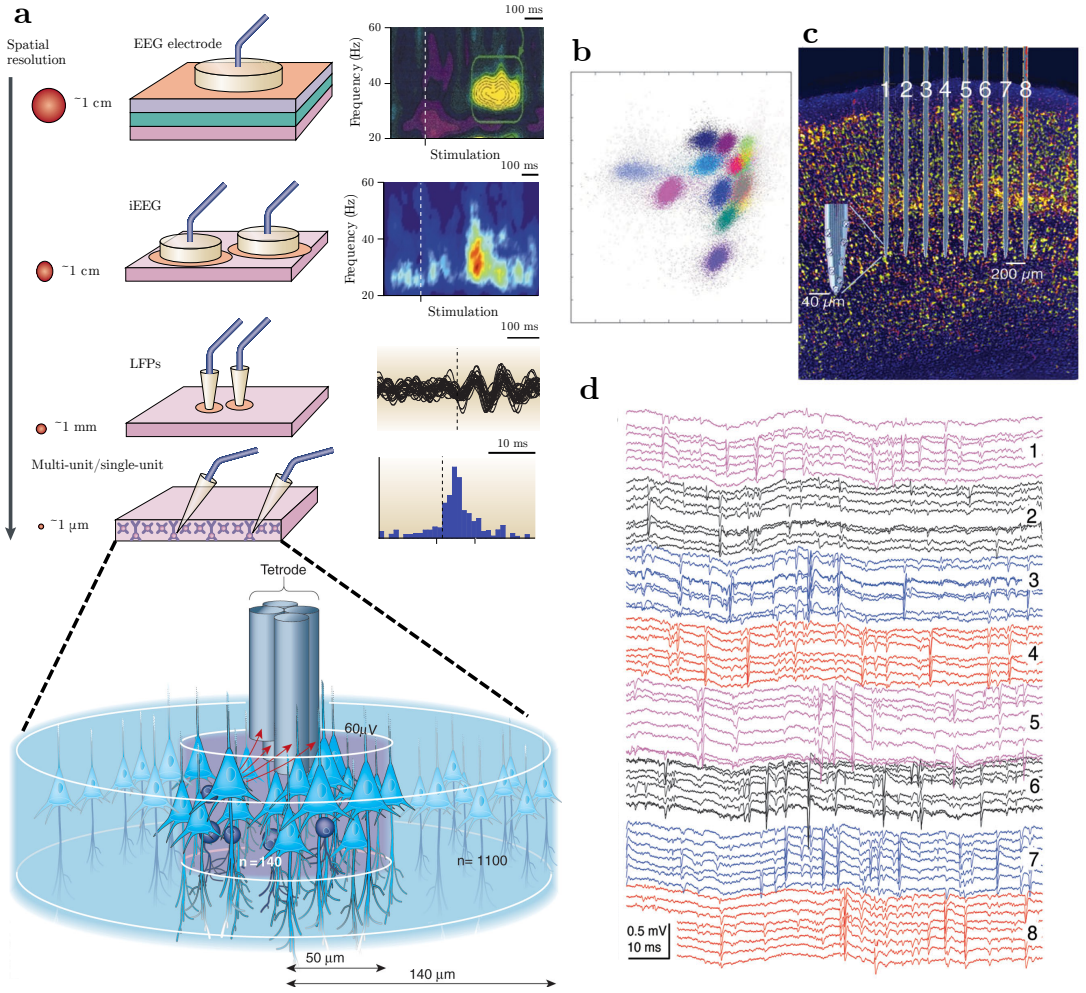

Figure 1.6: Recording brain rhythms and neurons. **a** Different spatial scales of recording of neural activity. From top to bottom: scalp electrodes and intracranial electrodes on the brain surface record EEG signals (see Box 1.3). Intracerebral electrodes record LFP signals, which are a spatially more precise version of the EEG and the spiking activity of neurons nearby the electrode. Single electrodes cannot always distinguish the spikes coming a nearby cell or another and record a signal called Multi Unit Activity (MUA). Electrodes with multiple recording sites (like the tetrode depicted in the zoom) record the same signal in parallel on different recording sites but from slightly different distances. This affects the amplitude and the waveform characteristics of the signal recorded by each channel, which form clusters corresponding to the recorded cells (**b**). (**c**) Array of another type of multi-electrode, the silicon probe. Each of these eight shanks has eight recording sites which recorded the signal depicted in **d** (channels from the same probe have the same color). Note how channels from the same shank record the same spikes but with different amplitudes and shapes (adapted from Varela *et al.* 2001 and Buzsáki & Draguhn 2004). See also *Box 1.3*.

I will expand on three parallel line of research: the work of Singer & Gray and coll., on the visual system and binding mechanisms, the work of Laurent and coll., on the olfactory system and finally the work Buzsáki and coll., on the temporal organization within the hippocampus by oscillations.

1.5.2 Generation of gamma oscillations

How are gamma oscillations generated? Two major models have been proposed (for reviews, see Whittington *et al.* 2000, Tiesinga & Sejnowski 2009). One model involves only reciprocally connected inhibitory neurons (I-I models) whereas the other is based on reciprocally connected pools of excitatory and inhibitory neurons (E-I models; see Figure 1.7a). In I-I models, gamma oscillations are generated by two pools of inhibitory neurons which reciprocally inhibit them cells and in turn whill synchronize the E cells. In E-I models, it is the alternation of excitation and feedback inhibition that generates gamma oscillation. Both models could co-exist whithin a single area. Thus a key component of gamma generation is inhibition, mediated by local fast-spiking interneurons. In the hippocampus, this role is thought to be carried by parvalbumin-containing basket cells, as evidence from electrophysiological recordings demonstrated a strong modulation (Buzsáki, Lai-Wo S., *et al.* 1983, Csicsvari *et al.* 2003).

1.5.3 Gamma oscillations in the visual system as a feature binding mechanism

Pioneering studies investigated the response of neurons in the primary visual cortex of cats to different stimulus (Gray & Singer 1989, Engel, Kreiter, *et al.* 1991, Singer & Gray 1995). These neurons have receptive fields, i.e. they respond to specific orientations of a visual stimulus (see Figure 1.1a) and are organized in columns. Neurons within a column exhibit similar receptive fields (Hubel & Wiesel 1962). In 1989, Gray & Singer demonstrated that neurons in different columns, engaged in synchronous oscillatory activity (in the range of 40 Hz) when presented to simultaneously moving stimulus, across their respective field. However, when the stimuli were in different directions, the synchronization was absent. These results suggested that the cerebral cortex might exploit synchronous oscillatory activity in order to bind these for further processing. This provided first experimental evidence to support the 'binding by synchrony theory' (Singer & Gray 1995, Roskies 1999). This theory postulates that the different features of an object (e.g. smell, color, texture, etc.) are treated by subsets of neurons in different part of the cortex and are associated together in a whole to reconstruct the object, through synchronizing oscillations (as I mentioned in 1.1). In further studies, gamma synchronizations has been observed in more ecologically relevant conditions, in monkeys freely viewing natural images (Brunet *et al.* 2013).

Box 1.4. Coherence between two oscillations

The coherence measures the consistency of the phase relation between two oscillations. Coherence ranges from 0 and 1 and corresponds to the spectral analog of the cross-correlation function in the time domain. Its squared value represents the amount of variance in one oscillation explained by the other and vice-versa. The coherence is high when the two signals maintain a constant phase relation (but not necessarily at a 0 lag). Note that the coherence also measures correlations in amplitude. Unfortunately, it is not possible to disentangle the contributions from amplitude and phase. To overcome this caveat, other measures have been defined, such as the phase locking value (Lachaux *et al.* 1999).

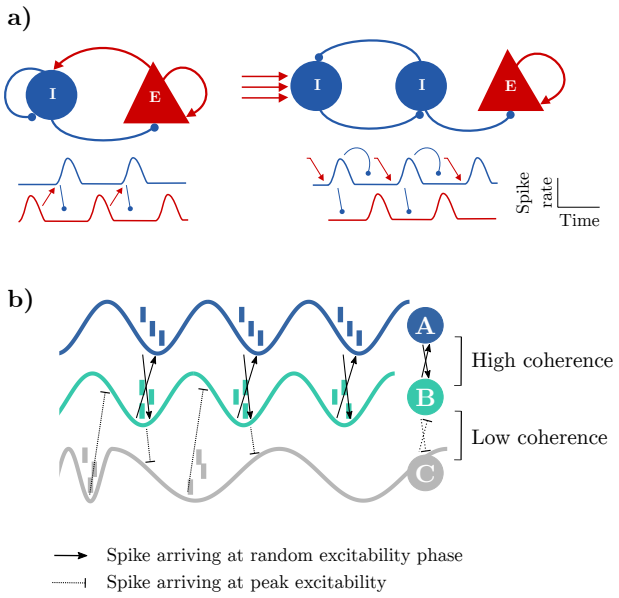

Figure 1.7: Generation of gamma oscillations and the Communication Through Coherence hypothesis. **a)** Two-models of generation of gamma oscillations. Left: Reciprocal connections between excitatory pyramidal neurons E and inhibitory interneurons I produce an alternation of excitation and inhibition. Right: Reciprocal connections between two pools of interneurons generate an oscillatory exert rhythmic inhibition on the adjacent population of pyramidal neurons E. Note that these two kind of mechanisms may co-exist within the same brain area. Adapted from Bosman, Lansink, *et al.* 2014. **b)** Schematic representation of three inter-connected brain regions (A,B and C), each rhythmically active. Traces are local network states and vertical ticks are spikes. A and B oscillate with "good phase relation", meaning that the neurons of each region fire during excitable states of the other region. In contrast, the phase relation between B and C is not suitable for communication. Indeed the neural populations have an incoherent phase relationship and the action potentials coming, for instance, from C arrive in B when neurons are inhibited there with low probability to fire. Panel adapted from Womelsdorf *et al.* 2007.

Gamma synchronization is not limited to cortical columns only. Several studies suggested a role of gamma oscillations in long-range synchronization of different brain areas (Engel, Kreiter, *et al.* 1991, Roelfsema *et al.* 1997, Rodriguez *et al.* 1999, Buschman & Miller 2007, Gregoriou *et al.* 2009). Such synchronization would be mediated by long-range inhibitory neurons (Buzsáki & Draguhn 2004). In 2005, Fries formulated the Communication Through Coherence (CTC) hypothesis to explain how gamma-band (or any band in general) synchronization may affect neuronal processing (for a review and an updated version, see Fries 2015). The CTC hypothesis suggests that effective communication between two oscillating neuronal populations depends, at least in part, on their phase relation. If upstream and downstream oscillations become coherent such that the EPSPs of the upstream region arrive at the downstream one during its phase of maximum excitability (trough of the oscillation), communication between the two brain region is facilitated (Figure 1.7b, see also Box 1.4). Even though the CTC is a general hypothesis applicable for any oscillation frequency bands, evidences have been provided mostly within the gamma band in the visual system (Womelsdorf *et al.* 2007, Bosman, Schoffelen, *et al.* 2012, Grothe *et al.* 2012, but see Benchenane *et al.* 2010, who reported prefrontal cell assemblies when the hippocampus and the prefrontal cortex exhibited high coherence).

1.5.4 Gamma oscillations and coincidental detection in the olfactory system

In the antennal lobe (AL) of insects, gamma oscillations (20-35 Hz) are thought to organize neuronal responses to odors in projection neurons (Laurent 2002). An elegant study from the Gilles Laurent's lab showed that these neurons activate synchronously within gamma cycles and project onto Kenyon cells of the mushroom bodies. Kenyon cells then act as coincidence detectors, that is, they spikes when the input (i.e. the projection neuron assembly), is synchronized (Perez-Orive *et al.* 2002). In turn, Kenyon cell exhibit oscillatory activity and their downstream target (β-lobe neurons) act as coincidence detectors as well Cassenaer & Laurent 2007. Interestingly,Cassenaer & Laurent reported spike-timing dependent plasticity between the Kenyon cells and the β-lobe neurons, on a $\pm$ 25 ms timescale that is the half-cycle of the gamma oscillation. Thus, if Kenyon cells discharge on average at a phase of $\pi/2$ (which corresponds to the delay conduction between the two neuronal populations), the population of β-lobe neurons will fire on average at the trough of the oscillation. However, if a single β-lobe cell fires in advance (because it received to much excitation), this cell will be depreciated Thus, the cell will receive less excitation in the next cycle and will fire later in phase, toward the trough of the oscillation. This work provided new insights on the interplay between rhythmic oscillations and plasticity mechanisms to shape cell assemblies.

The disruption of such oscillations in the honey bee AL (with picrotoxin disabling GABA receptors) resulted in a performance impairment in an odor discrimination paradigm coupled with conditioning. Bees failed to discrim-

inate between similar odors. Thus, gamma oscillations and cell assemblies could play a role in encoding features and reduce the overlap between neural representation (Stopfer *et al.* 1997). In mice, deleting GABA receptors in the olfactory bulb also disrupted gamma oscillation and these mice failed to generalize among similar odors (Nusser *et al.* 2001).

1.5.5 Temporal organization by oscillations within the hippocampus

Seminal work in the Buzsaki lab, led by K.D Harris, reported temporally organized activity of CA1 hippocampal neurons at the trough of theta oscillations ($\sim$ 8 Hz; Figure 1.8). The authors investigated the hypothesis that firing of CA1 hippocampal neurons in rats is organized in time into cell assemblies. Pyramidal cells in the hippocampus have place correlates ('place cells'; O'Keefe & Dostrovsky 1971), where they selectively fire when a rat is located in a specific location of the environment. Hence, the instantaneous firing probability of a place cell can be predicted from the spatial position of the rat. Harris *et al.* hypothesized that within an assembly, cells should show synchronous activation beyond that predicted by their common modulation by sensory input (which, here, concerns spatial position). Using a Generalized Linear Model (see 2.2.2 for methodological details), the authors demonstrated that the prediction of place cell spiking was greater when considering the activity of its peers, in addition to the location of the animal, compared to a model taking only into account the location of the animal. Interestingly, the prediction was optimal in 10-30 ms window, that is, the duration of slow (30-50 Hz) and medium (50-90 Hz) gamma cycles (see Box 1.5. for further details on gamma bands in the hippocampus) .

However, taking into account the velocity of the animal and theta modulation, during spatial navigation, a recent study showed that the coordinated activity observed in the hippocampus can be explained by the independent coding of each cell (Chadwick *et al.* 2015). Hence, this contradicts Harris *et al.* conclusion, and the hypothesis that synaptically coupled assemblies are formed with members predicting each other's activity beyond sensory inputs. Yet, assuming that cell assemblies are meaningful from the perspective of downstream reader, Harris *et al.*'s findings are still of importance, since they highlight the fine time scale synchronization of hippocampal place cells within the duration of a gamma cycle, at the trough of theta (even if this can be explained by independent coding).

To conclude, gamma oscillations are ubiquitous and have been reported in many brain areas. Evidence suggests that gamma oscillations organize local activity of cell assemblies, but can also mediate long-range synchronization, as theorized by the CTC hypothesis.

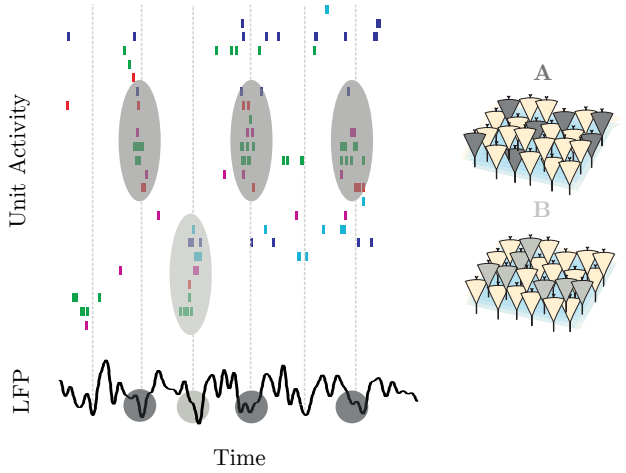

Figure 1.8: Temporal organization of neural activity in the hippocampus. Top: Raster plot of rat hippocampal pyramidal cells recorded during spatial exploration in an open field, ordered to highlight their temporal organization into two cell assemblies (A and B; right schematics). Synchronous activations of cell assemblies are shaded in gray. Bottom: the Local Field Potential (LFP) recorded in the hippocampal CA1 area displays theta oscillation. Vertical lines indicate troughs of theta waves. Assemblies are thought to be organized in a time scale similar to the one of gamma oscillations (10-30ms). Also, note that cell assemblies occur at a precise phase of theta rhythm. Based on Harris *et al.* 2003.

Box 1.5. Gamma oscillations in the hippocampus

Gamma band definition may vary greatly in the literature, which might complicate cross-referencing. Yet, for a few years now, a consensus seems to have been established. The three gamma bands band were distinguished by studying how they were modulated by a slower oscillation, theta ("cross-frequency coupling", see also section 1.6 for a functional role of theta-gamma coupling): slow gamma (30-50 Hz), medium gamma (50-90 Hz) and fast gamma (90-140 Hz). Similar results have been obtained with source separation by Independent Component Analysis (ICA, Schomburg *et al.* 2014). Note that fast gamma is also referred to as epsilon (Freeman 2007), since the mechanisms to generate the epsilon and gamma oscillations (slow and medium) differ (Belluscio *et al.* 2012). Indeed, entorhinal and CA3 input networks transmit slow and medium gamma whereas fast gamma oscillations are generated by local CA1 pyramidal cells and interneurons (Bragin *et al.* 1995, Colgin *et al.* 2009, Lasztóczi & Klausberger 2016).

1.6 Longer time scale mechanisms to build neural words

Cell assemblies are presumed to be the functional units of the brain, the building bricks of neural computation. Sequences of cell assemblies ('neural words', Buzsáki) have been hypothesized to underlie complex cognitive processes (Hebb 1949; Harris 2005; Buzsáki 2010). Such sequences may require mechanisms operating at a longer time scale (Figure 1.2 b, reader s). In this section, I will explain how nested oscillations could give rise to sequences of assemblies and review experimental evidence of their existence.

1.6.1 Nested oscillations

Nested oscillations (or 'cross-frequency coupling') occur when a faster rhythm is coupled to the phase of a slower rhythm[13]. Theoretical work by Lisman & Idiart (1995) proposed that sequences of assemblies could emerge from the successive gamma ('fast-oscillation') cycles nested within a single theta ('slow-oscillation') cycle (see Figure 1.9a). The authors suggested a functional role of such sequences in simultaneously maintaining several items in the working memory (7±2, consistent with the 'magic number' of Miller 1956[14]). Many studies have reported cross-frequency phase-amplitude coupling between gamma with theta (Buzsáki, Lai-Wo S., *et al.* 1983, Bragin *et al.* 1995,Canolty *et al.* 2006, Sirota, Montgomery, *et al.* 2008, Colgin *et al.* 2009) but also slower oscillations such as delta (Lakatos *et al.* 2005), alpha (Von Stein & Sarnthein 2000,Palva *et al.* 2005,Cohen *et al.* 2009), spindle (Peyrache, Battaglia, *et al.* 2011).

Experimental evidence supporting a role of oscillations in parsing neural words were provided by a recent study. Using an unsupervised approach driven by Independent Component Analysis (ICA, see 2.3 for methodological details), Lopes-dos-Santos, van de Ven, *et al.* 2018 detected nested oscillations within theta cycles. The authors identified spectral components ('tSCs', see Figure 1.9b) corresponding to the frequencies of beta, slow, medium and fast gamma oscillations. Using Generalized Linear Models (GLMs)[15], the strength of each spectral component was successfully predicted from the spiking activity of CA1 hippocampal principal cells within theta cycles. Interestingly spectral components were associated with different principal cells (Figure 1.9c,d). Even though authors did not investigate the precise temporal organization of cell spiking within nested oscillations, these results suggests that distinguishable neuronal ensembles correlate with nested oscillations in theta cycles (whether these ensembles are cell assemblies or neural words).

[13] Slow oscillations can modulate fast ones in two ways: the amplitude of the fast oscillation is phase-locked to the slow oscillation (phase-amplitude coupling) or the phases of the fast and the slow oscillations exhibit a constant relationship (phase-phase coupling; for more detail on methodological caveats see Aru *et al.* 2015).

[14] In one of the best-known articles in psychology, Miller suggested that human adult could store 5 to 9 items in their working memory, hence the 'magic number' 7±2

[15] See section 2.2.2 for methodological explanation on GLMs

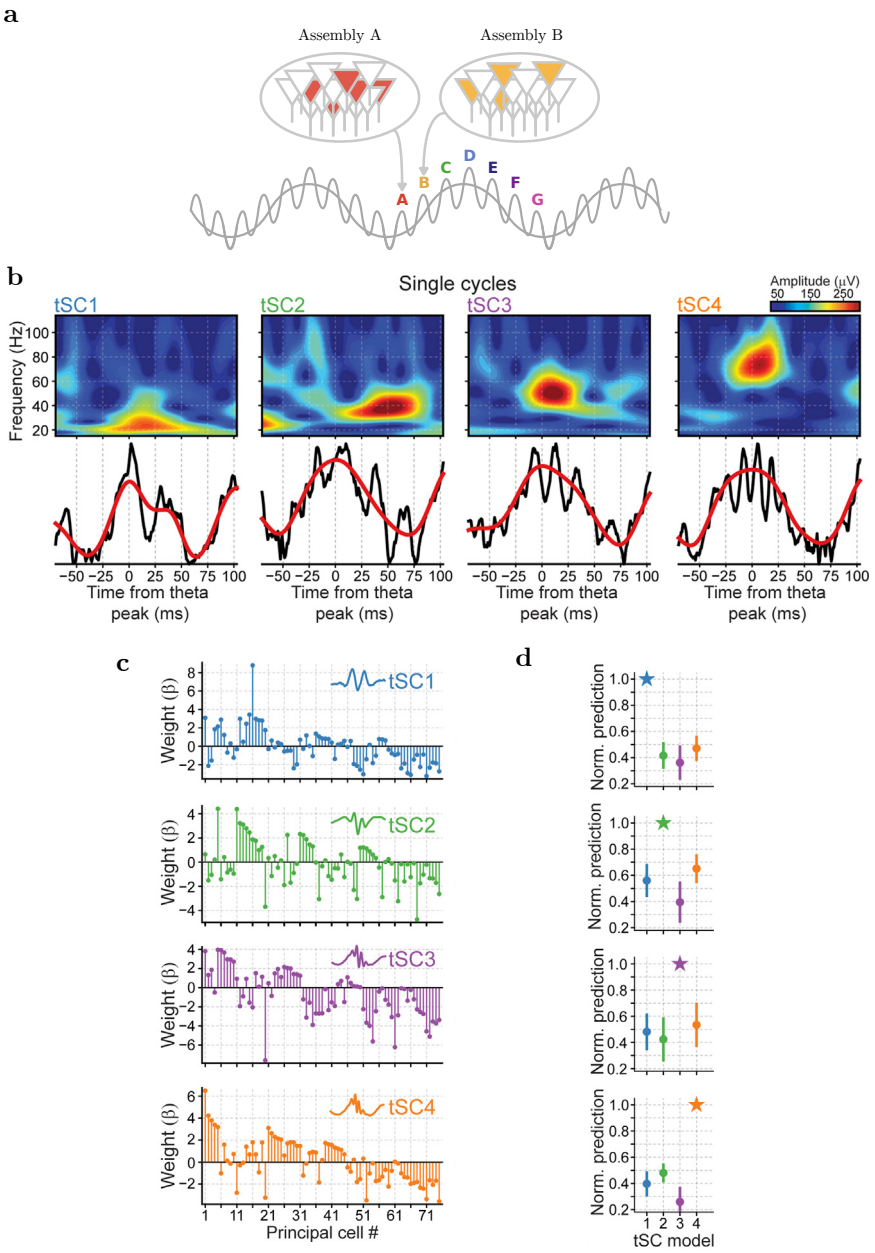

Figure 1.9: Nested oscillations within theta cycles. **a)** Gamma oscillations are nested in theta cycle. Different assemblies (represented by letters) are active in different gamma cycles. Neural words are formed by the sequences of cell assemblies activations. The number of gamma cycles per theta cycle (4 to 8) is thought to determine the span of working memory. Adapted from Lisman & Idiart 1995.

Figure 1.9: **b)** Raw LFP spectrogram (top) along with the raw LFP and theta signal of single-cycle examples drawn. tSC1 band corresponds to beta frequencies, tSC2 to slow gamma, tSC3 to medium gamma and tSC4 to fast gamma. **c)** Example weight vectors containing the contribution of each principal cell fitted to predict the strength of a given tSC (with a GLM). The distribution of weights differ for each tSC. **d)** Right: predictions (mean *pm* 95% confidence interval) obtained from the GLMs fitted for the different tSCs. Note that GLM predictions were normalized by their original value (i.e., GLMs predicting same tSC for which they were fitted), to make performance loss across tSC models explicit. Pannels b-c are adapted from Lopes-dos-Santos, van de Ven, *et al.* 2018.

1.6.2 Example of neural words

Experimental evidences of neural words have been found in the antenna lobe of insects. Wehr & Laurent 1996 reported that different subsets of projection neurons were active within consecutive gamma cycles after odor presentation (Wehr & Laurent 1996). Interestingly, successive presentation of the same odor elicited similar sequences whereas distinct odors generate unique neuronal sequences of projection neurons (Mazor & Laurent 2005,Broome *et al.* 2006). Another example of externally generated neural words are the stereotyped sequencess of assemblies produced by the high vocal centre during bird song. These sequences drive similar stereotyped patterned in downstream structures, and in turn to motor neuron of the vocal organ (Hahnloser *et al.* 2002). These two examples promote the idea that external stimuli can elicit sequences of cell assemblies, yet, experimental evidence from the Buzsaki lab suggests that internal processes also generate sequences. In an elegant study, Pastalkova *et al.* 2008, reported hippocampal sequences of activation during maze navigation but also during a delay memory task, when rats were running i wheel (i.e. while the sensory cues did not change, Figure 1.10). Interestingly, the internally generated sequences in the wheel could actually predict upcoming arm choice (rewarded as well as errors). The authors hypothesized that the hippocampus can generate sequences of assemblies in two ways: under the influence of sensory/external cues or by self-organized mechanisms (see also Chapter 3 about reactivation and replay processes during a state with very weak sensory inputs: sleep). Neural sequences have been observed in other structures as well, including the prefrontal cortex (Fujisawa, Amarasingham, *et al.* 2008), the parietal cortex (Harvey *et al.* 2012), or the striatum (Akhlaghpour *et al.* 2016).

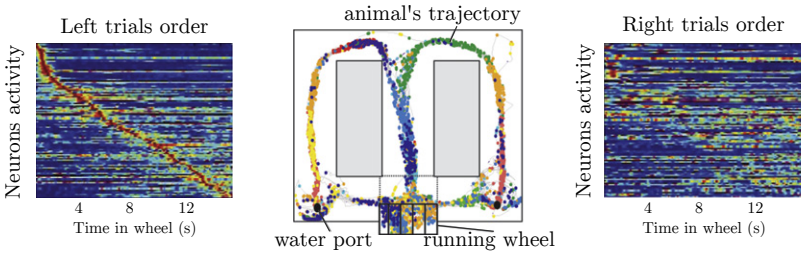

Figure 1.10: Internally generated sequences during a working memory task. Center: rats were trained to run in a wheel facing to the left during the delay between runs in the maze (left or right trajectory). Dots are color-coded spikes from simultaneously recorded neurons in hippocampal CA1. Color maps represent normalized firing rate profiles of neurons during wheel running (left) and right trials (right). Profiles are ordered by the latency of their peak during left trials. The stereotyped sequences observed during the left trajectory are similar to the ones internally generated during wheel running. Note that the left sequences differ from the right ones. Adapted from Pastalkova *et al.* 2008 and Buzsáki 2010.

Conclusion

In attempt to 'crack the neural code', many of the pioneer works studied single cell response to visual stimuli since at the time, recording simultaneously more few cells was a tremendous achievement (Barlow 1953,Hubel & Wiesel 1962). These studies and subsequent research established that some neurons in the cortex were tuned to particular visual stimuli, even to faces in higher order areas. In the past decades, recording simultaneously large numbers of neurons in multiple brain regions was no longer beyond the bounds of possibility. It became clear that one stimuli could evoke similar responses in several neurons, thus multiple cells could work together to code an object for example. This led to the resurgence of the 'cell assembly' idea, proposed by Hebb in 1949. Groups of interconnected neurons would work together to combine features of a stimuli and represent it. Chaining of such assemblies ('phase sequences') can give rise to complex cognitive function such as thinking, planning or dreaming. However, Buzsáki proposed a refinement: brains organize themselves and can generate internal stereotyped spiking patterns rather. He proposed that cell assemblies are groups of cells, not necessarily anatomically wired, that can synchronize within a given window to generate an organized and coherent input to downstream neurons or to other assemblies. Thus an assembly can be viewed as synchronous inputs to coincidence detector neurons within a time window the width of an EPSP or of the membrane time constant. These time scales may vary between cell types or brain areas but typically range from 10 to 30 ms. This window is of particular significance, since it corresponds to the time scale of plasticity phenomena but also to the period of a gamma oscillation. Similar to Hebb's phase sequences, Buzsaki suggested that longer-timescale mechanisms (such as nested oscillations) group several assemblies into sequences ('neural words'), thus providing a neural syntax as the basis

of elaborated cognitive processes. These two definitions of cell assemblies (Hebb 1949 and Buzsáki 2010) are not completely antagonistic and both are referred to in the literature [16]. Here, cell assemblies are intended a group of co-active cell in a meaningful time window. The next chapter is dedicated to the numerous existing methods to identify such cell assemblies,

[16] Even though these two major works are cited, definition of cell assemblies are rarely explicit in papers.

Reference	Brain area	Timescale (ms)	Method	Species	Pattern
(Pre)frontal Cortex					
Vaadia *et al.* 1995	FC	5	JPTH	Monkey	Pairs
Sakurai & Takahashi 2006	PFC	1	Cross-correlogram	Monkey	Pairs
Baeg *et al.* 2007	PFC	50	Cross-correlation	Rat	Pairs
Euston *et al.* 2007	mPFC	40	EV-REV	Rat	Pairs
Fujisawa, Amarasingham, *et al.* 2008	mPFC	5	Cross-correlogram	Rat	Assembly
Sigala *et al.* 2008	FC	200	Pearson correlation	Monkey	Pairs
Tsujimoto 2008	PFC	75	JPTH	Monkey	Pairs
Burgos-Robles, Vidal-Gonzalez, *et al.* 2009	mPFC	100	Cross-correlogram	Rat	Pairs
Peyrache, Khamassi, *et al.* 2009	mPFC	100	PCA	Rat	Assembly
Benchenane *et al.* 2010	mPFC	30	PCA	Rat	Assembly
Pipa & Munk 2011	vPFC	3	Comparing coincidental detection to jitters	Monkey	assembly
Dejean *et al.* 2016	dmPFC	150	PCA	Rat	Assembly
Tavoni *et al.* 2017	mPFC	10	Ising model	Rat	Assembly
Deolindo *et al.* 2018	PFC	10	ICA	Rat	Assembly
Todorova & Zugaro 2019	mPFC	15	ICA	Rat	Assembly
Hippocampus					
Wilson & McNaughton 1994	HPC	100	Cross-correlogram	Rat	Pairs
Kudrimoti *et al.* 1999	HPC	100	EV-REV	Rat	Pairs
Harris *et al.* 2003	HPC	20	GLM	Rat	Assembly.
O'Neill, Senior, *et al.* 2008	HPC	50	Cross-correlogram	Rat	Pairs
Kelemen & Fenton 2010	HPC	25	Cross-correlogram	Rat	Pairs
Malvache *et al.* 2016*	HPC	200	Comparing coincidental detection to shuffle	Mouse	Assembly
van de Ven *et al.* 2016	HPC	25	ICA	Mouse	Assembly
Girardeau, Inema, *et al.* 2017	HPC	50	EV-REV	Rat	Pairs
Sjulson *et al.* 2018	HPC	25	PCA	Rat	Assembly.
Giri *et al.* 2019	HPC	250	EV-REV, ICA	Rat	Assembly
Trouche, Koren, *et al.* 2019	HPC	25	ICA	Mouse	Assembly.
Nucleus Accumbens					
Pennartz, Lee, *et al.* 2004	vSTR	50	EV-REV	Rat	Pairs
Carrillo-Reid *et al.* 2008*	STR	250	Pearson correlation + Monte-carlo	Rat	assembly
Lansink, Goltstein, Lankelma, Joosten, *et al.* 2008	vSTR	50	EV-REV	Rat	Pairs
Sjulson *et al.* 2018	vSTR	25	PCA	Rat	Assembly.
Trouche, Koren, *et al.* 2019	vSTR	25	ICA	Mouse	Assembly.
Auditory cortex					
Decharms & Merzenich 1996	A1	25	Cross-correlogram	Monkey	Pairs
Bathellier *et al.* 2012*	Auditory cortex	250	Pearson correlation	Mouse	assembly.
See *et al.* 2018	Auditory cortex	10	ICA	Rat	assembly
Motor cortex					
Riehle *et al.* 1997	M1	5	Comparing coincidental detection to jitters	Monkey	assembly
Laubach, Wessberg, *et al.* 2000	M1	1	ICA	Rat	Assembly
Hoffman & Mcnaughton 2002	Motor cortex	50	EV	Monkey	Pairs
Gulati, Tsodikov, *et al.* 2014	M1	50	PCA	Rat	Assembly
Gulati, Won, *et al.* 2015	M1	50	PCA	Rat	Assembly
Ramanathan *et al.* 2015	M1	25	PCA	Rat	Assembly
Eckert *et al.* 2020	M1	50	PCA	Rat	Assembly
Somatosensory cortex					
Hoffman & Mcnaughton 2002	Somatosensory cortex	50	EV	Monkey	Pairs
Deolindo *et al.* 2018	S1	10	ICA	Rat	Assembly
Amygdala					
Quirk, Repa, *et al.* 1995	BLA	5	Cross-correlogram	Rat	Pairs
Paré & Collins 2000	LA	100	Cross-correlogram	Cat	Pairs
Girardeau, Inema, *et al.* 2017	BLA	50	EV-REV	Rat	Pairs
Zaki *et al.* 2019*	BLA	30000	ICA	Mouse	Assembly
Associative cortices (other than prefrontal cortex)					
Hoffman & Mcnaughton 2002	Parietal cortex	50	EV	Monkey	Pairs
Deolindo *et al.* 2018	Parietal cortex	10	ICA	Rat	Assembly
Chang, Esteves, *et al.* 2020	Retrosplenial cortex	250	Pearson correlation	Mouse	Assembly
Visual cortex					
Martin & von der Heydt 2015	V1,V2	5	Cross-correlation	Monkey	Pairs
Dong *et al.* 2008	V1,V2, V1-V2	20	Cross-correlation	Monkey	pairs
Deolindo *et al.* 2018	V1	10	ICA	Rat	Assembly
Others					
Tingley, Alexander, *et al.* 2015	Basal forebrain	50	GLM	Rat	Assembly.
Valdés *et al.* 2015	VTA	100	EV-REV	Rat	Pairs

Table *1*: Synchrony time scale in the literature (1/2).

Reference	Brain area	Timescale (ms)	Method	Species	Pattern
Cross-structural					
Nicolelis *et al.* 1995	Trigeminal sensory system	10	PCA	Rat	Assembly
Qin *et al.* 1997	HPC-parietal	100	Pearson correlation	Rat	Pairs
Hoffman & Mcnaughton 2002	Parietal-motor cortex	50	EV	Monkey	Pairs
Hoffman & Mcnaughton 2002	Somatosensory-motor cortex	50	EV	Monkey	Pairs
Hoffman & Mcnaughton 2002	Parietal-somatosensory cortex	50	EV	Monkey	Pairs
Lansink, Goltstein, Lankelma, McNaughton, *et al.* 2009	HPC-vSTR	50	EV-REV	Rat	Pairs
Girardeau, Inema, *et al.* 2017	BLA-HPC	50	EV-REV	Rat	Pairs
Tang, Shin, *et al.* 2017	HPC-PFC	100	ICA	Rat	Assembly

Table 2: Synchrony time scale in the literature (2/2). This table summarizes the time scale of synchrony reported in many brain areas in the literature. The fourth column described the methods used to detect co-activated cell pairs or cell assemblies. These methods are further detailed in Chapters 2 and 3. *****: authors used calcium imaging, hence time scales are bigger. **Brain area abbreviation**: frontal cortex (FC), prefrontal cortex (PFC), medial prefrontal cortex (mPFC), hippocampus (HPC), striatum (STR), ventral striatum (vSTR), primary auditory cortex (A1), primary motor cortex (M1), primary somatosensory cortex (S1), basolatral amygdala (BLA), lateral amygdala (LA), primary visual cortex (V1), secondary visual cortex (V2), ventral tegmental area (VTA). **Methods abbreviation**: joint-peri-event-histogram (JPTH), explained variance (EV), reverse explained variance (REV), principal component analysis (PCA), independent component analysis (ICA), General linearized model (GLM).

2 Methods to detect cell assemblies

Recent progress in large-scale recordings have permitted increases in the numbers of simultaneously recorded neurons, providing opportunities to identify cell assemblies (Buzsáki & Draguhn 2004). Along with experimental advances, numerous sophisticated computational methods have been developed, to track down cell assemblies. Here I will review the most prominent statistical tools in the literature as they evolved through the years: from elementary cross-correlations to model-based techniques. This section focuses mainly on methods based on pairwise correlations, even though more recent techniques relies on higher order correlation approaches which are more suited for identifying sequential rather than synchronous activity.

2.1 Descriptive statistics of correlation

An elementary tool to study the correlation between spiking in two neurons i and j is their cross-correlogram. To build this, for each spike emitted by neuron i, the time latencies of spikes emitted by neuron j are determined and counted. Cross-correlograms (CCG) are useful for estimating the time-lag between the activity of two spiking cells. Moreover, the latencies of peaks in cross-correlograms can be used to infer the number of synapses between each neuron, assuming knowledge about spike conduction speeds and their variability. Sharp short latency peaks usually indicates mono-synaptic connection whereas broader, longer latency peaks suggest multiple relays (Barthó *et al.* 2004; see Figure 2.1,a-b).

However cross-correlation histograms do not allow to distinguish correlations due to a direct synaptic connection from independent coincidental correlations with a third neuron, or driven by a common input with a conduction delay. Indeed, interpretation of cross correlations often assumes stationarity of neuronal activity. But in the brain many non-stationarities are present (e.g. current behavioral motivation, satiety states, oscillations of excitation/inhibition). For

example, neurons responding to the same stimulus, or firing at the same phase of an oscillation will have inflated CCGs. To correct for non-stationnarities , one may use the joint-peristimulus time histogram (JPSTH; Figure 2.1c-d).

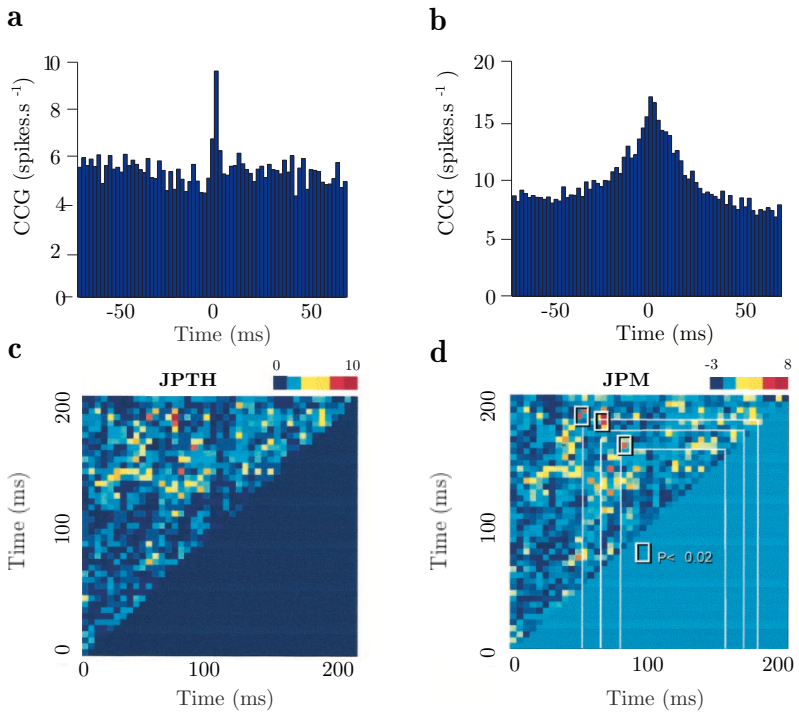

Figure 2.1: Elementary tools for correlation analysis: CCG and JPSTH. **a,b)** Cross-correlograms (CCGs) of simultaneously recorded neurons in neocortex. a) CCG shows a sharp peak (duration = 2 ms), which reflects putative mono-synaptic connections between cells. b) CCG shows a broader peak (duration = 20 ms), which probably results from more complex network processes. Adapted from Harris 2005. **c)** Observed JPSTH of a spike triplet. **d)** Corrected JPSTH of a spike triplet expressed as the difference between the observed JPSTH and the shift predictor (obtained from shuffled data). Boxes frame significant coincidences (50-182 ms, 64-173 ms, 72-154ms; Fisher's exact probability test; p<0.02). Modified from Nádasdy *et al.* 1999

JPSTH are useful to isolate correlation caused by a stimulus or an event from true network organisation. They are an extension of single neuron peri-event time histogram (PETH), that is, a neuron's discharge probability across time relative to event onsets. Each repetition of an event defines a trial. The (k,l) element of the JPSTH matrix represents the number of trial the neuron i fired in the k^{th} time bin and neuron j fired in the l^{th}. To eliminate cross-correlation induced by stimulus, a shift predictor is computed similarly to the JPSTH matrix after shuffling or shifting trial/event orders. Subtracting bin by bin the shift predictor from the JPSTH, one obtains a corrected JPSTH.

Determining JPSTH significance can be difficult. Usually control matrices are generated with the same procedure but on trial-shuffled data. Significant values are expected to exceed 95th percent of the shuffled control population. Reference events are not necessarily stimulus onset, Nádasdy *et al.* 1999 computed JPSTH between two cells while using spikes of a third cell as reference time/event (Figure 2.1,c-d). Thus, JPSTH can be a way to track down temporal relationships of neuronal triplets. However JPSTH techniques suffers from the same caveats as cross-correlation histograms (possible effects of other non-stationnarities than the one corrected for, correlation induced by a third/fourth neuron, etc.).
Searching for evidence of synaptic connections or correlation between pairs of neurons (or triplets) was popular in earlier multi-electrode recordings. With increasing numbers of simultaneously recorded neurons, the focus shifted to detecting synchronous patterns at a larger scale.

2.2 Model-based methods

2.2.1 Maximum Entropy Models

Maximum entropy models (MEMs) were introduced to evaluate the occurrence probability of each possible spike pattern (doublets, triplets, etc.) given the observed firing rates, pairwise correlations, and possibly higher-order moments of a population of recorded neurons. This kind of model describes the correlation structure of the network activity without assumptions about its mechanistic origin.
Briefly, spike trains are considered as a binary sequence of on/off states. In a brief time window, the state of a given neuron i, σ_i, is either 1 or 0 (Figure 2.2a-b). Thus the network has $\Omega = 2^N$ possible states, N being the number of recorded cells. A maximum entropy model with no constraint would assume that each of these states has an equal probability to be visited, i.e each neuron has an equal probability to be silent or active at a given time, which is far from reality. The network is supposed to be organized (with excitatory and inhibitory connections) and does not wander among all these possible states. One way to characterize the network organization is to build the distribution of visited states $P(\sigma_i)$. This distribution is fully described by all multivariate moments N (i.e. the vector of average firing rates, the matrix of second order correlation coefficients, the tensor of third order correlations, and so on...).
To estimate this distribution, the maximum entropy method derives a 'probabilistic model' of neural activity that matches correlation moments up to an order but otherwise have as little structure as possible. Pioneering studies chose to match only the mean activity of individual neurons and their pairwise correlations[1], (Schneidman *et al.* 2006; Shlens *et al.* 2006; Tkacik *et al.* 2006; Tang, Jackson, *et al.* 2008). Such models are termed Ising models.
To build a model that has the least possible structure, one can maximize the entropy of the distribution $P(\sigma_i)$. The entropy of the distribution $P(\sigma_i)$ is the only consistent way to measure the degree of randomness in a probability

[1] Note that higher-order may also be used to constrain MEMs.

distribution (Shannon 1948) and is defined as:

$$S = -\sum_{\{\sigma_i\}} P(\sigma_i) log(P(\sigma i)$$

With constraints of order 1 and 2, the solution of the MEM is mathematically equivalent to the Boltzmann distribution for a set of Ising spins σ_i that are subjected external magnetic fields h_i and interact with one another through couplings J_{ij} (Mézard *et al.* 1987). Thus to maximize the entropy one need to determine the parameters h_i and J_{ij} which would match individual firing rates and pairwise cross-correlations.

Maximum Entropy Models have been been largely applied to investigate the nature of neural correlations, especially in the retina (Schneidman *et al.* 2006, Shlens *et al.* 2006, Ganmor *et al.* 2011, Tkačik, Granot-Atedgi, *et al.* 2013, Tkačik, Marre, *et al.* 2014). Seminal work (Schneidman *et al.* 2006), used MEMs to demonstrate that pairwise interactions are dominant compared to higher order interactions in the vertebrate retina. They compared the performance of an independent model, a MEMs constrained with order 1 (that is the average firing rate) versus an Ising model (constraints of order 1 and 2, i.e. average firing rate and pairwise correlation). Authors found out that Ising models could predict the rates of commonly occurring 10-neuron patterns much better than the independent model (Figure 2.2c).

The same year, also based on Ising models, the work of Shlens *et al.* 2006 demonstrated not only that high order (up to 10) firing patterns arise from multiple pairwise interactions (Schneidman *et al.* 2006) but also that these high order firing pattern could be predicted from pairwise correlations restricted to anatomically adjacent parasol retinal ganglion cells (in the macaque monkey retina). Since these high order firing patterns emerge from non-neighbouring cells, it is likely they derive from propagation of the signal from pairs of adjacent cells. Interestingly an MEM was recently applied to calcium imaging recordings of hippocampal CA1 neurons in mice (Meshulam *et al.* 2017). In line with the Schneidman *et al.* 2006 results in the retina, the authors observed that the full probability distribution of spike patterns (thus including high-order phenomena) was successfully described with inferences based solely on average firing rate and pairwise correlation. Interestingly, this Ising model yielded accurate predictions both for the activity of individual place and non-place neurons in relation to the rest of the network. In another recent study, coupling between neurons J_{ij} was inferred from an Ising model applied to recordings of PFC neurons in rats learning task. Tavoni *et al.* 2017 found that the coupling (a proxy for pairwise correlation strength) in a subset of neuronal pairs was strengthened after learning, when comparing coupling in pre versus post sleep. These results are in line with those of Peyrache, Khamassi, *et al.* 2009, the original work which provided the data set for their model[2]. Note that this method is rarely used to identify specific patterns but

[2] see also the following Chapter 3 about Reactivations

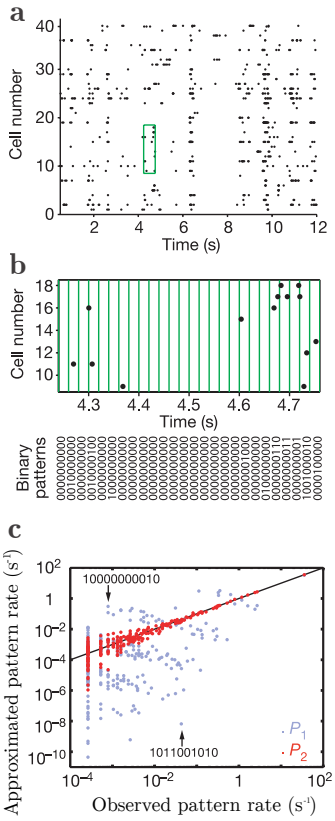

Figure 2.2: Maximum Entropy Models to study network activity. **a)** Raster plot of the neuronal responses of 40 retinal ganglion cells in the salamander to a natural movie clip. Each dot represents the occurence of an action potential. **b)** Discretization of population spike trains into a binary pattern is shown for the green boxed area in a). For clarity, 10 out of 40 cells are shown. **c)** Rate of occurrence of each firing pattern predicted from the Ising model that takes into account all pairwise correlations is plotted against the measured rate (P2; red dots). Each dot stands for one of the $2^{10} = 1,024$ possible binary activity patterns for 10 cells. Black line shows equality. For comparison, predictions from the independent model are also plotted (P1; grey dots). Two examples of highly erroneous estimates of the actual pattern rate by the independent model are highlighted. Adapted from Schneidman *et al.* 2006.

rather to determine the order of correlation that can best account for the observed patterns of activity.

One of the main drawbacks of these models is that maximizing the entropy of a large number of neurons is computationally demanding due to the large number of parameters to be determined (e.g. $N^2/2 = 1250$ for an Ising model with N=50 recorded neurons; parameters h_i and J_{ij}). Moreover assessing the statistical significance of the detected patterns remains challenging and can result in multiple testing issues. Note that classical MEM models do not distinguish correlation induced by non-stationarities (e.g. the visual stimulus in the case of retinal studies) from network-generated correlations (Tyrcha *et al.* 2012). To isolate contributions from several variables, we can turn to Generalized Linear Models.

2.2.2 Generalized Linear Models

Generalized Linear Models (GLMs) can attribute the variability in a spike train to several factors such as sensory input, spiking history, network synchronous activation (peer prediction), etc. GLMs estimate the value f_t of a given variable (e.g. the firing rate of a neuron at time t) as a function of predictors, that is, a set of observed values. This predicted value f_t is related to a linear combination of the model parameters through a so-called link function g. In the case of Poisson processes, the link function g is usually the exponential function. For example, to calculate peer prediction, one can estimate f_t, the intensity prediction function:

$$f_t = g(\sum_{\alpha} s_{t\alpha} w_\alpha)$$

where $s_{t\alpha}$ is the estimation the spike train of cell α spike train smoothed by a Gaussian kernel (of width σ) $s_{t\alpha} = \frac{1}{\sqrt{2\pi\sigma^2}} \sum_{\tau_\alpha} exp((t-\tau_\alpha)^2/2\sigma^2)$ and w_α are the prediction weights that are determined by maximizing the penalized log-likelihood.

This method was notably used by Harris *et al.* 2003 to predict the firing of rat hippocampal place cells ('targets') during spatial navigation based on the location of the animal and the spiking activity of the other recorded cells ('peers')[3]. Each peer was assigned a weight (w_α in the above formula) which represents its respective contribution in the prediction f_t of the target cell. For example, in Figure 2.3the prediction intensity increased when red color-coded peer cells (high positive weights) were active. This coincided with the spiking of the target place cell. Conversely when blue color-coded peers (negative weights) were active, the prediction intensity decreased and the target cell firing probability was lower. Thus for each target, the distribution of GLM weights provide a useful insight of peer contributions. However, this can not identify groups of co-active cells directly. To do so, one would have, at least, to compare the GLMs (i.e., w_α distributions) obtained for each target cell and try to cluster groups that can accurately predict each other (overlapping high weight cells). Thus, while GLM can isolate correlations induced by stationarities (but only those selected by the experimenter), it is not well suited for identifying cell assemblies per se. To that end, one of the more popular technique relies on Principal Component Analysis (PCA), which is also based on pairwise correlations (that are considered to account for higher order correlation Schneidman *et al.* 2006, Shlens *et al.* 2006, Meshulam *et al.* 2017).

[3]Scientific results of this study were discussed in 1.5.5. Here, the focus is only on the GLM method

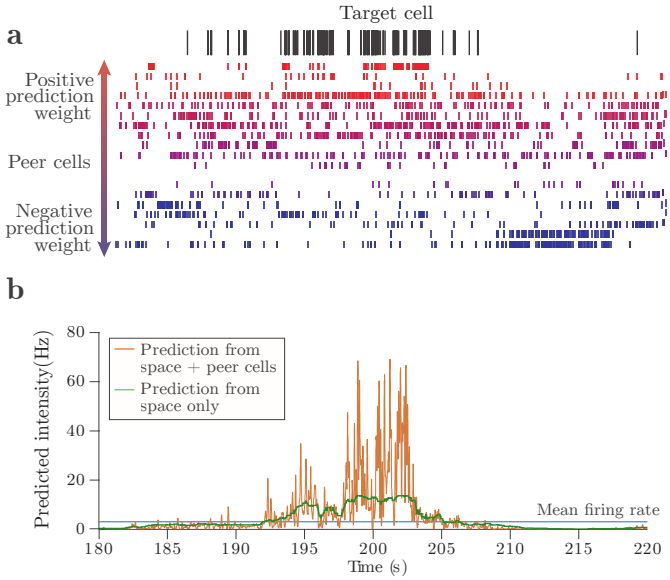

Figure 2.3: Peer prediction in the hippocampus. **a)** Activity of a target place cell (black, top), and a population of simultaneously recorded (peer) pyramidal cells (below). Each peer cell is assigned a prediction weight, with activity of positively or negatively weighted cells predicting increased or decreased probability of synchronous target-cell spikes . **b)** Target-cell firing probability that is predicted from the animal's position (green), or from position and peer activity (orange). Adapted from Harris *et al.* 2003.

2.3 PCA based methods

2.3.1 Detecting co-activations

The main goal of principal component analysis (PCA) is to reduce the dimensionality of a data set consisting of a large number of interrelated variables, while retaining as much of the data set's variation as possible. Here, the data sets are simultaneously recorded spike trains. This is achieved by transforming these to a new set of variables, the principal components (PCs), which are orthogonal, and which are ordered so that the first few retain most of the variation present in all of the original variables (Jolliffe 1986). PCA can be done by eigen-decomposition of a correlation matrix, usually after normalizing initial data. Using PCA to detect synchronous activity goes back to Nicolelis *et al.* (1995), Chapin & Nicolelis (1999) but was extended further by Peyrache, Khamassi, *et al.* 2009, Peyrache, Benchenane, *et al.* 2010.

First, the spike trains of n neurons are binned into B intervals to build a $n \times B$ spike matrix S. The (i, t) element of S represents the number of spikes emitted by the i^{th} cell within the t^{th} window. Then the spike matrix is z-scored resulting in a matrix Q (see Figure 2.4; steps 1, 2 and 3):

$$Q_{i,t} = \frac{S_{i,t} - \mu_i}{\sigma_i}$$

where μ_t and σ_t are respectively the mean and the standard deviation of the spike count of the i^{tj} neuron over time, i.e., $\mu_i = \frac{1}{B}\sum_{t=1}^{B} S_{i,t}$ and $\sigma_i = \frac{1}{B-1}\sqrt{\sum_{t=1}^{B}(S_{i,t} - \mu_t)^2}$. The cross-correlation matrix C is obtained by computing :

$$C_{i,j} = \frac{1}{B}\sum_{t=1}^{B} Q_{i,t} Qj, t = \frac{1}{n} Q^T Q$$

where $C_{i,j}$ is the Pearson correlation coefficient between the i^{th} and the j^{th} cell. Then, the eigenvalue decomposition of C is computed yielding in a set of n orthogonal PCs p_i and associated eigenvalues λ_i (ensured from the spectral theorem, since C is real and symmetric).

$$C = \sum_{i=1}^{n} \lambda_i^T p_i p_i$$

where the outer product ${}^T p_i p_i$ is the projection matrix onto the direction of p_i, and λ_i is the variance of the data along the same axis (Figure 2.4; steps 4, 5). To assess the number of significant PC's (i.e. components that are more likely to represent cell assemblies rather than correlation caused by random fluctuations), Peyrache, Khamassi, *et al.* 2009 proposed the Marčenko & Pastur distribution as a null hypothesis (Marčenko & Pastur 1967). Authors demonstrated that the singular values (square root of the eigenvalue of the correlation matrix) of large rectangular matrices ($N_{rows} \to \infty$, $N_{column} \to \infty$

and $N_{column}/N_{row} \geq 1$) with statistically independent rows follow a probability function $\rho(\lambda)$:

$$\rho(\lambda) = \frac{N}{2\pi\sigma^2 B} \frac{\sqrt{(\lambda_{max} - \lambda)(\lambda - \lambda_{min})}}{\lambda}$$

where σ^2 is the variance of the elements (σ^2 =1 with z-scored normalization). Thus, when neurons are uncorrelated, λ must vary between λ_{min} andλ_{max}, i.e. the variance can not be larger than λ_{max}. Hence PCs with eigenvalues exceeding λ_{max} are considered significant. However, the use of Marcenko Pastur threshold under non-stationnarity (for example, correlation produced by slower (co)variations compared to the chosen bin width) has been recently criticized (Russo & Durstewitz 2017). One possible alternative is to shuffle spike trains to create surrogate data and apply PCA once again. Repeating this operation will yield a distribution of eigenvalues. A statistical threshold can be derived from the 95th of this distribution. Despite the Russo & Durstewitz issues, the surrogate data and Marcenko Pastur provides similar results (see 4.4 in Result section). One of the main issues with PCA is that PCs are orthogonal by construction but this not be necessarily be the case in the brain. Moreover, when two assemblies concentrate the same amount of variance, PCA may failed to distinguish them and the two corresponding PCs may rather be a mixture of the two assemblies (Lopes-dos-Santos, Ribeiro, *et al.* 2013). Additionally, assemblies with overlapping members will not be properly detected.

To address this issue, Lopes-dos-Santos, Ribeiro, *et al.* 2013 used Independent Component Analysis (ICA) ensuing components selection with PCA (see Figure 2.4; step 6). Traditionally, ICA is used to solve the blind source problem also known as the cocktail-party problem, where one tries to separate the speech of several people talking simultaneously in a room. The Central Limit theorem states that the sum of independent variables (e.g the sound recording at the cocktail or PCs) is more Gaussian the variables them selves (each individual person or each 'true' assembly). Therefore to 'de-mix' components, ICA rotates PCs weights to maximizes measures of non-Gaussianity (kurtosis or negentropy, see Hyvärinen & Oja 2000 for more details) in order to make each component as independent as possible. It should be mentionnend that ICA was first used for neural data by Laubach, Shuler, *et al.* 1999, Laubach, Wessberg, *et al.* 2000 to detect synchronous activity in the motor cortex as rats performed a reaction-time task. However, in these studies, ICA was applied to too many components (with eigenvalues greater than 1) which can lead to spurious results (Lopes-dos-Santos, Ribeiro, *et al.* 2013). It remains crucial to apply ICA once and only once significant PCs have been identified (using Marčenko & Pastur threshold or surrogate data). Note that results may vary greatly with the choice of the bin duration. Therefore it is essential (but rare) to investigate the stability of the detected components with regards to this parameters (further discussed in Chapters 4 and 7). Note that the number of significant independent components (ICs) is necessarily less than or equal to the number of recorded neurons.

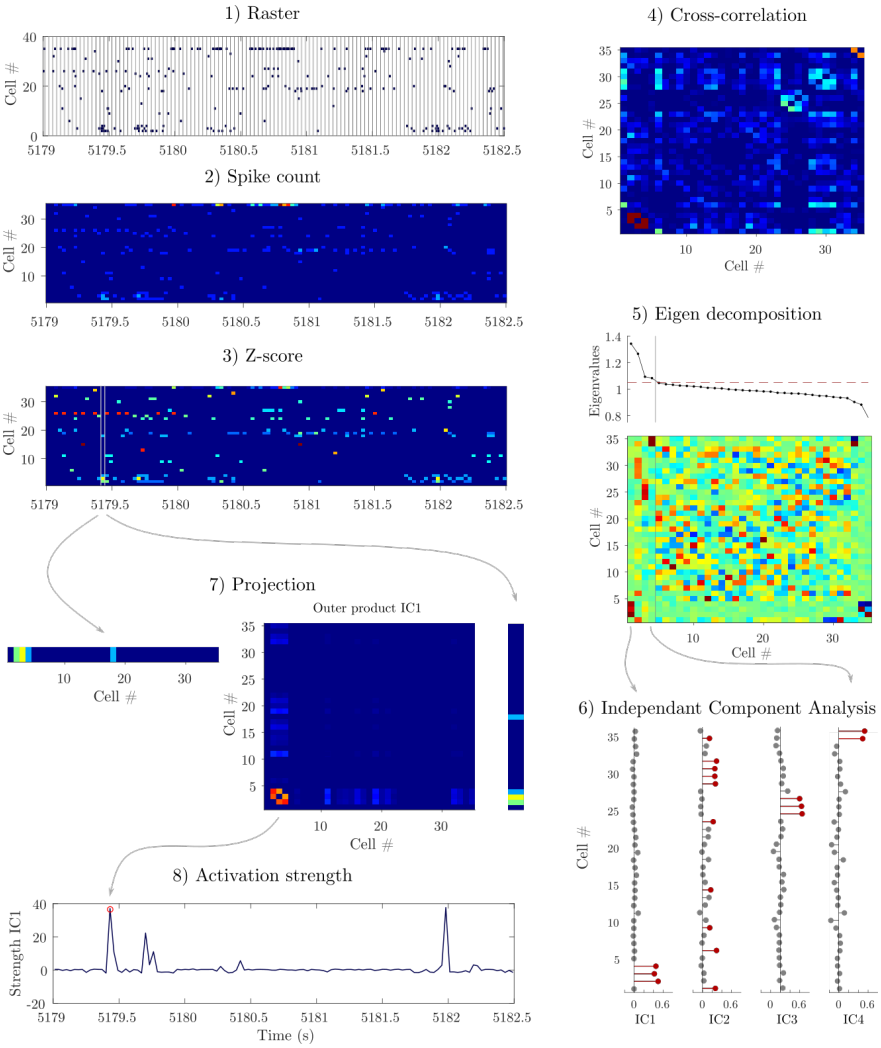

Figure 2.4: Cell assembly detection using PCA-ICA. **1)** Raster plot of activity of 35 PFC neurons. Spike trains are binned in 30 ms windows (vertical lines). **2)** Spike matrix for this data sample shows spike counts for each cell within each window. **3)** Z-scored spike matrix. **4)** Cross-correlation of the z-scored matrix for the entire recording session (duration ∼2h). **5)** Eigen decomposition of the cross-correlation matrix. Above : Eigenvalues. The horizontal dashed line indicates the Marcenko-Pastur threshold. The vertical grey line delimit the 4 sub-threshold eigenvalues. Below : Eigenvectors appear in columns. **6)** Independent Component Analysis. Each column represents an Independent Component (IC). Height of lollipop indicates weight of neurons. Weights exceeding Otsu's threshold are colored in red. **7)** For each bin, activation strengths are calculated as the projection projection of population vector from the z-scored matrix (delimited by white vertical lines in 3) onto the outer product of IC1. **8)** Activation strength of IC1 in the data sample of 1 and2. Note the peak caped by a red dot that correspond to the computation from 7. Co-activation of neuron 2,3 and 4 yield a peak in activation strength of IC1.

2.3.2 Activation strength

One of the greatest advantages of PCA-based methods is the possibility to track the dynamical activation strength of an identified independent components over time ('IC'; Figure 2.4; step 3, 7 and 8). First, the spike matrix is generated and z-scored resulting in a matrix Z (time bins can differ from the ones previously used for component detection). The outer product $Ic_i^T Ic_i$ creates a template, for each significant component ICs. The diagonal of the template matrix is set to 0 so that single neuron spiking does not contribute to the activation strength. Activation strength of the i^{th} component is computed by projecting population vector at a given time z(t) (columns of the Z matrix) onto the component template.

$$A_i(t) = z(t)^T (Ic_i^T Ic_i) z(t)$$

Thus the activation strength is high when multiple neurons with same-sign high weights fire synchronously and increases when these synchronous neurons fire more.

2.3.3 Interpreting PCA-ICA results

Usually the independent components are considered as proxies for cell assemblies (Peyrache, Khamassi, *et al.* 2009; Benchenane *et al.* 2010; van de Ven *et al.* 2016; Trouche, Koren, *et al.* 2019). Primarily, high weight neurons are thought to be part of the assembly. However PCA-ICA does not provide a proper way to identify cell assembly members. Usually, an arbitrary threshold is set (Z=2, van de Ven *et al.* 2016) or the n-th biggest weights are considered only (Benchenane *et al.* 2010, n = 5). In the result section of this manuscript, two different rules have been applied:

- a threshold of $1/\sqrt{N}$, with N being the number of cells recorded. This threshold represents the expected weight of neurons if they were all members of one only massive assembly (criterion selected in Results 4).
- using Otsu's method Otsu 1979, initially developed in image processing to separate pixels into two classes, foreground and background. This algorithm divides the data (here, weights of respective neurons) into two classes while maximizing the inter-class variance. The goodness of separation is quantified by Otsu's metric, the ratio of the inter-class variance and the total variance. When data are well separated well, Otsu's metric tends toward one, whereas a poor cut-off yield returns a near-0 value (selected method in Chapter 5).

Thus interpreting PCA-ICA components might be difficult especially the weight distribution is not bimodal. Interpreting activation strength signals may also be problematic. Usually, peaks in activation strength are thought to correspond to assembly expression. However, since activation strength computation is based on the whole distribution of weights, activation strength peaks might not correspond to co-activation of high weights neurons. Peaks can also emerge from co-activation of low weights neurons or bursting of a

low-spiking neuron[4].

Despite these difficulties, PCA-ICA techniques remain a reference method to detect co-activation pattern and are widely adopted by the scientific community (Peyrache, Khamassi, *et al.* 2009; Benchenane *et al.* 2010; Lopes-dos-Santos, Ribeiro, *et al.* 2013; Gulati, Tsodikov, *et al.* 2014; Gulati, Won, *et al.* 2015; Ramanathan *et al.* 2015; Dejean *et al.* 2016; van de Ven *et al.* 2016; Rothschild *et al.* 2017; Deolindo *et al.* 2018; See *et al.* 2018; Sjulson *et al.* 2018; Giri *et al.* 2019; Todorova & Zugaro 2019; Trouche, Koren, *et al.* 2019; Eckert *et al.* 2020).

2.4 Higher-order correlation

PCA and Ising models take into account correlations of order two. Even though pairwise correlations are thought to account for higher order correlations within the cortex (Schneidman *et al.* 2006), in recent years, several methods for the detection of higher-order correlation have been developed Grün *et al.* 2008; Staude, Grün, *et al.* 2010; Staude, Rotter, *et al.* 2010; Picado-Muiño *et al.* 2013, for a review see Quaglio, Rostami, *et al.* 2018). These methods are usually computationally demanding and remain best suited to identify precise spike sequences (Torre, Picado-Muiño, *et al.* 2013; Torre, Canova, *et al.* 2016; Quaglio, Yegenoglu, *et al.* 2017; Russo & Durstewitz 2017, see also 'Replay methods' in the next Chapter).

Conclusion

Historically, cross-correlation histograms and joint peri-stimulus histogram were the two principal methods to investigate correlations between pairs or triplets of neurons. Model-based methods have been recently developed to study larger patterns. Interestingly, larger patterns (n>3) can be inferred from pairwise correlation only, within the neocortex, but also within limbic structures such as the hippocampus. Moreover, model-based methods such as General Linearized Models can decompose the contributions of several factors (sensory input, peer cells etc.), to better understand the spiking activity of observed cells. However, to identify significant patterns of co-activation within spike trains, perhaps one of the most appropriate and popular approach remain PCA-ICA methods. Based on pairwise correlation, these techniques can detect independent components (proxies of cell assemblies), assess their activity over time, and are computationally less demanding than recently developed unsupervised methods (which best suited for sequence identification).

[4]These issues are further discussed and illustrated in Figure 5.11, see Chapter 5.

3 Reactivation of cell assemblies in off-line states

During sleep, repeated occurrences of stereotyped neural pattern such as synchronous cell assembly activation ('reactivation') or temporal sequences ('replay') have been hypothesized to be neural bases of memory consolidation (Buzsáki 1989). These reactivations are thought to help stabilize labile memories for long term-storage. This process would involve the coordination of a fast encoding temporary store, in the hippocampus and a slow-learning long-term store, in the neocortex (Marr 1971). Reactivations of cell assemblies have been extensively studied in the hippocampus, but also in downstream cortical and sub-cortical structures. Interestingly, reactivations are tightly associated with hippocampal SPW-Rs and/or cortical rhythms. In this chapter, I will first briefly describe sleep. Then, I will discuss seminal works on reactivation and replay in the hippocampus. As evidence of hippocampal replay grew, so did the methods for detecting it. These methods overlap with those reviewed in the Chapter 2 *Methods for cell assembly detection* but are presented separately here (see Boexes) because they were specifically developed to tackle the issue of pattern reinstatement, which slightly differs from pattern detection. In a recent review, Tingley & Peyrache (2020) stressed that discrepancies in interpretations in the literature could be caused by the use of different methods andor parameters, and that the community would gain from standardizing techniques or to apply common benchmarks. Finally, I will discuss how these recent techniques facilitated the examination of reactivation in multiple areas, often in concert with the hippocampus.

3.1 What is sleep?

Sleep is defined as a natural and reversible state of reduced responsiveness to external stimuli and relative inactivity, accompanied by a loss of reactivity to the outside world (except possibly some auditory signals). It occurs at regular intervals and, in mammals, sleep is homeostatically regulated (i.e. a loss or delay of sleep results in subsequent prolonged sleep periods) (Rasch & Born 2013). Sleep probably occurs in all vertebrates, including birds, fishes, and reptiles, and sleep-like states are similarly observed in invertebrates like flies, bees, and cockroaches (Cirelli & Tononi 2008).

Sleep is not a singular entity but is rather composed of two physiologically distinct states: rapid eye movement (REM), or paradoxical sleep, and non-rapid eye movement sleep (nREM), which can be divided into 3 stages. These states cyclically alternate during sleep even though nREM sleep is predominant at the beginning of the night and REM sleep later (Figure 3.2a). Rodents do not sleep in a single period like humans, but rather have several alternating cycles of REM and nREM sleep (see Figure 3.2b).

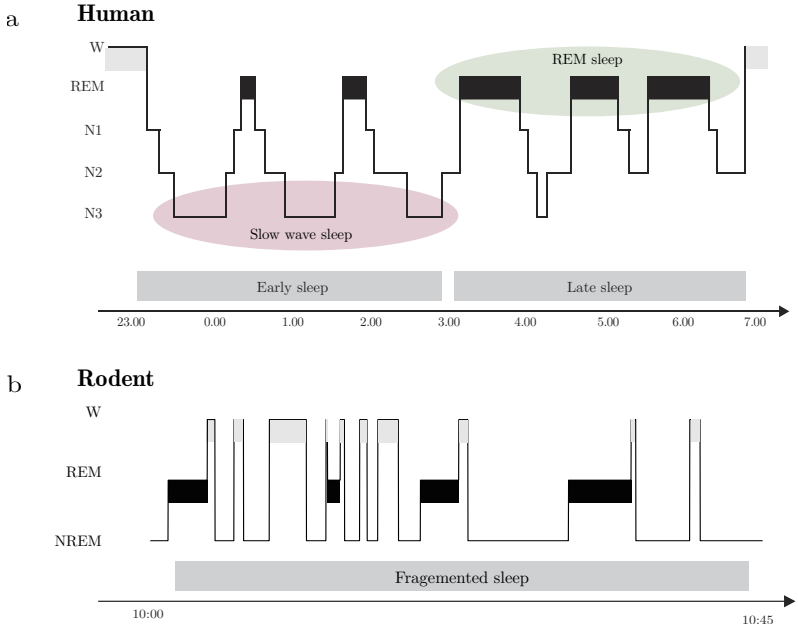

Figure 3.1: Sleep architecture. **a)** Example of a human hypnogram. Human sleep is composed of alternating periods of nREM and REM sleep, with nREM subdivided into a further 3 stages. nREM sleep occurs mostly during early sleep whereas REM sleep becomes more frequent later. Adapted from Rasch & Born 2013. **b)** Example of a rodent hypnogram (unpublished data from our lab). In rodents, sleep is more fragmented and composed of alternating bouts of nREM, REM, and brief awakening.

In the rodent literature (and more generally, the experimental animal literature), nREM sleep is referred to as Slow Wave Sleep (SWS), which in humans represents the deepest stage of nREM sleep only (N3).[1]. In this manuscript, the terms SWS and nREM will be used interchangeably to designate non-REM sleep periods in rats.

SWS and REM sleep stages display highly dissimilar electrophysiological patterns. In humans, these patterns, i.e. sleep rhythms, are best studied in the neocortex since they can be recorded with scalp EEG electrodes. Using this non-invasive technique, Loomis *et al.* 1935 shed light on different characteristic patterns of sleep EEG. If local field potential (LFP) recordings of REM sleep look very similar to those of the waking state, neocortical LFP during slow-wave sleep drastically differs. The hallmark rhythms of neocortex during SWS are (Figure 3.1 a):

- **Slow oscillations:** cortical cells spontaneously fluctuate between a depolarized state of sustained spiking activity, the UP state and a hyperpolarized state favoring interruption of neuronal firing, the DOWN state Steriade, Contreras, *et al.* 1993.

- **Delta waves:** positive deflections of the LFP in neocortical deep layers accompanying transient (200-500 ms) firing cessation[2]. Delta waves are thought to reflect UP-DOWN-UP transitions.

- **Sleep spindles:** thalamocortical waxing-and-waning oscillatory events (10-15 Hz) (Steriade, McCormick, *et al.* 1993) which occur mostly in the light stages of NREM sleep. Spindles are embedded in the cortical slow oscillation, closely following delta waves (∼40% of events; Maingret *et al.* 2016), but can also occur in an isolated manner (Sirota & Buzsáki 2005; Peyrache, Battaglia, *et al.* 2011).

Like in the cortex, during slow-wave sleep (but also quiet wakefulness, drowsiness), LFP in the hippocampus is characterized by large-amplitude irregular activity (LIA), with sporadically occurring transient deflection of the signal called sharp waves (Buzsáki 1986). Sharp waves co-occur with brief (50-150 ms) and fast oscillations (∼200 ms), called ripples which originate in the CA1 pyramidal layer (Buzsáki, Horváth, *et al.* 1992). These two events occur together as sharp-wave ripples (SPW-R; see Figure 3.1b)[3]. To this day, hippocampal sharp wave-ripples remain the best described neurophysiological correlate of reactivation and replay events.

[1] Even though a recent study in the mouse proposed a novel sleep scoring method to characterize 3 stages of non REM sleep, similar to the human taxonomy (Lacroix *et al.* 2018)

[2] In a recent study from our lab, Todorova & Zugaro 2019 demonstrated that delta waves are not complete silent but rather they represent isolated cortical computations closely related to ongoing information processing underlying memory consolidation

[3] Sharp-wave ripples are also observed during offline waking states Foster & Wilson 2006

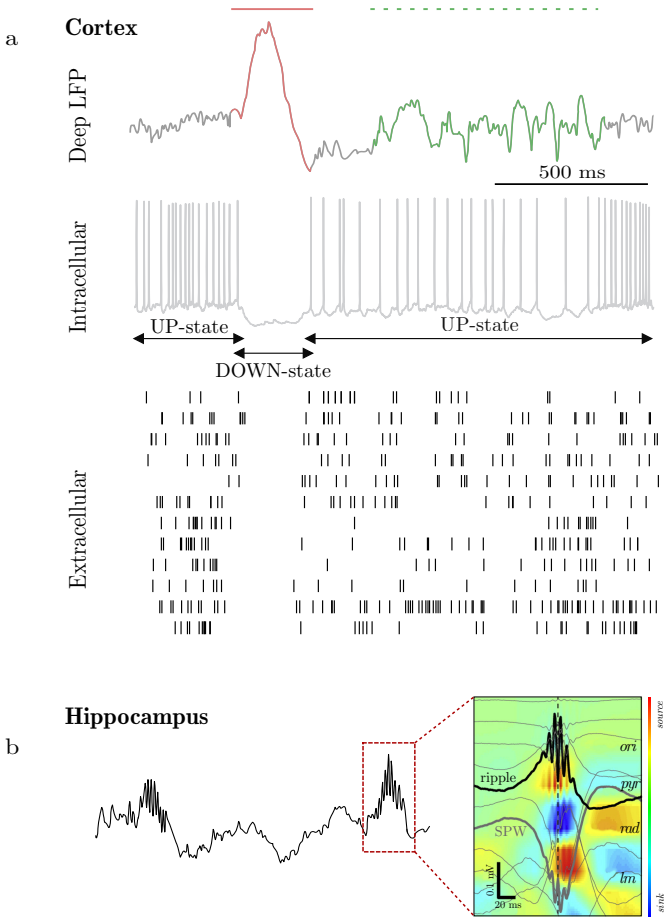

Figure 3.2: Slow wave sleep brain rhythms and cell activity. **a)** Example of simultaneous LFP (top) and extracellular recordings (bottom) in deep layers of prefrontal cortex in the rat. Each row of rasters corresponds to a different neuron and each tick represents a spike. Middle: intracellular recording of a layer V neocortical neuron. The cells' membrane potential drop during the DOWN-states, associated with a positive wave at the LFP level (delta wave; red solid line) and absence of neuronal activity. Unit activity resumes at the end of the delta wave (UP-state). Note the spindle (green; dashed line) following the delta wave in the LFP signal. **b)** Left: hippocampal LFP recorded in CA1 stratum pyramidale during sleep. Right: depth profile of sharp-wave ripples (solid lines) superimposed on a current source density map of the same events. Note the large sink in the stratum radiatum (sharp wave, SPW) and the fast alternation between sinks (blue) and sources (red) in the pyramidal layer (ripple). Adapted from Sullivan *et al.* 2014

.

3.2 Reactivation and replay in the hippocampus

In 1989, Buzsaki proposed that hippocampal cell assemblies are reactivated during ripples to transfer information to the neocortex (Buzsáki 1989). The purpose of such repetitive activation would be to subsequently consolidate memories via STDP mechanisms (since LTP involves much more intense activity than the low firing rate hippocampal projection neurons). The same year, Pavlides & Winson demonstrated that place cells active during behavior fired at higher rates during subsequent sleep. Conversely, cells associated with non-visited places did not show such changes.
Building on this work, Wilson & McNaughton (1994) recorded large ensembles of individual hippocampal place cells and demonstrated that multiple cell pairs which tended to fire together (100 ms) during experience were also synchronous during post behavior sleep ('POST'), but not during pre-behavior sleep ('PRE'), see Figure 3.3a. Reactivation was assessed by comparing the average cross-correlation in post sleep for two different type of cell pairs: pairs with overlapping fields versus pairs of non-overlapping ones. Interestingly, the authors found that reactivation occurred especially during sharp wave ripples, consistent with Buzsaki's prediction.
Later on, Skaggs & McNaughton (1996) hypothesized that hippocampal sequences during behavior were replayed in the same temporal order later during sleep. They examined the asymmetrical bias B_{ij} of the cross-correlogram between hippocampal place cells i and j :

$$B_{ij} = \int_{0}^{\Delta t} \chi_{ij}(t)dt - \int_{-\Delta t}^{0} \chi_{ij}(t)dt$$

where $\Delta t = 200$ ms. They observed that pairs that displayed strong temporal ordering on the track exhibited the same asymmetrical bias during POST but not during PRE sleep.
However, global changes in correlations could be caused by external modulation such as oscillations or changes in neuromodulator concentrations without changing the relative cross-correlation within the network. Moreover, the measure of replay proposed by Skaggs & McNaughton implies arbitrarily separating the cells into weak and strong correlated groups. Wilson & McNaughton partitioned the data into overlapping and non-overlapping place cell groups which may also be arbitrary and can not be applied to structure that does not have cells with proper fields.

To overcome these issues, a mathematical refinement, the explained variance method, was introduced by Kudrimoti *et al.* (1999, see Box 3.1). This more elegant approach confirmed results from previous experiments, i.e., pairwise correlations are relatively more similar in POST and during awake state ('WAKE') compared to PRE sleep and WAKE. Pattern reinstatement was strongest during SPW-R and decayed within ∼30 minutes.

Box 3.1. Explained and reverse explained variance (Kudrimoti *et al.* 1999; Pennartz, Lee, *et al.* 2004)

The first steps of the explained variance method consist in computing the cross-correlation matrix C, where $C_{i,j}$ is the Pearson correlation coefficient between the i^{th} and the j^{th} cell, for three different epochs: PRE sleep, WAKE and POST sleep. The explained variance measure (EV) assesses the relative similarity of C matrices in these periods. More precisely, the explained variance quantifies how much of the variance in the element of C in POST sleep can be explained by their variance in awake state given their relative magnitude in PRE sleep:

$$EV = r^2_{wake,POST|PRE} = \left(\frac{r_{wake,POST} - r_{wake,PRE} \times r_{POST,PRE}}{\sqrt{(1 - r^2_{wake,PRE})(1 - r^2_{POST,PRE})}} \right)^2$$

with $r_{A,B}$ being the correlation of matrices C computed during epochs A and B. However Kudrimoti *et al.* 1999 compared EV to $r_{wake,pre}$ e.g the correlation of C matrices during wake and pre instead of comparing the EV to a proper control. This problem was solved by Pennartz, Lee, *et al.* 2004 who introduced the reverse explained variance (REV). By switching pre and post epochs in the EV formula, REV captures the percentage of pre sleep variance explained by awake state given their relative magnitude. Reactivation is then assessed by a significance difference between EV and REV. To date, explained variance remains one of the more popular method to characterize pairwise reactivation (Kudrimoti *et al.* 1999; Hoffman & Mcnaughton 2002; Pennartz, Lee, *et al.* 2004; Euston *et al.* 2007; Lansink, Goltstein, Lankelma, Joosten, *et al.* 2008; Lansink, Goltstein, Lankelma, McNaughton, *et al.* 2009; Girardeau, Inema, *et al.* 2017; Tang, Shin, *et al.* 2017; Chang, Esteves, *et al.* 2020). Even though this method is more rigorous than direct cross-correlation comparison, it has some limitations:

- The explained variance measure can not track the timing of reactivations since it accounts for the total variance over a period of time. Furthermore, the variance values depend on the time bin chosen. The time bin parameter varies from one study to another, but this is rarely varied systematically or discussed.
- Explained variance calculations take into account every possible pairwise correlation among neurons even though some correlations could be due to chance.

To overcome the first limitation, other approaches are available such as template matching (but best suited for patterns with a fine temporal relationship such as sequences, Box 3.2) or reactivation strength techniques (Box 3.4).

Rather than focusing solely on pairwise correlations, subsequent studies

searched for a more quantitative estimate of neuronal reinstatement and tried to detect entire sequences of activity (Nádasdy *et al.* 1999; Lee & Wilson 2002). Nádasdy *et al.* 1999 relied on joint-peristimulus time histogram to identify sequences of triplets significantly occurring during WAKE and replayed at a faster rate during SPW-R (see Chapter 2 for methodological details). Lee & Wilson 2002 went further, using a combinatorial decoding method to identify sequences of more than four neurons (Figure 3.3b-e). They demonstrated that the probability of these long sequences ($n \geqslant 4$) to be replayed was higher than for isolated doublets. Consistent with previous findings, authors found out that replay happened at a faster time scale than encoding during behavior. While all of these studies provided experimental evidence of replay during nREM sleep, the pioneering work of Foster & Wilson 2006 demonstrated that replay can also take place during the awake state, when the animal pauses in its environment. Interestingly, sequences tended to be reversed with respect to the order of the field order sequence ('reverse replay'), contrasting to the forward sequences documented during nREM sleep (see Box 3.2 for details on the recent méthods to detect replay).

Box 3.2. Popular methods to detect replay

- **Bayesian reconstruction**: In recent studies, bayesian decoding seems to be the preferred method to investigate sequential replay (Johnson & Redish 2007; Davidson *et al.* 2009; Dragoi & Tonegawa 2011; Pfeiffer & Foster 2013; Grosmark & Buzsáki 2016; Drieu *et al.* 2018). Zhang *et al.* (1998) estimated the position x of the animal given the average firing rate map $f_i(x)$ of N neurons and the spike count n_i of all cells in a given window.

$$P(x|n) = P(x)(\prod_{i=1}^{N} f_i(x)^{n_i})exp(-\tau \sum_{i=1}^{N} f_i(x))$$

  where τ represents the window size of the discretized spike trains and $P(x)$ the probability for the animal to be at the position x (i.e. the normalized occupancy map). Computing this probability of each bin generates a reconstructed trajectory which is compared to the real one. It should be noted that this techniques relies on the average firing rate maps, i.e. a template. To assess the significance of detected replayed events, data from a candidate event are shuffled and true replayed event would be expected to appear less than 5% of the time.

- **Unsupervised methods**: A major limitation of bayesian decoding is to extend it to brain activity where behavioral correlates (such as spatial firing) are less precise (e.g, in brain structures other than the hippocampus). Recently, to tackle this issue several unsupervised methods were developed to identify sequences within data (see Grossberger *et al.* 2018; van der Meij & Voytek 2018; Mackevicius *et al.* 2019; Watanabe *et al.* 2019).

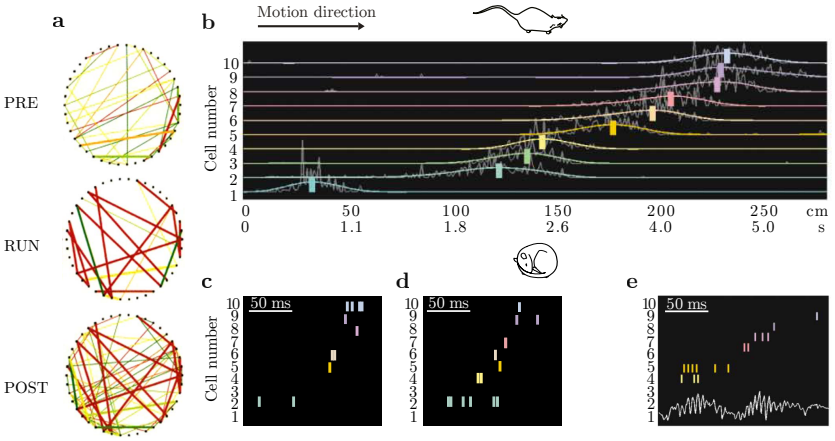

Figure 3.3: Hippocampal reactivations and replay **a)** The first compelling demonstration of experience-dependent reactivation of hippocampal activity. Diagram of the co-activation matrix of 42 simultaneously recorded neurons (dots on the circle). Lines indicate the small subset of all positive correlation (>0.2) between the pairs, with color reflecting the magnitude of the correlation (red, high; green, low). Bold lines indicate cell pairs that were correlated during waking activity (RUN) and also correlated during either sleep before (PRE) or after (POST). These panels reveal that most of the highly correlated pairs that appear during the run phase also appear in the POST phase but are typically absent from the PRE phase. **b)** Average firing rate of 10 hippocampal place cells ordered by their preferred position on a linear track (30 trials; y-axis, cell number; x-axis, position on the track). Colored vertical ticks indicate peak firing location for each cell. Responses for the respective laps are stacked for each cell. Time axis below shows time within an average lap (total: ∼5 s). **c-d)** Replay of place cell sequences. Examples of compressed replay during sleep. Note the faster time scale (∼20-fold compression). **e)** Replay coincides with sharp-wave-ripple (SPW-R) events. Panel a) adapted from Wilson & McNaughton 1994, b-e) from Lee & Wilson 2002.

A causal role of hippocampal reactivation Two studies first investigated the role of hippocampal ripples in memory consolidation, during nREM sleep (Girardeau, Benchenane, *et al.* 2009; Ego-Stengel & Wilson 2009). With closed-loop appartus authors disrupted hippocampal ripples — and therefore the associated neuronal activity (putative replay) — following training on a spatial task. This resulted in subsequent performance impairment, suggesting a causal role of SPW-R in memory consolidation. The same protocol was used to disrupt awake ripples during quiet wakefulness and yielded similar performance impairment (Jadhav, Kemere, *et al.* 2012). Interestingly, disrupting the reactivation of those cell assemblies that emerged in a novel environment drastically altered the activity of the cell assembly during re-exposure (Gridchyn *et al.* 2020). These findings led Gridchyn *et al.* to examine whether learning impairment results from the disruption of SPW-Rs alone or from the specific disruption of assembly firing patterns that presumably encode memory traces. They found that the disruption of the reactivation of synchronous place cell

patterns (∼20 ms) in CA1, with an optogenetic apparatus, led to impaired recall of spatial goal memories represented by these place cells, without impacting memory traces concerning other places. These results support the role of reactivation and replay as neural mechanisms of memory consolidation.

Box 3.3. Template Matching (Louie & Wilson 2001)

This method detect spike train pattern similarities with a chosen template. Usually templates correspond to sequential activation of neurons during WAKE. To create a template, spike trains occurring during a particular event (e.g., a trial) are binned resulting in a (n x B) matrix T, where n is the number of recorded cells and B the number of bins. All events in the recording session are similarly binned to generate (n x B) target spike matrices S. S and T can be normalized (e.g. z-score, setting the norm of each column to 1 etc.) before using the Pearson coefficient for matrices to compare them.

$$Coef = \frac{\sum_{i=1}^{n}\sum_{j=1}^{B}(T_{ij} - < T >)(S_{ij} - < S >)}{\sqrt{\sum_{i=1}^{n}\sum_{j=1}^{B}(T_{ij} - < T >)^2}\sqrt{\sum_{i=1}^{n}\sum_{j=1}^{B}(S_{ij} - < S >)^2}}$$

where the means $< S >$ and $< T >$ are respectively calculated as $< T >= \frac{1}{nB}\sum_{i=1}^{n}\sum_{j=1}^{B} T_{ij}$ and $< S >= \frac{1}{nB}\sum_{i=1}^{n}\sum_{j=1}^{B} S_{ij}$. Note that the sizes of S and T are similar but the binning width can vary to examine temporal compression and/or distension of behavioral sequences in sleep. However, this method should be used carefully as it presents some pitfalls:

- Results are extremely sensitive to the normalization method selected. Tatsuno *et al.* (2006) demonstrated that when normalizing columns of the matrices using their euclidean norm (Louie & Wilson 2001), the template matching measure was influenced by changes in mean firing rate of neurons and not just the fine structure of spike timing. Using z-scored matrices prevents this problem (Euston *et al.* 2007).

- Tatsuno *et al.* 2006 also reported that when comparing correlation of target matrices with two templates from distinct epochs, for example T_{PRE} in PRE and T_{POST} in POST sleep, it is crucial that target matrices remain the same. For example, one can not compare the correlation of template T_{PRE} matched with target in PRE only versus T_{POST} with POST target only. Such partial calculation of template-matching correlations, may lead to erroneous conclusions as the correlations have been proven to fluctuate with firing rate changes (De La Rocha *et al.* 2007).

- Since templates are based only on one instance, this measure can be sensitive to noise.

- Even if template matching can highlight temporal compression or distension, this method assumes that the temporal relations between neurons is linear. For example, let us consider a template where neurons A, B and C fire in sequence with similar inter-spike interval. Then, the template correlation with a target will be high, only if the initial order of discharge is preserved but also if the intervals of spiking between A,B and C are equal (but note that this interval might be shorter or longer compare to the template one, when investigating compression or distension).

Replay in REM sleep? Evidence of reactivation during REM sleep is rare and may results from the difficulty, in rodents, to collect enough data during this stage, since it represents only 10% of total sleep. Even though Pavlides & Winson (1989) observed an increase in firing rate of place cells during REM sleep after exposure to an environment, Kudrimoti *et al.* (1999) showed that the explained variance in the hippocampus is lower during REM than in SWS. However, Louie & Wilson (2001), used template matching (see Box 3.2) to demonstrate that temporally sequenced ensemble firing rate patterns reflecting tens of seconds to minutes of behavioral experience are reproduced during REM episodes at an equivalent timescale. Contrary to highly compressed SWS reactivation, these sequences were reactivated at an equivalent timescale, consistent with the similar LFP patterns observed during REM and awake. Unfortunately, to the best of my knowledge, these results have never been replicated in the hippocampus.

3.3 Extrahippocampal reactivations

Building on hippocampal research and methods, many studies addressed the question whether reactivation and/or replay were more widespread in the brain. Indeed, off-line reactivation might serve to strengthen synaptic connections among hippocampal place cells, storing spatial representations, but may also help coordinate consolidation in target structures. Especially, in light of Marr's two-stage model memory, coordinated reactivation between the hippocampus and the neocortex could facilitate the gradual transfer of memories for long-term storage. Hippocampal–neocortical interactions, however, are unlikely to account for the entire spectrum of memory consolidation processes. Consolidation of nondeclarative or procedural memories, may well involve subcortical routes, including basal ganglia structures such as the amygdala or the striatum (for reviews on extrahippocampal reactivation in concert with neocortical and subcortical structures, see Todorova & Zugaro 2019 and Skelin *et al.* 2019) .

3.3.1 Associative cortex reactivations

Associative cortices are involved in processing multimodal sensory information and include the PFC, cingulate, retrosplenial, posterior parietal (PPC), perirhinal and postrhinal cortices.

Parietal, cingulate and retrosplenial cortex. The dirst evidence of reactivation in association cortices were provided by Qin *et al.* 1997 in the parietal cortex. Hippocampo-parietal cell pairs were more correlated during sleep following track running compared to the sleep before. However, the temporal order of the awake correlation between these two structures was not preserved during sleep (although this remained present in correlation between neurons within the structures). Recently, Wilber *et al.* 2017 observed that multi-unit activity (i.e., all the undiscriminated spikes recorded from a single tetrode) in the parietal cortex was reactivated in a compressed manner (four- to ten-fold) following a spatial sequential memory task. Interestingly, reactivation was coordinated with hippocampal replay onset, with a peak of parietal activity, 50 to 150 ms afterwards. Similarly, in the anterior cingulate cortex (ACC), the majority of neurons are activated just before ripple onsets during sleep, but not before awake state. A subset of neurons (17%) exhibits a peak of activation after sleep ripple onsets (Wang & Ikemoto 2016). Recently, pairs of retrosplenial neurons were found to reactivate after sessions of virtual navigation on a linear treadmill populated with tactile landmarks (Chang, Esteves, *et al.* 2020). Interestingly, another recent paper reported ripples in the retrosplenial cortex, tightly coupled to hippocampal SPW-R, supporting the hypothesis that hippocampal ripples can drive reactivations in associative cortices (Nitzan *et al.* 2020).
Even though hippocampal coordinated reactivation has been reported in the PPC, the ACC and the retrosplenial cortex, the prefrontal cortex (PFC) is the cortical structure most extensively studied in the context of hippocampo-cortical communication.

Prefrontal cortex. THe PFC receives monosynaptic inputs from the ventral hippocampus and is thought to play a role in long-term storage of memory traces (Marr 1971, Squire 1992, Frankland & Bontempi 2005). Recently, Maingret *et al.* 2016, provided first evidence of a causal role of the hippocampo-prefrontal dialog during sleep. With a closed-loop apparatus, artificially enhanced coupling of hippocampal ripples and delta waves resulted in better memory recall performance during the following day. At the single unit level, the first evidence of hippocampo-prefrontal coordination was provided by Siapas & Wilson (1998) who observed a peak of activity of mPFC neurons up to one second after SPW-R onset. Wierzynski *et al.* (2009) examined the timing of mPFC neurons firing relative to HPC neurons. They found out that cross-covariance between single cells from the two structures was maximal in [0 100ms] window (CA1 leading mPFC). Yet, when excluding SPW-R periods from the analysis, the cross-covariance peak is diminished. The same year, Peyrache, Khamassi, *et al.* 2009 reported cell assemblies within mPFC dur-

ing a set-shifting task (see Box 3.4 for methodological détails). In subsequent SWS sleep, cell assemblies displayed, on average, higher activation strength compared to PRE sleep. Interestingly, activation strength peaked 40 ms after HPC ripples (Figure 3.4b). Furthermore, cell assemblies that appeared during response selection were reactivated prominently. This tight synchronization of ripple onset and mPFC reactivation supports the hypothesis that ripples can trigger reinstatement of neocortical assemblies in a process that would underlie the reorganization and stabilization of neocortical memory traces (Frankland & Bontempi 2005)[4]. Interestingly, similar to the hippocampus, replay of task-related neuronal sequences in the mPFC was observed during sleep (Figure 3.4a; Euston *et al.* 2007). Sequences were also replayed at 6-7 times faster than their sequence speed during behavior, in line with hippocampus compressed replay.

Box 3.4. Reactivation strength

Another current technique for studying reactivation is reactivation strength. This method assesses the similarity of co-firing at a given time during sleep with correlation during WAKE.

$$R_{sleep(t)} = z^T_{sleep}(t) P_{wake} z_{sleep}(t)$$

where $z_{sleep}(t)$ is the z-scored population vector and P_{wake} is a projector that represents correlation during the WAKE epochs. In the simplest case P_{wake} can be the correlation matrix (Girardeau, Inema, *et al.* 2017) even though it takes into account noisy correlation (as in Kudrimoti *et al.* 1999). In search for a better template, Peyrache, Khamassi, *et al.* 2009 used Principal Component Analysis (PCA) and Lopes-dos-Santos, Ribeiro, *et al.* 2013 used Independent Component Analysis (ICA) to extract meaningful correlation from the spike matrix (for more details and discussion about activation strength and PCA/ICA, see Chapter *Methods for cell assembly detection* 2).

3.3.2 Entorhinal cortex

In recent years, several studies investigated reactivation in the Medial Entohinal Cortex (MEC), which project to the hippocampus. Conflicting results have been reported regarding the coordination of hippocampal replay and the activity of grid cells, neurons within the entorhinal cortex that exhibit grid-like place correlation (Ólafsdóttir *et al.* 2016; O'Neill, Boccara, *et al.* 2017). Ólafsdóttir *et al.* (2016) showed that grid cells in deep layer of the Medial

[4] SPW-R modulation of mPFC neurons is also observed in awake offline state. Indeed, ∼35% of mPFC population exhibit excitatory or inhibitory modulation within 200 ms window following SPW-R (Jadhav, Rothschild, *et al.* 2016). Interestingly, distinct population of mPFC neurons were modulated during awake SPW-R and sleep SPW-R, with inhibited responses exhibited mostly during WAKE (Tang, Shin, *et al.* 2017). Moreover, HPC-PFC reactivations were stronger during awake SPW-R compared to sleep and the average activation strength of HPC-PFC cross structural assemblies was higher.

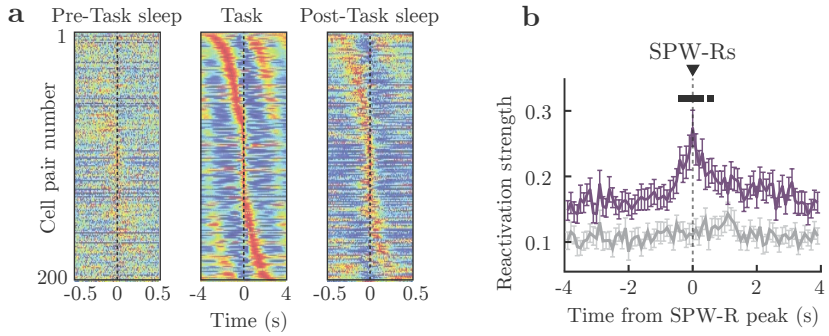

Figure 3.4: Reactivation and replay in the prefrontal cortex. a) Cross correlation between mPFC cell pairs formed during training are preserved during following sleep, in a temporally compressed manner (each row is a cross-correlogram between two mPFC cells shown as a heat map; adapted from Euston *et al.* 2007). Note that only cell pairs showing a peak z score exceeding 11 during the task were included (∼5 to 15%of the total number of cell pairs). Red indicates the highest coincidence rate and blue, the lowest. The time axis during sleep epochs is magnified. b) Cell assemblies reactivation strength in mPFC is increased during SPW-R events in sleep following training (purple) compared to sleep preceding training (gray) on a set-shifting task. The peak correlation occurs 40 ms after the peak of the ripples, indicating that SPW-Rs lead mPFC reactivations. Adapted from Peyrache, Khamassi, *et al.* 2009.

Entorhinal Cortex (MEC) are more active during forward replay events, with a peak of activity at 10 ms. The positions encoded by grid cells lagged 11 ms behind those of CA1. However, in recordings from the superficial layers of the MEC, O'Neill, Boccara, *et al.* 2017 reported independent replay of hippocampal and entorhinal neuronal sequences. Moreover, entorhinal replay was also independent of ripple timing, which is quite surprising given that the superficial MEC is the main input area of the hippocampus. The authors suggested that the EC could act independently in mnemonic processes rather than having a subservient role to the hippocampus. Methodological caveats regarding these two studies have been discussed in Trimper *et al.* 2017. One main issue is that grid cells exhibit regularly spaced spatial receptive fields in all environments and, therefore, coordinated replay between place cells and grid cells may be detected by chance. To account for these issues, recent studies relied on continuous-attactor models to investigate MEC patterns during sleep (Trettel *et al.* 2019; Gardner *et al.* 2019). Authors reported that in the superficial layer of the MEC pairwise correlation of grid cells was preserved during nREM but also REM sleep. However these entorhinal reactivations were not explained by hippocampal theta oscillations nor by the replayed activity in the hippocampal subregion CA1. Thus, the pattern of correlations likely originates within the MEC superficial layers rather than being inherited, through feed-forward projections, from circuitry in the hippocampus. Note that these recent studies (Trettel *et al.* 2019; Gardner *et al.* 2019) are limited to superficial layers and the field would benefit further investigation in the deep layer of the MEC, given the reported methodological caveats of Ólafsdóttir *et al.* 2016.

3.3.3 Sensory cortices

Aside from association cortices, coordinated replay have also been found in sensory cortices. In the visual cortex, sequential activations of neurons recorded in the deep layer of the primary visual cortex are reinstated during sleep, as in the hippocampus (Ji & Wilson 2007; Figure 3.5a,b). Interestingly, the replay of the same trajectories tended to occur at the same time in the hippocampus and the visual cortex. However, even though the authors reported a trend toward hippocampal replays leading those in the neocortex, they were unable to definitively establish the direction of interaction. As opposed to the prefrontal reactivation, authors suggested a bidirectional interaction, with the visual cortex first biasing hippocampal activity, to establish context. In turn, hippocampal replay would then bias the cortical activity towards cortical matching replay. This result is in line with the findings of Sirota, Csicsvari, *et al.* (2003), in the somatosensory cortex. On average neocortical population activity preceded hippocampal discharges and ripples (50 to 100 ms) during non-REM sleep. Similarly, in the Auditory Cortex (AC), Rothschild *et al.* (2017) reported an increase in activity of a sub-population of neurons up to 200 ms prior to SPW-R onset. Moreover, the activity of auditory neurons could predict hippocampal firing during the following ripple while the hippocampal pattern during ripple predicted subsequent AC activity. Interestingly, auditory stimulation could bias hippocampal replay up to 15 seconds following a stimulation (see also Bendor & Wilson 2012, for similar results). Sensory cue presentation during sleep in humans plays a causal role in memory-associated reactivation. During slow-wave sleep, participants were re-exposed to the odors (Rasch, Buchel, *et al.* 2007) or the sounds (Rudoy *et al.* 2009) they experienced earlier during a memory task. This 'cueing' significantly enhanced their recall performance afterwards. Overall, neural activity in sensory cortices during non-REM sleep tends to precede and potentially bias hippocampal SWRs and reactivation events, although the communication is likely bidirectional.

3.3.4 Reactivation of emotional memories

Appetitive memories The ventral striatum (vSTR) receives strong input from the hippocampal system and subiculum and is involved in motivational behavior. Hence, Pennartz, Lee, *et al.* 2004 investigated whether reactivation in the ventral striatum exists and its potential coordination with the hippocampus. They demonstrated that cell pairs in rats vSTR were reactivated during slow-wave sleep and that ripple modulated neurons tended to be more reactivated, following a track-running task. Interestingly, reward modulated neurons were more reactivated in vSTR (Lansink, Goltstein, Lankelma, Joosten, *et al.* 2008) and in the ventral tegmental area, another brain area implicated in the reward circuits. (Valdés *et al.* 2015)[5]. In a follow-up study, Lansink, Goltstein, Lankelma, McNaughton, *et al.* (2009) went further by examining cross-structural reactivation of hippocampal and ventral striatal

[5] Even though in the ventral tegmental area, coordination with ripples is restricted to quiet wakefulness and does not occur duirng nREM sleep per se (Gomperts *et al.* 2015)

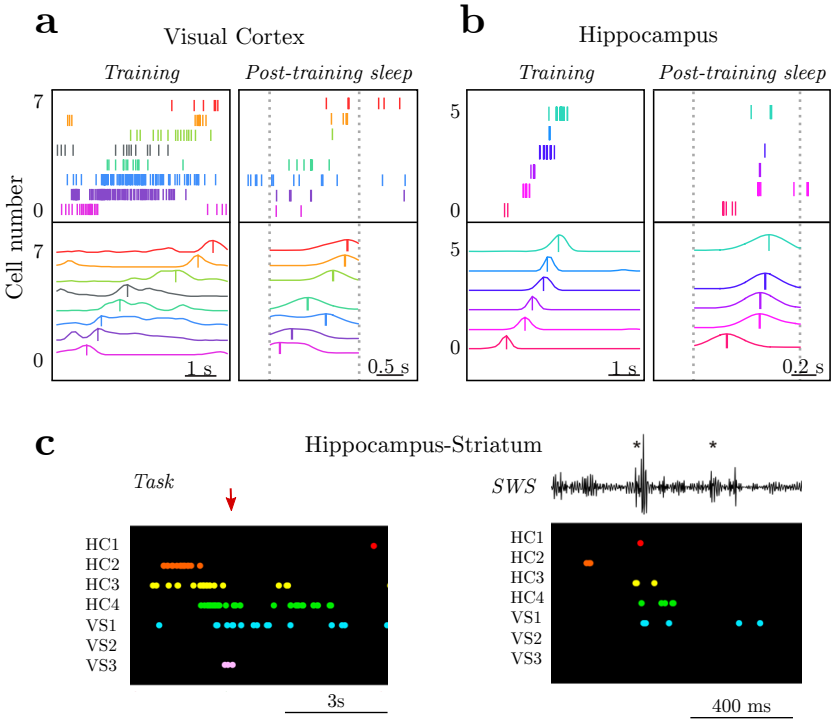

Figure 3.5: Neural reactivations in concert with the hippocampus. **a,b)** Sequential cell activity emerges both in the visual cortex and in the hippocampus during behaviour. Top: example raster plots for a single trial. Bottom: average firing rate for each cell over all trials, ordered according to their firing peak. During subsequent sleep, sequence replays occur in both regions, sometimes in an inter-area temporally correlated manner. Furthermore, in a few cases, joint reactivations represented the same experience. Adapted from Ji & Wilson 2007. **c)** Reactivation of reward-related memories. Left: Example of the firing patterns of simultaneously recorded hippocampal (HC1–HC4) and ventral striatal (VS1–VS3) cells during track running. Each row in the black field represents one cell; its spikes are shown with colored dots. Note that when the rat encounters a reward (labeled with the red arrow), some units of the hippocampus and the ventral striatum co-activate. Only cells that exhibited a place field or a reward-related correlate are shown here. Right: During SWS, the LFP displays large irregular activity intermitted with SPW-R (filtered trace [100–250 Hz]). Identified ripples are indicated with asterisks (*). Several units that were activated during track running were reactivated within a short time period, in concert with SPW-R. Note the different time scales at the left and right. Adapted from Lansink, Goltstein, Lankelma, McNaughton, *et al.* 2009.

neurons. Specifically, striatal reward cells and hippocampal place cells were more likely to reactivate especially if the place field was located just before the reward location. Reactivation occurred in the same order, mostly from the hippocampus to the striatum and was compressed 10 times (from 500 ms during track running to 50 ms in sleep, see Figure 3.5c). In order to test the causality of place-reward reactivations, De Lavilléon *et al.* (2015) used a closed-loop protocol in mice that paired the activity of one place cell with stimulation of the medial forebrain bundle, known to elicit reward signals, in particular via the VTA. Afterward, the mouse, upon awakening, tended to go toward places associated with the artificial reward signal. This suggests that the emotional valence of spatial representations can be updated throughout memory consolidation during sleep

Aversive memories Aversive emotional processing during sleep has been extensively studied in humans but less in rodents (for a review, see Trouche, Pompili, *et al.* 2020). A major structure of interest is the basolateral amygdala (BLA), notably involved in associating the emotional valence of a stimulus (aversive or appetitive) with a sensory and/or contextual stimulus. Recently, Girardeau, Inema, *et al.* 2017, demonstrated that neurons from the dorsal hippocampus and the BLA are conjointly reactivated during sleep. The reactivation decayed within hours. Moreover, BLA ripple-modulated neurons tended to be more reactivated. Interestingly, the reactivation was stronger for the joint patterns representing a threatening pathway (along which an air-puff was delivered) compared to a safe one.
These results suggest that joint reactivations of hippocampal spatially tuned neurons with neurons encoding positive or negative valence of stimuli (in the striatum, the VTA or the amygdala) could potentially support memory consolidation in reinforcement learning paradigms.

3.4 Reactivation of procedural memory traces

Slow-wave sleep has also been directly implicated in the consolidation of motor skills, however the neural mechanisms underlying such processes remain poorly understood, and evidence for reactivation in motor areas is scarce. Still, the reactivation of task-related cell assemblies in the motor cortex during SWS have been reported following neuroprosthetic learning (Gulati, Tsodikov, *et al.* 2014) and a food-pellet grasping task (Ramanathan *et al.* 2015, Eckert *et al.* 2020). Interestingly, sequences of activation of task-related neurons were significantly replayed after learning sessions, but the best results were obtained with large bin size template-matching, suggesting that synchronous activations rather than fine temporal ordering were more relevant (Ramanathan *et al.* 2015). Cell assembly reactivations were tightly locked to spindles, in line with prior studies, suggesting that spindles may mediate offline gains in motor performance (Walker *et al.* 2002). Interestingly, late stage learning was not associated with reactivation. Recently, Eckert *et al.* 2020 suggested that reactivation would occur during post nREM sleep whereas "pre-activation", that is an increased cell assembly activity prior to the task, would occur in REM.

The authors found that coordinated reactivation in both sleep states was beneficial for skill learning in two rats. Replay of neuronal sequences associated with vocal bird song has also been observed during sleep in motor areas of the zebra finch brain (Dave & Margoliash 2000). Even though, some evidence of motor reactivation exists, the field would benefit from further investigations.

Conclusion

Sleep is crucial for certain types of memory consolidation. Respective sleep stages have been suggested to play distinct roles in these processes. The reactivation of synchronous activity and the replay of entire neuronal sequences have been proposed as the neural basis for memory consolidation. Since the seminal works from Pavlides & Winson 1989 and Wilson & McNaughton 1994, reactivation and replay have extensively studied in the hippocampus and several techniques have been developed (e.g. explained variance, template matching etc.). These events can happen during quiet wakefulness, slow-wave sleep and in forward and backward fashion (Foster & Wilson 2006). Importantly, replay events are tightly synchronized with sharp-wave ripples. Several studies suggested that hippocampal replay and ripples orchestrate similar reactivation in connected areas such as the prefrontal cortex (Peyrache, Khamassi, *et al.* 2009) for long-term memory storage or in the ventral striatum and the basolateral amygdala for emotion-place associations (Lansink, Goltstein, Lankelma, McNaughton, *et al.* 2009, Girardeau, Inema, *et al.* 2017). However, in sensory cortices, it is difficult to establish a clear directionality pattern in hippocampal-cortical communication. Reactivation may rather be bi-directional (Ji & Wilson 2007, Rothschild *et al.* 2017). Sensory cortices would first bias hippocampal activity, to establish context, triggering associated hippocampal replay which would then bias the cortical activity towards matching replay. Interestingly, reactivation in the enthorinal cortex takes place, in SWS but also in REM sleep, independently, despite their connections with the hippocampus (Trettel *et al.* 2019; Gardner *et al.* 2019). Finally, a few studies have demonstrated that similar mechanisms could take place in the motor cortex during sleep following procedural learning, in conjunction with cortical spindles (Gulati, Tsodikov, *et al.* 2014, Ramanathan *et al.* 2015, Eckert *et al.* 2020). Thus, reaction of cell assemblies and replay of neural sequences are ubiquitous phenomena within the brain and are presumed to be major neural mechanism underpinning declarative and procedural memories.

Part II

Results

4 Distributed cell assemblies spanning prefrontal cortex and striatum

C Boucly*,[1], V Oberto*,[1], HY Gao*,[1], R Todorova[1], MB Zugaro[1], SI Wiener[1]

[1] Center for Interdisciplinary Research in Biology (CIRB), College de France, CNRS, INSERM, PSL Research University, Paris, France.

* Equal contributions.

Corresponding author: Sidney Wiener, CIRB Collège de France, 11 pl Marcelin Berthelot, 75231 Paris, France. sidney.wiener@college-de-france.fr

Acknowledgements Thanks to France Maloumian for help preparing figures, and to Marie-Annick Thomas and Suzette Doutremer for training and advice for histology. Nicole Quenech'du and Jérémie Teillon for advice and training for image processing. Thanks to Drs. M. Khamassi, C. Lansink, and C. Lena for helpful suggestions. Support came from French National Research Agency ANR-2010-BLAN-0217-01 Neurobot, French Ministry of Research, Collège de France, MEMOLIFE Laboratory of Excellence, Paris Science & Letters Research University, Paris.

Submitted to Nature Communications

Abstract

Highly synchronous neuronal assembly activity is deemed essential for sensory, motor, and integrative processes. These would require the coordination of multiple brain areas, even though assemblies have typically been observed only in single structures. Here, for the first time, we demonstrate distributed assembly activation in a cortical-subcortical pathway. The assemblies spanned functionally distinct sub-regions of rat medial prefrontal cortex and striatum at high synchrony (∼10 ms). They emerged when members shifted their firing phase relative to ongoing 4 Hz and theta, in association with high gamma oscillations. Weak behavioral correlates dispersed among single neurons could coalesce into potent assembly codes for impending choice, reward, or rule order. Thus, cell assemblies are a more general coding mechanism than previously envisioned, linking distributed cortical and subcortical areas at high synchrony.

4.1 Introduction

Complex brain functions have long been proposed to be mediated by the concerted action of groups of neurons ('cell assemblies', Hebb 1949; Buzsáki 2010). Yet, experimental evidence for this remains scarce. While coordinated neuronal firing has been reported in some cortical areas (see, e.g., Harris *et al.* 2003, Uhlhaas *et al.* 2009; Peyrache, Khamassi, *et al.* 2009), this has rarely been observed in subcortical areas (Trouche, Koren, *et al.* 2019; Lansink, Goltstein, Lankelma, Joosten, *et al.* 2008). Further, the reported time scales of coordination have generally been one or two orders of magnitude above those required for neuronal communication or plasticity mechanisms (e.g., post-synaptic membrane time constants, Koch *et al.* 1996 or spike timing dependent plasticity rules, Markram *et al.* 1997; Magee & Johnston 1997), challenging their functional relevance. Conversely, there is little evidence for distributed synchrony, i.e., neuronal assemblies spanning multiple areas and co-activated at a fast (10 ms) time scale (Deolindo *et al.* 2018)

A candidate system to study distributed synchrony in cortical-subcortical areas is the cortico-striatal pathway. The convergence and overlap from multiple cortical areas (Haber 2016) raises the question of whether and how precisely cortical and striatal neurons can be synchronized while integrating information across hierarchical and functional territories (Alexander *et al.* 1986). Of particular interest are the functionally distinct dorsal and ventral zones of the medial prefrontal cortex (PFC) of rats, and their ventral and medial striatal (STR) projection zones.

One potential mechanism for achieving precise temporal coordination in distributed cell assemblies is phase locking to oscillations of brain activity (Fries 2015). Indeed,previous studies have shown that neurons are synchronized to regular rhythms in PFC(Benchenane *et al.* 2010; Fujisawa & Buzsáki 2011) and in STR (DeCoteau *et al.* 2007;Van Der Meer & Redish 2011), as well as synchrony between cortical and striatal oscillations(Donnelly *et al.* 2014; von Nicolai *et al.* 2014; Catanese, Carmichael, *et al.* 2016).

Here we demonstrate that groups of PFC and STR neurons fire synchronously at high precision. Surprisingly, these cell assemblies integrate neuronal activity from sub-regions of both PFC and STR which have generally been considered functionally distinct. Assemblies emerged as individual neurons shifted their preferred phase relative to ongoing rhythms. They had robust behavioral correlates that appeared weakly

or not at all in their members, and assemblies were reactivated during sleep, indicating that they were endogenously generated, and not simply driven by behavioral events.

4.2 Results

Cortical and subcortical neurons form cross-structural assemblies

We performed large-scale simultaneous recordings in medial PFC and downstream medial and ventral STR neurons (Supp. Figure 4.7, Supp. Table *1*) of rats performing a task designed to engage these structures (Ragozzino 2007, Floresco *et al.* 2006, Oualian & Gisquet-Verrier 2010, Hart *et al.* 2014; Bissonette & Roesch 2015). To test for coordinated activity between PFC and STR, we first performed a combined principal and independent component analysis (PCA-ICA). This identified numerous stereotyped spiking patterns spanning both structures at a time scale consistent with cross-structural communication (Figure 4.1a,b; Supp. Table *2*). To quantify this time scale, we systematically varied the time windows analyzed. Unexpectedly, most (70%) of these motifs persisted for time windows as brief as 10 ms (Supp. Fig. 4.8), indicating that they formed cell assemblies (Harris 2005).

Of the 74 detected assemblies (containing 2 to 16 members, mean=6.8 ± 3.1 cells; see Supp. Table *2*), approximately half were cortical-subcortical, spanning both STR and PFC ('STR + PFC', n=32; e.g., Figure 4.1a, assemblies 1 and 3). While the remaining half were detected in only a single structure ('STR-only', n=33; Figure 4.1a, assembly 4; 'PFC-only', n=9; Figure 4.1a, assembly 2), this generally occurred when very few neurons (one or two) were recorded in the other structure (Supp. Table 2), suggesting that most assemblies might in fact span both structures.

Another unforeseen result was that in almost all sessions, assemblies included neurons of functionally distinct sub-regions of both PFC and STR (83% sessions for dorsomedial and ventral STR, Figure 4.1a, assembly 4; 85% sessions for dPFC and vPFC, Figure 4.1a, assembly 2; counted for sessions with >2 neurons in each structure).

To further investigate the synchrony of assembly members at a fine time scale, we cross-correlated spikes of PFC-STR neuron pairs. Incidences of STR spiking were significantly elevated in a [-15, 30] ms window around PFC spikes (shaded gray area in Figure 4.1c, left).
The cross-correlograms were significantly asymmetric (median asymme-

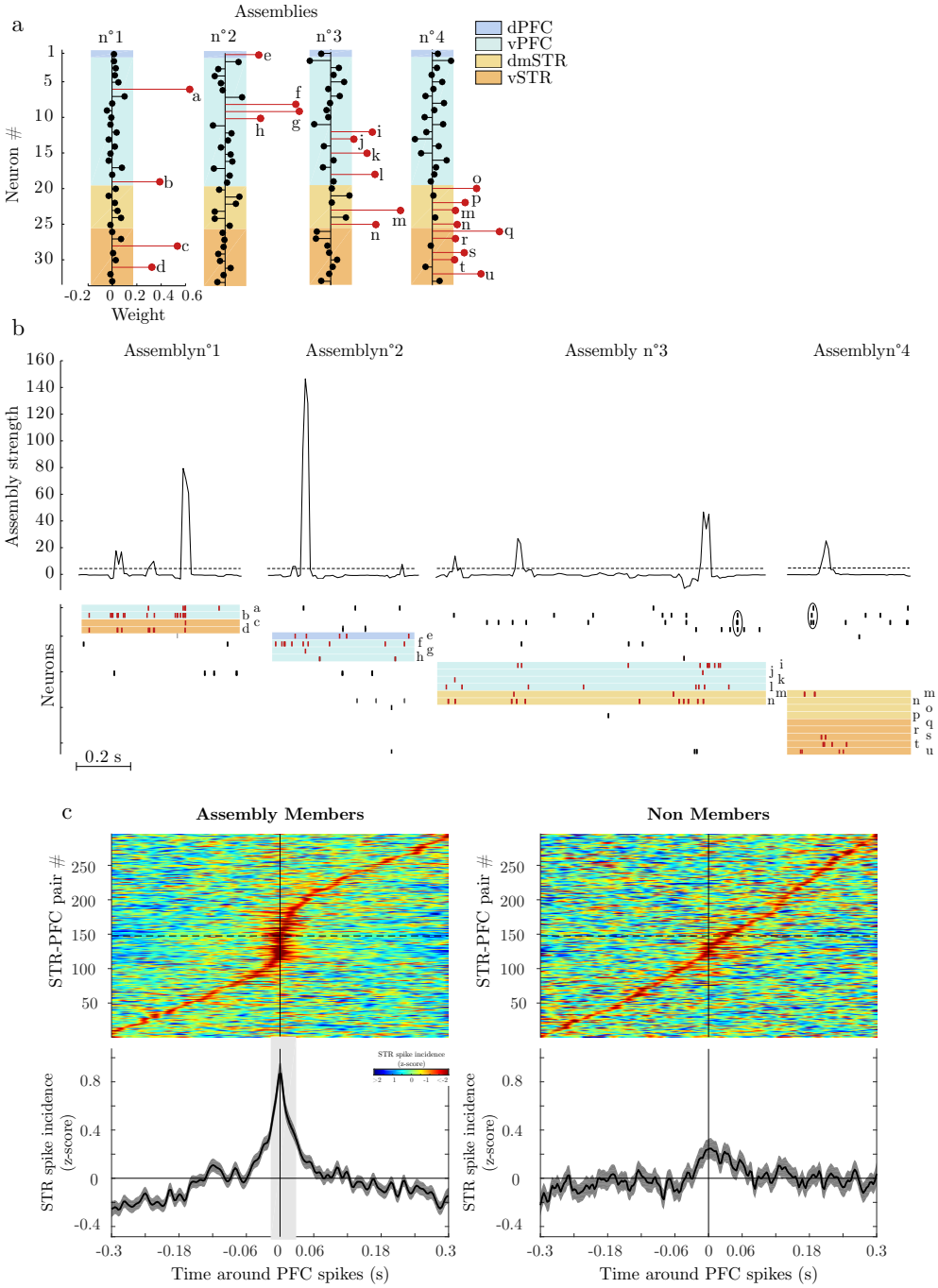

Figure 4.1: Assemblies of STR and PFC neurons.

Figure 4.1: a) The four assemblies exceeding the Marčenko-Pastur threshold (cf., Supp. Fig. 4.8a) in a representative session. Assembly 'members' (red 'lollipops') exceeded the ICA weight threshold ($abs(1/\sqrt{N})$: lateral edges of colored bars). Infralimbic and prelimbic cortex (IL and PL) are grouped together as 'vPFC' while cingulate cortex (Cg1) is labelled 'dPFC'. Core and shell zones of the nucleus accumbens are grouped together as 'vSTR'. dmSTR is dorso-medial striatum. **b)** Examples of assembly activations. Cells are identified by letters (re-ordered from panel a) to highlight the respective assemblies. The dashed horizontal lines indicate the activation strength threshold. Color-code and identifying letters are the same as in panel a. **c)** Cross-correlations of STR-PFC cell pairs from all cross-structural assemblies. Top: Color raster plots ordered by the onset of the peak z-score value (3 ms bins). Bottom: Averages of the above data (shaded area: $p<0.05$, Monte-Carlo bootstrap). The bin width selected for assembly detection here was 30 ms (cf., Supp. Fig. 4.8e). Left: All neuron pairs that were both members of the same assembly. Right: CCRs of randomly selected pairs of neurons that were not members of the same assemblies.

try index = 0.1; Wilcoxon sign rank test p = 6.9e-27), consistent with PFC neurons driving STR neurons during assembly activations. No significant peak was detected in cross-correlations between pairs of PFC and STR neurons that were not members of the same assemblies (Figure 4.1c, right; the non-significant bump at zero could be due to pairs belonging to undetected assemblies).

Assemblies emerge as member neurons shift phase to align with brain rhythms

Prefrontal assemblies form during bouts of synchronous theta oscillations in hippocampus and PFC (Benchenane *et al.* 2010), suggesting distributed PFC-STR assemblies could also emerge from phase realignment with ongoing rhythms (Fries 2015). In a T-maze task, two principal bands dominated the LFPs (Figure 4.2a,b, right columns). Consistent with synchronization of cells by oscillatory rhythms (Supp. Fig. 4.9c), nearly half of the assemblies were phase locked to 4 Hz (∼40%) or theta (∼50%) (Figure 4.2d,e; whether they included neurons from only one or both structures, Supp. Table *3*). Notably, oscillatory power and coherence were significantly elevated on delimited segments of the maze requiring distinct behaviors and cognitive processes (on the central vs. return arms for 4 Hz or theta respectively; Figure 4.2a,b and Supp. Fig. 4.9b). A Granger analysis revealed that PFC oscillations led STR at both 4 Hz and theta (Figure 4.2c), again consistent with the uni-directionality of monosynaptic PFC-STR projections (although, alternatively, PFC and STR could receive common inputs). Note that although analyses below refer to PFC oscillations, results were similar with reference to STR oscillations (not shown).

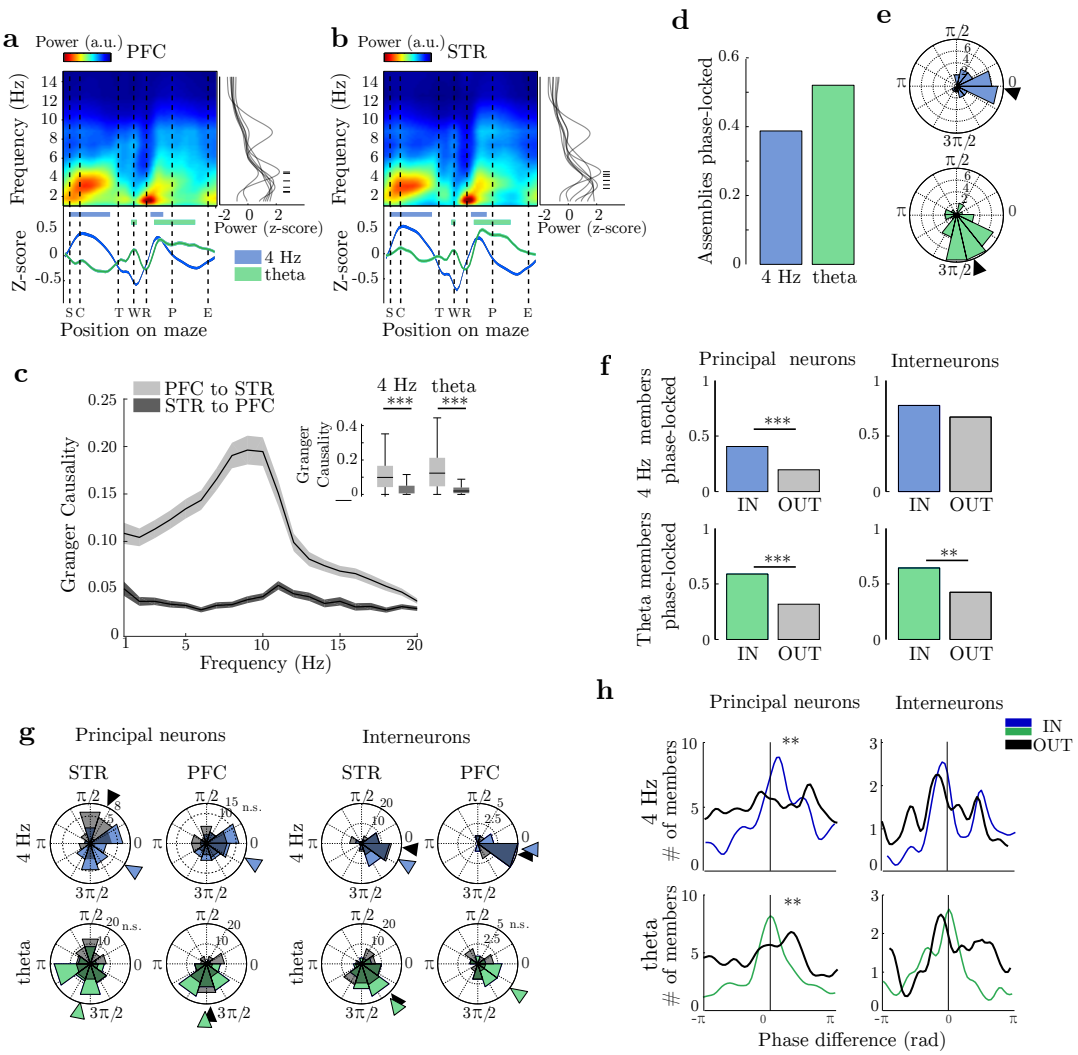

Figure 4.2: Assemblies and their members are modulated by 4 Hz and theta oscillations. **a,b)** Mean spectrogram (top) and 4 Hz and theta power (bottom; linear scale) distributions on a linearized projection of the maze (S-Start point; C-Cue onset; T-Turn; W-Reward photodetector; R-Reward site; P-Cue off; E-Trial end; cf. Figure 4). Horizontal color-coded bars indicate maze segments with significantly higher z-scores ($p<0.05$, Monte Carlo bootstrap). Right panels: Average power of the spectrograms for each rat (gray traces) and overall average (black trace)from data recorded in the central arm. Hashmarks show modes for the respective rats. The color scales are linear. **c)** Average Spectral Granger Causality between PFC and STR LFPs of all session data. Inset compares the two directional values for 4 Hz (Wilcoxon sign rank test: p=1.9e-79) and 8 Hz (p=9.8e-77, n=20 sessions for each). Horizontal bars represent the median, boxes indicate the 25th and 75th percentiles, and whiskers are minimum and maximum values. **d)** Proportions of assemblies phase-locked to 4 Hz and theta bands in data from all sessions (n=74 assemblies).

Figure 4.2: e) Distribution of the mean phases for all assemblies significantly phase-locked to PFC 4 Hz or theta oscillations. Arrowheads indicate the distribution means. For assemblies phase locked to 4 Hz, Rayleigh test: mean angle m=0 rad, p=7.2e-06; for theta, Rayleigh test: m=-1.3, p=1.3e-06. **f)** Proportions of principal and interneuron members phase-locked during oscillation cycles with assembly activations (IN) and those without (OUT) (binomial tests: 4 Hz p=1.0e-04 and 0.17; theta p=9.7e-08 and 3.8e-03, respectively). **g)** Distributions of the mean phases of phase-locked members IN (color) and OUT (gray). Arrowheads mark significant distribution means(Rayleigh test: $p<0.05$). h) Distribution of the differences between mean phase angle of each assembly (at zero) and the mean for each individual phase-locked member IN (color) and OUT(gray). Kuiper test (comparison of two circular distributions): 4 Hz p=0.001 and 1; theta p=0.002 and 1, respectively for principal neurons and interneurons. See Supplementary Table *4* for detailed circular statistical results.

We predicted that assembly activations would be dynamically associated with phase locking of individual members, and thus tested for this. For both 4 Hz and theta, oscillatory cycles containing assembly activations ('IN') were compared to all other cycles ('OUT'). As predicted, substantially more assembly members were phase locked to 4 Hz and theta during 'IN' cycles (Figure 4.2f; except for interneurons at 4 Hz). These results were replicated in an independent analysis based on pairwise phase consistency (Supp. Figure 4.9d). Furthermore, during IN cycles, both STR and PFC principal neuron members were phase-locked to the average preferred phase of the assemblies (compare Figs. 4.2e and g), contrary to OUT cycles (Figure 4.2g). (Down-sampling the number of data points to balance them across conditions yielded the same results; not shown). Thus, on average principal neurons shifted their preferred phase to the overall mean phase of assembly activation. We further tested whether members shifted to the phase of their respective assemblies, even when taking into account variations in the latter's preferred phases. While this did occur for principal neurons of both STR and PFC, for both 4 Hz and theta (Figure 4.2h), interneurons, on the other hand, remained at the assemblies' preferred phases during both IN and OUT cycles (Figure 4.2h). This was not due to analyzing only phase-locked members: the same result was observed using all assembly members (Supp. Fig 4.9e). Overall, this suggests that entrainment of principal neurons to a common preferred phase is crucial for assembly formation.

Both 4 Hz and theta modulated gamma oscillations in STR (Figure 4.3a), which, in turn, could help govern precise synchrony among PFC and STR neurons. Several frequency bands were modulated by 4 Hz or theta oscillations (including 'gamma-50' at 40–70 Hz, and 'beta' at 15–35 Hz), but only 'gamma-80' (70-100 Hz) was modulated at a phase near that of the assemblies, and thus was analyzed further (cf., Figures

4.2e and 4.3a). Assembly activations were more frequent during gamma-80 bursts (Figure 4.3c), and reciprocally, in cycles containing assembly activations there were more gamma-80 bursts (and higher gamma-80 power, not shown; Friedman test, $p<0.05$).

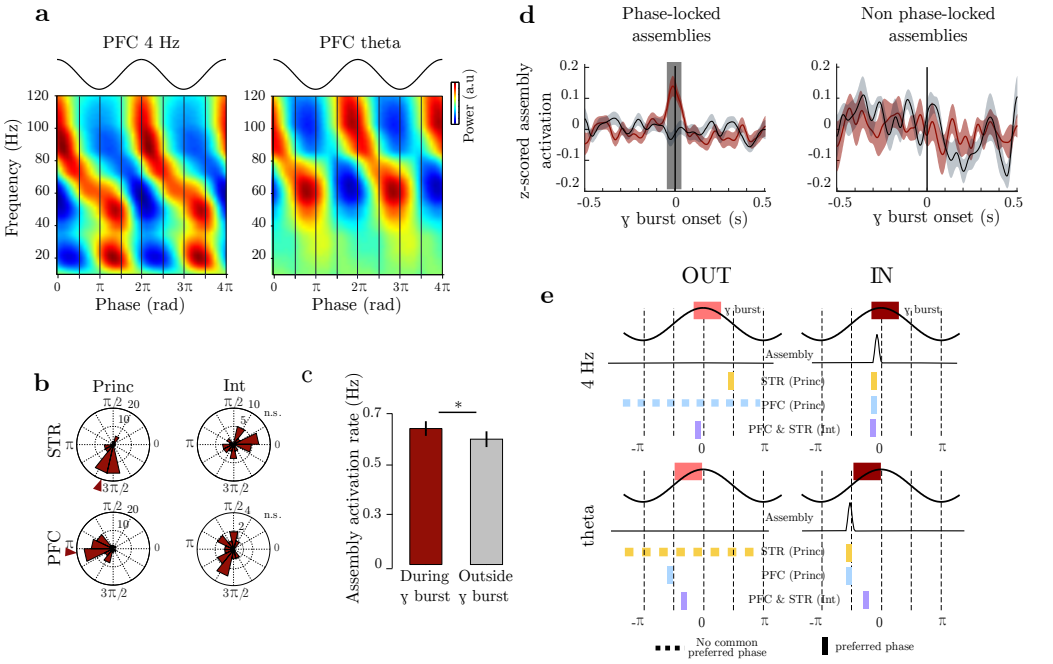

Figure 4.3: Gamma-80 oscillations and synchrony. **a)** Average PFC 4 Hz and theta LFP modulation of higher frequency bands of PFC LFPs (n= 20 sessions). **b)** Distributions and preferred angles of phase locking to PFC gamma-80 in all STR and PFC principal neuron and interneuron members. Arrowheads indicate significant mean angles (n.s.: not significant). **c)** Activation of assemblies is greater within than outside of gamma-80 bursts (Wilcoxon signed-ranktest, p=0.043, n=74 assemblies). **d)** Mean (traces) and SEM (shading) of PETHs of assembly activations triggered at the onset of gamma-80 bursts for assemblies phase-locked to 4 Hz and/or theta Hz (left; n=52), and others with no 4 Hz or theta phase-locking (right; n=22) (red: during gamma bursts; gray: outside of gamma bursts; shaded vertical bar: $p<0.05$, Monte-Carlo bootstrap). **e)** Summary of alignments of the respective phase relations OUT vs. IN for 4 Hz and theta.

More precisely, 4 Hz and theta phase-locked assemblies were tightly synchronized with gamma burst onsets (Figure 4.3d; Supp. Figure

4.9a), but this was not the case for assemblies with no phase locking. This is consistent with the hypothesis that gamma-80 onset facilitates assembly member synchrony.

Gamma-80 phase-locking of PFC principal neuron members differed from that of STR principal neuron members by a quarter of a cycle (corresponding to 3 ms, Figure 4.3b), consistent with tight coupling, and on the order of the time scale of the PFC to STR conduction time (Fino *et al.* 2005). The timing of assembly activation relative to 4 Hz, theta and gamma-80 is summarized in Fig. 4.3e.

Functional correlates in cortico-subcortical assemblies

Cell assemblies are expected to underlie some brain computation or cognitive function, possibly beyond that of their individual members. We thus investigated the functional correlates of the cross-structural assemblies. In a flexible decision task (Figure 4.4a), 31% of the 74 assemblies were preferentially activated on limited segments of the maze corresponding to different behavioral and cognitive aspects of the task (Figure 4.4d-f, top row, 4.4g and 4.4j) such as decision-making and reward approach. These spatial correlates were often modulated by other behavioral factors, such as left vs right choice or rewarded vs non-rewarded choice (see Figure 4.4j and Supp. Figure 4.10). The rats alternated between two goal-directed tasks in a T-maze (Figure 4.4a). First animals performed a visual discrimination task (VD1), then a spatial discrimination (SD), and finally the visual task again (VD2; Figure 4.4b,c). Assemblies were selective for 'task conditions' (VD1, SD, VD2; Figure 4.4e,f). Interestingly, more assemblies discriminated between repetitions of the same task (VD1 vs VD2) than between different tasks (SD vs VD1, or SD vs VD2; Figure 4.4e, f and i), and these were distinctly distributed on the maze (Figure 4.4h). This did not result from linear drift in firing rate during the sessions, or behavioral parameters such as reward arm choice, speed, or vicarious trial and error behavior (see Methods 4.4, and Supp. Figures 4.11 and 4.12).

To assess whether behavioral correlates of assemblies merely derived from those of their members, or whether more complex integration took place, we first determined the selectivity of individual members. Substantial numbers of individual STR and PFC neurons fired selectively for several trial characteristics, including reward arm choice (left or right), reward outcome (Figure 4.5e, Supp. Figure 4.10), and between task conditions (Figure 4.5a-d, Supp. Figure 4.13).

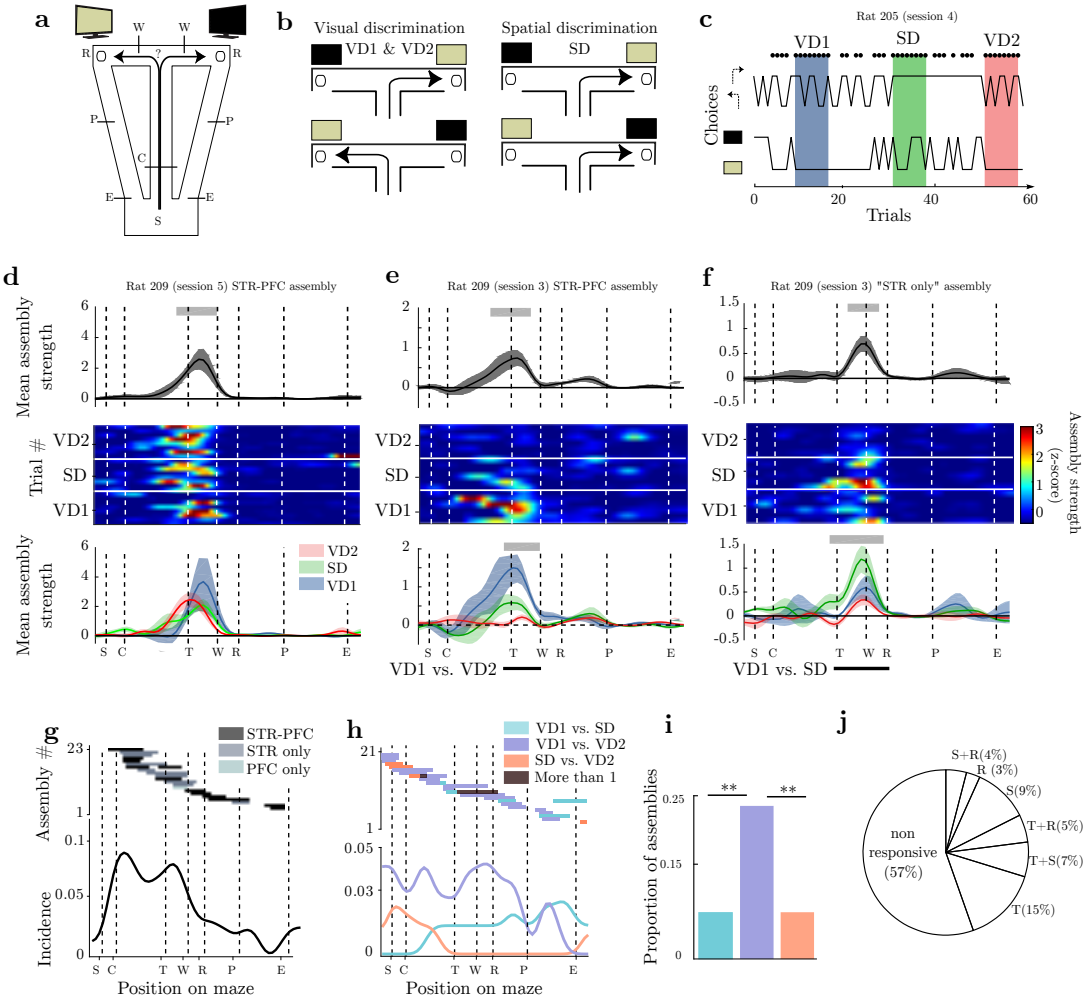

Figure 4.4: STR-PFC assembly activations are behaviorally selective. **a)** In this completely automated T-maze, rats self-initiated trials by crossing a photo-detector C near the beginning of the central arm to trigger visual cues on two TV screens behind the reward arms (in pseudo-random sequence). Following correct choices, a photo-detector W on the reward arm triggered release of a sweetened liquid reward at a reward site R. S- trial start point; P- photo-detectors triggering cues off; E- trial end point. **b)** In the VD task, the screens indicated the rewarded arm, while in SD, the rat's non-preferred arm (right or left) was rewarded, irrespective of the cue screens. **c)** Behavioral responses during a representative session. Dots above indicate rewarded trials. The upper and lower traces track performance for the SD or VD contingencies. Color-shaded zones indicate criterion performance trials. The rule was changed after criterion performance was reached.

Figure 4.4: d,e,f) Example assembly activations on a linearized projection of the maze. Top row: Mean (traces) and SEM (shading) of activation strengths over the entire session.Significant deviations from baseline are marked by light gray shaded rectangles ($p<0.05$, Monte-Carlo bootstrap). Middle row: z-scored assembly activation strengths for each trial during the three task conditions. Bottom row: Mean (± SEM) assembly activation strengths in the respective task conditions. **d)** An assembly active during reward arm selection but with no significant differences between task conditions. **e)** A task-order selective assembly (shaded region indicates where activity was higher during VD1 than VD2). **f)** An assembly selective for the SD rule (vs. VD1 and VD2). **g)** Distribution of assembly selectivity for maze segments (horizontal bars; Monte Carlo bootstrap $p<0.05$). Bottom) Summary histogram. Incidence is the fraction of assemblies selective for each spatial bin. **h)** Maze distribution of task condition selectivity of assemblies.

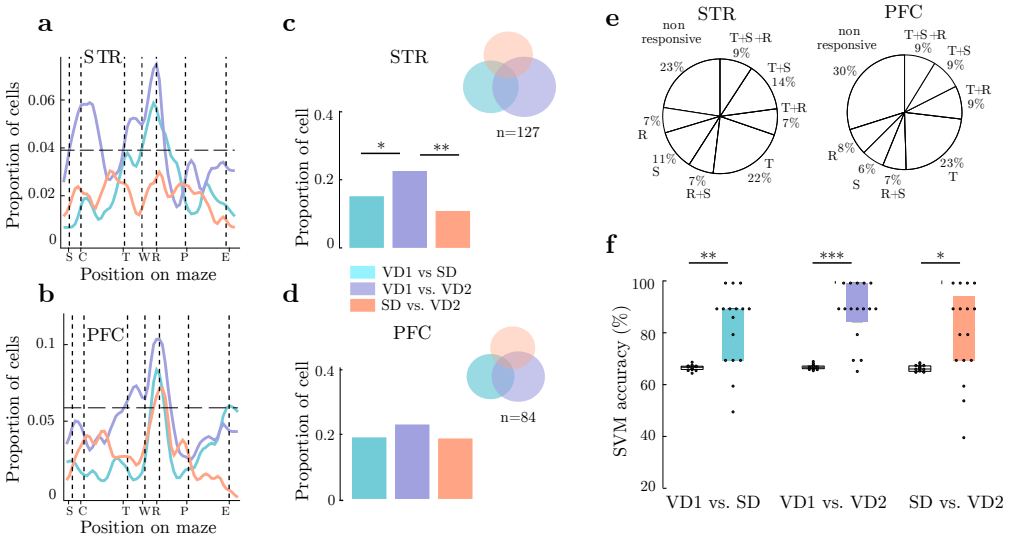

Figure 4.5: Behavioral correlates of STR and PFC neurons. a,b) Distributions of significant task condition differences of single neurons along the linearized maze (cf., Supp. Fig. 4.13 for details). The horizontal dashed lines represent the 95% confidence limit for uniform data. **c,d)** Proportions of cells selective for each task condition comparison (binomial tests: p=0.02, 0.13, 2.1e-4, and p=0.31, 0.79, 0.20, respectively for STR (n=295) and PFC (n=185). Upper right: Proportions of cells (areas of circles) selective for single and multiple task condition comparisons. **e)** Behavioral correlates (same abbreviations as Fig. 4.4j). **f)** Support vector machine models trained on STR population activity successfully classify task conditions. The SVM prediction accuracies (color-coded boxplots) are significantly higher than those for randomized data sets (white boxplots to the left) (Wilcoxon signed-rank test: VD1 vs SD; p =0.0027; VD2 vs SD, p=0.02; VD1 vs VD2,p=0.0008, n=16 sessions). Each point represents one session.

Among the three task condition comparisons, VD1 vs VD2 firing rate differences were predominant, but only in STR neurons (Figure 4.5c,d). Firing rate differences between task conditions had characteristic distributions on the maze (Figure 4.5a,b; corrected for linear drift, Supp Fig. 4.11b), and a support vector machine model (SVM) trained on STR neuronal activity reliably classified the ongoing task conditions, including VD1 vs VD2 (Figure 4.5f; this was also found for PFC: Supp. Figure 4.14). Not surprisingly, many of these behavioral correlates mirrored those of assemblies (compare Figures 4.4 and 4.5; e.g. Figure 4.6b 'reward' and 'spatial'; data summary in filled bars in Figure 4.6e).

To control that this overlapping selectivity between assemblies and their members was not coincidental, behavioral correlates were randomly re-assigned among simultaneously recorded cells (members and non-members). The actual ('real') members shared selectivity with the assembly significantly more often than the randomly assigned groups (Figure 4.6e). On the other hand, members could be selective where assemblies were not (e.g., Fig 4.6b, 'Side', 'VD1 vs. VD2'), consistent with our hypothesis that assemblies may not merely reflect the properties of their members.

Indeed, assemblies appeared to express behavioral correlates for which none of their members showed significance (e.g., Fig 4.6b, 'VD2 vs SD'). We thus tested for a relationship between non-significant members and their assembly's behavioral correlate. We selected cell assemblies that significantly discriminated between alternative trial characteristics (e.g., VD1 vs. VD2, rewarded vs. unrewarded choice, leftward vs. rightward choice, or positions on the maze), and focused on their members that did not. In order to investigate a possible 'trend' across these members, we measured the difference in firing rates between the pairs of trial characteristics. As a control, we also measured their differences in firing rates at randomly selected locations on the maze. The resulting distributions (trends vs controls) were significantly different (Figure 4.6f; Supp. Figure 4.15, confirming that mere trends for behavioral correlates in individual neurons could be detected as significant events at the population level. This supports the hypothesis that cell assemblies can bring forth behavioral correlates reflecting non-significant tendencies in their individual members.

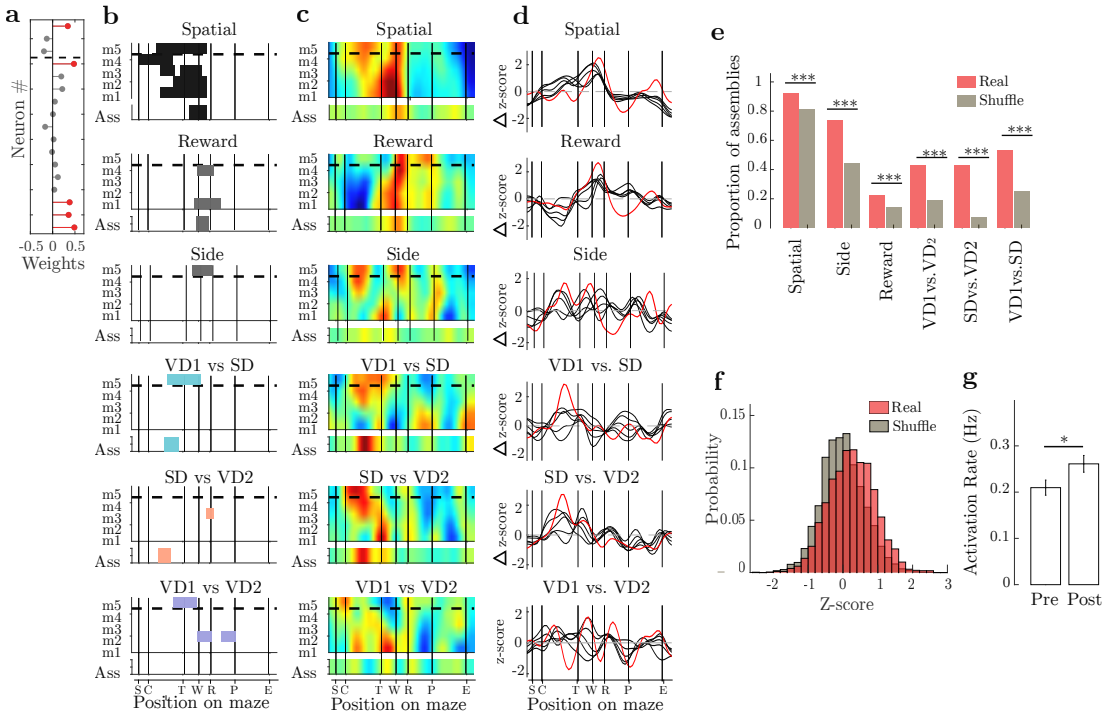

Figure 4.6: Comparison of behavioral correlates of assemblies and their members. a-d) Comparison of behavioral correlates of a representative assembly (Ass) and its members (m).a) Lollipop plot of strengths of the members. Dashed lines separate PFC and STR neurons in a, band c. b) Significant behavioral correlation of the assembly and its members (Monte Carlo bootstrap, $p<0.05$). 'Reward' indicates significant differences between rewarded and unrewarded trials. 'Side' indicates significant differences between leftward and rightward choice trials. 'Spatial'indicates activation on certain maze segments (shown as z-score in c and d). c and d) Z-scored differences in assembly activation rates and member firing rates (except z-score for 'Spatial').Color code scales range from -0.5 to 5 for assembly activations and -2 to 2 for members. e) Test for whether the same correlates in members and assemblies is coincidental. Proportion of assemblies sharing the same selectivity as at least one member, for the actual data ('Real') and for the random shuffles of weights among the members (binomial test $p<0.001$). f) Testing for firing rate changes in non-significantly correlated members for the same behavioral correlate of the assembly.

Figure 4.6: Pooled distribution of the z-scored activity differences between the pairs of trial characteristics of all behavioral correlates (e.g., leftward vs. rightward choices, VD2 vs SD) vs. the z-scored distribution of differences for the same cells, but at randomly selected locations (Wilcoxon signed rank test: p=6.3e-46). Positive z-scores indicate that activity changes of members for the same comparison and in the same direction as the assembly. g) Assembly activation rate was greater during post-task (Post) than pre-task (Pre) sleep (Wilcoxon signed rank test: p=1.3e-04,n=59).

Cortico-subcortical assemblies can be internally generated

The above analyses indicate that synchronous activity among neurons did not simply result from common inputs triggered by behavioral events (for instance, the same sensory and motor processes triggered different assembly activation rates in VD1 vs VD2). Yet, a more direct proof would be to show that distributed assemblies also activate in the absence of behavioral events. We thus tested for endogenous assembly reactivation during sleep. Not only did we find assembly reactivation, but in addition PFC-STR assembly activity was significantly higher during post-task sleep than during pre-task sleep (Figure 4.6 g). In individual assemblies, activation rates of 34% of the assemblies significantly increased during post-task sleep relative to pre-task sleep, while they decreased in only 7% (binomial comparison, $p<0.05$; see Supplementary Table *2*). Since reactivation of neural patterns of activity during sleep, including from PFC and vSTR, has been linked with memory consolidation (Maingret *et al.* 2016; Todorova & Zugaro 2019; Lansink, Goltstein, Lankelma, Joosten, *et al.* 2008); this suggests that distributed assemblies could participate in offline memory consolidation.

4.3 Discussion

Here we showed highly synchronous cortical-subcortical neuronal assemblies. Not only did these assemblies unexpectedly include members from hierarchically distinct brain areas (cortex vs non-cortex), they also integrated members from functionally diverse and reportedly distinct loops in the cortico-striatal pathway. Assemblies emerged when spikes of principal neurons shifted in phase relative to 4 Hz and theta, and were accompanied by increased gamma activity. Assembly activations were associated with specific behavioral components of a set-shifting task. In many cases, assemblies amplified non-significant firing trends of individual members, bringing forth significant behavioral correlates. Finally, assemblies were selectively reactivated during sleep after behavioral sessions, indicating that they were independent of specific behavioral inputs and that they could be involved in memory consolidation processes.

Distributed assemblies coordinate functionally distinct sub-regions at a precise time scale

Distributed cell assemblies included members from PFC and STR, extending beyond previous observations of assemblies confined to PFC (Peyrache, Khamassi, *et al.* 2009; Sakurai, Nakazono, *et al.* 2013) or to rare reports of synchronous activation in STR (at the cell pair level: Pennartz, Lee, *et al.* 2004; Lansink, Goltstein, Lankelma, Joosten, *et al.* 2008; at the assembly level: Trouche, Koren, *et al.* 2019). In such studies, the time bins ranged from 25 to 100 ms. However, for coincidence detection in downstream readers (Buzsáki 2010), convergent inputs from assemblies must be in brief time windows on the order of 8 ms (Roy & Alloway 2001), consistent with our observations. This fine time scale of distributed synchronization could support binding of information processed by distinct brain areas (Engel, Fries, *et al.* 2001).

Here, assemblies bridged STR and PFC sub-regions with markedly distinct functions ranging from associative learning to goal-directed behavior (Alexander *et al.* 1986; Hart *et al.* 2014; Ito & Doya 2015; Sierra-Mercado *et al.* 2011). The wealth of evidence indicating that PFC and STR sub-regions execute distinct functional processes does not preclude the possibility of precisely timed cooperation by these 'complementary', or even 'competing', structures. Membership in assemblies by neurons from functionally distinct prefrontal and striatal subregions could be related to the overlapped interconnections among these areas (Mailly *et al.* 2013; Haber 2016) or common inputs (e.g., from hippocampus, dopaminergic nuclei).

Interestingly, assemblies also included interneurons, which could contribute either directly via both local and long-range projections, or indirectly by silencing competing assemblies (Stark *et al.* 2015, Geisler *et al.* 2007). Indeed, the PFC projection to STR medium spiny neurons is a feed-forward loop going through parvalbumin fast spiking interneurons.

Hebb (1949) postulated that strengthening of excitatory synaptic connections among members would help give rise to cell assemblies. Because the vast majority of striatal neurons are inhibitory and have sparse local connectivity (Koos *et al.* 2004), it seems unlikely that cell assemblies could emerge only from local striatal circuit interactions. Instead, consistent with the known anatomical projections (Mailly *et al.* 2013), conduction delays (Fino *et al.* 2005), and computational simulations (Humphries *et al.* 2009; Ponzi & Wickens 2012; Carrillo-Reid *et al.*

2008), timed prefrontal inputs could leverage synchronous striatal activity and/or oscillatory coherence with striatum for distributed assembly activations. Our data are consistent with PFC monosynaptically driving the STR during assembly activations since PFC and STR neurons fire synchronously at time scales as brief as 10 ms. This is also consistent with greater PFC to STR (than STR to PFC) results of the Granger analysis, as well as the asymmetry of the cross-correlograms.

Brain rhythms may synchronize cortico-subcortical assemblies

The communication through coherence hypothesis (Fries 2015) postulates that cross-structural communication is facilitated when their respective local oscillations are synchronized, concentrating spike activity into brief temporal windows. Here, several rhythms strongly modulated the assembly activations as well as spike timing of their members. These diverse rhythms could exert parallel, alternating and/or interacting influences to orchestrate brain network activity. Furthermore, the highest amplitudes of 4 Hz and theta LFPs were at different locations on the maze (choice point vs post-reward), and these are associated with respectively different cognitive processes. Indeed, 4 Hz has been described in coupling with amygdala, dopaminergic nuclei, and respiratory coordinating signals (e.g., Fujisawa & Buzsáki 2011; Karalis *et al.* 2016; Carmichael *et al.* 2017) while theta rhythms in PFC and STR could be related to hippocampal theta (Tabuchi *et al.* 2000;Jones & Wilson 2005; DeCoteau *et al.* 2007; Benchenane *et al.* 2010; Van Der Meer & Redish 2011). Moreover, during spatial exploration, theta rhythms synchronize the hippocampus and the vSTR, whereas during lever presses, vSTR is dominated by a transient low frequency rhythm from the PFC (e.g, Gruber *et al.* 2009; see also Stenner *et al.* 2015). This is consistent with diverse rhythms recruiting distributed assemblies in relation to ongoing behavioral challenges. While some assemblies are synchronized by 4 Hz and/or theta, others may well depend on other mechanisms, perhaps involving other frequencies such as 20 Hz (Howe *et al.* 2011).

Several results here point to gamma-80 oscillations as a more precise synchronizing influence. Indeed, gamma oscillations have been proposed to shape the formation of cell assemblies (Gray & Singer 1989; Engel, Fries, *et al.* 2001; Buzsáki 2010). The one-quarter cycle (3 ms) difference of phase locking of STR and PFC spikes to gamma-80 is consistent with the strong synchrony of the onset of gamma-80 bursts in PFC and vSTR LFPs with PFC leading (Catanese, Carmichael, *et al.* 2016), although the phase lag there averaged only 0.59 ms. While the origin of many rhythms in STR and PFC remains unclear (Carmichael *et al.* 2017, Tort,

Ponsel, *et al.* 2018), their modulation of single neurons provides evidence that they are not simply volume conduction artifacts here.

Behavioral correlates of distributed cell assemblies

Previous work has shown rule selectivity in STR and PFC (Asaad *et al.* 1998; White & Wise 1999: Bissonette & Roesch 2015; Sleezer *et al.* 2016). In contrast with rule selective responses, assemblies, as well as individual STR and PFC neurons, had different activation rates in the same task (VD1 vs VD2), and these had a higher incidence than other comparisons. This is consistent with previous PFC population analyses revealing discrimination between repetitions of the same rule later in a behavioral session (Guise & Shapiro 2017; Malagon-Vina *et al.* 2018). This has been only rarely reported in single neurons in STR (Shibata *et al.* 2001).

However, to our knowledge, this is the first report of behavioral correlated activity of assemblies in a distributed cortical-subcortical network. Previous studies of such correlates in single structure assemblies could well represent only a part of more extensively distributed network activity. Indeed, when we observed assemblies limited to a single structure, this generally occurred when there was weaker sampling of the other structure. We propose that cross-structural assemblies are likely to be a general mechanism that extends to other brain areas and networks, and underlie other highly integrated representations.

4.4 Materials and methods

Animals and pretraining

Six male Long-Evans rats (from René Janvier, Genest-St-Isle, weight 350–400 g) were housed on a 12:12-h light-dark cycle, with experiments performed during the day in facilities authorized by the Veterinary Services of the city of Paris (n° B75-05-12). Rats were handled each workday in the experimental room. They were first familiarized with the experimental environment by free exploration of the maze (foraging for scattered pieces of chocolate puffed rice breakfast cereal) for at least three days. When the pre-training and training began, animals were partially water-restricted (10 min per day or more as required) to no less than 85% of their free-feeding weight. All procedures were in accord with local (autorisation d'expérimenter n°75-1328-R; Comité d'Ethique pour l'Expérimentation Animal no. 59 dossier 2012-0007) and international (European Directive 2010/63/EU; US National Institutes of

Health guidelines) standards and legal regulations regarding the use and care of animals.

Surgery

Rats were allowed at least 2 days before surgery with ad libitum water and no training. Rats were deeply anesthetized (xylazine, 20 mg/ml, 0.1 ml intramuscular; sodium pentobarbital, 40 mg per kg of body weight, intraperitoneal, with a 5 mg supplement i.p. every hour as needed). The head was placed in a Kopf stereotaxic instrument, the cranial surface was prepared, jeweler's screws were attached with dental cement reinforcement, and trephination was performed. Then rats were implanted with a custom-built microdrive holding 15 independently movable tetrodes (groups of four twisted 13 µm tungsten wires, gold-plated to 200 kohm). Usually eight tetrodes were placed in the ventral or dorso-medial STR (AP 1.0-2.5 mm and ML 0.8–1.8 mm relative to bregma), and seven in the medial prefrontal cortex (AP 2.5–3.4 mm and ML 0.3–0.9 mm). The implant was secured to the skull screws with dental cement. Miniature stainless steel screws were implanted above the cerebellum as reference and ground electrodes. After surgery, rats were allowed to recover for at least one week with ad libitum food and water, before any further training. The electrodes were then progressively lowered until they reached their targets and then adjusted every day to optimize unit isolation and recording quality.

The automated T-maze with return arms

See Figure 4.4a; cf. Catanese, Cerasti, *et al.* 2012; Wood *et al.* 2000. The experimental chamber was a 3 m diameter cylindrical space, enclosed by black curtains running from floor to ceiling and was lit by a ceiling mounted light bulb. The maze was constructed from matte black painted wood. Maze arms were 8 cm wide with 2 cm high borders. The central arm was 1 m long and the reward arms were each 50 cm long. At the junction of the return arms and the central arm was a return/start zone measuring 35x38 cm. The maze was elevated 70 cm above the floor. The experimental protocol was automated and paced by the rat. As the rat spontaneously crossed a photodetector near the beginning of the central arm ('C' in Fig. 4a), this triggered the display of visual cues on two TV screens (80 cm diagonal; 76 cm above the floor) centered behind the two reward sites. The visual cues were vertical bars (spatial frequency of 0.13 cpd) projected on one screen and horizontal bars on the other, or, in later experiments, to facilitate learning, simply one white and one black screen. Following correct choices, a photodetector on the reward arm ('W') triggered distribution of a saccharinated (0.25%, 30

µl) water reward via a solenoid valve controlled by a CED Power1401 interface (Cambridge, UK) with our scripts. Cues remained on until the rat crossed the photodetector at the middle of the return arm ('P').

Recording, data processing, and spike sorting

Brain signals were pre-amplified (unity-gain headstage, Noted Bt), amplified 500x (Neuralynx L8), acquired and digitized with two synchronized Power1401 systems (CED, Cambridge, UK). To track the position of the animal, two light–emitting diodes were fixed to the front of the head-mounted microdrive. These were detected by an overhead video camera (sampling rate 30 Hz). Off-line spike sorting was carried out with Principal Component Analysis with NDManager for preprocessing (Hazan *et al.* 2006, http://neurosuite.sourceforge.net), and a semi-automatic cluster cutting procedure combining KlustaKwik (K.D. Harris, http://klustakwik. sourceforge.net) and Klusters (L. Hazan, http://neurosuite.sourceforge.net). LFPs were derived from wideband signals that had been down-sampled to 1250 Hz on all channels.

Histology and electrode position verification

To confirm recording sites, electrolytic lesions (cathodal current injection: 30 µA for 30 s) were applied to each tetrode. Two days later, the rats were administered a lethal dose of pentobarbital and were intracardially perfused with saline (0.9%, wt/vol) followed by paraformaldehyde solution (10%, wt/vol). Brain regions of interest were sliced into 40 µm coronal sections and stained with cresyl violet. For 3 of the rats, prior to implant surgery, electrode tips were dipped in fluorescent marking dyes (Sigma-Aldrich). In those cases, half of the histology sections were set aside for fluorescence microscopy observations. Electrode positions were then reconstructed in 3D with the Neurolucida system on the basis of lesion location and the depths the electrodes had been lowered. Only data from electrodes with confirmed recording locations were further analyzed.

Behavioral protocol

During the pre-training phase (10±3 days, mean±SD), the rats were trained to follow forward paths on the T-maze. Backtracking was prevented with manual placement of transparent Plexiglas barriers or a pulley-driven barrier on the reward arms. Rats were trained on the T-maze to acquire and alternate between the two tasks. Daily training and recording sessions consisted of one or two blocks of 20-30 min (the average time to perform one trial was 25±1.5 s). On average, post-

surgery training and recording sessions for a given rat lasted about 90 days. In order to obtain liquid rewards, the rats had to visit the correct arm according to the current rule. Visual cues were displayed on the two screens in pseudorandom order: each screen did not display the same cue more than four times successively. First, in the visual cue task (VD), one cue indicated the rewarded arm, irrespective of whether it was to the left or right (Figure 4.4a). Once the rat reached a criterion of a minimum of 10 consecutive correct trials, or 80% correct choices for the whole session, in the following session training commenced in the spatial discrimination task (SD). In the SD task, reward was provided on only one (right or left) arm, irrespective of the visual cue displays. This was selected as their non-preferred arm, as determined during pre-training. Once the rat reached the same criterion performance as above, the next session started with retraining in a few more VD sessions. Rats were then trained to flexibly switch between the two rules within the same session. Since the rats had found the VD task more difficult (27 ± 5 sessions for VD versus 2.0 ± 0.7 sessions for SD), the rule sequence of all sessions required the rats to first reach criterion (eight consecutive correct trials) in VD (these high performance trials are called 'VD1'). Then the rule was changed to SD and the trials where the rat subsequently performed at criterion level are called 'SD'. Similarly, following the rule change to VD, the next series of criterion performance trials is referred to as 'VD2'. Data from the twenty sessions with criterion level performance in these three task conditions are presented here. There were no significant differences in overall performance between the first and last sessions (Wilcoxon signed-rank, $n=6$ rats, $p=0.0625$). No cue was presented for incorrect trials, and thus the rats learned by trial and error. The current rule was signaled by the presence (SD task) or absence (VD task) of a sound cue (repetition of the Microsoft Windows standard system 'Asterisk' sound) by a loudspeaker in front of the T-maze. The tone went on when the central arm photodetector was crossed and was turned off when the return arm photodetector was crossed. Rule changes were extra-dimensional, that is, between VD and SD. This protocol was designed so that the sensory inputs and motor outputs remained virtually the same in both tasks, permitting distinction of neural activity specific to the cognitive demands of the respective tasks.

Sleep Detection

Each behavioral recording was preceded and followed by a rest/sleep recording session in a terra cotta flowerpot lined with a towel. These sessions lasted at least 10 min (2 of the 6 rats) or 1 hour (the other 4 rats). Sleep data were recorded in 10 of the sessions, when 58 of the

assemblies were recorded (Supplementary Table 2). Sleep was detected by low movement speed. Headstage LED signals were first smoothed and periods when the speed did not exceed 0.05 m/s for a duration of at least 120 s (with a tolerance of two s when this velocity could be exceeded).

Data analyses

Data were analyzed using programs custom-written in Matlab (Statistical Toolbox; FMAToolbox, http://fmatoolbox.sourceforge.net).

Statistics

Statistics are reported as the median±25% confidence intervals otherwise. Monte Carlo bootstrap analyses were done (detailed below). For non-normal distributions, multiple comparisons were made with the Kruskal-Wallis test (or, for paired data, the Friedman test), for post-hoc tests, the (Bonferroni-corrected when necessary) Wilcoxon rank sum (or signed rank) tests, and for proportion comparisons, the binomial test.

Cell assembly detection

A method based on principal and independent component analyses (PCA and ICA) detected the co-activation of simultaneously recorded neurons referred to as 'assemblies'. First PCA was performed. The activity of the neurons was binned into 30 ms time bins to build a spike matrix S, where S_{ij} represents the firing of neuron i in spatial bin j. The matrix was z-scored, resulting in the Z matrix, where the i-th row of Z represents the z-scored activity of neuron i over all spatial bins. We calculated Q, the pairwise cell activity correlation matrix where N is the total number of neurons. We then computed the eigenvalue decomposition of Q. Eigenvalues that exceeded the upper bounds of the Marcenko-Pastur distribution were considered significant. However PCs are, by definition, orthogonal, a constraint that is not necessarily respected in the brain. To address this issue we carried out ICA on the major PCs (Lopes-dos-Santos, Ribeiro, *et al.* 2013) using the fast independent component analysis (fastICA) algorithm for MATLAB (H Gävert, J Hurri, J Särelä, and A Hyvärinen, http://research.ics.aalto.fi/ica/fastica). This ICA returned assemblies as vectors of N weights, corresponding to the respective cell's contributions. Since the signs of the output weights are arbitrary, weights were inverted as necessary to render the highest absolute weight positive. Components were normalized such that a component with equal contribution from all N neurons recorded in a session would be composed of N equal weights each with absolute value $1/\sqrt{N}$. Thus neurons with weights exceeding $1/\sqrt{N}$ are referred to as 'assembly

members'. The activation strength of each assembly within a given time bin is computed by projecting the matrix Z (constructed with 30 ms bins and a 10 ms sliding window) onto a template matrix obtained by the matrix product of the component and its transpose. The diagonal of the template matrix is set to zero so that single neuron spiking does not contribute to the activation strength. Thus the activation strength is high when multiple neurons with high weights fire synchronously and increases when synchronous high weight neurons fire more. Assemblies were considered to be active when their activation strength exceeded 5, which corresponds to the median of the 99th quantile distribution of activation strength.

Matching assemblies calculated with different bin widths

The PCA-ICA analyses of the data set were performed with bin widths ranging from 10 to 150 ms. Assemblies detected at different time scales were iteratively matched by selecting pairs with maximum correlations (Spearman coefficient). First, we computed correlations between each possible pair of assemblies computed with two different bin widths. The pair with the highest coefficient was set aside and the procedure was repeated with the remaining assemblies until all assemblies were paired. When the number of assemblies was different from one time scale to another, the remaining assemblies were left unmatched. Matched pairs with significant Spearman coefficients were considered as 'highly correlated.'

Marčenko & Pastur threshold

Note that this threshold is derived from a random matrices theorem and its use for selecting major principal components has been criticized (Russo & Durstewitz 2017). We shuffled spike identity while preserving spike time stamps to create surrogate data and then ran PCA. This procedure was repeated 1000 times to build a distribution of eigenvalues. The 95% quantile of this distribution was considered as an alternative threshold to Marčenko-Pastur. No significant differences were found when comparing data from the Marčenko-Pastur threshold to the present one derived from surrogate data ($p = 0.77$; Wilcoxon paired rank test).

Asymmetry of the cross-correlations of STR-PFC cell pairs

We calculated an asymmetry index (inspired by Belluscio *et al.* 2012): for each STR-PFC member pair, the normalized ratio of area under the positive part of the crosscorrelogram curve (]0 ms, 30 ms]) over the area

under the negative part ([-15 ms, 0 ms[). Thus when the index is positive, there are more cross-correlated STR spikes after the PFC spike, while when the ratio is negative, it is the opposite. A Wilcoxon sign rank test determined whether the median of the distribution was greater than 0.

Local field potential (LFP) analyses

Power spectra were calculated with wavelet methods. The spectrogram was also calculated with multi-taper Fourier methods. Since the results were similar for the two methods, the wavelet method was retained. These were performed over parts of or for the entire session, and then averaged for each spatial bin. Since there is controversy about the origin of some STR LFP oscillations (Lalla *et al.* 2017; Carmichael *et al.* 2017), two types of signals were analyzed. 'Raw' signals from a single STR tetrode wire were referenced to the cerebellar skull screw. To control for possible volume conduction and reference channel activity in STR, 'locally referenced signals' were derived from a single STR tetrode wire, subtracting the average LFP recorded across the other tetrodes there for 4 and 8 Hz analyses. However no major difference was observed compared to raw signals, so the latter are reported. Since results were similar with only one selected channel by area or with the average of all recorded channels (data not shown), the former were used. Coherence calculations were based on a multi-taper Fourier analysis (Mitra & Pesaran 1999) and performed with custom-written, MATLAB-based programs. We used the MATLAB mtspecgramc function with a time window of 2 s, a step size of 0.1 s and a bandwidth product of 3 with 5 tapers. Then the average coherence spectrum was computed for each spatial bin of the maze.

Granger Causality Analysis

To determine whether PFC oscillations precede STR oscillations, Granger causality was measured with the Fieldtrip toolbox (Oostenveld *et al.* 2011; http://fieldtriptoolbox.org). We used non-parametric Granger causality based on Fourier transforms (Dhamala *et al.* 2008) within windows of 1 s for frequencies from 1 to 20 Hz.

Spike-LFP analyses

To examine modulation of spiking activity by LFP oscillations first, instantaneous signal power and phase were derived from the Hilbert transform of the bandpass-filtered signal. We quantified phase consistency of spikes relative to the LFP band with both the Rayleigh test of circular uniformity and the unbiased pairwise phase consistency (PPC) devel-

oped by Vinck *et al.* 2012. For each unit and assembly, we first tested for significant entrainment to the LFP at low frequencies: 4 Hz (from 2 to 6 Hz) and theta (from 6 to 12 Hz). To characterize phase locking in neurons, we used two methods. With the Rayleigh test, a neuron or an assembly was considered as phase locked if $p<0.05$ and kappa>0.1. This criterion was chosen on the basis of k-means separation and confirmed by eye. Moreover to take into account the non-uniformity of the signal (cycle asymmetry) we use the correction of Siapas, Lubenov, *et al.* 2005. Even though the main results did not change, we reported the corrected data. In the second method (used for neurons only), PPC threshold was determined from a jitter analysis: in data from each single unit, spikes were randomly jittered within a time window equivalent to a single cycle of the band under study. The actual values were considered significant if they exceeded the 95th percentile of this distribution. Since the results were similar between the two methods, the Rayleigh result is reported.

Comparison of phase-locking in members and assemblies

To determine whether STR and PFC members were phase-locked only during assembly activations modulation was compared between cycles containing assembly activations ('IN') and other cycles ('OUT'). First instantaneous signal power and unwrap phase were derived from the Hilbert transform of the bandpass-filtered signal. Each individual cycle (multiples of 2*pi) was determined. For each assembly, if the cycle contained an activation, then it was 'IN', otherwise it was 'OUT'. Then phase locking was calculated individually for each member for 'IN' and 'OUT', as described above. However since there was slight variability in the preferred phases among different assemblies, the difference between the assembly's preferred phases and the actual spike phases were calculated for each member of each assembly (and were calculated separately for 'IN' and 'OUT'. Then the Kuiper test compared the 'IN' and 'OUT' circular distributions. Note that power was not significantly different in 'IN' vs 'OUT' cycles (Friedman test: $p>0.05$) for both 4 and 8 Hz. Gamma burst detection. We detected transient gamma burst events in both the STR and PFC LFPs. LFPs were first filtered in the high-gamma band (70–110 Hz) using the MATLAB filtfilt function (4th order Chebyshev filter). Instantaneous signal amplitude was obtained by taking the modulus of the Hilbert-transformed signal. Gamma events were defined as when the amplitude envelope exceeded the 95th percentile of the amplitude distribution and contained at least three gamma cycles. Events separated by less than 1/2 cycle were merged. Cell activity analyses. A k-means analysis distinguished putative PFC and STR interneurons and principal cells based on spike waveform half-amplitude

duration and trough-to-peak delay (Barthó *et al.* 2004). For STR neurons, a firing rate criterion was also applied (Berke *et al.* 2004). The STR units were classified as putative MSN projection neurons (83%) or fast spiking interneurons (15%), leaving 2% unclassified. In the PFC recordings, these two waveform parameters alone permitted classification of 85% as projection neurons and 13% as interneurons, leaving 2% unclassified. Further analyses focused on neurons with average firing rates equal to or greater than 0.1 Hz.

Spatial distribution of neuron firing

The maze was linearized and divided into equal segments (bin size=4.5 cm). Then firing rate vectors over respective bins were computed using a kernel based method. The firing rate was estimated at each bin x as: $f(x) = \sum(n_t * K(|x - xt|) / \sum(dt * K(|x - x_t|))$, where n_t is the number of action potentials emitted in a given bin, dt is the amount of time spent in the bin, and K is the smoothing Gaussian kernel function (4.5 cm). The firing vector of each neuron was then z-transformed, and these were averaged together to derive the population responses.

Monte Carlo bootstrap analyses

This method (Fujisawa, Amarasingham, *et al.* 2008) was selected since it requires no assumptions about the underlying distribution of the data and provides greater spatial resolution than comparable approaches. It tested the statistical significance of the firing rate differences of individual neurons between VD1, VD2 and SD task conditions in the sessions as well as the differences between right vs. left reward arm choice trials and rewarded vs. non-rewarded trials. (Of course, SD trials could not be compared for right vs. left choices.) Let us take as an example testing for differences in firing rate between two series of trials when the rat performed at criterion levels the VD task the first time vs. the SD task. For each neuron, the average firing rate F was calculated at each bin x for each condition and the difference was taken: $D(x) = F_{SD}(x) - F_{VD1}(x)$. To test the statistical significance of the rate differences D(x) with the bootstrap procedure, the distribution of possible rate differences Dr(x) is estimated by randomly permuting the identity of each trial into proxy groups $F'_{SD}(x)$ and $F_{VD1}(x)$. This process was repeated 5000 times to obtain the distribution from the resampled data, $D_{r_1}(x)$,..., $D_{r_n}(x)$. With this shuffled dataset, the pointwise confidence limits (demarcating the upper and lower 2.5% of the distributions) were computed for each bin x. To deal with multiple comparison issues, the method also computes the global 5% bands. A maze zone (i.e., contiguous series of spatial bins) is considered to have significant different firing only when

D(x) crosses both the global and pointwise bands, and the zone extent is determined only by the points where D(x) lies beyond the pointwise band. To test for behavioral correlates in assemblies or neurons (task condition, rewarded vs non-rewarded trials, etc) the Monte Carlo bootstrap test had to be significant for at least one bin of the maze. This is referred to as 'selectivity'.

Slope correction

To correct for gradual upward or downward drifts in assembly activations (or neuron firing rates) over the course of the recording sessions, a linear regression computed each assembly average activation (or neuron's average firing rate) for each trial as a function of trial number (excluding the VD1, SD and VD2 criterion performance trials). The assembly with significant regressions (Spearman correlation $p<0.05$, $n=11$ assemblies) were discarded from further analysis. All neurons with significant drift (Spearman correlation $p<0.05$, $n=105$ neurons) were corrected (rather than discarded) by calculating the slope and subtracting the product of the (trial number minus 1) and the slope from the rate for each trial for the neuron

Support Vector Machine analysis

With the libSVM library (Chang & Lin 2011), support vector machines (SVMs) with RBF kernel quantified how well STR or PFC population activity distinguished between trials in different pairs of trial conditions, namely VD1 vs SD, VD1 vs VD2, and VD2 vs SD. Each neuron's firing rate was averaged over each trial in a given task condition to obtain a population vector of length N, with N corresponding to the number of cells recorded during the session. Population vectors were z-scored in order to prevent neurons with high firing rates from having excessive influence on classification. Population vectors were then normalized by setting their euclidean norm to 1. First, data were split in two balanced set (e.g., 4 VD1 trials and 4 VD2 trials in each set). The first set was used to find optimal SVM hyperparameters γ and C, with γ as the exponent of a radial basis function kernel and C, the penalty parameter of the error term. A grid of values between 0.01 and 30 was searched to find (C, γ) values that optimized a leave-one-out cross validation accuracy. The accuracy of the SVM, i.e., its ability to correctly predict the epoch of the single left-out trial, was quantified. This procedure was iterated on each possible permutation ($n = 8$) of the data set and for each pair (C, γ). The parameters with the best averaged cross-validation accuracy in each session were retained for subsequent analyses. With the second data set, SVM were fit similarly using a leave-one-out

cross validation procedure but with fixed hyper parameters (C, γ). To build a null distribution of prediction accuracy, the population activity vectors for each trial in each task condition were randomly assigned to one of the task conditions being compared. SVMs were then recomputed from these randomized data sets using again the first half of the data set for setting hyper parameters and the second half to compute SVM accuracies. This procedure was repeated 500 times. The actual prediction accuracy distributions (from second set) were then compared to the null distributions with the Wilcoxon rank-sum test.

Comparison of behavioral correlates of assemblies vs. their members lacking significance for the correlate

The aim here was to determine if, when the assembly showed a behavioral correlate, whether those members lacking significance for this correlate (in the bootstrap analyses) nevertheless tended to show it. (Members were excluded if their significant behavioral correlate was in bins overlapping with the same selectivity in the assembly.) For each member, z-scores were computed for the difference between the member's firing rate for the two trial characteristics (e.g., VD1 vs. VD2, rewarded vs. unrewarded, leftward vs. rightward choice). For spatially selective activity, the z-score was taken relative to the mean firing or activity rate. The signs of values for the members were rectified to correspond to the sign of the change of activation of the assembly. To provide a benchmark randomized distribution, differences of z-scores were again computed, but with activity of members at randomly selected locations on the maze (maintaining the same number of bins as for the initial distribution). Members were excluded if their significant behavioral correlate was in bins overlapping with the same selectivity in the assembly. A Wilcoxon signed rank test assessed if the differences between the median of the surrogate distribution and the true distribution was different. This procedure was repeated for each behavioral correlate of the assembly.

4.5 Supplementary materials

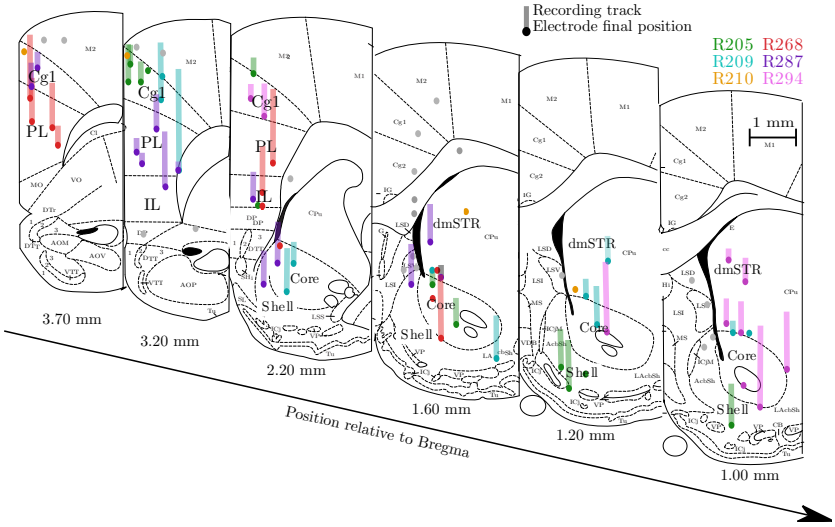

Figure 4.7: Recording sites Histologically identified locations of tetrode recording sites projected onto atlas images of coronal sections (adapted from Paxinos & Watson 2006). Each color corresponds to a different rat. Multiple tetrodes oriented in two parasagittal rows recorded neuronal activity and local field potentials (LFPs) at multiple sites in dorsomedial STR (dmS), vSTR (composed of nucleus accumbens core and shell subregions, and PFC cingulate (Cg1), prelimbic (PL) and infralimbic (IL) areas (cf., Supplementary Table *1*).

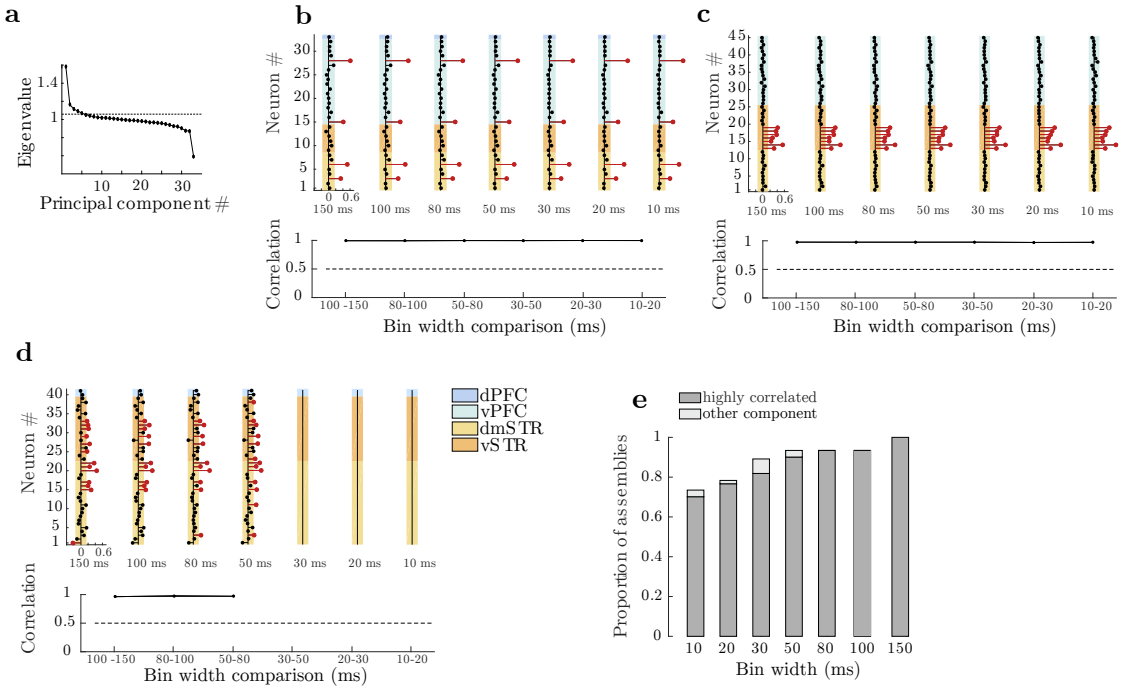

Figure 4.8: STR and PFC assemblies are maintained in bin widths ranging from 150 to 10 ms. a) Eigenvalues of the assemblies from the recording session of Figure 4.1. The horizontal line is the Marčenko-Pastur threshold. The assemblies are numbered in order of decreasing eigenvalues. b,c,d) Top: Matched assemblies are shown for different bin widths (same format as Figure 1a). Bottom: Spearman correlation coefficients compare matched assemblies detected with indicated bin widths. b,c) Examples of assemblies detected at all bin widths. d) An assembly not detected at bin widths briefer than 50 ms. Assembly members shown in b, c and d were recorded from at least 2 different tetrodes. e) Proportion of significantly correlated assemblies (Spearman correlation; $p<0.05$) detected at the various bin widths relative to those observed at 150 ms. 'Other component' refers to detected assemblies with no significant matches with 150 ms assemblies with the Spearman correlation test.

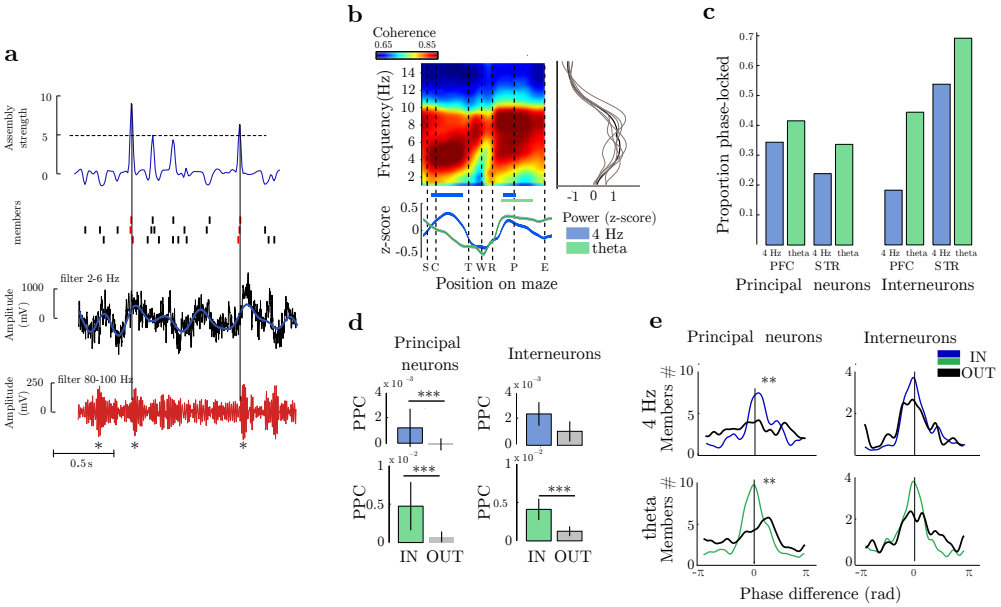

Figure 4.9: Assembly and member modulation by fast and slow oscillations. a) Representative example of activation of a 4 Hz phase-locked assembly at the onset (vertical lines) of two gamma-80 bursts (stars). Top: Assembly activations above threshold (dashed horizontal line) with members' spikes (red rasters). Bottom: PFC LFPs filtered for 4 Hz or gamma-80. b) Top: Mean PFC-STR coherence distribution on the maze for all sessions. Bottom: Coherence between PFC and STR LFPs at 4 Hz and theta. Color-coded horizontal bars represent significant segments (Monte Carlo bootstrap: $p<0.05$). Right panel) The average z-score of the frequency distribution of PFC-STR coherence in the central arm for individual rats (gray) and overall mean (black). c) Proportions of cells phase-locked to 4 Hz and theta bands of PFC LFP (i.e., with PPC values exceeding the 95th percentile of shuffled distributions; data from all sessions). d) Comparison of IN vs. OUT phase-locking of the two types of members to 4 Hz and theta (Friedman test: p=2.2e-06, 0.0022, 8.9e-10, and 4.6e-07 respectively). e) Distribution of the differences between mean phase angle of the assembly (at zero) and each individual member IN or OUT for the two cell types. Kuiper test (comparison of two circular distributions): 4 Hz p=0.001 and 1; theta p=0.001 and 0.05, respectively. See Supplementary Table *4* for all details of circular statistics.

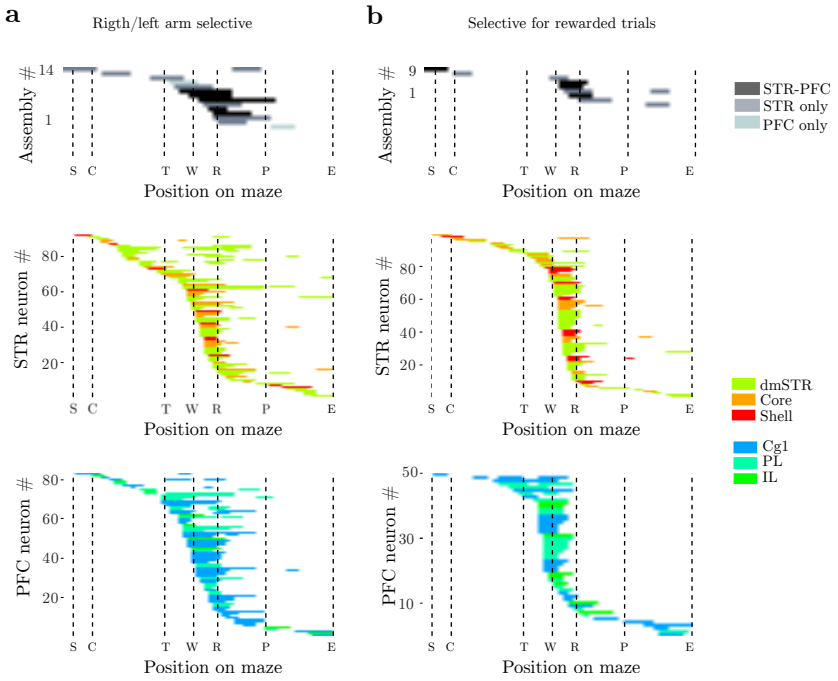

Figure 4.10: Maze distribution of arm choice and reward correlates. Significant differences in assembly activations or neuron firing rates between trials: (a) on trials with left vs. right reward arm choices, or (b) rewarded vs unrewarded trials. a,b) Each row shows the maze segment(s) where differences were significant for an assembly or a neuron. Same format as figures 4g and h. Cells are ordered by the position of the first significant bin.

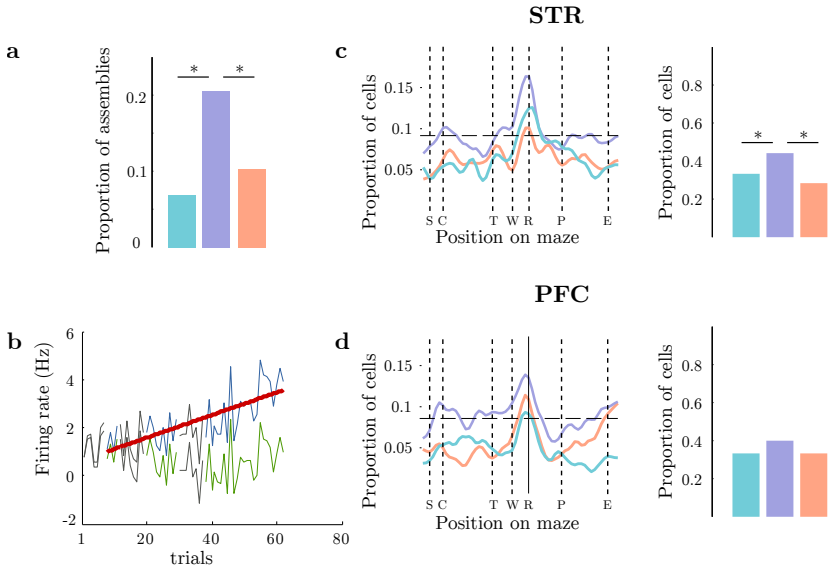

Figure 4.11: Correction for drift in firing rate over the course of the session. a) Proportions of assemblies showing task condition selectivity after removing assemblies with significant drift in activation rate over the course of the session. Binomial tests: p=0.016, 0.034, and 0.75 respectively. n=63 assemblies. b) Example of drift correction for an example neuron. The blue trace indicates average firing rate trial by trial. The regression bar for all (except criterion performance) trials is in red. The corrected values are in green. The black traces correspond to firing rates in criterion performance periods before (above) and after (below) correction. Note that 21% of the neurons showed significant drift but, within the same session, different neurons could have positive or negative regression slopes (not shown). c,d) Proportions of cells showing task condition selectivity after slope correction. VD1 vs. SD (cyan), VD1 vs. VD2 (violet) and SD vs. VD2 (salmon) (same format as Fig. 5). Binomial tests: p=0.033, 0.006, 0.53 and p=0.24, 0.51, and 0.06 respectively. STR (n=185 cells) and PFC (n=295 cells).

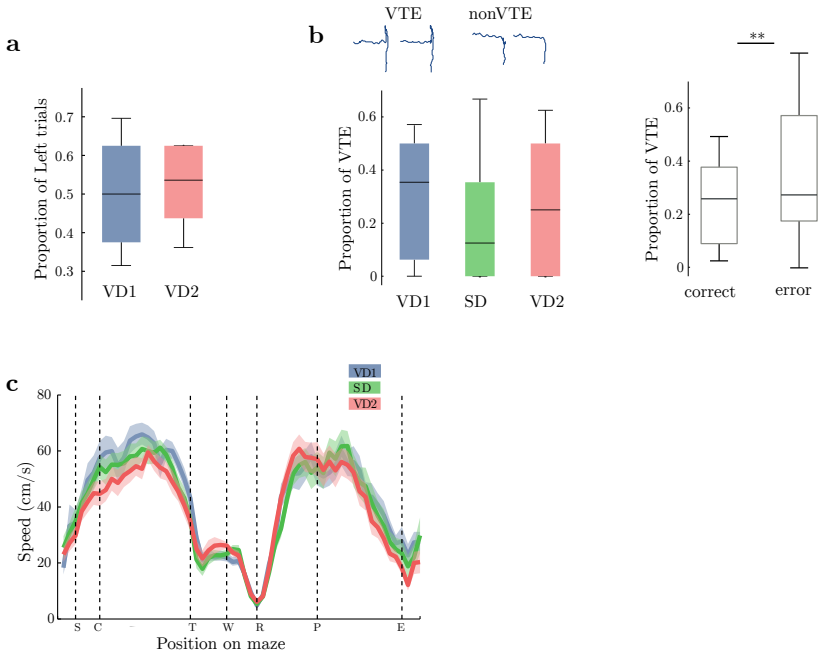

Figure 4.12: Behavioral parameters were not significantly different between VD1, SD and VD2 task conditions. a) Proportion of left reward arm choices during criterion performance for VD1 vs VD2 (Wilcoxon signed-rank test, p=0.85, n=20 sessions) b) Proportion of trials with vicarious trial and error (VTE) behavior. Top) Example of trajectories in two VTE trials (left) and two non-VTE ('ballistic') trials (right). Bottom) Proportion of VTE trials for the respective epochs for all sessions (Friedman test: p=0.32, n=20 sessions). Right) The proportion of VTE for correct and error trials. Boxplots show the median, the 25th and 75th percentiles, and the extreme values. c) Comparison of average running speed along the maze in the three task conditions for all sessions. Solid lines are means and shaded areas are SEMs (p>0.05, Monte Carlo bootstrap).

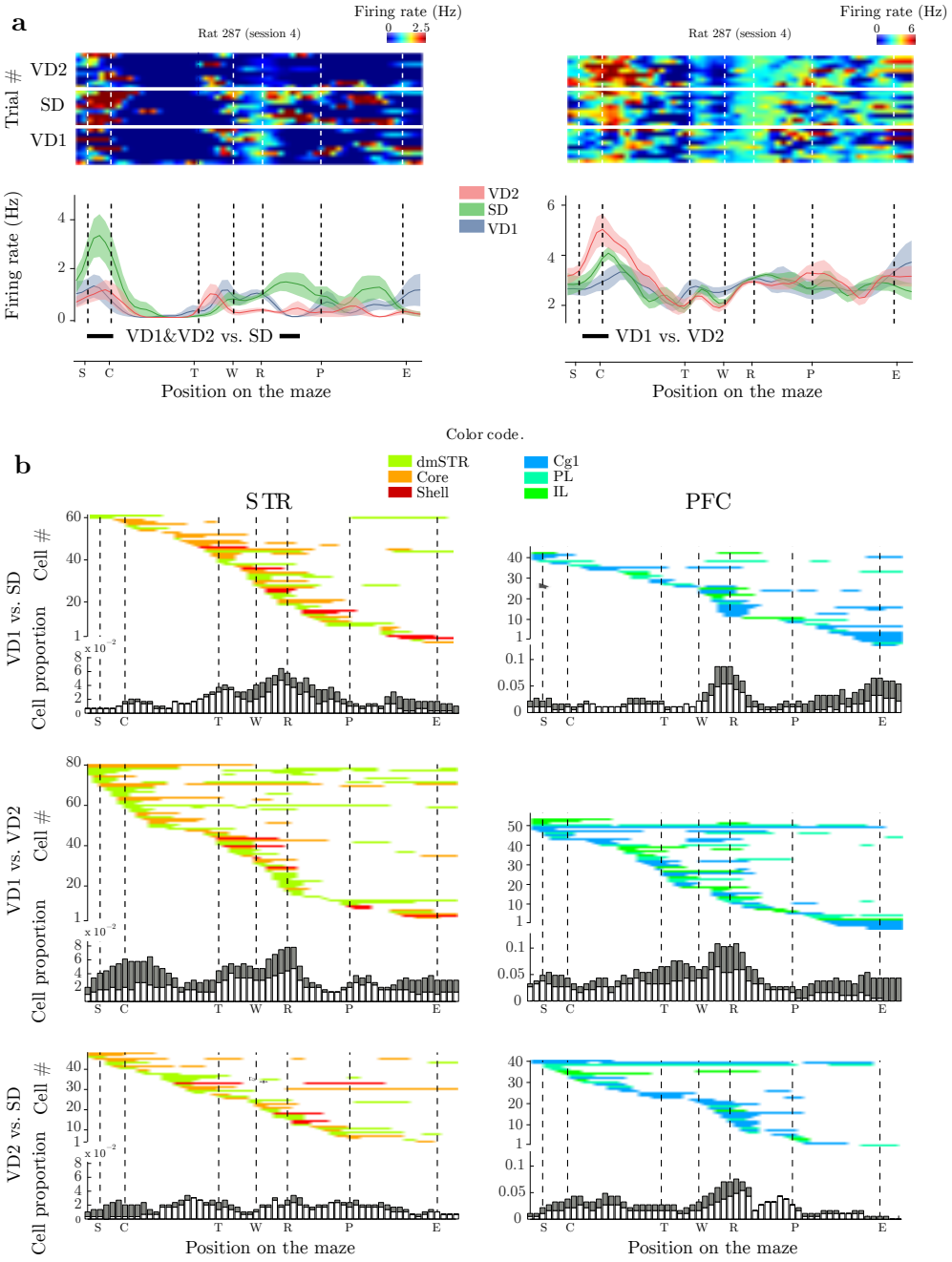

Figure 4.13: Activity of single neurons in STR and PFC distinguishes task conditions. a) Color rasters of the firing rates of two vSTR neurons on a linearized projection of the maze. Below, mean firing rates (solid traces) and their SEMs (shading around traces) for the three task conditions.

Figure 4.13: Zones with significant differences (Monte Carlo bootstrap, $p<0.05$) are indicated by horizontal bars. b) Maze distributions of significant firing differences for task condition comparisons in individual neurons, distinguishing their anatomical locations ($p<0.05$, Monte Carlo bootstrap). Same format as Supp. Fig. 4.10. The histograms below indicate the proportions of these cells for which the difference was positive (grey) or negative (white) for the respective bins.

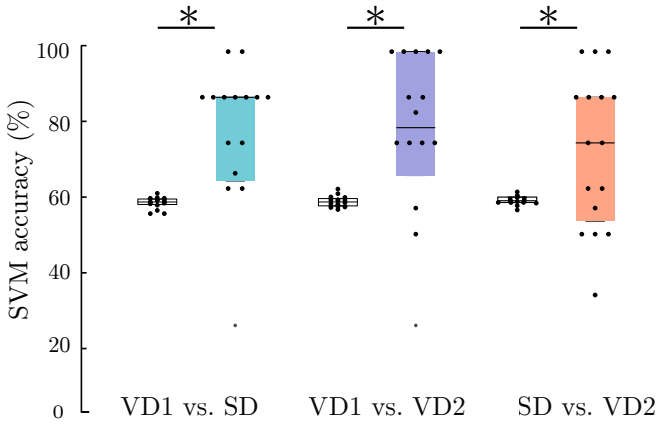

Figure 4.14: PFC population coding predicts epochs. The distribution of SVM prediction accuracy from PFC populations is significantly higher for all three comparisons than for randomized (at the left of each pair) data sets (Wilcoxon signed-rank tests; $p=0.0386$, 0.043, and 0.034, respectively, $n=16$ sessions). Boxplots show median and the 25th and 75th percentiles. Each point represents one session.

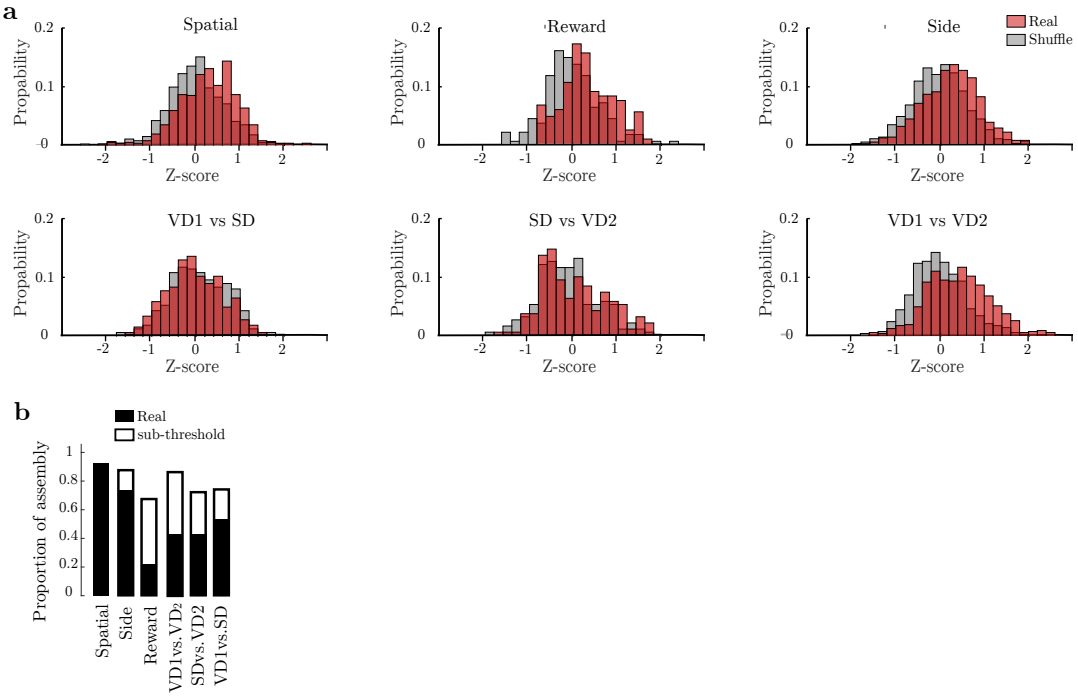

Figure 4.15: Non-significantly behaviorally correlated activity of members resembles the behavioral correlates of their assemblies. a) As in Figure 4.6f, comparisons of distribution of the z-scored activity differences between the pairs of trial characteristics for the behavioral correlates (e.g., rewarded and non-rewarded trials) vs. the z-scored distribution of differences for the same cells but at randomly selected locations on the maze (Wilcoxon signed rank tests for first row, then second row: p=1.2e-21, p=3.4e-8, p=1.1e-22, p=0.07, p=0.05 and p=1.3e-25 respectively). b) Incidences of overlap of significant behavioral correlates between members and assemblies ('Real'; filled bars). In cases of no significant overlapping members, sub-significant activity was examined (Figure 4.6d). Those non-significant members with firing rate differences z-scored values exceeding 1.5 in positions overlapping with those of the behavioral correlate of the assembly are indicated 'subthreshold' (white bars).

Rat	# sessions	dPFC (Cg1)	vPFC (PL+IL)	all PFC	dmSTR	vSTR (core+shell)	all STR
205	3	38	6	44	10	31	41
209	3	0	5	5	48	63	111
210	4	27	0	27	0	0	0
268	2	0	11	11	15	6	21
287	5	15	78	93	39	43	82
294	3	11	0	11	40	0	40
Total	**20**	91	100	**191**	152	143	**295**
# of rats		4	4	**6**	5	6	**5**

Table *1*: Summary of total numbers of neurons recorded in the six rats. Four sessions from rat 210 are not included for assembly analyses because only PFC neurons were recorded. However this rat's data was used for single unit and LFP analyses.

	High Weights					Behavior correlates		Phase Locking		Sleep
	dPFC	vPFC	dmSTR	vSTR	Type	all epochs	Inter-epochs differences	4Hz	8Hz	
Session 1 R205-20120902	**2**	**1**	**4**	**10**						
Group 1	0	**1**	**1**	**3**	STR+PFC	✓	✓	x	x	x
Group 2	**2**	0	0	**4**	STR+PFC	x	x	x	x	x
Group 3	**1**	0	**1**	**5**	STR+PFC	x	x	x	x	x
Session 2 R205-20120903	**22**	**2**	**6**	**12**						
Group 4	0	0	0	**5**	STR-only	x	x	x	x	nan
Group 5	**9**	0	0	0	PFC-only	✓	x	x	x	nan
Group 6	**9**	0	0	**2**	STR+PFC	✓	x	x	x	nan
Group 7	**11**	0	**1**	**2**	STR+PFC	x	x	x	✓	nan
Group 8	**8**	**1**	**5**	**2**	STR+PFC	✓	x	x	x	nan
Group 9	**5**	0	**3**	**5**	STR+PFC	✓	x	✓	x	nan
Session 3 R205-20120904	**14**	**3**	**0**	**9**						
Group 10	**5**	0	0	0	PFC-only	x	x	✓	x	✓
Group 11	**5**	0	0	**2**	STR+PFC	x	x	x	x	x
Group 12	**7**	**1**	0	**2**	PFC-only	x	x	✓	x	x
Session 4 R209-20121113	**0**	**2**	**16**	**17**						
Group 13	0	0	**6**	0	STR-only	x	✓	✓	✓	x
Group 14	0	**1**	**2**	**3**	STR+PFC	✓	✓	x	✓	x
Group 15	0	0	**2**	**5**	STR-only	x	x	x	x	x
Group 16	0	0	**2**	**5**	STR-only	✓	✓	x	✓	x
Group 17	0	**1**	**5**	**3**	STR+PFC	✓	✓	x	x	x
Group 18	0	**1**	**5**	**3**	STR+PFC	x	x	x	x	x
Session 5 R209-20121114	**0**	**1**	**15**	**24**						
Group 19	0	0	**3**	**3**	STR-only	✓	x	x	x	✓
Group 20	0	0	**8**	0	STR-only	x	x	✓	✓	x
Group 21	0	0	**4**	**3**	STR-only	✓	✓	x	x	x
Group 22	0	0	**2**	**7**	STR-only	x	x	✓	x	x
Group 23	0	**1**	**6**	**7**	STR+PFC	x	x	✓	✓	x
Group 24	0	0	**1**	**9**	STR-only	x	x	x	x	x
Session 6 R209-20121115	**0**	**2**	**17**	**22**						
Group 25	0	0	**4**	**3**	STR-only	✓	✓	x	x	nan
Group 26	0	0	0	**5**	STR-only	x	x	x	x	nan
Group 27	0	0	**6**	**1**	STR-only	x	✓	✓	✓	nan
Group 28	0	0	**3**	**5**	STR-only	✓	✓	x	x	nan
Group 29	0	0	**2**	**6**	STR-only	✓	x	x	x	nan
Group 30	0	0	**2**	**8**	STR-only	x	x	x	x	nan
Group 31	0	0	**6**	**7**	STR-only	x	x	x	x	nan
Session 7 R268-20140930	**0**	**2**	**6**	**1**						
Group 32	0	0	**4**	0	STR-only	x	x	✓	✓	nan
Group 33	0	0	**3**	0	STR-only	x	x	✓	x	nan
Session 8 R268-20141016	**0**	**9**	**9**	**5**						
Group 34	0	0	**6**	0	STR-only	x	x	✓	✓	x
Group 35	0	**3**	**1**	**1**	STR+PFC	x	x	x	✓	✓
Group 36	0	**4**	**5**	0	STR+PFC	x	x	x	x	✓
Group 37	0	**5**	**1**	**2**	STR+PFC	x	x	x	x	x
Session 9 R287-20150105	**7**	**17**	**4**	**7**						
Group 38	0	0	**3**	0	STR-only	x	✓	✓	✓	✓
Group 39	0	**3**	0	**1**	STR+PFC	x	x	x	✓	x
Group 40	**1**	**3**	0	0	PFC-only	x	x	x	✓	✓
Group 41	**4**	**3**	0	**3**	STR+PFC	x	✓	x	✓	x
Session 10 R287-20150107	**1**	**18**	**6**	**8**						
Group 42	0	**2**	0	**2**	STR+PFC	✓	x	✓	✓	x
Group 43	**1**	**3**	0	0	PFC-only	x	x	x	x	x
Group 44	0	**4**	**2**	0	STR+PFC	x	x	✓	✓	✓
Group 45	0	**6**	0	**1**	STR+PFC	x	✓	x	x	x
Group 46	0	0	**4**	**5**	STR-only	x	x	x	✓	x
Session 11 R287-20150113	**4**	**10**	**7**	**5**						
Group 47	0	0	0	**2**	STR-only	x	✓	✓	✓	✓
Group 48	0	0	**4**	0	STR-only	x	x	✓	✓	x
Group 49	0	**3**	0	0	PFC-only	x	x	x	x	✓
Group 50	**2**	**2**	**1**	**1**	STR+PFC	x	x	✓	x	✓

	High Weights					Behavior correlates		Phase Locking		Sleep
	dPFC	vPFC	dmSTR	vSTR	Type	all epochs	Inter-epochs differences	4Hz	8Hz	
Session 12 R287-20150114	**3**	**13**	**9**	**11**						
Group 51	0	0	0	**2**	STR-only	x	✓	x	x	x
Group 52	0	0	**4**	0	STR-only	x	x	x	x	x
Group 53	0	0	0	**2**	STR-only	x	x	x	x	✓
Group 54	0	**4**	0	0	PFC-only	x	x	x	x	✓
Group 55	**3**	**7**	**2**	0	STR+PFC	x	✓	x	x	✓
Group 56	**2**	**3**	**1**	**3**	STR+PFC	x	x	x	x	✓
Group 57	**2**	**2**	**3**	**1**	STR+PFC	✓	x	x	x	✓
Session 13 R287-20150115	**0**	**20**	**13**	**12**						
Group 58	0	0	0	**4**	STR-only	x	✓	✓	x	✓
Group 59	0	**4**	0	0	PFC-only	x	x	x	✓	x
Group 60	0	0	0	**5**	STR-only	x	✓	x	x	✓
Group 61	0	0	**7**	0	STR-only	x	✓	✓	x	✓
Group 62	0	**7**	0	0	PFC-only	x	x	x	✓	✓
Group 63	0	**6**	**1**	**2**	STR+PFC	✓	x	x	x	x
Group 64	0	**6**	**4**	**2**	STR+PFC	✓	✓	✓	x	✓
Session 14 R294-20150313	**5**	**0**	**10**	**0**						
Group 65	**2**	0	**4**	0	STR+PFC	x	x	✓	x	✓
Group 66	**4**	0	**2**	0	STR+PFC	x	x	x	x	✓
Session 15 R294-20150317	**5**	**0**	**18**							
Group 67	0	0	**3**	0	STR-only	x	x	✓	x	x
Group 68	0	0	**3**	0	STR-only	x	✓	x	✓	✓
Group 69	**4**	0	**2**	0	STR+PFC	✓	✓	✓	x	x
Group 70	**1**	0	**4**	0	STR+PFC	x	x	x	x	x
Group 71	**1**	0	**6**	0	STR+PFC	✓	x	✓	x	✓
Session 16 R294-20150401	**1**	**0**	**12**	**0**						
Group 72	0	0	**2**	0	STR-only	✓	x	nan	nan	x
Group 73	**1**	0	**2**	0	STR+PFC	x	x	nan	nan	✓
Group 74	0	0	**6**	0	STR-only	x	x	nan	nan	x

Table *2*: Summary of assembly recordings. In the row with session number, values indicate total numbers of cells recorded by structure. In the rows with group numbers, the values indicate the number of members by structure. Checkmarks indicate that the behavioral correlate was significant for the assembly. X's indicate that they were not, and Nan's indicate that the test could not be performed.

	Count	Behavioral correlates		Phase Locking		Sleep
		all epochs	Inter-epochs differences	4Hz	8Hz	
STR-only	33	8	15	13	11	8
PFC-only	8	1	1	1	3	5
STR+PFC	33	12	7	10	8	12
Total	**74**	**21**	**23**	**24**	**22**	**25**

Table *3*: Summary of assembly modulation

	Figure 2.g		**Figure 3.a**		**Figure 3.b**			
					Principal neurons		Interneurons	
	Assemblies		Gamma-80		PFC	STR	PFC	STR
Rayleigh test	4 Hz	8 Hz	4 Hz	8 Hz	Gamma-80	Gamma-80	Gamma-80	Gamma-80
mean angle(rad)	0	-1.3	0.1	-0.3	-3.09	-2.01	-2.94	-0.31
p value	7.16E-006	1.31E-006	1.45E-007	1.21E-007	1.19E-012	1.30E-008	0.0774	0.151
Kappa	1.59	1.38	3.18	3.24	1.61	1.36	0.753	0.47
Resultant	0.621	0.567	0.824	0.827	0.625	0.562	0.411	0.228
n	28	39	20	20	63	53	15	36
Figure 2.g	Principal neurons							
	PFC				STR			
	4 Hz		8 Hz		4 Hz		8 Hz	
Rayleigh test	IN	OUT	IN	OUT	IN	OUT	IN	OUT
mean angle(rad)	-0.4	0	-1.5	-1.5	-0.6	1.1	-2	2.5
p value	0,00114	0.415	1.16E-012	0.000392	0.00892	0.0397	1.87E-005	0.717
Kappa	0,000178	0.274	1.66	0.758	0.926	0.747	0.781	0.13
Resultant	0,371	0.136	0.635	0.354	0.42	0.35	0.364	0.065
n	48	48	61	61	26	26	80	80
	Interneurons							
	PFC				STR			
	4 Hz		8 Hz		4 Hz		8 Hz	
Rayleigh test	IN	OUT	IN	OUT	IN	OUT	IN	OUT
mean angle(rad)	-0.1	0.2	-0.6	-0.5	-0.4	-0.1	-1	-0.9
p value	0.00323	0.00101	0.0348	0.888	1.18E-008	5.06E-005	2.52E-009	3.56E-005
Kappa	1.67	2.11	1.15	0	1.49	1.004	1.27	0.856
Resultant	0.756	0.814	0.544	0.106	0.596	0.449	0.537	0.394
n	9	9	11	11	47	47	64	64

Table 4: Values for circular statistical test results

5 'Reading cell' assemblies in the cortico-amygdalar circuit

CJ Boucly[*,1], R Todorova[*,1], EM Leroux[1], SI Wiener[1], MB Zugaro[1], MN Pompili[1,2]

[1] Center for Interdisciplinary Research in Biology (CIRB), Collège de France, CNRS, INSERM, PSL Research University, Paris, France.

[2] Institute of Psychiatry and Neuroscience of Paris (IPNP), Hopital Sainte-Anne, INSERM, Université de Paris, Paris, France.

[*] Equal contributions

Author contributions: MNP, RT, and CJB conceived the project. Data was acquired by MNP and EML and processed by MNP, CJB, EML, and RT. Data analysis was designed by RT, CJB, MNP, MBZ, and SIW and performed by CJB and RT. CJB, MNP, RT, SIW, and MBZ wrote the paper.

Acknowledgements: we thank Gabriel Makdah for help with data acquisition, Yves Dupraz for help designing the electrophysiological implants, and Gyorgy Buzsaki for useful discussions. This project was funded from the Labex MemoLife and the Pierre Deniker Foundation (to MNP). CB is supported by the French ministry of higher education and research, and RT by Collège de France

Manuscript in preparation

Abstract

Hebb (1949) proposed that cell assemblies are a fundamental functional unit of the brain. With recent advances in large-scale neuronal recordings, ensembles of cells that repeatedly fire in synchrony within brief time windows have been reported in multiple brain regions. Yet, the functional relevance of these ensembles remains largely unexplored, especially in higher order brain areas. An influential hypothesis is that the biological relevance of precisely timed co-activation is to more effectively trigger responses in downstream cells, termed 'readers' of the cell assembly (Buzsáki 2010). In simultaneous recordings of hundreds of neurons in the medial prefrontal cortex (mPFC) and amygdala (AMY), we found assembly-reader pairs, where activation of an assembly was followed by the firing of a reader cell. This response of the reader cell was supra-linear, amplified by the synchrony of the firing of member

cells. Finally we found that the assembly-reader relationship changes with learning. Our results are in line with a role of cell assemblies in efficient cross-structural communication.

5.1 Introduction

An increasingly influential hypothesis in neuroscience posits that cell assemblies are the computational unit of the brain, underlying complex information encoding beyond the processing power of single cells (Hebb 1949; Braitenberg 1978; Hopfield 1982; Pouget *et al.* 2000; Varela *et al.* 2001; Harris 2005; Eichenbaum 2018). Techniques allowing the simultaneous recordings of large numbers of neurons have resulted in an increasing body of research tracking down the cell assembly dynamics in multiple brain systems (Harris *et al.* 2003; Fujisawa, Amarasingham, *et al.* 2008; Peyrache, Khamassi, *et al.* 2009; Benchenane *et al.* 2010; Dejean *et al.* 2016). In addition to the classical perspective that the function of cell assemblies is to represent information on the population level (Hebb 1949; Barlow 1972), from a physiological perspective, the key function of the coincident firing of cell assemblies may be to trigger a downstream neuron (Buzsáki 2010). Such a downstream neuron responding to the synchronous activations of an assembly can be considered as observer-classifier-reader neuron, from hereon referred to as 'reader'. Yet while coincidence detectors have been described in sensory systems (Alonso *et al.* 1996; Usrey *et al.* 2000; Roy & Alloway 2001), for the detection of convergent sensory information, evidence for 'reader' cells responding to cell assemblies representing more abstract information in higher order brain areas is lacking.

Here we report single units responding to cell assemblies in the reciprocally connected (Vertes 2004; Hoover & Vertes 2007; Hübner *et al.* 2014; Adhikari *et al.* 2015; Reppucci & Petrovich 2016; Marek *et al.* 2018) cortico-amygdalar circuit in rats during sleep, when brain activity is dominated by internal dynamics rather than responding to external stimuli. We found neurons responding to cell assemblies in both structures. Their response to assemblies was supra-linear, indicating that the synchronous activation of cell assemblies is an effective mechanism of cross-structural communication. Finally, we show that reader responses to assemblies can change after learning, supporting the hypothesis of a role of cell assemblies in cognitive processes.

5.2 Results

Cell assemblies are ubiquitous in the brain

In order to study the communication between cell assemblies and downstream readers, we recorded simultaneously hundreds of single units in the medial prefrontal cortex (mPFC) and the amygdala (AMY) during slow-wave sleep (Figure 5.5; n = 4 rats; 6 sessions each) and we first detected cell assemblies using a PCA-ICA algorithm (see Methods 5.4; Supp. Figure 5.10 and 5.11; Lopes-dos-Santos, Ribeiro, *et al.* 2013). As previously reported (Fujisawa, Amarasingham, *et al.* 2008; Peyrache, Khamassi, *et al.* 2009; Benchenane *et al.* 2010; Dejean *et al.* 2016), prefrontal unit activity exhibited synchrony (Figure 5.1a) and we found multiple cell assemblies in each sleep session (median = 18; Figure 5.1f). Interestingly, we also observed similar coincidental firing in the amygdala (Figure 5.1b,f). To further investigate the synchrony of assemblies, we compared the cross-correlation between the units belonging to the same assembly ('co-member' pairs) to the cross-correlation of neurons that were never part of the same assembly ('control' pairs). Cells sharing an assembly were significantly more correlated than control pairs (Figure 5.1c-e). Moreover, the spiking activity of one member could be accurately predicted from the activity of the other members, in 15 ms windows, as shown in Figure 5.1g ('peer prediction', see Harris *et al.* 2003 and Methods 5.4). Thus, in both the prefrontal cortex and the amygdala, neurons exhibited fine time scale synchrony consistent with the idea that cell assemblies are ubiquitous in the brain.

'Reader' neurons responding to cell assemblies

We hypothesized that the activation of these cell assemblies would evoke spiking responses in downstream brain regions receiving projections, as per the 'reader' hypothesis. Indeed, we found 503 assembly-reader pairs (Figure 5.2a,c,d), in which an amygdala reader unit significantly responded to activations of mPFC assemblies ($p<0.05$, Monte-Carlo bootstrap). Similarly, we also investigated whether synchronous amygdalar activity might trigger mPFC responses. This analysis revealed amygdala assemblies consistently followed by mPFC 'reader' responses (n = 622, Figure 5.2b-f), reinforcing the hypothesis of assembly readers as a general mechanism of cross-structural communication (see also Supp. Figures 5.6 and 5.7).

Reader responses to cell assemblies are supra-linear

Our hypothesis was that the synchronous activation of a cell assembly drives the response of the reader cell beyond what could be achieved by activations of individual members. Indeed, we observed that the readers

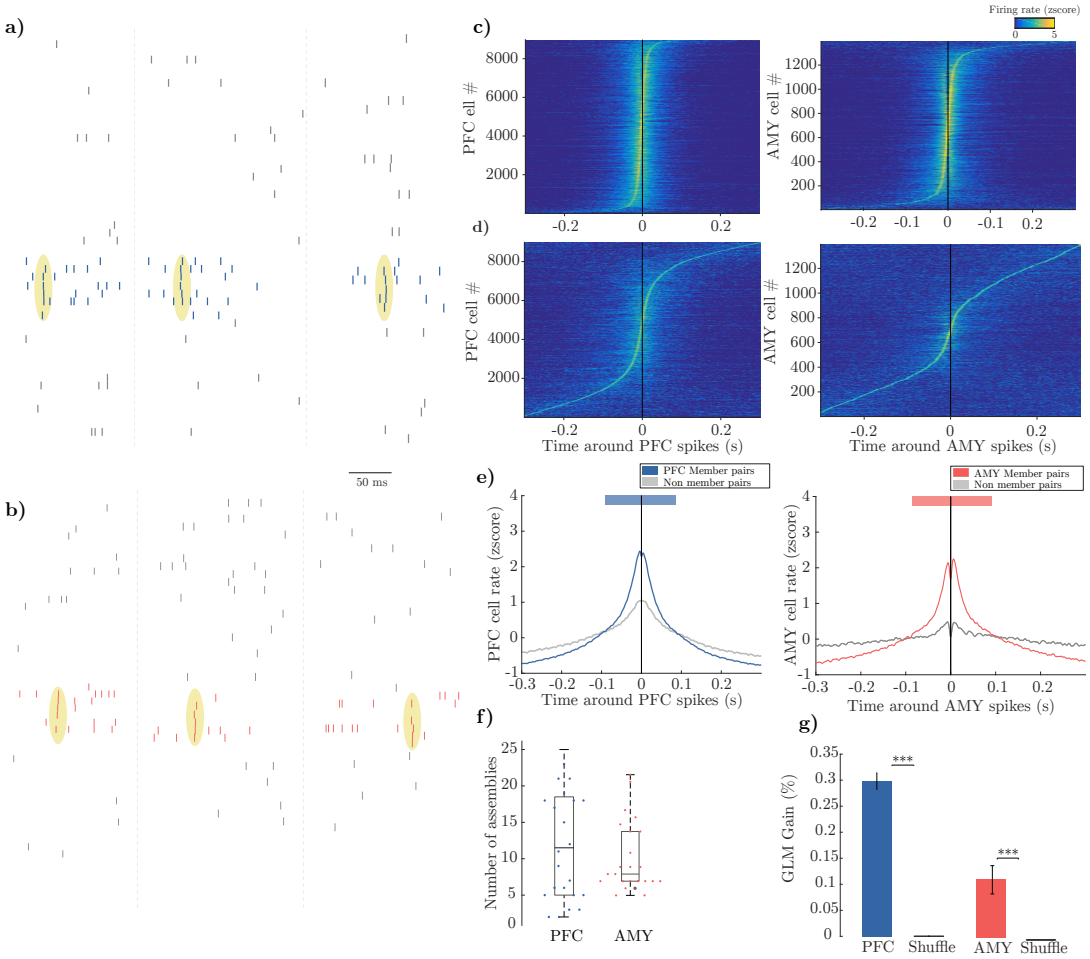

Figure 5.1: Cell assemblies are ubiquitous. **a,b)** Raster plots of prefrontal (a) and amygdalar (b) units recorded during sleep. Colored ticks: neurons exhibiting tight co-activations (yellow ovals). Gray ticks: other recorded units. **c)** Cross-correlations of members of the same assemblies (z-scored). Pairs are ordered by the timing of the peak z-scored correlation. Left: prefrontal assemblies. Right: amygdalar assemblies. **d)** Cross-correlations of 'control' pairs, that is randomly selected pairs of cells that were not members of the same assembly (left: in the prefrontal cortex; right: in the amygdala). **e)** Average cross-correlation of c) and d). The correlation between members of the same assembly is significantly higher than for control pairs ($p<0.05$, Monte-Carlo bootstrap; shaded bars). **f)** Number of detected assemblies per session. Left: in the prefrontal cortex, median = 18. Right: in the amygdala, median = 9.5. The boxes indicate distribution quartiles and the horizontal bars, the medians. Each individual colored dot represents one session. **g)** GLM prediction gain of member activity from the other assembly members, compared to the prediction from shuffled data. Left: prefrontal assemblies ($p<0.001$; Wilcoxon signed-rank test). Right: amygdalar assemblies ($p < 0.001$; Wilcoxon signed-rank test)

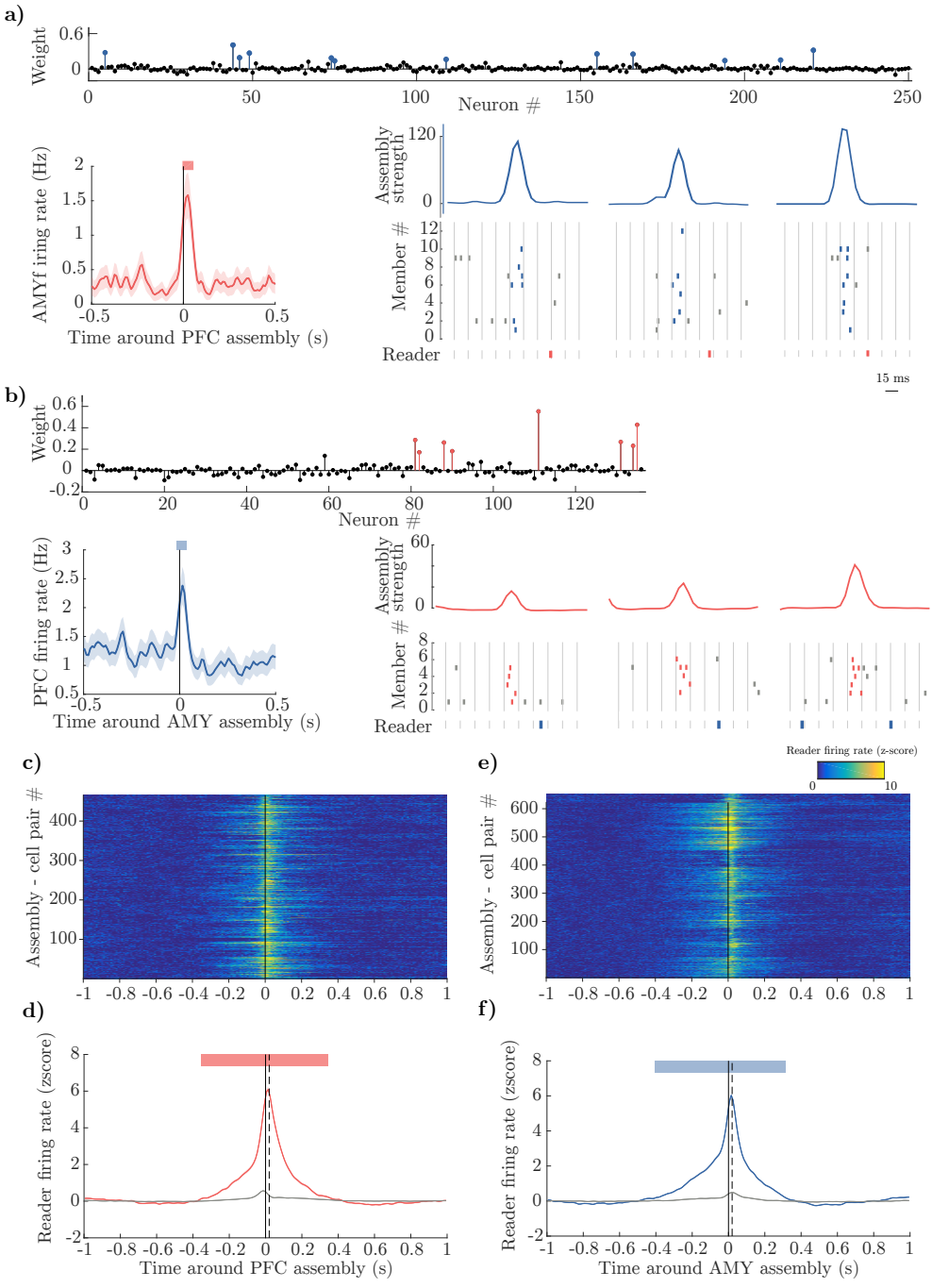

Figure 5.2: Readers of cell assemblies

Figure 5.2: a,b) Examples of significant neuron responses 10 to 30 ms after assembly activation (a: AMY neurons, PFC assemblies; b: PFC neurons, AMY assemblies). Top: cell assembly weights of members (colored circles) and non-members (black circles). Bottom left: mean ± s.e.m. of the 'reader' cell firing rate centered on assembly activation. Shaded bars on top indicate significant responses ($p<0.05$: Monte-Carlo bootstrap test; see Methods 5.4). Bottom right: assembly strength and associated raster plots. Assembly member ticks appear in color during the assembly activation and in gray outside. Blue: prefrontal spikes; red: amygdala spikes. Note the reader response $\sim$ 20 ms after the assembly activation. **c,e)** Reader activity centered on assembly activations for the significant assembly - reader pairs (pooled data). c) PFC assembly - AMY reader. e) AMY assembly - PFC reader. **d,f)** Average reader activity centered on assembly activations, over all significant pairs (colored line). Note that reader responses peaked at 20 ms (dashed line). Gray: average 'reader' activity for non-significant pairs. d) PFC assembly - AMY reader. f) AMY assembly - PFC reader.

were more likely to discharge when an increasing number of assembly members were active together (see Figure 5.3a-c for PFC assemblies and 5.3d-f for AMY assemblies). We then investigated whether this increase derived from the linear summation of the responses to each member. To test this, for each assembly activation, we computed the expected linear reader response as the weighted sum of the responses to all the active members taken individually (see Methods 5.4). The observed reader responses exceeded this linear estimate $\sim$ 20 ms after assembly activations, indicating that the reader response was driven by the assembly synchrony (Figure 5.3g-j, for PFC assemblies; Figure 5.3k-n, for AMY assemblies).

Learning-related changes in amygdalar assembly reading rate

We next investigated the behavioral relevance of cell assembly reading and in particular whether it evolved with learning. To test this, animals underwent a standard fear conditioning and extinction protocol known to involve both the prefrontal cortex and the amygdala (Morgan & LeDoux 1995; Muller *et al.* 1997; Herry *et al.* 2008; Sierra-Mercado *et al.* 2011; see Figure 5.4a and Methods 5.4; for more details on the behavioral protocol). We observed significant changes of prefrontal reader responses to amygdalar assemblies in sleep following both fear conditioning and extinction in sleep after learning compared to sleep before (Figure 5.4b,c). When we took into account possible network changes due to the passage of time, the effect of fear conditioning, but not extinction, was significantly greater than expected (Figure 5.4d-f).

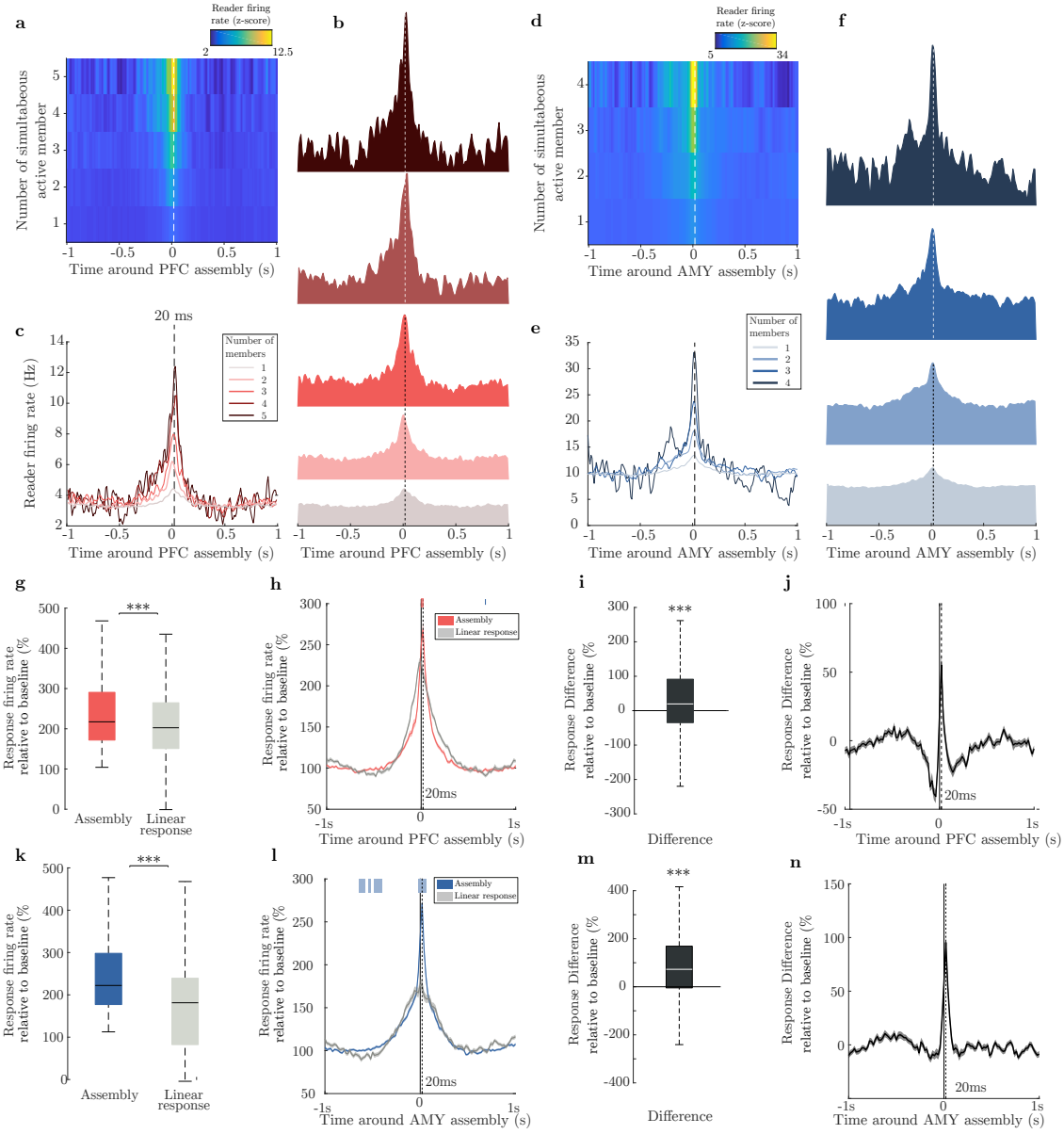

Figure 5.3: Reader responses are supra-linear. **a-c)** Example of an amygdalar neuron response as a function of the number of simultaneously active PFC members. **d-f)** Example of a prefrontal neuron response as a function of the number of simultaneously active AMY members. **g,k)** Colored: Increases in reader firing in the window 15 to 25 ms following assembly activation. In gray: estimated linear response (sum of the reader responses to each active member individually, see Methods 5.4). Reader responses to synchronous assembly activations significantly exceeded the linear responses. g) PFC assembly - AMY ($p<0.001$; Wilcoxon signed-rank test). k) AMY assembly - PFC reader ($p<0.001$; Wilcoxon signed-rank test).

Figure 5.3: **h,l)** Normalized reader firing rate centered on assembly activation (shaded area. mean +/- s.e.m.). Colored: observed; grey: estimated linear response. Note that unlike the linear response, the observed response peaks at 20 ms (shaded bars; p<0.05; Monter-Carlo Bootsrap). **i,m)** Difference of the responses in g and k, respectively. **j,n)** Difference (shaded area. mean +/- s.e.m.) of the responses in h and l, respectively.

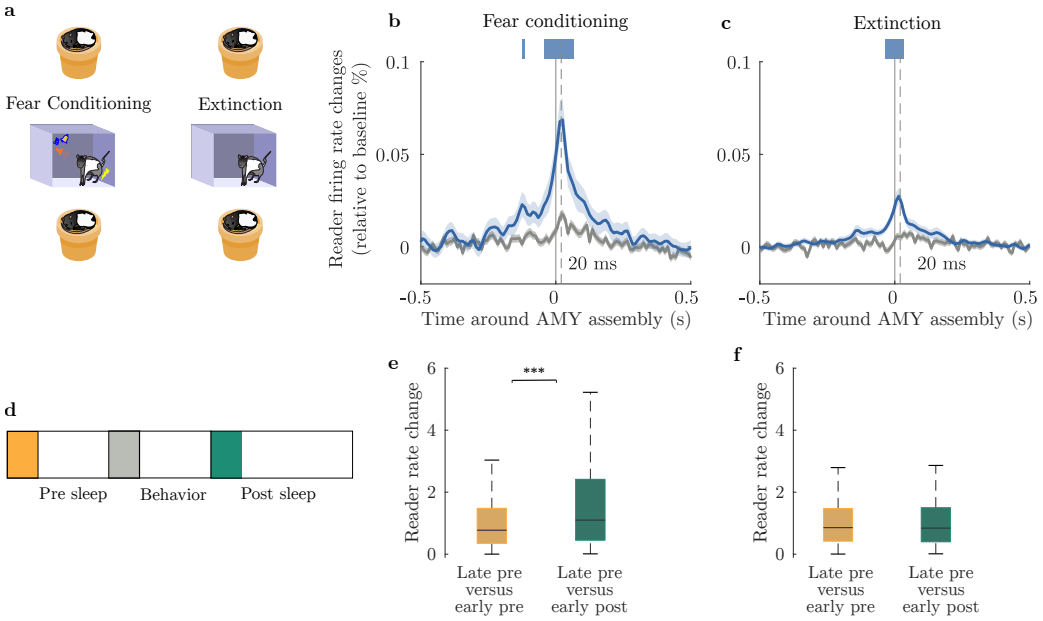

Figure 5.4: Learning-related changes in the assembly-reader relationship **a)** Sleep sessions (duration: ∼2 hours) took place before and after each training session (duration: ∼30 minutes). **b,c)** PFC reader absolute firing rate changes between post and pre sleep (normalized relative to baseline), centered on AMY assembly activations (shaded area: mean ± s.e.m.). The blue line highlights the interval where the increase was significant (p<0.05, Monte-Carlo bootstrap test). **d)** Passage of time analysis schema. Yellow segment: 'early pre sleep' period; gray: 'late pre sleep'; green: 'early post sleep'. Note that the same amount of time elapsed between early and late pre sleep and between late pre sleep and early post sleep. **e,f)** Reader response changes (in absolute value) ∼ 10-30 ms following assembly activations, in the early vs late pre sleep (yellow) and late pre sleep vs early post sleep (green). Reader rate changes were significantly higher when periods were separated by a fear conditioning session (e: p<0.001 ; Wilcoxon signed-rank test) but not by an extinction session (f: p=0.22).

In the other direction, amygdarar reader responses to prefrontal assemblies changed after learning, but we could not rule out that these were caused by the mere passage of time (see Supp Fig. 5.8). Thus, assembly-

reader coupling appeared to reorganize over time and in particular, prefrontal reader responses to amygdalar assemblies changed after fear conditioning, which is consistent with a role of amygdala-prefrontal communication in fear conditioning (Popa, Duvarci, *et al.* 2010; Senn *et al.* 2014; Burgos-Robles, Kimchi, *et al.* 2017; Klavir *et al.* 2017).

5.3 Discussion

This work was aimed at investigating whether cell assembly activity evoked firing responses in downstream brain regions as predicted by the assembly 'reader' hypothesis. We studied this in the prefrontal-amygdalar system and found that neural activity in each structure neural activity was organized in brief timescale cell assemblies. Moreover, specific downstream units or 'readers' increased their firing rates ∼10 to 30 ms following cell assembly activations, which is consistent with the conduction delay between the two structures (Quirk, Likhtik, *et al.* 2003; Likhtik *et al.* 2005). The response increased with the number of co-activated assembly members in a supra-linear fashion, indicating that the synchrony of the active members amplified the 'reader' response. Moreover, assembly-reader association re-organized with time and was not invariant with learning, supporting the idea that this communication mechanism is plastic and can be shaped by experience, following the ever changing information encoded by neural populations.

Cell assemblies are ubiquitous

Cell assemblies have been reported in various brain regions: the hippocampus (Harris *et al.* 2003), the prefrontal cortex (Fujisawa, Amarasingham, *et al.* 2008; Peyrache, Khamassi, *et al.* 2009; Benchenane *et al.* 2010; Dejean *et al.* 2016) sensory cortices (Bathellier *et al.* 2012), motor cortices (Riehle *et al.* 1997) as well as in the basal ganglia (Trouche, Koren, *et al.* 2019). In the amygdala, previous work investigated the cross-correlation of the firing of cell-pairs (Quirk, Repa, *et al.* 1995; Paré & Collins 2000; Girardeau, Inema, *et al.* 2017). Here we report for the first time, brief time scale synchrony within the amygdala (∼15 ms). Hence, our result further corroborate the hypothesis that cell assemblies are an ubiquituous brain phenomenon in line with the assumption of cell assemblies as the functional unit of the brain.

Readers of cell assemblies

Theoretical work has suggested that neurons act as coincidence detectors, that is, a 'target' would discharge when it receives inputs from multiple neurons ('sources') within a short time scale (Abeles 1982, Koch

et al. 1996). Indeed, to reach the spiking threshold, a single excitatory post-synaptic potential is usually not sufficient. Integration time in the prefrontal cortex and the amygdala are ∼20 ms (Tripathy *et al.* 2015). Within such brief window, 'source' neurons may spike only once or twice. Thus, the target may likely discharge when multiple 'source' cells fire together, rather than when a single source bursts. Experimentally, the mechanism of coincidence detection has been demonstrated in brain slices, and in vivo in anaesthetized animals. it has been reported in the auditory, visual, and somatosensory systems (Alonso *et al.* 1996; Roy & Alloway 2001). However, cell assemblies have been proposed to play a role in sophisticated cognitive functions such as learning, decision-making, and cognitive processing (Fujisawa, Amarasingham, *et al.* 2008; Benchenane *et al.* 2010; Ramanathan *et al.* 2015). Here, we provide evidence for the role of cell assemblies in high order brain areas to discharge 'reader' neurons in a downstream structure. This corroborates the hypothesis that responding to cell assemblies might be the mechanism by which information flow is achieved between brain areas (Buzsáki 2010).

Reader responses are supra-linear

Cell assemblies are believed to carry additional information beyond the information relayed by each member individually. If a downstream neuron specifically responds to the activation of a cell assembly, then its responses should be specifically evoked by the assembly as a whole rather than reflect a summation of the responses to assembly members taken individually. Previous work demonstrated supra-linear summation of two coincidental input in the lateral geniculate nucleus in cats (Alonso *et al.* 1996). Within the prefrontal cortex, Fujisawa, Amarasingham, *et al.* 2008 reported that coincidental firing of more than one neuron facilitated spike transmission, with supra-linear effect within 0 to 5 ms. In contrast, spike occurrences of more than one neuron in time windows $\geq$10 ms showed only a linear additive effect on the cooperative ability of presynaptic neurons to discharge a postsynaptic partner. Similarly, we observed that reader responses were supra-linear.

Assembly-reader relationships are shaped by learning

The meaning of the information represented by a cell assembly is likely to change in an ever changing environment, being shaped by experience. Therefore downstream circuits may need to adapt their responses upon assembly activation. One possibility is that the reactivation of specific assemblies might strengthen their connections with a reader. During sleep, reinstatment of learning related assemblies has been extensively

documented in the hippocampus (Wilson & McNaughton 1994; Kudrimoti *et al.* 1999; Nádasdy *et al.* 1999) but also in the prefrontal cortex (Euston *et al.* 2007; Peyrache, Khamassi, *et al.* 2009). Moreover, a recent study demonstrated that correlated pairs of neurons in the amygdala emerge during fear conditioning training (Girardeau, Inema, *et al.* 2017). Here we show that cell assembly-reader relationship is not only shaped by experience but also changes with the passage of time. This is consistent with the evidence demonstrating a constant drift with time of brain representations (Hasz & Redish 2020) and as a consequence downstream decoders likely change their responses accordingly. Moreover here we also show that prefrontal readers of amygdalar cell assemblies evolve with fear conditioning, beyond what can be accounted for by the mere passage of time. Amygdala to mPFC communication has been shown to underpin conditioned fear retention (Klavir *et al.* 2017), recall (Burgos-Robles, Kimchi, *et al.* 2017), and consolidation (Popa, Duvarci, *et al.* 2010). Our results are in line with these findings. It is likely that other learning paradigms would affect specifically the communication between other structures in a specific direction like we found here for AMY-mPFC communication. Finally, we suggest that reader mechanisms may be a general process within the brain beyond this specific network.

5.4 Methods

Animals

Six male Long-Evans rats (350 – 400 g at the time of the surgery, 2-5 months old) were housed individually in monitored conditions (21°C and 45% humidity) and maintained on a 12h light- 12h dark cycle. In order to avoid obesity, rats feeding was restricted to 13-16 g of rat chow per day, with water available *ad libitum*. To habituate the rats to human manipulation they were handled each workday. All experiments conformed to the approved protocols and regulations of the local ethics committee (Comité d'Ethique en matière d'expérimentation animale Paris Centre et Sud n°59), the French ministries of agriculture, and higher education and research.

Surgery

Rats were deeply anesthetized using a ketamine-xylazine mixture (Imalgene and Rompun, 180 mg/kg and 10 mg/kg, respectively) and anesthesia was maintained with isoflurane (0.1-1.5% in oxygen). Analgesia was assured by subcutaneous injection of buprenorphine (Buprecaire, 0.025 mg/kg) and meloxicam (Metacam, 3 mg/kg). We implanted the animals bilaterally with a custom build microdrive with either 24, 32,

or 42 bundles of independently movable twisted electrodes (12 µm tungsten wires twisted in groups of either 6 or 8 wires and gold-plated to ∼200 kΩ) 0.5mm above the target brain regions. Miniature stainless steel screws (serving as electrical reference and ground) were implanted above the cerebellum. During recovery from surgery (minimum 7 days), the rats received antibiotical (Marbofloxacine, 2 mg/kg) and analgesic (Meloxicam, 3 mg/kg) treatments via subcutaneous injections, and were provided with food and water ad libitum. The recording electrodes were then progressively lowered until they reached their targets and then adjusted to optimize yield and stability. Eletrode bundles dorsoventral locations were estimated in vivo using microdriver screw turn counts.

Behavioral apparati

During the experiments, the rats were exposed to three different environments: 2 testing contexts (A and B), one plastic pot for sleep sessions. The **context A** was a cubicle conditioning chamber (40 x 40 x 40 cm) with gray plexiglass walls lined with ribbed black rubber sheets and a floor composed of nineteen stainless steel rods (0.48 cm diameter with 1.6 cm spacing connected to a scrambled shock generator (ENV-414S, Med Associates, USA). It was mildly scented daily with mint-perfumed cleaning solution (Simple Green, Sunshine Makers). The **context B** was a stadium-shaped PVC enclosure (30 cm of straight side and 15 cm of radius) with a black wooden floor and walls lined with light brown pieces of rope rug. It was mildly scented daily with a baking vanilla extract solution. The sleeping pot was a cloth-lined plastic flowerpot (30 cm upper diameter, 20 cm lower diameter, 25 cm high). A custom-made electronic system presented the animals with two auditory CSs (80 dB, 20 s long, each composed of 1 Hz, 250 ms long pips of either white noise, CS+, or 8 kHz pure tones, CS-).

Behavioral protocol

To balance the time spent in each context by the animals, every day of the experimental protocol consisted of one 37 min (n=4 rats). When introduced in the contexts the animals were either presented with the auditory CSs (after a baseline period of 3 min, the animals were presented to 16 CSs, 8 CS+ and 8 CS-, separated by random-duration inter-trial intervals ranging between 120 and 240 s) or received no auditory stimuli (context exposure sessions). Each day of the protocol consisted of a silent context exposure session in one context and a session with CS presentations in the other, except for the fear renewal test day where both sessions had CS presentations. Before and after each session the animals were left undisturbed for at least 2h in the sleeping pot to record sleep

activity. Note that results from Figure 5.1, 5.2 and 5.3 were obtained with data from the pre-training sleep session only whereas Figure 5.4 compares pre and post sleep sessions.
Habituation took place on days 1 and 2. On day 1, habituation to the CSs took place in one context while on day, 2 in the other. On days 3 and 4, the animals were fear conditioned in the BOX where CS+ presentations were coupled with foot shocks (1 s, 0.6 mA, co-terminating with CS+ presentations). During habituation and fear conditioning CS+ and CS- were presented in pseudorandom order (no more than 2 consecutive presentations of the same-type CS). Extinction training began on day 5. In the CYL, after the baseline, 4 CS- were presented followed by 8 CS+ and then 4 CS-. Extinction training was repeated every day until the rat was seen sleeping during CS+ presentations.

Data acquisition and processing

An inertial measurement unit (IMU, custom made) recorded 3D angular velocity and linear acceleration of the animals' heads (sampled at 300 Hz). A red LED mounted on the headstage signalled the instantaneous position of the animals sampled by overhead webcams (30 Hz). Animal behavior was also recorded (50 Hz) by lateral video cameras in A and B (acA25000, Basler). Brain activity was recorded using a 256-channel digital data acquisition system (KJE-1001, Amplipex, Szeged, Hungary). The signals were digitized with three or four 64-channel headstages (Amplipex HS2) and were sampled wideband at 20,000 Hz. Off-line spike sorting of mPFC data was performed by a custom written Matlab program (MathWorks, Natick, MA) implementing the Kilosort algorithm (Pachitariu *et al.* 2016). AMY data was spike sorted with KlustaKwik (K.D. Harris, http://klustakwik. sourceforge.net). Obtained clusters were manually inspected to reject noise and to merge erroneously discriminated units with Klusters (Hazan *et al.* 2006). Neurophysiological and behavioral data were explored with NeuroScope (Hazan *et al.* 2006). LFPs were derived from wideband signals by downsampling all channels to 1,250 Hz.
At the end of the experiments, recording sites were marked with small electrolytic lesions (∼20 µA for 20 seconds, one lesion per bundle). After a delay of at least three days to permit glial scar, rats were deeply anesthetized with a lethal dose of pentobarbital, and intracardially perfused with saline (0.9%) followed by paraformaldehyde (4%). Coronal slices (35 µm) were stained with cresyl-violet and imaged with conventional transmission light microscopy. Recording positions were reconstructed comparing the images with the stereotactic diagrams in Paxinos and Watson (2013).

Slow-Wave Sleep Detection

Automatic detection of immobility was performed by applying a threshold detection routine to the angular speed calculated from gyroscopic data. When data from inertial sensors was not available, position data was used instead. LFP data was visualized using Neuroscope (Hazan *et al.* 2006) and channels with distinct spindles during sleep (mPFC) and theta oscillations during exploration (HPC) were identified. All immobility periods where the z-scored LFP signal filtered in the spindle band (9-17 Hz) exceeded a k-means identified threshold (Supplementary Figure 5.9a) were classified as SWS.

Data analysis and statistics

Data were analyzed in Matlab (MathWorks, Natick, MA), using Freely Moving Animal Toolbox (M.Zugaro and R.Todorova, http://fmatoolbox.sourceforge.net) and custom written programs. Descriptive statistics are reported as median ± standard error of the median.

Cell assembly detection

A unsupervised method based on principal and independent component analyses (PCA; Peyrache, Khamassi, *et al.* 2009 and ICA; Lopes-dos-Santos, Ribeiro, *et al.* 2013) detected the co-activation of simultaneously recorded neurons referred to as 'assemblies'. First, spike trains were binned into 15 ms bins an z-scored to generate a zscored spike count matrix Z, where $Z_{i,j}$ represents the number of spike emitted by the cell i during the time bin j. Then, we extracted assemblies with a two-step procedure. First, principal components (PCs) were computed by eigen decomposition of the correlation of the matrix Z. Principal components associated with eigenvalues exceeding the upperbounds of the Marčenko-Pastur distribution were considered significant (Marčenko & Pastur 1967). Then, we carried out ICA (using the fastICA algorithm, H Gävert,J Hurri, J Särelä, and A Hyvärinen, http://research.ics.aalto.fi/ica/fastica) on the spike train projections onto the subspace spanned by significant PCs. This yielded a set of vectors Ic, of N weights, interpreted as cell assemblies, with weights corresponding to the respective cell's contributions to the assembly (N being the number of recorded cells). Since the signs of the output weights are arbitrary, weights were inverted as necessary to render the highest absolute weight positive. Assembly weights were also normalized.

Identification of cell assembly members

Members of cell assemblies, i.e. cells with the highest absolute weights were identified using Otsu's method (Otsu 1979). Initially developed for image processing, this algorithm divides neuron absolute weights into two groups while maximizing the inter-class variance (the upper group being labeled as 'members'). The goodness of separation was quantified with Otsu's metric (between 0 and 1), that is the ratio of the inter-class variance and the total variance.

Rejection of assemblies with negative weights

In theory, assemblies could be formed with both positive and negative weight members ('mixed' assemblies), representing two groups of anti-correlated neurons that inhibit each other. However, the mixed assemblies we detected tended to be associated with weak eigenvalues and low Otsu's metric compared to assemblies with positive weights members only (see Supp. Figure 5.10c). It is possible that these mixed assemblies resulted from ICA's failure to identify independent component from PCs (see Lopes-dos-Santos, Ribeiro, *et al.* 2013). Thus, we chose to discard 'mixed-assemblies' from further analysis.

Assembly activations

To study the reader responses to synchronous activations of assembly members, we excluded the activity on non-member cells when computing the activation strength of a given assembly (see Supp. Figure 5.11). For each time bin, the assembly activation strength was computed as :

$$A_i(t) = z(t)^T (Ic_i^T Ic_i) z(t)$$

where Ic_i corresponds to the i^{th} and $z(t)$ to the population vector at a given time i.e. columns of the Z matrix). Note that to compute activation strength, the Z matrix was constructed with 15 ms bins and a 5 ms sliding window. The diagonal of the outer product $Ic_i^T Ic_i$ was set to 0 so that single neuron spiking does not contribute to the activation strength. Peaks of the activation strength were detected to identify the precise moments when assembly members were co-firing. Assemblies were considered to be active when their activation strength exceeded the 95th quantile distribution of their peak values.

Readers of cell assemblies

Reader responses to assembly activations were computed as follows. For each reader cell i, spikes were counted in 2 s windows, centered on assembly activation peaks and binned in 10 ms. Assembly-reader candidate

pairs with the reader emitting fewer than 30 spikes around assembly activations were discarded. Candidate assembly-reader pairs were pre-selected for further analyses if the z-scored mean reader response exceeded 2 SDs in the 10-30 ms window following assembly activations; this pre-selection step was required to reduce the computation demands of the analysis below. For each candidate assembly-reader pair, its response matrix was shuffled 200 times to create surrogate data. With this shuffled dataset, the pointwise confidence limits (demarcating the upper and lower 2.5% of the distributions) were computed for each time bin. To account for possible multiple comparisons issues, global bands were also constructed from the maximum and minimum distribution (upper and lower 2.5%). Pairs of assembly-readers were retained for further analysis if they met the following criteria:

1. The cross-correlation exhibited a significant increase in at least one bin within 10-30 ms around assembly activation. To reach significance, the cross-correlation values had to cross both the global and the pointwise band. But note that the time zone extent was determined only by the bins where the cross-correlation lied beyond the pointwise band.

2. Based on the assumption that reader should respond subsequent to assembly activation, the mode of the mean cross-correlogram should be positive (i.e. within]0 1] second, here).

Peer prediction

Population coupling of assembly members was assessed by quantifying to what extent the spike activity of one member could be predicted from the spike activity of all other members ("peer prediction", Harris *et al.* 2003). First, spike trains were divided into two non-overlapping partitions. Using one partition, for each member i of an assembly, a Generalized Linear Model (GLM) was trained to predict its activity from the matrix S_i, containing the spike counts of all units members of the same assembly as the predicted cell. The GLM was tested on the remaining partition. This procedure was repeated two times, switching the training and testing sets, resulting in a two-fold cross-validation. The quality of the prediction was assessed by comparing the median prediction error e to the median error $e_{shuffled}$ obtained by shuffling 50 times the predictions relative to the observed spike counts S_i. The prediction gain g was defined as $g = 1 - e_{shuffled}/e$ ensemble activity rather than neuron pairs (Rothschild *et al.* 2017).

Supra-linearity of reader responses to assembly activations

To assess the supra-linearity of reader responses to assembly activation, we computed an expected reader linear response based on individual member activations. First, we computed the average response curve of the reader to each of the member cells firing unsynchronously (not within $\sim$ 15 ms of other members). Then, for each assembly activation, the estimated linear response was the sum of these individual response curves, weighted by the number of spikes emitted by each member around the assembly activation [-15,15] ms.

Learning-related changes: time control

To ensure that learning related changes between pre and post sleep were not merely caused by time, we compared significant assembly-reader pairs detected in three different periods (see Figure 5.4 d). Period 1 and 2 were selected from pre sleep whereas the third period was from post sleep, defined as meeting the following criteria:

1. The duration between the end of period 1 and the beginning of period 2 was the same as between the end of period 2 and the beginning of period 3.

2. The three periods contained the same amount of slow-wave sleep ($\pm$ 30%).

5.5 Supplementary Material

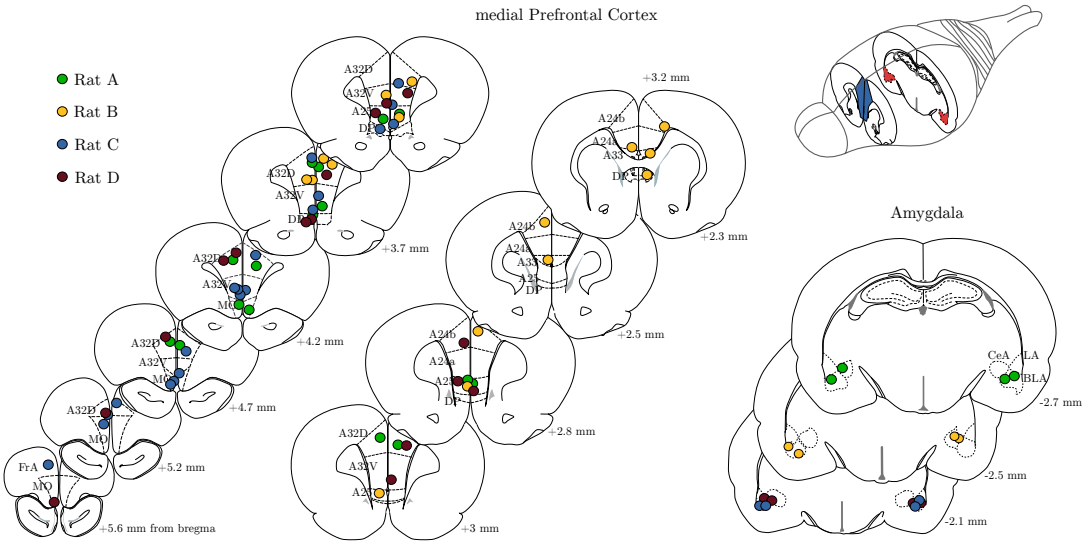

Figure 5.5: Histology Mapping of approximate recording locations (color-coded by rat) in the medial prefrontal cortex (left and middle stacks) and amygdala (right stacks) recording sites. MO = Medial Orbital cortex; DP = Dorsal Peduncular cortex; FrA = Frontal Association cortex; A32D = cingulate cortex area 32 dorsal; A32V = cingulate cortex area 32 ventral; A25 = cingulate cortex area 25; A24a = cingulate cortex area 24a; A24b = cingulate cortex area 24b; CeA = Central nucleus of the Amygdala; LA = lateral amygdala; BLA = Basolateral Amygdala.

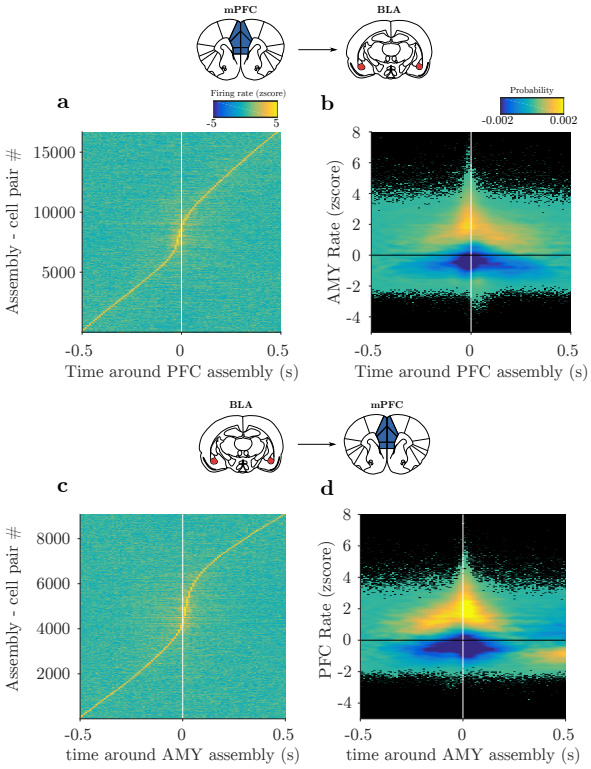

Figure 5.6: Cross-correlation between all possible pairs of assembly-reader **a)** Raster plot of the cross-correlation between prefrontal assemblies and amygdala cells (z-scored; all 16888 pairwise possible combinations). **b)** Distribution of data in a), normalized to baseline (between -500 and -450 ms). The yellow area indicates an increase of reader rate around assembly activation. **c and d)** Same as a and b but for amygdalar assemblies and prefrontal cells.

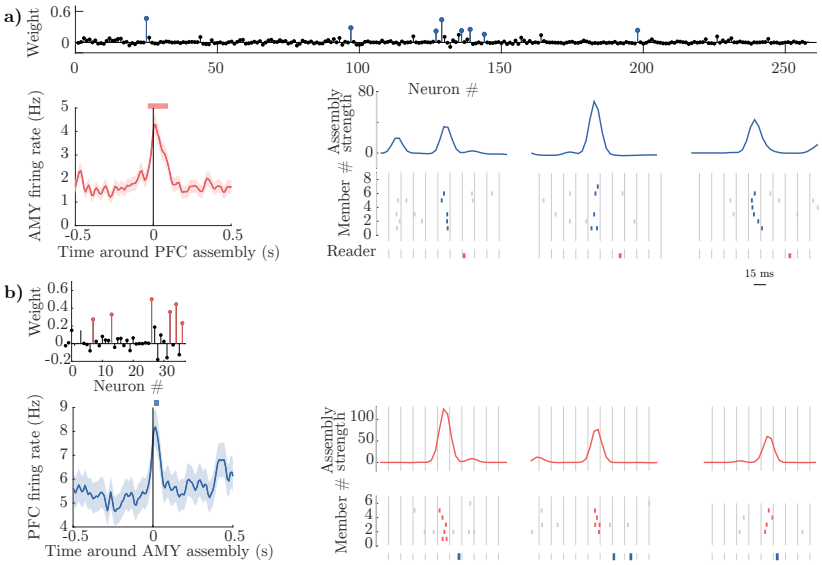

Figure 5.7: Supplementary assembly-reader examples a, b) Respective examples of significant neuron response 10 to 30 ms after assembly activation onset (a: AMY neurons, PFC assemblies; b: PFC neurons, AMY assemblies) Examples were from different sleep session, prior to any behavioral training. Top: cell assemblies. Weights represent each cell's contribution to the assembly. Colored weights: assembly members. Bottom left : 'reader' cell firing rate centered on assembly activation. Shaded bars on top indicate significant responses ($p<0.05$: Monte-Carlo bootstrap test; see Methods 5.4). Bottom right: assembly strength and associated raster plots. Assembly member ticks appear in color during the assembly activation and in gray outside. Blue: prefrontal spikes; red: amygdala spikes. Note the reader response $\sim$ 20 ms after the assembly activation.

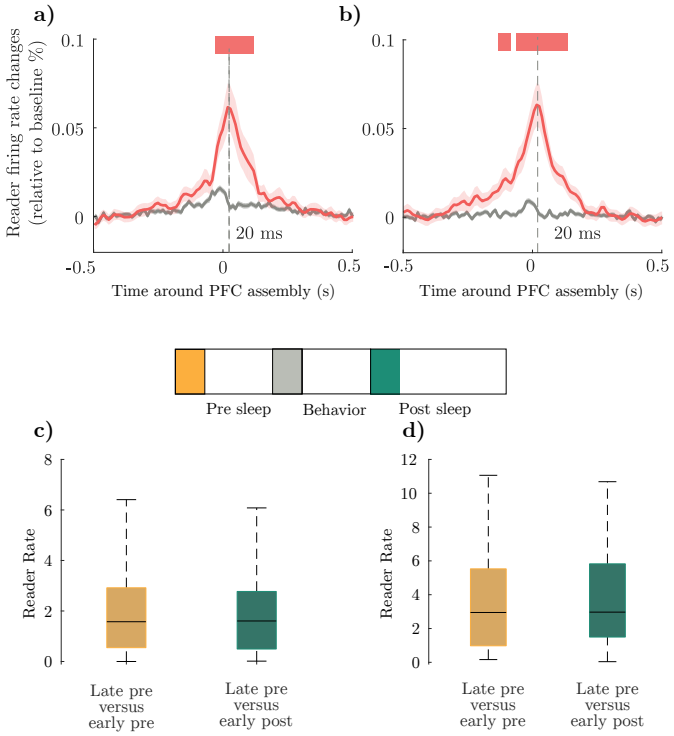

Figure 5.8: AMY reader to PFC assemblies reorganize with time **a) and b)** AMY reader normalized firing rate changes between post and pre sleep (in absolute value), centered on PFC assembly activations (shaded area: mean ± s.e.m.). The red line highlights the interval where the increase was significant ($p<0.05$, Monte-Carlo bootstrap test). **c) and d)** Reader response changes (in absolute value) ∼ 10-30 ms following assembly activations, in the early vs late pre sleep (yellow) and late pre sleep vs early post sleep (green). Reader rate changes were not significantly different when periods were separated by a training session c) Fear conditioning sessions ($p=0.56$; Wilcoxon signed-rank test). d) Extinction sessions ($p=0.66$; Wilcoxon signed-rank test).

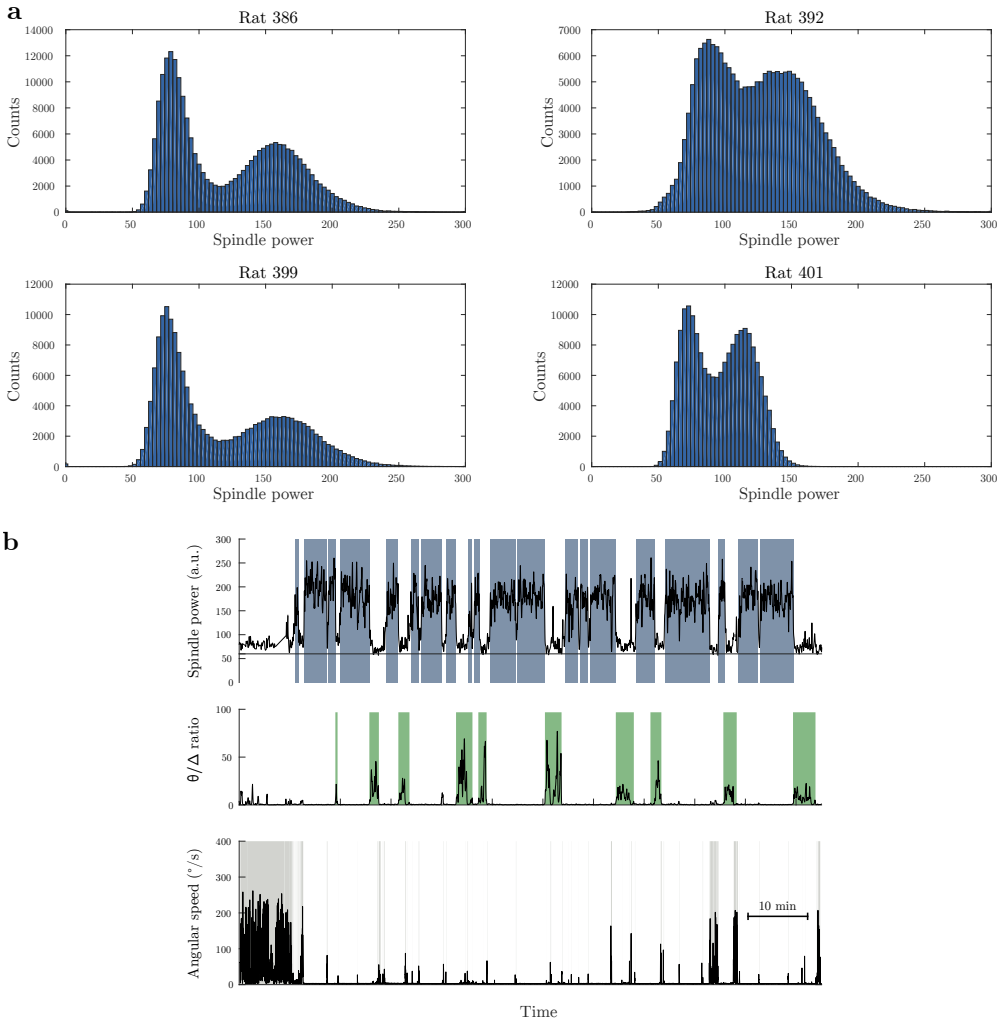

Figure 5.9: Slow wave sleep detection. **a)** Sleep threshold identification from mPFC LFP. Distributions of the spindle power. For each rat the minimum between the two peaks of the distributions was taken as the threshold for sleep detection during periods of immobility. **b)** Example of sleep scoring for $\sim$ 1h30 of recording in the flower pot. Top: Power of the prefrontal LFP signal filtered in the spindle band(9-17 Hz). Blue squares mark the episodes scored as SWS. Middle: Ratio between the theta (6-9 Hz) and delta (0.5-4 Hz) power of the LFP from electrode in the HPC. Green squares mark the episodes scored as REM. Bottom: Angular speed of the animal's head. Gray squares mark episodes of non-immobility.

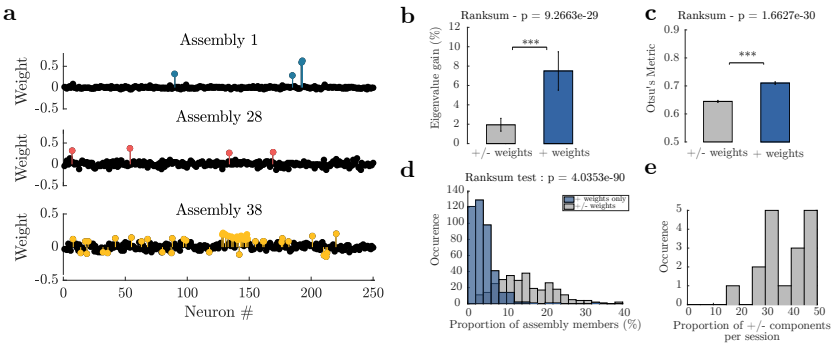

Figure 5.10: Mixed assemblies carry positive and negative weight members
a) Three examples of PFC assemblies. Weights represent each cell's contribution to the assembly. Colored weights indicate assembly members. Assemblies are order by eigenvalue amplitude (that is 1, 28 and 38). Note that assembly 1 and 28 have positive members ('uniform assembly') only whereas the third assembly is composed of both negative and positive members ('mixed-sassembly'). Such assembly is referred to as 'mixed assembly', as opposed to 'uniform assembly' composed of same-sign members only. **b)** Comparison of eigenvalues for two types of assemblies: uniform and mixed assembly. Eigenvalues of mixed assemblies are significantly smaller than those of uniform assemblies. Thus mixed assemblies are less relevant than uniform ones (p = 9.2e-29; Wilcoxon signed-rank test). Colored bars represent median and error bars correspond to the standard error of the median; **c)** Comparison of Otu's metric for two types of assembly: uniform and mixed. Otsu's metric is significantly lower for mixed assemblies (p = 1.7e-30; Wilcoxon signed-rank test), suggesting that the identification of members is less accurate for mixed components. **d)** Proportion of units being part of assemblies, compared to the number of recorded neurons in a session. The number of members in mixed assemblies is significantly higher compared to standard assemblies (up to 40%). **e)** Proportion of mixed assemblies per session.

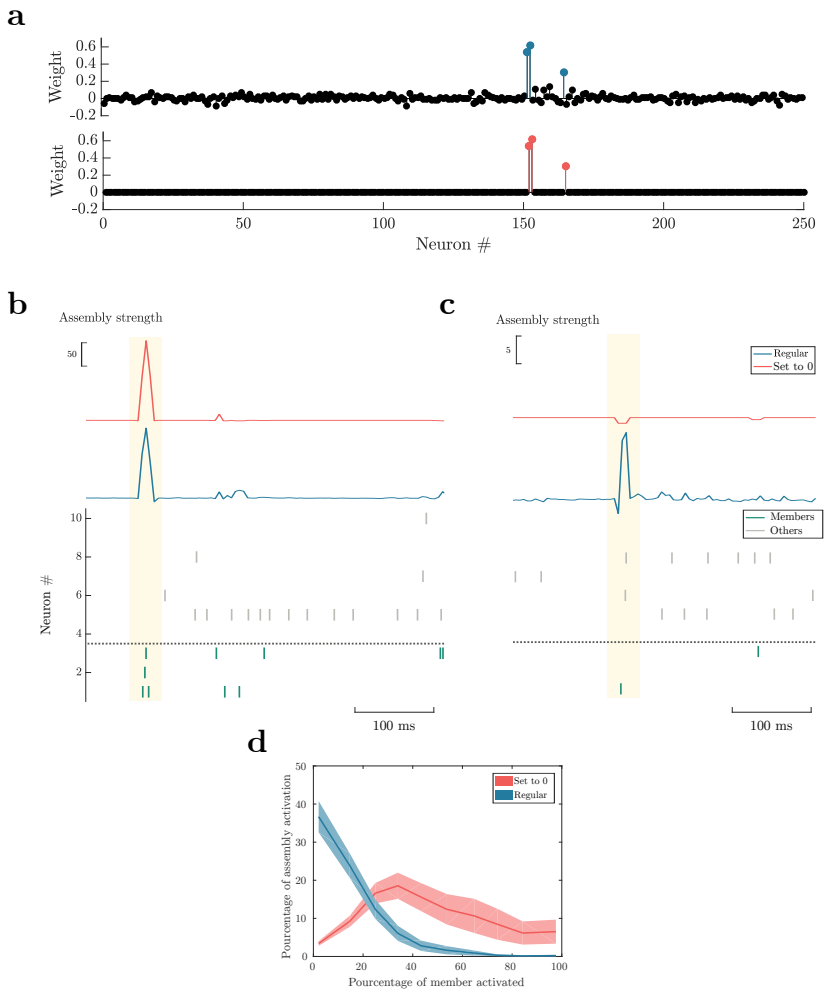

Figure 5.11: Setting non-member weights to 0. **a)** Top: an exemple of a PFC assembly. The weights represent each cell's contribution to the assembly. Colored weights indicate assembly members. Bottom: the same assembly but with non-members weight set to 0. **b and c)** Top: Curves represent assembly activation strength computed with regular weights (blue) and non-member weights set to zero (red). Bottom: Raster plots of neurons ordered by absolute weights. The horizontal dashed line separate members (green ticks) from non-members (grey ticks). Shaded yellow rectangles indicate putative activations. **b)** All three members are active resulting in a peak of activation strength, with both computation methods. **c)** Only one member fires an action potential however a peak is detected with the regular activation strength computation method. Note that there no peaks appear with the other method (i.e. setting non-member weights to zero). **d)** Percentage of firing member during assembly activation. When setting weights to 0, activation strength peaks correspond to co-activations of a higher number of members.

	Number of neurons		Number of assemblies	
session	PFC	AMY	PFC	AMY
Rat392-20181028	68	38	12	3
Rat392-20181029	103	53	16	6
Rat392-20181030	82	51	14	9
Rat392-20181031	38	45	10	10
Rat392-20181101	39	41	10	6
Rat392-20181102	110	60	20	5
Rat386-20180917	250	131	37	18
Rat386-20180918	260	136	36	13
Rat386-20180919	217	135	33	16
Rat386-20180920	258	83	37	12
Rat386-20180921	291	136	40	11
Rat386-20180922	285	124	42	12
Rat399-20190402	155	36	26	5
Rat399-20190403	145	43	26	5
Rat399-20190404	141	42	25	6
Rat399-20190405	149	39	25	4
Rat399-20190406	141	47	26	5
Rat399-20190407	60	38	13	7
Rat401-20190605	12	11	3	3
Rat401-20190606	17	15	5	4
Rat401-20190607	13	16	3	4
Rat401-20190608	20	16	4	3
Rat401-20190609	23	10	5	2
Rat401-20190610	24	9	5	2

Table *1*: Number of recorded neurons and cell assemblies

Part III

General Discussion

6 Discussion

While the experimental results of this thesis have been thoroughly discussed in their respective chapters, this section aims at reviewing our key findings and addressing perspectives for future work.

6.1 Cross-structural coordination

In chapter *Distributed cell assemblies spanning prefrontal cortex and striatum* 4, one of our main findings is the existence of cross-structural assemblies. Cross-structural synchrony has been previously observed between pairs of neurons (Qin *et al.* 1997; Hoffman & Mcnaughton 2002; Lansink, Goltstein, Lankelma, McNaughton, *et al.* 2009; Girardeau, Inema, *et al.* 2017). However, at the assembly level, evidence of cross-structural synchrony remains scarce and mostly restricted to the neocortex (Deolindo *et al.* 2018). Here, our results suggest that within PFC-STR cross-structural assemblies, striatal neurons jointly discharge $\sim 3ms$ subsequent to prefrontal synchronous activity (see the asymmetry of the cross-correlation of PFC-STR member pairs in Figure 4.1c and the phase shift between STR and PFC spikes to gamma-80 in Figure 4.3b). Hence it is possible that PFC-STR assemblies reflect the responses of striatal cells ('readers') to prefrontal assembly activations. Conversely, the conduction delay between the amygdala and the prefrontal cortex is longer, $\sim 20ms$, and thus ideal for studying responses to assemblies without temporal ambiguity.

Alternatively, PFC-STR assemblies could emerge through the common input of a third structure, for example the hippocampus. Indeed, both the striatum and the prefrontal cortex have been shown to coordinate with the hippocampus during learning tasks (Lansink, Golt-

stein, Lankelma, McNaughton, *et al.* 2009; HPC-STR pair correlation; Benchenane *et al.* 2010; PFC spike-HPC field coherence; Sjulson *et al.* 2018; HPC and STR assembly coupling). Future work could investigate temporal coordination of single units within the hippocampo-prefrontal-striatal network during a similar behavioral task. Notably, it would be interesting to determine whether PFC-STR assembly reactivations are coupled to awake and/or sleep ripples.

6.2 Synchronization through oscillations

Oscillations are thought to organize neural network dynamics. They can shape local cell assemblies but also mediate long-range synchronization across distinct areas (Varela *et al.* 2001; Fries 2005), leading to the formation of distributed cell assemblies. In particular, gamma oscillations have been suggested to coordinate neural activity in the mammalian visual cortex (Gray & Singer 1989; Engel, Fries, *et al.* 2001) and also in insect olfactory bulbs (Wehr & Laurent 1996; Perez-Orive *et al.* 2002; Mazor & Laurent 2005).

Here we reported a precise phase relationship of cell assemblies relative to prefrontal rhythms, 4 Hz and theta. Assemblies emerged when spikes of principal neurons shifted in phase, and were accompanied by increased gamma activity. Interestingly, in the ventral palladium, a brain area downstream to the ventral striatum, cell assemblies have been found between ∼24 ms and 80 ms (average time scale = 50 ms), consistent with the beta oscillation period (Tingley, Alexander, *et al.* 2015). Even though we did not observe beta band in our recordings, beta rhythms have been hypothesized to play a role in the coordination of activity among spatially distributed brain regions (in addition to gamma oscillations, Kopell *et al.* 2000; Bibbig *et al.* 2002). How these assemblies in the ventral palladium relate to the prefrontal-striatal assemblies we described, remains unclear.

Conversely, future work could focus on the role of oscillations in shaping amygdalar cell assemblies. Also, one may investigate whether oscillations coordinate assembly and their downstream reader responses. During awake states, converging evidence showed the amygdala and the mPFC exhibited both theta and gamma synchrony, associated with fear behavior control (Stujenske *et al.* 2014). Furthermore, some studies also suggested that oscillatory coupling between these structures, particularly during REM sleep, may be crucial for fear learning (Popa, Duvarci, *et al.* 2010). As postulated by the Coherence Through Communication

theory, such coordination may strengthen connections between cell assemblies and their output target.

6.3 The importance of time scale

In the literature, the time scale of cell assemblies varies greatly, from 1 ms to hundreds of milliseconds, especially in calcium imaging studies. Here we proposed to investigate the formation of cell assemblies within brief timescale close to the membrane time constant of hypothetical targets. We hypothesized that one role of cell assemblies is to produce a coherent synchronous output. In the chapter *Distributed cell assemblies spanning prefrontal cortex and striatum* 4, we investigated the stability of the assemblies detected by PCA-ICA at multiple time scales. Surprisingly, 70% of the detected components at 150 ms persisted at 10 ms (Figure 4.8). Hence, it is possible that some of the assemblies detected in previous studies using larger time bins may have reflected brief synchronous patterns. In the chapter *'Reading cell' assemblies in the cortico-amygdalar circuit* 5, we did not study assembly variability related to the time scale. We directly selected a short time window (15 ms), in the range of the membrane time constant of both the amygdala and the prefrontal cortex (see Tripathy *et al.* 2015; Figure 1.3). Future work should investigate the precise timescales at which an assembly is effective at triggering a downstream response, a parameter which may depend on the biophysics of the downstream neuron.

6.4 Perspectives

While the results presented in *Distributed cell assemblies spanning prefrontal cortex and striatum* 4 are currently under consideration at Nature Communcations, the project on assembly 'readers' in the prefrontal-amygdala network is still ongoing work. The following section is dedicated to the future questions we aim to address.

6.4.1 Characterizing mono-synaptic connections

First, we would like to identify putative mono-synaptic connections within and between the prefrontal cortex and the amygdala. With this information, we will investigate whether cell assembly members are connected to their presumed targets (as shown in Figure 6.1a). Also, it would be interesting to see if, within an assembly, members are reciprocally connected (in line with Hebb's definition of a cell assembly).

6.4.2 Further investigation of the reader response supra-linearity

In Figure 5.3, we demonstrated that the response of reader neurons to cell assembly activations exhibited supra-linear effects. This has been previously reported within the prefrontal cortex (Fujisawa, Amarasingham, *et al.* 2008) and the visual system (Alonso *et al.* 1996; see Figure 6.1b-f). However, one can argue that the supra-linearity might be biased by the activity of unrecorded assembly members. For example, let us consider the assembly ABC and the reader R. We noticed that the reader response to ABC exceed the linear contribution of the individual members A,B and C. However, if a neuron D, not recorded was also active at the same time as ABC (thus the actual assembly was ABCD), the response we observe might be simply explained by the linear summation of A,B,C and D. While it is not possible to experimentally disprove this possibility, short of exhaustively recording all the inputs of a target cell, it is worth considering that the non-linearity is actually expected from the biophysics of neurons, as detailed in the vast literature of coincidence detection (Koch *et al.* 1996).

6.4.3 Extinction learning-related changes

Fear conditioning learning had clear effects on the coupling of amygdalar assemblies and PFC readers. However, when investigating the opposite direction (that is, PFC assemblies and neurons in the amygdala), the changes in the assembly-reader responses were not higher than what would be expected with the passage of time. In a parallel project on the same data set (lead by MN Pompili and R Todorova), preliminary analyses suggest distinct roles of cell assemblies in extinction consolidation whether members are from the ventral part of the medial prefrontal cortex or the dorsal one. Hence, we may detect cell assemblies (and then hypothetical AMY readers) within these two sub-regions to further study extinction related changes. Also, in the chapter *'Reading cell' assemblies in the cortico-amygdalar circuit* 5, we focused on the early extinction sessions (i.e. the two first days) but we might as well investigate late extinction sessions.

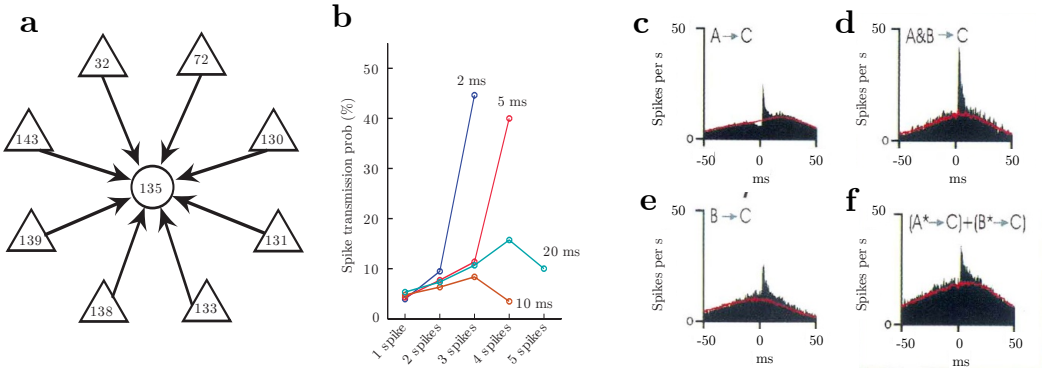

Figure 6.1: Coincidental firing of more facilitates spike transmission supra-linearly. **a)** Representative cell assembly of eight putative pyramidal cells converging on an interneuron ('reader'), in rat prefrontal cortex. **b)** Spike transmission probability as a function of the number of coincident spikes among two or more neurons within increasing time windows. Note the supra-linear facilitation below 5 ms intervals. **c,e)** Cross correlations between a simple cell C in the primary visual cortex and two geniculate cells A, B in cats. The cross-correlations show peaks displaced 2-3 ms to the right of zero which indicate that the simple cell C receives monosynaptic inputs from each geniculate cell A, B (schematically represented by arrows). **d,f)** The spike trains of neurons A and B were divided into two categories: those that occurred within 1.0 ms of each other (A&B) and those of either neuron that did not (A* and B*). The influence of the simultaneous spikes A&B (d) was compared to that of the non-simultaneous spikes (f) by adding together the correlograms from A* –> C and B* –> C. Note the supra-linear effect in d, compared to f. Pannels a-b are adapted from Fujisawa, Amarasingham, *et al.* 2008, and pannels c-f from Alonso *et al.* 1996.

7 On the limitation of Principal and Independent Component Analysis to detect cell assemblies

The results of this thesis mostly derived from the PCA-ICA computation method used for cell assembly detection. This method extracted, with a relatively low computation time, independent components, proxies of cell assemblies.

7.1 Identifying cell assembly members

An independent component is a collection of weights that account for the contribution of each cell within this putative assembly. A central question is: how to identify members of cell assemblies, i.e. the cells that significantly participate in the assemblies?

To this end, in a first attempt, we used Monte-Carlo simulations to estimate the range of weights that could be obtain by chance for each component. To test whether a neuron n_j was a member of the assembly $A = [w_1, w_2, ...w_N]$, we shuffled the inter-spike intervals of n_j, while preserving the activity of all other units. Then assemblies A' were detected within these surrogate data. We expected to identify an assembly A'_i, with a weight distribution similar to A, except for the weight of the cell w'_j. Repeating this procedure 1000 times, we would obtain a distribution of w'_j to compare to the actual weight of the neuron j in A, w_j. However, in many cases, we were unable to reliably match the assembly A with any surrogate assembly A'_i. These cases were a drawback in estimating the control distribution of weights of neuron j in assembly i. We considered that if assembly i could not be retrived without the activity of a neuron j, this may be evidence that neuron j is indeed a member of assembly i. However, we sometimes failed to retrieve a match for A_i even when shuffling the activity of neurons with

very small weights. We therefore moved on to using other method to determine assembly membership.

In the chapter 4, we used the threshold $1/\sqrt{N}$, with N being the number of cells recorded. This threshold represents the expected weight of neurons if all N units were members of one only massive assembly. This threshold was necessary to discriminate cross-structural from single-structure assemblies, investigate the phase-locking of members, relative to ongoing rhythms, as well as quantify their behavior correlate.

In chapter 5 *'Reading cell' assemblies in the cortico-amygdalar circuit*, identifying members was critical to pinpoint exactly which co-active cells could trigger a downstream neuron. To this end, we used a slighly more stringent threshold, based on Otsu's method to distinguish the foreground from the background of gray-scaled pictures. This method provides a metric to quantify the goodness of the separation (between 0 and 1).

7.2 The 'mixed-component' issue

When searching for cell assembly members we noticed that some components exhibited both positive and negative weight members[1] ('mixed-component, see examples in Figure 5.10). In theory, these mixed-components could represent two groups of synchronous neurons that activate in alternation. This could be mediated by interneurons within each group, inhibiting the other group.

However, similar 'mixed-component' were reported by Lopes-dos-Santos, Ribeiro, *et al.* 2013, when dissecting the Principal Component Method (Peyrache, Khamassi, *et al.* 2009, see Figure 7.1). In simulated data sets, the authors found out that 'mixed-components' appeared when the cell assemblies overlapped i.e., they share one or some of their members . For example, using PCA to detect assemblies with neurons [#11, #12, #13, #14] and [#14, #15, #16, #17] yielded a component with high weights for neurons #11 to #18 and a 'mixed-component' with negative weights for [#11, #12, #13] but positive for [#15, #16, #17] (see Figure 7.1b, middle and bottom components). The independent component analysis is supposed to overcome this issue (as shown in Figure 7.1c). We hypothesized that ICA may fail to disentangle assembly patterns that concentrate weak amount of co-variance, hence associated we small

[1] Recall that the sign of weights is arbitrary and weights were inverted as necessary to render the highest absolute weight positive.

eigenvalues (see Figure5.10).

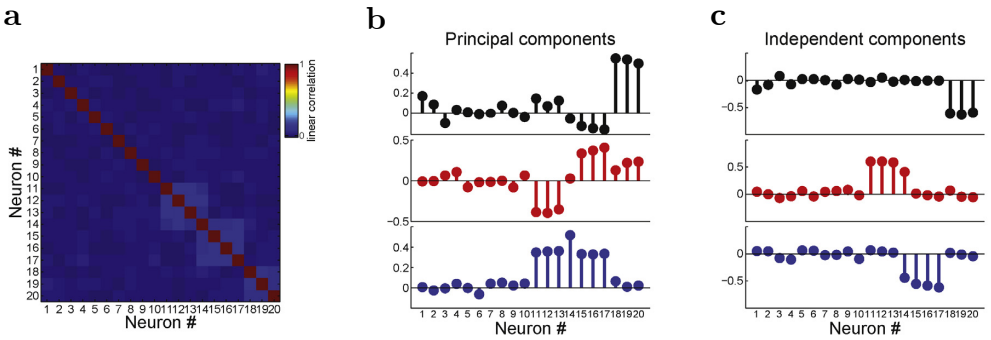

Figure 7.1: 'De-mixing' principal components with independent component analysis. **a)** Correlation matrix of a spike matrix with 20 neurons. Three assemblies were present in a simulated network (light blue squares in the correlation matrix). Assembly 1: neurons #11, #12, #13, #14; assembly 2: neurons #14, #15, #16, #17; assembly 3: neurons #18, #19, #20). **b,c)** Assembly patterns estimated by principal components (b) and by independent components (c). PCA accurately detected assembly 1 but failed to distinguish the overlapping assembly 2 and 3 (both include neuron #14). Note that the second principal component mixes both positive and negative weights. Conversely, assembly patterns were better segregated with ICA, i.e., each assembly pattern has large weights for its corresponding members.

Given that the eigenvalues of the mixed components were lower than average, perhaps one solution would be to increase the eigenvalue threshold from Marčenko & Pastur. This threshold is used because it captures well the distribution of eigenvalues of shuffled matrices, i.e. when no assemblies are present (chapter 2; Peyrache, Benchenane, *et al.* 2010). However, it is possible that the non-linearities due to some assemblies present in the data might distort the distribution of eigenvalues to the point where Marčenko & Pastur's threshold is not a good threshold for separating out assembly patters from noise (Russo & Durstewitz 2017). However, increasing the threshold to using the Tracy-Widom correction (Peyrache, Benchenane, *et al.* 2010) did not abolish mixed assemblies. Therefore, while it is possible to consider mixed components as a symptom of poor assembly separation, there doesn't seem to be a trivial way to avoid them apart from discarding them after detection. Indeed, despite being different on average, the distributions of eigenvalues of mixed and non-mixed components overlapped (data not shown), and therefore no eigenvalue threshold could reliably separate between the two distributions at the risk of also rejecting the majority of non-mixed components.

7.3 Assessing the strength of co-activations

To track over time the dynamic of assembly activity, we computed the activation strength. While the greatest peaks of this measure can reliably highlight high-weight cell co-activations (see the striking examples in the raster plot 4.1, 5.1, 5.2), minor peaks can be caused by the fluctuations of non -member cells, without any members firing (see Figure 5.11). Thus, in Chapter *'Reading' cell assemblies in the cortico-amygdalar circuit* 5, assembly activation strength was computed from the spiking activity of members only. With this restriction, the activation strength peaks reflected accurate member co-activations (n≥2).

7.4 Cell assembly sizes

We also observed that co-activations were composed of different combination of members. For example, if we consider an assembly composed of ABCDEFGHI. Assembly activations could be any duet, (eg. AB, DI, GH), triplet (e.g ABC, CDE, GHI) etc. Should these constellations of different patterns be integrated in the same assembly? Typically, PCA-ICA can detect cell assemblies as big as 20 neurons (in a session of 250 recorded neurons), however, simultaneous co-activations barely exceed 8 or 9 members. Let us recall that the number of assembly is also necessarily lesser than the number of recorded neurons. Considering these observations one can wonder, what reasonable cell assembly size can we expect? How many assemblies are there? We hypothesized that each individual member does not necessarily participate in every single assembly activation but to what extent patterns of activation should overlap to be considered from the same assembly? These questions remain open to debate. To tackle these size issues, in our lab, we are currently developing an algorithm to detect patterns of simultaneous co-activations. This method progressively adds neurons to each assembly, as long as two criteria are fulfilled. For adding neuron X to the pair AB to make an assembly ABX:

1. X needs to fire significantly more synchronously with the activations of AB than with the activity of A or B (both comparisons need to be significant).

2. X needs to fire significantly more synchronously with the activations of AB than the multi-unit activity does (excluding A, B).

Conclusion

Principal Component Analysis and Independent Component Analysis are fast, accessible and popular methods to identify cell assemblies within simultaneously recorded spike trains. While, this technique can accurately detect strong co-activations in the first place, weak correlations might yield more puzzling results. Hence, one might turn to alternative solutions. In chapter 2 and 3, I discussed the numerous existing methods to detect synchronous activity within multiple spike trains ($n>2$). Most of these techniques are usually computationally demanding and remain best suited to identify precise spike sequences. Since every method comes with some drawbacks, the best option may be to use one's favorite method while keeping in mind eventual caveats and last but least, interpreting results with caution.

Bibliography

1. Abeles, M. Role of the cortical neuron: integrator or coincidence detector? eng. *Israel journal of medical sciences* **18,** 83–92 (1982).
2. Abraham, W. C., Logan, B., Greenwood, J. M. & Dragunow, M. Induction and experience-dependent consolidation of stable long-term potentiation lasting months in the Hippocampus. *Journal of Neuroscience* **22,** 9626–9634 (2002).
3. Adhikari, A., Lerner, T. N., Finkelstein, J., Pak, S., Jennings, J. H., Davidson, T. J., Ferenczi, E., Gunaydin, L. A., Mirzabekov, J. J. & Ye, L. Basomedial amygdala mediates top-down control of anxiety and fear. *Nature* **527,** 179–185 (2015).
4. Adrian, E. D. Olfactory reactions in the brain of the hedgehog. *The Journal of Physiology* **100,** 459–473 (1942).
5. Akhlaghpour, H., Wiskerke, J., Choi, J. Y., Taliaferro, J. P., Au, J. & Witten, I. B. Dissociated sequential activity and stimulus encoding in the dorsomedial striatum during spatial working memory. *eLife* **5.** doi:10.7554/eLife.19507 (2016).
6. Alexander, G. E., DeLong, M. R. & Strick, P. L. Parallel Organization of Functionally Segregated Circuits Linking Basal Ganglia and Cortex. *Annual Review of Neuroscience* **9,** 357–381 (1986).
7. Alonso, J. M., Usrey, W. M. & Reid, R. C. Precisely correlated firing in cells of the lateral geniculate nucleus. *Nature* **383,** 815–819 (1996).
8. Artola, A. & Singer, W. Long-term potentiation and NMDA receptors in rat visual cortex. *Nature* **330,** 649–652 (1987).
9. Aru, J., Aru, J., Priesemann, V., Wibral, M., Lana, L., Pipa, G., Singer, W. & Vicente, R. *Untangling cross-frequency coupling in neuroscience* 2015. doi:10.1016/j.conb.2014.08.002.
10. Asaad, W. F., Rainer, G. & Miller, E. K. Neural activity in the primate prefrontal cortex during associative learning. *Neuron* **21,** 1399–1407 (1998).
11. Baeg, E. H., Kim, Y. B., Kim, J., Ghim, J. W., Kim, J. J. & Jung, M. W. Learning-induced enduring changes in functional connectivity among prefrontal cortical neurons. *Journal of Neuroscience* **27,** 909–918 (2007).
12. Barlow, H. B. Summation and inhibition in the frog's retina. *The Journal of Physiology* **119,** 69–88 (1953).
13. Barlow, H. B. Single units and sensation: A neuron doctrine for perceptual psychology? *Perception* **1,** 371–394 (1972).
14. Barthó, P., Hirase, H., Monconduit, L., Zugaro, M., Harris, K. D. & Buzsáki, G. Characterization of neocortical principal cells and interneurons by network interactions and extracellular features. *Journal of Neurophysiology* **92,** 600–608 (2004).
15. Bathellier, B., Ushakova, L. & Rumpel, S. Discrete Neocortical Dynamics Predict Behavioral Categorization of Sounds. *Neuron* **76,** 435–449 (2012).
16. Belluscio, M. A., Mizuseki, K., Schmidt, R., Kempter, R. & Buzsáki, G. Cross-frequency phase-phase coupling between theta and gamma oscillations in the hippocampus. *Journal of Neuroscience* **32,** 423–435 (2012).
17. Benchenane, K., Peyrache, A., Khamassi, M., Tierney, P. L., Gioanni, Y., Battaglia, F. P. & Wiener, S. I. Coherent Theta Oscillations and Reorganization of Spike Timing in the Hippocampal- Prefrontal Network upon Learning. *Neuron* **66,** 921–936 (2010).
18. Bendor, D. & Wilson, M. A. Biasing the content of hippocampal replay during sleep. *Nature Neuroscience* **15,** 1439–1444 (2012).

19. Berger, H. Über das Elektrenkephalogramm des Menschen. *Archiv für Psychiatrie und Nervenkrankheiten* **87,** 527–570 (1929).

20. Berke, J. D., Okatan, M., Skurski, J. & Eichenbaum, H. B. Oscillatory entrainment of striatal neurons in freely moving rats. *Neuron* **43,** 883–896 (2004).

21. Bi, G.-q. & Poo, M.-m. Synaptic Modification by Correlated Activity: Hebb's Postulate Revisited. *Annual Review of Neuroscience* **24,** 139–166 (2001).

22. Bibbig, A., Traub, R. D. & Whittington, M. A. Long-range synchronization of γ and β oscillations and the plasticity of excitatory and inhibitory synapses: A network model. *Journal of Neurophysiology* **88,** 1634–1654 (2002).

23. Bindman, L. J., Murphy, K. P. & Pockett, S. Postsynaptic control of the induction of long-term changes in efficacy of transmission at neocortical synapses in slices of rat brain. *Journal of Neurophysiology* **60,** 1053–1065 (1988).

24. Bissonette, G. B. & Roesch, M. R. Rule encoding in dorsal striatum impacts action selection. *European Journal of Neuroscience* **42,** 2555–2567 (2015).

25. Bliss, T. V. & Lømo, T. Longâlasting potentiation of synaptic transmission in the dentate area of the anaesthetized rabbit following stimulation of the perforant path. *The Journal of Physiology* **232,** 331–356 (1973).

26. Bosman, C. A., Lansink, C. S. & Pennartz, C. M. A. Functions of gamma-band synchronization in cognition: from single circuits to functional diversity across cortical and subcortical systems. *European Journal of Neuroscience* **39,** 1982–1999 (2014).

27. Bosman, C. A., Schoffelen, J. M., Brunet, N., Oostenveld, R., Bastos, A. M., Womelsdorf, T., Rubehn, B., Stieglitz, T., De Weerd, P. & Fries, P. Attentional Stimulus Selection through Selective Synchronization between Monkey Visual Areas. *Neuron* **75,** 875–888 (2012).

28. Bragin, A., Jandó, G., Nádasdy, Z., Hetke, J., Wise, K. & Buzsáki, G. Gamma (40-100 Hz) oscillation in the hippocampus of the behaving rat. *Journal of Neuroscience* **15,** 47–60 (1995).

29. Braitenberg, V. in, 171–188 (Springer, Berlin, Heidelberg, 1978). doi:10.1007/978-3-642-93083-6{_}9.

30. Broome, B. M., Jayaraman, V. & Laurent, G. Encoding and Decoding of Overlapping Odor Sequences. *Neuron* **51,** 467–482 (2006).

31. Brunet, N., Bosman, C. A., Roberts, M., Oostenveld, R., Womelsdorf, T., De Weerd, P. & Fries, P. Visual Cortical Gamma-Band Activity During Free Viewing of Natural Images. *Cerebral Cortex* **25,** 918–926 (2013).

32. Burgos-Robles, A., Kimchi, E. Y., Izadmehr, E. M., Porzenheim, M. J., Ramos-Guasp, W. A., Nieh, E. H., Felix-Ortiz, A. C., Namburi, P., Leppla, C. A. & Presbrey, K. N. Amygdala inputs to prefrontal cortex guide behavior amid conflicting cues of reward and punishment. *Nature neuroscience* **20,** 824–835 (2017).

33. Burgos-Robles, A., Vidal-Gonzalez, I. & Quirk, G. J. Sustained conditioned responses in prelimbic prefrontal neurons are correlated with fear expression and extinction failure. *Journal of Neuroscience* **29,** 8474–8482 (2009).

34. Buschman, T. J. & Miller, E. K. Top-down versus bottom-up control of attention in the prefrontal and posterior parietal cortices. *Science* **315,** 1860–1864 (2007).

35. Buzsáki, G. Two-stage model of memory trace formation: A role for "noisy" brain states. *Neuroscience* **31,** 551–570 (1989).

36. Buzsáki, G. Hippocampal sharp waves: Their origin and significance. *Brain Research* **398,** 242–252 (1986).

37. Buzsáki, G. *Neural Syntax: Cell Assemblies, Synapsembles, and Readers* 2010. doi:10.1016/j.neuron.2010.09.023.

38. Buzsáki, G. & Draguhn, A. *Neuronal olscillations in cortical networks* 2004. doi:10.1126/science.1099745.

39. Buzsáki, G., Horváth, Z., Urioste, R., Hetke, J. & Wise, K. High-frequency network oscillation in the hippocampus. *Science* **256,** 1025–1027 (1992).

40. Buzsáki, G., Lai-Wo S., L. & Vanderwolf, C. H. *Cellular bases of hippocampal EEG in the behaving rat* 1983. doi:10 . 1016 / 0165 - 0173(83) 90037-1.

41. Buzsáki, G. & Wang, X.-J. Mechanisms of Gamma Oscillations. *Annual Review of Neuroscience* **35,** 203–225 (2012).

42. Canolty, R. T., Edwards, E., Dalal, S. S., Soltani, M., Nagarajan, S. S., Kirsch, H. E., Berger, M. S., Barbare, N. M. & Knight, R. T. High gamma power is phase-locked to theta oscillations in human neocortex. *Science* **313,** 1626–1628 (2006).

43. Carmichael, J. E., Gmaz, J. M. & van der Meer, M. A. Gamma oscillations in the rat ventral striatum originate in the piriform cortex. *Journal of Neuroscience* **37,** 7962–7974 (2017).

44. Carrillo-Reid, L., Tecuapetla, F., Tapia, D., Hernández-Cruz, A., Galarraga, E., Drucker-Colin, R. & Bargas, J. Encoding network states by striatal cell assemblies. *Journal of Neurophysiology* **99,** 1435–1450 (2008).

45. Cassenaer, S. & Laurent, G. Hebbian STDP in mushroom bodies facilitates the synchronous flow of olfactory information in locusts. *Nature* **448,** 709–713 (2007).

46. Catanese, J., Carmichael, J. E. & van der Meer, M. A. Low- and high-gamma oscillations deviate in opposite directions from zero-phase synchrony in the limbic corticostriatal loop. *Journal of Neurophysiology* **116,** 5–17 (2016).

47. Catanese, J., Cerasti, E., Zugaro, M., Viggiano, A. & Wiener, S. I. Dynamics of decision-related activity in hippocampus. *Hippocampus* **22,** 1901–1911 (2012).

48. Chadwick, A., Van Rossum, M. C. & Nolan, M. F. Independent theta phase coding accounts for ca population sequences and enables flexible remapping. *eLife* **2015,** 1–51 (2015).

49. Chang, C.-C. & Lin, C.-J. LIBSVM: A library for support vector machines. *ACM Trans. Intell. Syst. Technol* **2,** 27 (2011).

50. Chang, H., Esteves, I. M., Neumann, A. R., Sun, J., Mohajerani, M. H. & McNaughton, B. L. Coordinated activities of retrosplenial ensembles during resting-state encode spatial landmarks. *Philosophical Transactions of the Royal Society B: Biological Sciences* **375,** 20190228 (2020).

51. Chapin, J. K. & Nicolelis, M. A. L. *Principal component analysis of neuronal ensemble activity reveals multidimensional somatosensory representations* tech. rep. (1999), 121–140.

52. Chrobak, J. J. & Buzsáki, G. Gamma oscillations in the entorhinal cortex of the freely behaving rat. *Journal of Neuroscience* **18,** 388–398 (1998).

53. Cirelli, C. & Tononi, G. Is Sleep Essential? *PLoS Biology* **6,** e216 (2008).

54. Clugnet, M. C. & LeDoux, J. E. Synaptic plasticity in fear conditioning circuits: Induction of LTP in the lateral nucleus of the amygdala by stimulation of the medial geniculate body. *Journal of Neuroscience* **10,** 2818–2824 (1990).

55. Cohen, M. X., Elger, C. E. & Fell, J. Oscillatory activity and phase-amplitude coupling in the human medial frontal cortex during decision making. *Journal of Cognitive Neuroscience* **21,** 390–402 (2009).

56. Colgin, L. L., Denninger, T., Fyhn, M., Hafting, T., Bonnevie, T., Jensen, O., Moser, M. B. & Moser, E. I. Frequency of gamma oscillations routes flow of information in the hippocampus. *Nature* **462,** 353–357 (2009).

57. Collingridge, G. L., Isaac, J. T. & Yu, T. W. *Receptor trafficking and synaptic plasticity* 2004. doi:10 . 1038/nrn1556.

58. Csicsvari, J., Jamieson, B., Wise, K. D. & Buzsáki, G. Mechanisms of gamma oscillations in the hippocampus of the behaving rat. *Neuron* **37,** 311–322 (2003).

59. Dave, A. S. & Margoliash, D. Song replay during sleep and computational rules for sensorimotor vocal learning. *Science* **290,** 812–816 (2000).

60. Davidson, T. J., Kloosterman, F. & Wilson, M. A. Hippocampal replay of extended experience. *Neuron* **63,** 497–507 (2009).

61. De La Rocha, J., Doiron, B., Shea-Brown, E., Josić, K. & Reyes, A. Correlation between neural spike trains increases with firing rate. *Nature* **448,** 802–806 (2007).

62. De Lavilléon, G., Lacroix, M. M., Rondi-Reig, L. & Benchenane, K. Explicit memory creation during sleep demonstrates a causal role of place cells in navigation. *Nature neuroscience* **18,** 493–495 (2015).

63. Decharms, R. & Merzenich, M. M. Primary cortical representation of sounds by the coordination of action-potential timing. *Nature* **381,** 610–613 (1996).

64. DeCoteau, W. E., Thorn, C., Gibson, D. J., Courtemanche, R., Mitra, P., Kubota, Y. & Graybiel, A. M. Learning-related coordination of striatal and hippocampal theta rhythms during acquisition of a procedural maze task. *Proceedings of the National Academy of Sciences of the United States of America* **104,** 5644–5649 (2007).

65. DeFelipe, J. & Fariñas, I. *The pyramidal neuron of the cerebral cortex: Morphological and chemical characteristics of the synaptic inputs* 1992. doi:10.1016/0301-0082(92)90015-7.

66. Dejean, C., Courtin, J., Karalis, N., Chaudun, F., Wurtz, H., Bienvenu, T. C. & Herry, C. Prefrontal neuronal assemblies temporally control fear behaviour. *Nature* **535,** 420–424 (2016).

67. Deolindo, C. S., Kunicki, A. C., Da Silva, M. I., Brasil, F. L. & Moioli, R. C. Neuronal assemblies evidence distributed interactions within a tactile discrimination task in rats. *Frontiers in Neural Circuits* **11,** 114 (2018).

68. Desimone, R., Albright, T. D., Gross, C. G. & Bruce, C. Stimulus-selective properties of inferior temporal neurons in the macaque. *Journal of Neuroscience* **4,** 2051–2062 (1984).

69. Destexhe, A., Rudolph, M. & Paré, D. The high-conductance state of neocortical neurons in vivo. *Nature Reviews Neuroscience* **4,** 739–751 (2003).

70. Dhamala, M., Rangarajan, G. & Ding, M. Estimating granger causality from fourier and wavelet transforms of time series data. *Physical Review Letters* **100,** 018701 (2008).

71. Dong, Y., Mihalas, S., Qiu, F., von der Heydt, R. & Niebur, E. Synchrony and the binding problem in macaque visual cortex. *Journal of Vision* **8,** 30–30 (2008).

72. Donnelly, N. A., Holtzman, T., Rich, P. D., Nevado-Holgado, A. J., Fernando, A. B. P., Van Dijck, G., Holzhammer, T., Paul, O., Ruther, P., Paulsen, O., Robbins, T. W. & Dalley, J. W. Oscillatory Activity in the Medial Prefrontal Cortex and Nucleus Accumbens Correlates with Impulsivity and Reward Outcome. *PLoS ONE* **9** (ed Tort, A. B. L.) e111300 (2014).

73. Dragoi, G. & Tonegawa, S. Preplay of future place cell sequences by hippocampal cellular assemblies. *Nature* **469,** 397–401 (2011).

74. Drieu, C., Todorova, R. & Zugaro, M. Nested sequences of hippocampal assemblies during behavior support subsequent sleep replay. *Science* **362,** 675–679 (2018).

75. Eckert, M. J., McNaughton, B. L. & Tatsuno, M. Neural ensemble reactivation in rapid eye movement and slow-wave sleep coordinate with muscle activity to promote rapid motor skill learning. *Philosophical Transactions of the Royal Society B: Biological Sciences* **375,** 20190655 (2020).

76. Ego-Stengel, V. & Wilson, M. A. Disruption of ripple-associated hippocampal activity during rest impairs spatial learning in the rat. *Hippocampus* **20,** NA–NA (2009).

77. Eichenbaum, H. Barlow versus Hebb: When is it time to abandon the notion of feature detectors and adopt the cell assembly as the unit of cognition? *Neuroscience Letters* **680,** 88–93 (2018).

78. Engel, A. K., Fries, P. & Singer, W. Dynamic predictions: Oscillations and synchrony in topâdown processing. *Nature Reviews Neuroscience* **2,** 704–716 (2001).

79. Engel, A. K., Kreiter, A. K., König, P. & Singer, W. Synchronization of oscillatory neuronal responses between striate and extrastriate visual cortical areas of the cat. *Proceedings of the National Academy of Sciences of the United States of America* **88,** 6048–6052 (1991).

80. Euston, D. R., Tatsuno, M. & McNaughton, B. L. Fast-Forward Playback of Recent Memory Sequences in Prefrontal Cortex During Sleep. *Science* **318,** 1147–1150 (2007).

81. Fino, E., Glowinski, J. & Venance, L. Bidirectional activity-dependent plasticity at corticostriatal synapses. *Journal of Neuroscience* **25,** 11279–11287 (2005).

82. Floresco, S. B., Ghods-Sharifi, S., Vexelman, C. & Magyar, O. Dissociable roles for the nucleus accumbens core and shell in regulating set shifting. *Journal of Neuroscience* **26,** 2449–2457 (2006).

83. Foster, D. J. & Wilson, M. A. Reverse replay of behavioural sequences in hippocampal place cells during the awake state. *Nature* **440,** 680–683 (2006).

84. Frankland, P. W. & Bontempi, B. The organization of recent and remote memories. *Nature Reviews Neuroscience* **6,** 119–130 (2005).

85. Freeman, W. J. Definitions of state variables and state space for brain-computer interface. *Cognitive Neurodynamics* **1,** 3–14 (2007).

86. Fries, P. A mechanism for cognitive dynamics: neuronal communication through neuronal coherence. *Trends in Cognitive Sciences* **9,** 474–480 (2005).

87. Fries, P. Neuronal Gamma-Band Synchronization as a Fundamental Process in Cortical Computation. *Annual Review of Neuroscience* **32,** 209–224 (2009).

88. Fries, P. *Rhythms for Cognition: Communication through Coherence* 2015. doi:10.1016/j.neuron.2015.09.034.

89. Fujisawa, S., Amarasingham, A., Harrison, M. T. & Buzsáki, G. Behavior-dependent short-term assembly dynamics in the medial prefrontal cortex. *Nature Neuroscience* **11,** 823–833 (2008).

90. Fujisawa, S. & Buzsáki, G. A 4 Hz Oscillation Adaptively Synchronizes Prefrontal, VTA, and Hippocampal Activities. *Neuron* **72,** 153–165 (2011).

91. Ganmor, E., Segev, R. & Schneidman, E. Sparse low-order interaction network underlies a highly correlated and learnable neural population code. *Proceedings of the National Academy of Sciences of the United States of America* **108,** 9679–9684 (2011).

92. Gardner, R. J., Lu, L., Wernle, T., Moser, M. B. & Moser, E. I. Correlation structure of grid cells is preserved during sleep. *Nature Neuroscience* **22,** 598–608 (2019).

93. Geisler, C., Robbe, D., Zugaro, M., Sirota, A. & Buzsáki, G. Hippocampal place cell assemblies are speed-controlled oscillators. *Proceedings of the National Academy of Sciences of the United States of America* **104,** 8149–8154 (2007).

94. Gelbard-Sagiv, H., Mukamel, R., Harel, M., Malach, R. & Fried, I. Internally generated reactivation of single neurons in human hippocampus during free recall. *Science* **322,** 96–101 (2008).

95. Girardeau, G., Benchenane, K., Wiener, S. I., Buzsáki, G. & Zugaro, M. B. Selective suppression of hippocampal ripples impairs spatial memory. *Nature Neuroscience* **12,** 1222–1223 (2009).

96. Girardeau, G., Inema, I. & Buzsáki, G. Reactivations of emotional memory in the hippocampus-amygdala system during sleep. *Nature Neuroscience* **20,** 1634–1642 (2017).

97. Giri, B., Miyawaki, H., Mizuseki, K., Cheng, S. & Diba, K. Hippocampal reactivation extends for several hours following novel experience. *Journal of Neuroscience* **39,** 866–875 (2019).

98. Gomperts, S. N., Kloosterman, F. & Wilson, M. A. VTA neurons coordinate with the hippocampal reactivation of spatial experience. *eLife* **4.** doi:10.7554/elife.05360 (2015).

99. Gray, C. M. & Singer, W. Stimulus-specific neuronal oscillations in orientation columns of cat visual cortex. *Proceedings of the National Academy of Sciences of the United States of America* **86,** 1698–1702 (1989).

100. Gregoriou, G. G., Gotts, S. J., Zhou, H. & Desimone, R. High-Frequency, long-range coupling between prefrontal and visual cortex during attention. *Science* **324,** 1207–1210 (2009).

101. Gridchyn, I., Schoenenberger, P., O'Neill, J. & Csicsvari, J. Assembly-Specific Disruption of Hippocampal Replay Leads to Selective Memory Deficit. *Neuron* **106,** 291–300 (2020).

102. Groenewegen, H. J., Wright, C. I. & Uylings, H. B. The anatomical relationships of the prefrontal cortex with limbic structures and the basal ganglia. *Journal of psychopharmacology (Oxford, England)* **11,** 99–106 (1997).

103. Grosmark, A. D. & Buzsáki, G. Diversity in neural firing dynamics supports both rigid and learned hippocampal sequences. *Science* **351,** 1440–1443 (2016).

104. Gross, C. G., Bender, D. B. & Rocha-Miranda, C. E. Visual receptive fields of neurons in inferotemporal cortex of the monkey. *Science* **166,** 1303–1306 (1969).

105. Gross, C. G. Genealogy of the "grandmother cell". *Neuroscientist* **8,** 512–518 (2002).

106. Grossberger, L., Battaglia, F. P. & Vinck, M. Unsupervised clustering of temporal patterns in high-dimensional neuronal ensembles using a novel dissimilarity measure. doi:10.1371/journal.pcbi.1006283 (2018).

107. Grothe, I., Neitzel, S. D., Mandon, S. & Kreiter, A. K. Switching neuronal inputs by differential modulations of gamma-band phase-coherence. *Journal of Neuroscience* **32,** 16172–16180 (2012).

108. Gruber, A. J., Hussain, R. J. & O'Donnell, P. The Nucleus Accumbens: A Switchboard for Goal-Directed Behaviors. *PLoS ONE* **4** (ed Albertson, D. N.) e5062 (2009).

109. Grün, S., Abeles, M. & Diesmann, M. in, 96–114 (2008). doi:10.1007/978-3-540-88853-6{_}8.

110. Guise, K. G. & Shapiro, M. L. Medial Prefrontal Cortex Reduces Memory Interference by Modifying Hippocampal Encoding. *Neuron* **94,** 183–192 (2017).

111. Gulati, R., Tsodikov, A., Etzioni, R., Hunter-Merrill, R. A., Gore, J. L., Mariotto, A. B. & Cooperberg, M. R. Expected population impacts of discontinued prostate-specific antigen screening. *Cancer* **120,** 3519–3526 (2014).

112. Gulati, T., Won, S. J., Ramanathan, D. S., Wong, C. C., Bodepudi, A., Swanson, R. A. & Ganguly, K. Robust neuroprosthetic control from the stroke perilesional cortex. *Journal of Neuroscience* **35,** 8653–8661 (2015).

113. Haber, S. N. Corticostriatal circuitry. *Dialogues in Clinical Neuroscience* **18,** 7–21 (2016).

114. Hahnloser, R. H., Kozhevnikov, A. A. & Fee, M. S. An ultra-sparse code underlies the generation of neural sequences in a songbird. *Nature* **419,** 65–70 (2002).

115. Halgren, E., Babb, T. L. & Crandall, P. H. Responses of human limbic neurons to induced changes in blood gases. *Brain Research* **132,** 43–63 (1977).

116. Harris, K. D. Neural signatures of cell assembly organization. *Nature Reviews Neuroscience* **6,** 399–407 (2005).

117. Harris, K. D., Csicsvari, J., Hirase, H., Dragoi, G. & Buzsáki, G. Organization of cell assemblies in the hippocampus. *Nature* **424,** 552–556 (2003).

118. Hart, G., Leung, B. K. & Balleine, B. W. *Dorsal and ventral streams: The distinct role of striatal subregions in the acquisition and performance of goal-directed actions* 2014. doi:10.1016/j.nlm.2013.11.003.

119. Harvey, C. D., Coen, P. & Tank, D. W. Choice-specific sequences in parietal cortex during a virtual-navigation decision task. *Nature* **484,** 62–68 (2012).

120. Hasz, B. M. & Redish, A. D. Dorsomedial prefrontal cortex and hippocampus represent strategic context even while simultaneously changing representation throughout a task session. *Neurobiology of Learning and Memory* **171,** 107215 (2020).

121. Hazan, L., Zugaro, M. & Buzsáki, G. Klusters, NeuroScope, NDManager: A free software suite for neurophysiological data processing and visualization. *Journal of Neuroscience Methods* **155,** 207–216 (2006).

122. Hebb, D. O. *The Organization of Behavior* (1949).

123. Herry, C., Ciocchi, S., Senn, V., Demmou, L., Müller, C. & Lüthi, A. Switching on and off fear by distinct neuronal circuits. *Nature* **454,** 600–606 (2008).

124. Hirsch, J. C. & Crepel, F. Postsynaptic calcium is necessary for the induction of LTP and LTD of monosynaptic EPSPs in prefrontal neurons: An in vitro study in the rat. *Synapse* **10,** 173–175 (1992).

125. Hoffman, K. L. & Mcnaughton, B. L. Coordinated reactivation of distributed memory traces in primate neocortex. *Science* **297,** 2070–2073 (2002).

126. Hoover, W. B. & Vertes, R. P. Anatomical analysis of afferent projections to the medial prefrontal cortex in the rat. *Brain Structure and Function* **212,** 149–179 (2007).

127. Hopfield, J. J. Neural networks and physical systems with emergent collective computational abilities. *Proceedings of the National Academy of Sciences of the United States of America* **79,** 2554–2558 (1982).

128. Howe, M. W., Atallah, H. E., McCool, A., Gibson, D. J. & Graybiel, A. M. Habit learning is associated with major shifts in frequencies of oscillatory activity and synchronized spike firing in striatum. *Proceedings of the National Academy of Sciences of the United States of America* **108,** 16801–16806 (2011).

129. Hubel, D. H. & Wiesel, T. N. Receptive fields, binocular interaction and functional architecture in the cat's visual cortex. *The Journal of Physiology* **160,** 106–154 (1962).

130. Hübner, C., Bosch, D., Gall, A., Lüthi, A. & Ehrlich, I. Ex vivo dissection of optogenetically activated mPFC and hippocampal inputs to neurons in the basolateral amygdala: implications for fear and emotional memory. *Frontiers in behavioral neuroscience* **8,** 64 (2014).

131. Humphries, M. D., Wood, R. & Gurney, K. Dopamine-modulated dynamic cell assemblies generated by the GABAergic striatal microcircuit. *Neural Networks* **22,** 1174–1188 (2009).

132. Hyvärinen, A. & Oja, E. Independent component analysis: Algorithms and applications. *Neural Networks* **13,** 411–430 (2000).

133. Iriki, A., Pavlides, C., Keller, A. & Asanuma, H. Long-term potentiation in the motor cortex. *Science* **245,** 1385–1387 (1989).

134. Ito, M. & Doya, K. Distinct neural representation in the dorsolateral, dorsomedial, and ventral parts of the striatum during fixed- and free-choice tasks. *Journal of Neuroscience* **35,** 3499–3514 (2015).

135. Ito, M. & Kano, M. Long-lasting depression of parallel fiber-Purkinje cell transmission induced by conjunctive stimulation of parallel fibers and climbing fibers in the cerebellar cortex. *Neuroscience Letters* **33,** 253–258 (1982).

136. Izhikevich, E. M. *Dynamical systems in neuroscience* (MIT press, 2007).

137. Jadhav, S. P., Kemere, C., German, P. W. & Frank, L. M. Awake hippocampal sharp-wave ripples support spatial memory. *Science* **336,** 1454–1458 (2012).

138. Jadhav, S. P. P., Rothschild, G., Roumis, D. K. K. & Frank, L. M. M. Coordinated Excitation and Inhibition of Prefrontal Ensembles during Awake Hippocampal Sharp-Wave Ripple Events. *Neuron* **90,** 113–127 (2016).

139. Ji, D. & Wilson, M. A. Coordinated memory replay in the visual cortex and hippocampus during sleep. *Nature Neuroscience* **10,** 100–107 (2007).

140. Johnson, A. & Redish, A. D. Neural ensembles in CA3 transiently encode paths forward of the animal at a decision point. *Journal of Neuroscience* **27,** 12176–12189 (2007).

141. Jolliffe, I. T. in *Principal component analysis* 129–155 (Springer, 1986).

142. Jones, M. W. & Wilson, M. A. Phase precession of medial prefrontal cortical activity relative to the hippocampal theta rhythm. *Hippocampus* **15,** 867–873 (2005).

143. Kandel, E. R., Schwartz, J. H., Jessell, T. M., Jessell, D. o. B., Thomas, M. B., Siegelbaum, S. & Hudspeth, A. J. *Principles of neural science* (McGraw-hill New York, 2000).

144. Karalis, N., Dejean, C., Chaudun, F., Khoder, S., R Rozeske, R., Wurtz, H., Bagur, S., Benchenane, K., Sirota, A., Courtin, J. & Herry, C. 4-Hz oscillations synchronize prefrontal-amygdala circuits during fear behavior. *Nature Neuroscience* **19,** 605–612 (2016).

145. Kay, L. M. *Olfactory system oscillations across phyla* 2015. doi:10.1016/j.conb.2014.10.004.

146. Kelemen, E. & Fenton, A. A. Dynamic grouping of hippocampal neural activity during cognitive control of two spatial frames. *PLoS Biology* **8.** doi:10.1371/journal.pbio.1000403 (2010).

147. Klavir, O., Prigge, M., Sarel, A., Paz, R. & Yizhar, O. Manipulating fear associations via optogenetic modulation of amygdala inputs to prefrontal cortex. *Nature neuroscience* **20,** 836–844 (2017).

148. Koch, C., Rapp, M. & Segev, I. A Brief History of Time (Constants). *Cerebral Cortex* **6,** 93–101 (1996).

149. König, P., Engel, A. K. & Singer, W. Integrator or coincidence detector? The role of the cortical neuron revisited. *Trends in Neurosciences* **19,** 130–137 (1996).

150. Konorski, J. *Integrative activity of the brain.* (Chicago, University of Chicago Press, 1967).

151. Koos, T., Tepper, J. M. & Wilson, C. J. Comparison of IPSCs evoked by spiny and fast-spiking neurons in the neostriatum. *Journal of Neuroscience* **24,** 7916–7922 (2004).

152. Kopell, N., Ermentrout, G. B., Whittington, M. A. & Traub, R. D. Gamma rhythms and beta rhythms have different synchronization properties. *Proceedings of the National Academy of Sciences of the United States of America* **97,** 1867–1872 (2000).

153. Kreiman, G., Koch, C. & Fried, I. Category-specific visual responses of single neurons in the human medial temporal lobe. *Nature Neuroscience* **3,** 946–953 (2000).

154. Kudrimoti, H. S., Barnes, C. A. & McNaughton, B. L. Reactivation of hippocampal cell assemblies: Effects of behavioral state, experience, and EEG dynamics. *Journal of Neuroscience* **19,** 4090–4101 (1999).

155. Lachaux, J., Rodriguez, E., Martinerie, J. & Varela, F. J. Measuring phase synchrony in brain signals. *Human Brain Mapping* **8,** 194–208 (1999).

156. Lacroix, M. M., de Lavilléon, G., Lefort, J., El Kanbi, K., Bagur, S., Laventure, S., Dauvilliers, Y., Peyron, C. & Benchenane, K. Improved sleep scoring in mice reveals human-like stages. *bioRxiv,* 489005 (2018).

157. Lakatos, P., Shah, A. S., Knuth, K. H., Ulbert, I., Karmos, G. & Schroeder, C. E. An oscillatory hierarchy controlling neuronal excitability and stimulus processing in the auditory cortex. *Journal of Neurophysiology* **94,** 1904–1911 (2005).

158. Lalla, L., Rueda Orozco, P. E., Jurado-Parras, M. T., Brovelli, A. & Robbe, D. Local or not local: Investigating the nature of striatal theta oscillations in behaving rats. *eNeuro* **4.** doi:10.1523/ENEURO.0128-17.2017 (2017).

159. Lansink, C. S., Goltstein, P. M., Lankelma, J. V., Joosten, R. N., McNaughton, B. L. & Pennartz, C. M. Preferential reactivation of motivationally relevant information in the ventral striatum. *Journal of Neuroscience* **28,** 6372–6382 (2008).

160. Lansink, C. S., Goltstein, P. M., Lankelma, J. V., McNaughton, B. L. & Pennartz, C. M. Hippocampus leads ventral striatum in replay of place-reward information. *PLoS Biology* **7,** e1000173 (2009).

161. Lasztóczi, B. & Klausberger, T. Hippocampal Place Cells Couple to Three Different Gamma Oscillations during Place Field Traversal. *Neuron* **91,** 34–40 (2016).

162. Laubach, M., Shuler, M. & Nicolelis, M. A. *Independent component analyses for quantifying neuronal ensemble interactions* in *Journal of Neuroscience Methods* **94** (Elsevier, 1999), 141–154. doi:10.1016/S0165-0270(99)00131-4.

163. Laubach, M., Wessberg, J. & Nicolelis, M. A. Cortical ensemble activity increasingly predicts behaviour outcomes during learning of a motor task. *Nature* **405,** 567–571 (2000).

164. Laurent, G. Olfactory network dynamics and the coding of multidimensional signals. *Nature Reviews Neuroscience* **3,** 884–895 (2002).

165. Laurent, G. & Davidowitz, H. Encoding of olfactory information with oscillating neural assemblies. *Science* **265,** 1872–1875 (1994).

166. Lee, A. K. & Wilson, M. A. Memory of sequential experience in the hippocampus during slow wave sleep. *Neuron* **36,** 1183–1194 (2002).

167. Likhtik, E., Pelletier, J. G., Paz, R. & Paré, D. Prefrontal control of the amygdala. *Journal of Neuroscience* **25,** 7429–7437 (2005).

168. Lisman, J. E. & Idiart, M. A. Storage of 7 Â± 2 short-term memories in oscillatory subcycles. *Science* **267,** 1512–1515 (1995).

169. Liu, Q. S., Pu, L. & Poo, M. M. Repeated cocaine exposure in vivo facilitates LTP induction in midbrain dopamine neurons. *Nature* **437,** 1027–1031 (2005).

170. Loomis, A. L., Harvey, E. N. & Hobart, G. Potential rhythms of the cerebral cortex during sleep. *Science* **81,** 597–598 (1935).

171. Lopes-dos-Santos, V., Ribeiro, S. & Tort, A. B. *Detecting cell assemblies in large neuronal populations* 2013. doi:10.1016/j.jneumeth.2013.04.010.

172. Lopes-dos-Santos, V., van de Ven, G. M., Morley, A., Trouche, S., Campo-Urriza, N. & Dupret, D. Parsing Hippocampal Theta Oscillations by Nested Spectral Components during Spatial Exploration and Memory-Guided Behavior. *Neuron* **100,** 940–952 (2018).

173. Louie, K. & Wilson, M. A. Temporally structured replay of awake hippocampal ensemble activity during rapid eye movement sleep. *Neuron* **29,** 145–156 (2001).

174. Mackevicius, E. L., Bahle, A. H., Williams, A. H., Gu, S., Denisenko, N. I., Goldman, M. S. & Fee, M. S. Unsupervised discovery of temporal sequences in high-dimensional datasets, with applications to neuroscience. *eLife* **8.** doi:10.7554/eLife.38471 (2019).

175. Magee, J. C. Dendritic integration of excitatory synaptic input. *Nature Reviews Neuroscience* **1,** 181–190 (2000).

176. Magee, J. C. & Johnston, D. A synaptically controlled, associative signal for Hebbian plasticity in hippocampal neurons. *Science* **275,** 209–213 (1997).

177. Mailly, P., Aliane, V., Groenewegen, H. J., Haber, S. N. & Deniau, J. M. The rat prefrontostriatal system analyzed in 3D: Evidence for multiple interacting functional units. *Journal of Neuroscience* **33,** 5718–5727 (2013).

178. Maingret, N., Girardeau, G., Todorova, R., Goutierre, M. & Zugaro, M. Hippocampo-cortical coupling mediates memory consolidation during sleep. *Nature Neuroscience* **19,** 959–964 (2016).

179. Malagon-Vina, H., Ciocchi, S., Passecker, J., Dorffner, G. & Klausberger, T. Fluid network dynamics in the prefrontal cortex during multiple strategy switching. *Nature Communications* **9,** 1–13 (2018).

180. Malvache, A., Reichinnek, S., Villette, V., Haimerl, C. & Cossart, R. Awake hippocampal reactivations project onto orthogonal neuronal assemblies. *Science* **353,** 1280–1283 (2016).

181. Marčenko, V. A. & Pastur, L. A. Distribution of eigenvalues for some sets fo random matrices. *Mathematics of the USSR-Sbornik* **1,** 457–483 (1967).

182. Marek, R., Xu, L., Sullivan, R. K. P. & Sah, P. Excitatory connections between the prelimbic and infralimbic medial prefrontal cortex show a role for the prelimbic cortex in fear extinction. *Nature neuroscience* **21,** 654–658 (2018).

183. Markram, H., Lübke, J., Frotscher, M. & Sakmann, B. Regulation of synaptic efficacy by coincidence of postsynaptic APs and EPSPs. *Science* **275,** 213–215 (1997).

184. Marr, D. Simple memory: a theory for archicortex. *Philosophical Transactions of the Royal Society of London. B, Biological Sciences* **262,** 23–81 (1971).

185. Martin, A. B. & von der Heydt, R. Spike synchrony reveals emergence of proto-objects in visual cortex. *Journal of Neuroscience* **35,** 6860–6870 (2015).

186. Mazor, O. & Laurent, G. Transient dynamics versus fixed points in odor representations by locust antennal lobe projection neurons. *Neuron* **48,** 661–673 (2005).

187. McGaugh, J. L. THE AMYGDALA MODULATES THE CONSOLIDATION OF MEMORIES OF EMOTIONALLY AROUSING EXPERIENCES. *Annual Review of Neuroscience* **27,** 1–28 (2004).

188. Meshulam, L., Gauthier, J. L., Brody, C. D., Tank, D. W. & Bialek, W. Collective Behavior of Place and Non-place Neurons in the Hippocampal Network. *Neuron* **96,** 1178–1191 (2017).

189. Mézard, M., Parisi, G. & Virasoro, M. *Spin glass theory and beyond: An Introduction to the Replica Method and Its Applications* (World Scientific Publishing Company, 1987).

190. Miller, G. A. The magical number seven, plus or minus two: some limits on our capacity for processing information. *Psychological Review* **63,** 81–97 (1956).

191. Mitra, P. P. & Pesaran, B. Analysis of dynamic brain imaging data. *Biophysical Journal* **76,** 691–708 (1999).

192. Morgan, M. A. & LeDoux, J. E. Differential contribution of dorsal and ventral medial prefrontal cortex to the acquisition and extinction of conditioned fear in rats. *Behavioral neuroscience* **109,** 681 (1995).

193. Muller, J., Corodimas, K. P., Fridel, Z. & LeDoux, J. E. Functional inactivation of the lateral and basal nuclei of the amygdala by muscimol infusion prevents fear conditioning to an explicit conditioned stimulus and to contextual stimuli. *Behavioral Neuroscience* **111,** 683–682 (1997).

194. Nádasdy, Z., Hirase, H., Czurkó, A., Csicsvari, J. & Buzsáki, G. Replay and time compression of recurring spike sequences in the hippocampus. *Journal of Neuroscience* **19,** 9497–9507 (1999).

195. Nicolelis, M. A., Baccala, L. A., Lin, R. C. & Chapin, J. K. Sensorimotor encoding by synchronous neural ensemble activity at multiple levels of the somatosensory system. *Science* **268,** 1353–1358 (1995).

196. Nitzan, N., McKenzie, S., Beed, P., English, D. F., Oldani, S., Tukker, J. J., Buzsáki, G. & Schmitz, D. Propagation of hippocampal ripples to the neocortex by way of a subiculum-retrosplenial pathway. *Nature Communications* **11,** 1–17 (2020).

197. Nusser, Z., Kay, L. M., Laurent, G., Homanics, G. E. & Mody, I. Disruption of GABAA receptors on GABAergic interneurons leads to increased oscillatory power in the olfactory bulb network. *Journal of Neurophysiology* **86,** 2823–2833 (2001).

198. O'Keefe, J. & Dostrovsky, J. The hippocampus as a spatial map. Preliminary evidence from unit activity in the freely-moving rat. *Brain Research* **34,** 171–175 (1971).

199. Ólafsdóttir, H. F., Carpenter, F. & Barry, C. Coordinated grid and place cell replay during rest. *Nature Neuroscience* **19,** 792–794 (2016).

200. O'Neill, J., Boccara, C. N., Stella, F., Schoenenberger, P. & Csicsvari, J. Superficial layers of the medial entorhinal cortex replay independently of the hippocampus. *Science* **355,** 184–188 (2017).

201. O'Neill, J., Senior, T. J., Allen, K., Huxter, J. R. & Csicsvari, J. Reactivation of experience-dependent cell assembly patterns in the hippocampus. *Nature Neuroscience* **11,** 209–215 (2008).

202. Oostenveld, R., Fries, P., Maris, E. & Schoffelen, J.-M. S. FieldTrip: Open Source Software for Advanced Analysis of MEG, EEG, and Invasive Electrophysiological Data. *Computational Intelligence and Neuroscience,* 9 (2011).

203. Otsu, N. Threshold selection method from gray-level histograms. *IEEE Trans Syst Man Cybern* **SMC-9,** 62–66 (1979).

204. Oualian, C. & Gisquet-Verrier, P. The differential involvement of the prelimbic and infralimbic cortices in response conflict affects behavioral flexibility in rats trained in a new automated strategy-switching task. *Learning and Memory* **17,** 654–668 (2010).

205. Pachitariu, M., Steinmetz, N., Kadir, S., Carandini, M. & Harris, K. D. *Kilosort: realtime spike-sorting for extracellular electrophysiology with hundreds of channels* tech. rep. (2016), 061481. doi:10.1101/061481.

206. Palva, J. M., Palva, S. & Kaila, K. Phase synchrony among neuronal oscillations in the human cortex. *Journal of Neuroscience* **25,** 3962–3972 (2005).

207. Paré, D. & Collins, D. R. Neuronal correlates of fear in the lateral amygdala: Multiple extracellular recordings in conscious cats. *Journal of Neuroscience* **20,** 2701–2710 (2000).

208. Pastalkova, E., Itskov, V., Amarasingham, A. & Buzsáki, G. Internally generated cell assembly sequences in the rat hippocampus. *Science* **321,** 1322–1327 (2008).

209. Pavlides, C. & Winson, J. Influences of hippocampal place cell firing in the awake state on the activity of these cells during subsequent sleep episodes. *Journal of Neuroscience* **9,** 2907–2918 (1989).

210. Paxinos, G. & Watson, C. *The Rat Brain in Stereotaxic Coordinates: Hard Cover Edition* 456 (2006).

211. Pennartz, C. M., Ameerun, R. F., Groenewegen, H. J. & Lopes da Silva, F. H. Synaptic Plasticity in an In Vitro Slice Preparation of the Rat Nucleus Accumbens. *European Journal of Neuroscience* **5,** 107–117 (1993).

212. Pennartz, C. M., Lee, E., Verheul, J., Lipa, P., Barnes, C. A. & McNaughton, B. L. The ventral striatum in off-line processing: Ensemble reactivation during sleep and modulation by hippocampal ripples. *Journal of Neuroscience* **24,** 6446–6456 (2004).

213. Perez-Orive, J., Mazor, O., Turner, G. C., Cassenaer, S., Wilson, R. I. & Laurent, G. Oscillations and sparsening of odor representations in the mushroom body. *Science* **297,** 359–365 (2002).

214. Perrett, D. I., Rolls, E. T. & Caan, W. Visual neurones responsive to faces in the monkey temporal cortex. *Experimental Brain Research* **47,** 329–342 (1982).

215. Peyrache, A., Battaglia, F. P. & Destexhe, A. Inhibition recruitment in prefrontal cortex during sleep spindles and gating of hippocampal inputs. *Proceedings of the National Academy of Sciences of the United States of America* **108,** 17207–17212 (2011).

216. Peyrache, A., Benchenane, K., Khamassi, M., Wiener, S. I., Battaglia, F. P., Peyrache, A., Benchenane, Â. K., Khamassi, Â. M., Wiener, Â. S. I., Battaglia, F. P., Wiener, S. I. & Khamassi, M. Principal component analysis of ensemble recordings reveals cell assemblies at high temporal resolution. *J Comput Neurosci* **29,** 309–325 (2010).

217. Peyrache, A., Khamassi, M., Benchenane, K., Wiener, S. I. & Battaglia, F. P. Replay of rule-learning related neural patterns in the prefrontal cortex during sleep. *Nature Neuroscience* **12,** 919–926 (2009).

218. Pfeiffer, B. E. & Foster, D. J. Hippocampal place-cell sequences depict future paths to remembered goals. *Nature* **497,** 74–79 (2013).

219. Picado-Muiño, D., Borgelt, C., Berger, D., Gerstein, G. & Grün, S. Finding neural assemblies with frequent item set mining. *Frontiers in Neuroinformatics* **7,** 9 (2013).

220. Pignatelli, M. & Beyeler, A. *Valence coding in amygdala circuits* 2019. doi:10.1016/j.cobeha.2018.10.010.

221. Pipa, G. & Munk, M. H. J. Higher Order Spike Synchrony in Prefrontal Cortex during Visual Memory. *Frontiers in Computational Neuroscience* **5,** 23 (2011).

222. Ponzi, A. & Wickens, J. R. Input dependent cell assembly dynamics in a model of the striatal medium spiny neuron network. *Frontiers in Systems Neuroscience* **6.** doi:10.3389/fnsys.2012.00006 (2012).

223. Popa, D., Duvarci, S., Popescu, A. T., Léna, C. & Paré, D. Coherent amygdalocortical theta promotes fear memory consolidation during paradoxical sleep. *Proceedings of the National Academy of Sciences* **107,** 6516–6519 (2010).

224. Popa, D., Spolidoro, M., Proville, R. D., Guyon, N., Belliveau, L. & Léna, C. Functional role of the cerebellum in gamma-band synchronization of the sensory and motor cortices. *Journal of Neuroscience* **33,** 6552–6556 (2013).

225. Pouget, A., Dayan, P. & Zemel, R. Information processing with population codes. *Nature Reviews Neuroscience* **1,** 125–132 (2000).

226. Qin, Y.-L., Mcnaughton, B. L., Skaggs, W. E. & Barnes, C. A. Memory reprocessing in corticocortical and hippocampocortical neuronal ensembles. *Philosophical Transactions of the Royal Society of London. Series B: Biological Sciences* **352** (eds Burgess, N. & Oapos;Keefe, J.) 1525–1533 (1997).

227. Quaglio, P., Rostami, V., Torre, E. & Grün, S. Methods for identification of spike patterns in massively parallel spike trains. *Biological Cybernetics* **112,** 57–80 (2018).

228. Quaglio, P., Yegenoglu, A., Torre, E., Endres, D. M. & Grün, S. Detection and Evaluation of Spatio-Temporal Spike Patterns in Massively Parallel Spike Train Data with SPADE. *Frontiers in Computational Neuroscience* **11,** 41 (2017).

229. Quian Quiroga, R., Kraskov, A., Koch, C. & Fried, I. Explicit Encoding of Multimodal Percepts by Single Neurons in the Human Brain. *Current Biology* **19,** 1308–1313 (2009).

230. Quirk, G. J., Likhtik, E., Pelletier, J. G. & Paré, D. Stimulation of medial prefrontal cortex decreases the responsiveness of central amygdala output neurons. *Journal of Neuroscience* **23,** 8800–8807 (2003).

231. Quirk, G. J., Repa, J. C. & LeDoux, J. E. Fear conditioning enhances short-latency auditory responses of lateral amygdala neurons: Parallel recordings in the freely behaving rat. *Neuron* **15,** 1029–1039 (1995).

232. Quiroga, R. Q., Kreiman, G., Koch, C. & Fried, I. Sparse but not 'Grandmother-cell' coding in the medial temporal lobe. *Trends in Cognitive Sciences* **12,** 87–91 (2008).

233. Quiroga, R. Q., Reddy, L., Kreiman, G., Koch, C. & Fried, I. Invariant visual representation by single neurons in the human brain. *Nature* **435,** 1102–1107 (2005).

234. Quiroga, R. Q. *Concept cells: the building blocks of declarative memory functions* 2012. doi:10.1038/nrn3251.

235. Ragozzino, M. E. *The contribution of the medial prefrontal cortex, orbitofrontal cortex, and dorsomedial striatum to behavioral flexibility* in *Annals of the New York Academy of Sciences* **1121** (Blackwell Publishing Inc., 2007), 355–375. doi:10.1196/annals.1401.013.

236. Ramanathan, D. S., Gulati, T. & Ganguly, K. Sleep-Dependent Reactivation of Ensembles in Motor Cortex Promotes Skill Consolidation. *PLOS Biology | DOI.* doi:10.1371/journal.pbio.1002263 (2015).

237. Rasch, B., Buchel, C., Gais, S. & Born, J. Odor Cues During Slow-Wave Sleep Prompt Declarative Memory Consolidation. *Science* **315,** 1426–1429 (2007).

238. Rasch, B. & Born, J. About sleep's role in memory. *Physiological Reviews* **93,** 681–766 (2013).

239. Ray, S. & Maunsell, J. H. R. Different Origins of Gamma Rhythm and High-Gamma Activity in Macaque Visual Cortex. *PLoS Biology* **9** (ed Ungerleider, L.) e1000610 (2011).

240. Reppucci, C. J. & Petrovich, G. D. Organization of connections between the amygdala, medial prefrontal cortex, and lateral hypothalamus: a single and double retrograde tracing study in rats. *Brain Structure and Function* **221,** 2937–2962 (2016).

241. Riehle, A., Grün, S., Diesmann, M. & Aertsen, A. Spike synchronization and rate modulation differentially involved in motor cortical function. *Science* **278,** 1950–1953 (1997).

242. Rodriguez, E., George, N., Lachaux, J. P., Martinerie, J., Renault, B. & Varela, F. J. Perception's shadow: Long-distance synchronization of human brain activity. *Nature* **397,** 430–433 (1999).

243. Roelfsema, P. R., Engel, A. K., König, P. & Singer, W. Visuomotor integration is associated with zero time-lag synchronization among cortical areas. *Nature* **385,** 157–161 (1997).

244. Roskies, A. L. *The binding problem* 1999. doi:10.1016/S0896-6273(00)80817-X.

245. Rothschild, G., Eban, E. & Frank, L. M. A cortical-hippocampal-cortical loop of information processing during memory consolidation. *Nature Neuroscience* **20,** 251–259 (2017).

246. Roy, S. A. & Alloway, K. D. Coincidence detection or temporal integration? What the neurons in somatosensory cortex are doing. *Journal of Neuroscience* **21,** 2462–2473 (2001).

247. Rudoy, J. D., Voss, J. L., Westerberg, C. E. & Paller, K. A. Strengthening individual memories by reactivating them during sleep. *Science* **326,** 1079 (2009).

248. Russo, E. & Durstewitz, D. Cell assemblies at multiple time scales with arbitrary lag constellations. *eLife* **6,** 1–31 (2017).

249. Sakurai, Y., Nakazono, T., Ishino, S., Terada, S., Yamaguchi, K. & Takahashi, S. *Diverse synchrony of firing reflects diverse cell-assembly coding in the prefrontal cortex* 2013. doi:10.1016/j.jphysparis.2013.05.004.

250. Sakurai, Y. & Takahashi, S. Dynamic synchrony of firing in the monkey prefrontal cortex during working-memory tasks. *Journal of Neuroscience* **26,** 10141–10153 (2006).

251. Schneidman, E., Berry, M. J., Segev, R. & Bialek, W. Weak pairwise correlations imply strongly correlated network states in a neural population. *Nature* **440,** 1007–1012 (2006).

252. Schomburg, E. W., Fernández-Ruiz, A., Mizuseki, K., Berényi, A., Anastassiou, C. A., Koch, C. & Buzsáki, G. Theta Phase Segregation of Input-Specific Gamma Patterns in Entorhinal-Hippocampal Networks. *Neuron* **84,** 470–485 (2014).

253. See, J. Z., Atencio, C. A., Sohal, V. S. & Schreiner, C. E. Coordinated neuronal ensembles in primary auditory cortical columns. *eLife* **7.** doi:10.7554/eLife.35587 (2018).

254. Segev, I. & London, M. *Untangling dendrites with quantitative models* 2000. doi:10.1126/science.290.5492.744.

255. Senn, V., Wolff, S. B. E., Herry, C., Grenier, F., Ehrlich, I., Gründemann, J., Fadok, J. P., Müller, C., Letzkus, J. J. & Lüthi, A. Long-range connectivity defines behavioral specificity of amygdala neurons. *Neuron* **81,** 428–437 (2014).

256. Shannon, C. E. A mathematical theory of communication. *The Bell system technical journal* **27,** 379–423 (1948).

257. Shatz, C. J. The Developing Brain. *Scientific American* **267,** 60–67 (1992).

258. Shibata, R., Mulder, A., Trullier, O. & Wiener, S. Position sensitivity in phasically discharging nucleus accumbens neurons of rats alternating between tasks requiring complementary types of spatial cues. *Neuroscience* **108,** 391–411 (2001).

259. Shlens, J., Field, G. D., Gauthier, J. L., Grivich, M. I., Petrusca, D., Sher, A., Litke, A. M. & Chichilnisky, E. J. Journal of Neuroscience. *J. Neurosci.* **13,** 5334–5355 (2006).

260. Siapas, A. G., Lubenov, E. V. & Wilson, M. A. Prefrontal phase locking to hippocampal theta oscillations. *Neuron* **46,** 141–151 (2005).

261. Siapas, A. G. & Wilson, M. A. Coordinated interactions between hippocampal ripples and cortical spindles during slow-wave sleep. *Neuron* **21,** 1123–1128 (1998).

262. Sierra-Mercado, D., Padilla-Coreano, N. & Quirk, G. J. Dissociable roles of prelimbic and infralimbic cortices, ventral hippocampus, and basolateral amygdala in the expression and extinction of conditioned fear. *Neuropsychopharmacology* **36,** 529–538 (2011).

263. Sigala, N., Kusunoki, M., Nimmo-Smith, I., Gaffan, D. & Duncan, J. Hierarchical coding for sequential task events in the monkey prefrontal cortex. *Proceedings of the National Academy of Sciences of the United States of America* **105,** 11969–11974 (2008).

264. Singer, W. & Gray, C. M. Visual Feature Integration and the Temporal Correlation Hypothesis. *Annual Review of Neuroscience* **18,** 555–586 (1995).

265. Sirota, A., Csicsvari, J., Buhl, D. & Buzsáki, G. Communication between neocortex and hippocampus during sleep in rodents. *Proceedings of the National Academy of Sciences* **100,** 2065–2069 (2003).

266. Sirota, A. & Buzsáki, G. Interaction between neocortical and hippocampal networks via slow oscillations. *Thalamus and Related Systems* **3,** 245–259 (2005).

267. Sirota, A., Montgomery, S., Fujisawa, S., Isomura, Y., Zugaro, M. & Buzsáki, G. Entrainment of Neocortical Neurons and Gamma Oscillations by the Hippocampal Theta Rhythm. *Neuron* **60,** 683–697 (2008).

268. Sjulson, L., Peyrache, A., Cumpelik, A., Cassataro, D. & Buzsáki, G. Cocaine Place Conditioning Strengthens Location-Specific Hippocampal Coupling to the Nucleus Accumbens. *Neuron* **98,** 926–934 (2018).

269. Skaggs, W. E. & McNaughton, B. L. Replay of neuronal firing sequences in rat hippocampus during sleep following spatial experience. *Science* **271,** 1870–1873 (1996).

270. Skelin, I., Kilianski, S. & McNaughton, B. L. Hippocampal coupling with cortical and subcortical structures in the context of memory consolidation. *Neurobiology of Learning and Memory* **160,** 21–31 (2019).

271. Sleezer, B. J., Castagno, M. D. & Hayden, B. Y. Rule encoding in orbitofrontal cortex and striatum guides selection. *Journal of Neuroscience* **36,** 11223–11237 (2016).

272. Spruston, N. & Johnston, D. Perforated patch-clamp analysis of the passive membrane properties of three classes of hippocampal neurons. *Journal of Neurophysiology* **67,** 508–529 (1992).

273. Squire, L. R. Memory and the hippocampus: a synthesis from findings with rats, monkeys, and humans [published erratum appears in Psychol Rev 1992 Jul;99(3):582]. *Psychol.Rev.* **99,** 195–231 (1992).

274. Stark, E., Roux, L., Eichler, R. & Buzsáki, G. Local generation of multineuronal spike sequences in the hippocampal CA1 region. *Proceedings of the National Academy of Sciences of the United States of America* **112,** 10521–10526 (2015).

275. Staude, B., Grün, S. & Rotter, S. Higher-order correlations in nonstationary parallel spike trains: Statistical modeling and inference. *Frontiers in Computational Neuroscience* **4.** doi:10.3389/fncom.2010.00016 (2010).

276. Staude, B., Rotter, S. & Grün, S. CuBIC: Cumulant based inference of higher-order correlations in massively parallel spike trains. *Journal of Computational Neuroscience* **29,** 327–350 (2010).

277. Stenner, M. P., Litvak, V., Rutledge, R. B., Zaehle, T., Schmitt, F. C., Voges, J., Heinze, H. J. & Dolan, R. J. Cortical drive of low-frequency oscillations in the human nucleus accumbens during action selection. *Journal of Neurophysiology* **114,** 29–39 (2015).

278. Steriade, M., Contreras, D., Dossi, R. C. & Nunez, A. The slow (<1 Hz) oscillation in reticular thalamic and thalamocortical neurons: Scenario of sleep rhythm generation in interacting thalamic and neocortical networks. *Journal of Neuroscience* **13,** 3284–3299 (1993).

279. Steriade, M., McCormick, D. A. & Sejnowski, T. J. Thalamocortical oscillations in the sleeping and aroused brain. *Science* **262,** 679–685 (1993).

280. Stopfer, M., Bhagavan, S., Smith, B. H. & Laurent, G. Impaired odour discrimination on desynchronization of odour-encoding neural assemblies. *Nature* **390,** 70–74 (1997).

281. Stujenske, J. M., Likhtik, E., Topiwala, M. A. & Gordon, J. A. Fear and Safety Engage Competing Patterns of Theta-Gamma Coupling in the Basolateral Amygdala. *Neuron* **83,** 919–933 (2014).

282. Sullivan, D., Mizuseki, K., Sorgi, A. & Buzsáki, G. Comparison of sleep spindles and theta oscillations in the hippocampus. *Journal of Neuroscience* **34,** 662–674 (2014).

283. Tabuchi, E., Mulder, A. & Wiener, S. Position and behavioral modulation of synchronization of hippocampal and accumbens neuronal discharges in freely moving rats. *Hippocampus* **10,** 717–728 (2000).

284. Tang, A., Jackson, D., Hobbs, J., Chen, W., Smith, J. L., Patel, H., Prieto, A., Petrusca, D., Grivich, M. I., Sher, A., Hottowy, P., Dabrowski, W., Litke, A. M. & Beggs, J. M. A maximum entropy model applied to spatial and temporal correlations from cortical networks in vitro. *Journal of Neuroscience* **28,** 505–518 (2008).

285. Tang, W., Shin, J. D., Frank, L. M. & Jadhav, S. P. Hippocampal-prefrontal reactivation during learning is stronger in awake compared with sleep states. *Journal of Neuroscience* **37,** 11789–11805 (2017).

286. Tatsuno, M., Lipa, P. & McNaughton, B. L. Methodological considerations on the use of template matching to study long-lasting memory trace replay. *Journal of Neuroscience* **26,** 10727–10742 (2006).

287. Tavoni, G., Ferrari, U., Battaglia, F. P., Cocco, S. & Monasson, R. Functional coupling networks inferred from prefrontal cortex activity show experience-related effective plasticity. *Network Neuroscience* **1,** 275–301 (2017).

288. Tiesinga, P. & Sejnowski, T. J. *Cortical Enlightenment: Are Attentional Gamma Oscillations Driven by ING or PING?* 2009. doi:10.1016/j.neuron.2009.09.009.

289. Tingley, D., Alexander, A. S., Quinn, L. K., Chiba, A. A. & Nitz, D. A. Cell assemblies of the basal forebrain. *Journal of Neuroscience* **35,** 2992–3000 (2015).

290. Tingley, D. & Peyrache, A. On the methods for reactivation and replay analysis. *Philosophical Transactions of the Royal Society B: Biological Sciences*. doi:https://doi.org/10.1098/rstb.2019.0231 (2020).

291. Tkačik, G., Granot-Atedgi, E., Segev, R. & Schneidman, E. Retinal metric: A stimulus distance measure derived from population neural responses. *Physical Review Letters* **110,** 058104 (2013).

292. Tkačik, G., Marre, O., Amodei, D., Schneidman, E., Bialek, W. & Berry, M. J. Searching for Collective Behavior in a Large Network of Sensory Neurons. *PLoS Computational Biology* **10,** e1003408 (2014).

293. Tkacik, G., Schneidman, E., Berry, M. J. & Bialek, W. Ising models for networks of real neurons (2006).

294. Todorova, R. & Zugaro, M. Isolated cortical computations during delta waves support memory consolidation. *Science* **366,** 377–381 (2019).

295. Torre, E., Canova, C., Denker, M., Gerstein, G., Helias, M. & Grün, S. ASSET: Analysis of Sequences of Synchronous Events in Massively Parallel Spike Trains. *PLoS Computational Biology* **12.** doi:10.1371/journal.pcbi.1004939 (2016).

296. Torre, E., Picado-Muiño, D., Denker, M., Borgelt, C. & Grün, S. Statistical evaluation of synchronous spike patterns extracted by frequent item set mining. *Frontiers in Computational Neuroscience*. doi:10.3389/fncom.2013.00132 (2013).

297. Tort, A. B., Kramer, M. A., Thorn, C., Gibson, D. J., Kubota, Y., Graybiel, A. M. & Kopell, N. J. Dynamic cross-frequency couplings of local field potential oscillations in rat striatum and hippocampus during performance of a T-maze task. *Proceedings of the National Academy of Sciences of the United States of America* **105,** 20517–20522 (2008).

298. Tort, A. B., Ponsel, S., Jessberger, J., Yanovsky, Y., Brankačk, J. & Draguhn, A. Parallel detection of theta and respiration-coupled oscillations throughout the mouse brain. *Scientific Reports* **8,** 1–14 (2018).

299. Trettel, S. G., Trimper, J. B., Hwaun, E., Fiete, I. R. & Colgin, L. L. Grid cell co-activity patterns during sleep reflect spatial overlap of grid fields during active behaviors. *Nature Neuroscience* **22,** 609–617 (2019).

300. Trimper, J. B., Trettel, S. G., Hwaun, E. & Colgin, L. L. Methodological Caveats in the Detection of Coordinated Replay between Place Cells and Grid Cells. *Frontiers in Systems Neuroscience* **11,** 57 (2017).

301. Tripathy, S. J., Burton, S. D., Geramita, M., Gerkin, R. C. & Urban, N. N. Brain-wide analysis of electrophysiological diversity yields novel categorization of mammalian neuron types. *Journal of Neurophysiology* **113,** 3474–3489 (2015).

302. Trouche, S., Koren, V., Doig, N. M., Ellender, T. J., El-Gaby, M., Lopes-dos-Santos, V., Reeve, H. M., Perestenko, P. V., Garas, F. N., Magill, P. J., Sharott, A. & Dupret, D. A Hippocampus-Accumbens Tripartite Neuronal Motif Guides Appetitive Memory in Space. *Cell* **176,** 1393–1406 (2019).

303. Trouche, S., Pompili, M. N. & Girardeau, G. The role of sleep in emotional processing: insights and unknowns from rodent research. *Current Opinion in Physiology* **15,** 230–237 (2020).

304. Tsujimoto, S. *Review: The prefrontal cortex: Functional neural development during early childhood* 2008. doi:10.1177/1073858408316002.

305. Tyrcha, J., Roudi, Y., Marsili, M. & Hertz, J. The Effect of Nonstationarity on Models Inferred from Neural Data. *Journal of Statistical Mechanics: Theory and Experiment* (2012).

306. Uhlhaas, P. J., Roux, F., Singer, W., Haenschel, C., Sireteanu, R. & Rodriguez, E. The development of neural synchrony reflects late maturation and restructuring of functional networks in humans. *Proceedings of the National Academy of Sciences of the United States of America* **106,** 9866–9871 (2009).

307. Usrey, W. M., Alonso, J. M. & Reid, R. C. Synaptic interactions between thalamic inputs to simple cells in cat visual cortex. *Journal of Neuroscience* **20,** 5461–5467 (2000).

308. Vaadia, E., Haalman, I., Abeles, M. & Bergman, H. Dynamics of neuronal interactions in monkey cortex in relation to behavioural events. *Nature* **373,** 515–518 (1995).

309. Valdés, J. L., McNaughton, B. L. & Fellous, J. M. Offline reactivation of experience-dependent neuronal firing patterns in the rat ventral tegmental area. *Journal of Neurophysiology* **114,** 1183–1195 (2015).

310. Van de Ven, G. M., Trouche, S., McNamara, C. G., Allen, K. & Dupret, D. Hippocampal Offline Reactivation Consolidates Recently Formed Cell Assembly Patterns during Sharp Wave-Ripples. *Neuron* **92,** 968–974 (2016).

311. Van Der Meer, M. A. & Redish, A. D. Theta phase precession in rat ventral striatum links place and reward information. *Journal of Neuroscience* **31,** 2843–2854 (2011).

312. Van der Meij, R. & Voytek, B. Uncovering neuronal networks defined by consistent between-neuron spike timing from neuronal spike recordings. *Eneuro* **5** (2018).

313. Varela, F., Lachaux, J. P., Rodriguez, E. & Martinerie, J. The brainweb: Phase synchronization and large-scale integration. *Nature Reviews Neuroscience* **2,** 229–239 (2001).

314. Vertes, R. P. Differential projections of the infralimbic and prelimbic cortex in the rat. *Synapse* **51,** 32–58 (2004).

315. Vinck, M., Battaglia, F. P., Womelsdorf, T. & Pennartz, C. Improved measures of phase-coupling between spikes and the Local Field Potential. *Journal of Computational Neuroscience* **33,** 53–75 (2012).

316. Von Stein, A. & Sarnthein, J. *Different frequencies for different scales of cortical integration: From local gamma to long range alpha/theta synchronization* in *International Journal of Psychophysiology* **38** (2000), 301–313. doi:10.1016/S0167-8760(00)00172-0.

317. Von Nicolai, C., Engler, G., Sharott, A., Engel, A. K., Moll, C. K. & Siegel, M. Corticostriatal coordination through coherent phase-amplitude coupling. *Journal of Neuroscience* **34,** 5938–5948 (2014).

318. Walker, M. P., Brakefield, T., Morgan, A., Hobson, J. A. & Stickgold, R. Practice with sleep makes perfect: Sleep-dependent motor skill learning. *Neuron* **35,** 205–211 (2002).

319. Wang, D. V. & Ikemoto, S. Coordinated interaction between hippocampal sharp-wave ripples and anterior cingulate unit activity. *Journal of Neuroscience* **36,** 10663–10672 (2016).

320. Wang, X. J. *Neurophysiological and computational principles of cortical rhythms in cognition* 2010. doi:10.1152/physrev.00035.2008.

321. Watanabe, K., Haga, T., Tatsuno, M., Euston, D. R. & Fukai, T. Unsupervised Detection of Cell-Assembly Sequences by Similarity-Based Clustering. *Frontiers in Neuroinformatics* **13,** 39 (2019).

322. Waydo, S., Kraskov, A., Quiroga, R. Q., Fried, I. & Koch, C. Sparse representation in the human medial temporal lobe. *Journal of Neuroscience* **26,** 10232–10234 (2006).

323. Wehr, M. & Laurent, G. Odour encoding by temporal sequences of firing in oscillating neural assemblies. *Nature* **384,** 162–166 (1996).

324. White, I. M. & Wise, S. P. Rule-dependent neuronal activity in the prefrontal cortex. *Experimental Brain Research* **126,** 315–335 (1999).

325. Whittington, M. A., Traub, R. D., Kopell, N., Ermentrout, B. & Buhl, E. H. *Inhibition-based rhythms: Experimental and mathematical observations on network dynamics* in *International Journal of Psychophysiology* **38** (Int J Psychophysiol, 2000), 315–336. doi:10.1016/S0167-8760(00)00173-2.

326. Wierzynski, C. M., Lubenov, E. V., Gu, M. & Siapas, A. G. State-Dependent Spike-Timing Relationships between Hippocampal and Prefrontal Circuits during Sleep. *Neuron* **61,** 587–596 (2009).

327. Wilber, A. A., Skelin, I., Wu, W. & McNaughton, B. L. Laminar Organization of Encoding and Memory Reactivation in the Parietal Cortex. *Neuron* **95,** 1406–1419 (2017).

328. Wilson, M. A. & McNaughton, B. L. Reactivation of hippocampal ensemble memories during sleep. *Science* **265,** 676–679 (1994).

329. Womelsdorf, T., Schoffelen, J. M., Oostenveld, R., Singer, W., Desimone, R., Engel, A. K. & Fries, P. Modulation of neuronal interactions through neuronal synchronization. *Science* **316,** 1609–1612 (2007).

330. Wood, E. R., Dudchenko, P. A., Robitsek, R. J. & Eichenbaum, H. Hippocampal neurons encode information about different types of memory episodes occurring in the same location. *Neuron* **27,** 623–633 (2000).

331. Yuste, R. From the neuron doctrine to neural networks. *Nature Reviews Neuroscience* **16,** 487–497 (2015).

332. Zaki, Y., Mau, W., Cincotta, C., Hamidi, A., Doucette, E., Grella, S. L., Merfeld, E., Murawski, N. J., Shpokayte, M. & Ramirez, S. Hippocampus and amygdala fear memory engrams re-emerge after contextual fear reinstatement. *bioRxiv,* 2019.12.19.882795 (2019).

333. Zhang, K., Ginzburg, I., McNaughton, B. L. & Sejnowski, T. J. Interpreting neuronal population activity by reconstruction: Unified framework with application to hippocampal place cells. *Journal of Neurophysiology* **79,** 1017–1044 (1998).

ABSTRACT

How do billions of neurons cooperate to process information and mediate cognitive function such as learning, planning or memory? An influential hypothesis is that groups of neurons can synchronize within brief time windows to represent a cognitive entity or a concept (e.g. an apple, a sonata, the thought of my grand-mother, Hebb 1949). These groups, called 'cell assemblies' are thought to be the functional units of the brain. Recent advances in large-scale neuronal recordings enabled to investigate such synchronous activity within single areas of the brain. Yet, the functional relevance of these ensembles remains largely unexplored, especially in higher order brain areas. To address this question, we designed two research projects based on extracellular recordings in rats.

First, we demonstrated and characterized synchronous activity spanning different parts of the prefrontal cortex and the striatum, constituting the cortico-basal ganglia loop. These distributed cell assemblies exhibited behaviorally correlated activation during a set-shifting task, and synchrony emerged when assembly members shifted their phase relative to ongoing brain rhythms. We propose that cross-structural assemblies are likely to be a general mechanism that can span across multiple brain area and networks, therefore underlying highly integrated representations.

Second, we analyzed the neural activity from hundreds of single units in the prefrontal-amygdalar networks during sleep to investigate the functional relevance of cell assemblies from the perspective of a downstream neuron. Our results suggest that the synchronous activity of cell assemblies facilitate and amplify the discharge of downstream neurons, termed ‘readers’ of the assembly. Interestingly, we showed that the assembly-reader communication changes with learning.

RÉSUMÉ

Par quels moyens des milliards de neurones coopèrent et communiquent afin de sous-tendre des fonctions cognitives telles que la planification, l’apprentissage ou bien la mémoire? Selon l’hypothèse influente de Hebb (1949), de petits groupes de neurones se synchroniseraient, sur une courte échelle de temps, afin de représenter une entité ou bien un concept (par exemple, une pomme, une sonate ou bien le souvenir de ma grand-mère). Ces groupes de neurones, des 'assemblées cellulaires', constitueraient ainsi les unités fonctionnelles du cerveau. De recents progrès techniques et expérimentaux ont permis de mettre en lumière l’existence de telles assemblées au sein de certaines régions cérébrales. Pourtant, le rôle et la pertinence fonctionnelle de ces ensembles restent largement inexplorés, en particulier dans les aires cérébrales qui sous-tendent des fonctions cognitivescomplexes. Pour étudier cette problématique, nous avons conçu deux projets de recherche à partir d’enregistrements éléctrophysiologiques extracellulaires chez le rat.

Premièrement, nous avons démontré et caractérisé des assemblées cellulaires incluant des neurones de différentes parties du cortex préfrontal et du striatum. Le mécanisme de formation de telles assemblées implique un changement de phase de leurs membres, par rapport aux rythmes cérébraux du cortex préfrontal. Lors d’une tâche de flexibilité cognitive, ces assemblées cellulaires distribuées s’activent sélectivement selon le comportement de l’animal (par exemple, lors de la prise de décision). Pour conclure, il est très probable que de telles assemblées distribuées reflètent un mécanisme général par lequel des neurones issus de différentes régions et réseaux du cerveau sesynchronisent, pour sous-tendre des représentations intégrant de multiples informations.

Dans un second temps, nous avons analysé l'activité de centaines de neurones dans le réseau préfrontal-amygdalien,enregistrés lors du sommeil, afin d’étudier la pertinence fonctionnelle des assemblées cellulaires du point de vue d'unneurone post-synaptique. Nos résultats suggèrent que l'activité synchrone des assemblées cellulaires facilite et amplifie la décharge de neurones post-synaptiques, appelés «lecteurs» de l’assemblée. Enfin, nous avons montré que la communication entre une assemblée et son ou ses lecteurs change avec l’apprentissage.